NON-CONTACT AND SECURE RADAR-BASED CONTINUOUS IDENTITY AUTHENTICATION IN MULTIPLE-SUBJECT ENVIRONMENTS

A DISSERTATION SUBMITTED TO THE GRADUATE DIVISION OF THE UNIVERSITY OF HAWAIʻI IN PARTIAL FULFILLMENT OF THE REQUIREMENTS FOR THE DEGREE OF

DOCTOR OF PHILOSOPHY

IN

ELECTRICAL ENGINEERING

December 2020

By
Shekh Md Mahmudul Islam

Dissertation Committee:

Victor M. Lubecke, Chairperson
Olga Boric-Lubecke
Aaron Ohta
Yao Zheng
Jelena Maricic

We certify that we have read this dissertation and that, in our opinion, it is satisfactory in scope and quality as a dissertation for the degree of Doctor of Philosophy in Electrical Engineering.

DISSERTATION COMMITTEE

Victor M. Lubecke, PhD

Olga Boric-Lubecke, PhD

Aaron Ohta, PhD

Yao Zheng, PhD

Jelena Maricic, PhD

Dedicated to
My father Md. Ayub Nabi and my mother Razia Begum
For their endless love, support, and encouragement.

Acknowledgements

I wish to acknowledge the many people who have helped to make this work possible, by contributing technically, by making my time at outside my home comfortable one, and/or by preparing me for my career.

First I would like to thank my adviser, Professor Victor Lubecke. He has always been enthusiastic both when talking with me and with others, which has helped me to keep motivated to work on this research project. He has helped me to make my research focused and practical by redirecting me when I get sidetracked on tangential or impractical research interest. I consider myself a very lucky person to have such an experienced and knowledgeable adviser. He could grasp the idea of my research very quickly and guide me readily towards the next steps. Finally, he has been a great mentor, encouraging my interest both within and outside of my research.

I wish to thank Professor Olga Boric-Lubecke for her excellent support as a mentor and committee member. I would like to thank Professor Olga Boric-Lubecke for introducing me to different research projects, for her consistent excellent technical advice, for teaching me to write good research papers and for encouraging me to publish early and often.

I would also like to thank Professor Yao Zheng for his excellent mentoring in researching security analysis. He was a great resource for me for further development of the security protocol that consists of a substantial part of the dissertation. I would like to thank all the committee members for their timely feedback and responses.

It was a great privilege to receive support from the alumni group of the lab. Ashikur Rahman shared useful insights when I faced obstacles in my research. Having him as a

colleague was great. Otherwise, I would have wasted a lot of time reinventing the wheels. Ehsan Yavari has been my great colleague and guide. He showed the path towards publishing my first paper and greatly contributed to the writing. I would especially like to thank him for being my consistent companion for coffee breaks and lunches, many of which had been lonely without him. I also want to mention Meheran Baboli and John E. Kiriazi who shared their experimental data set for contributing to other research projects.

Finally, my parents Md. Ayub Nabi and Razia Begum, whose encouragement to always explore my surroundings led to my early interest in science, and whose consistent focus on my academic achievement laid the groundwork for pursuing Ph.D. My mother always inspired me greatly and always spent my evening time in Skype throughout my graduate study in abroad. My father has always encouraged me to be self-sufficient, to be strong and courageous, to be realistic, and to be successful. In the absence of me, my elder brother Dr. Shekh Mamun Kabir, and my younger sister Israt Jahan supported my parents wholeheartedly. Without my family support, it would have been very difficult to continue my studies abroad.

Abstract

An unobtrusive, secure and non-contact continuous authentication system can potentially improve security throughout a login session. Traditional user authentication procedures such as fingerprint, password, or facial identification typically provide only an initial spot-check of identity at the start of a user session, potentially allowing undesired access to personal information (e. g. social security number) at some later point in an apparently continuous user session. The research goal of this PhD dissertation is to create a non-contact and secure continuous authentication system based on Doppler radar, which analyzes back-scattered RF signals which carry body motion information indicating a human subject's vital signs (breathing rate, heart rate) and associated unique patterns. An additional advantage to this radar technique is that continuous authentication is achieved without intrusive video imaging. Reported prior results are focused solely on use of respiratory motion to identify a single isolated subject. Simultaneous measurement of multiple subjects is a critical challenge. In realistic environments (airport security, in-home sleep apnea test, etc.) the presence of multiple subjects in front of the radar system is likely. To make this technology effective for real world applications, isolation of one particular subject's breathing pattern from the combined mixture of motion for multiple subjects is essential. Reported research has so far been limited to maintaining 1-m subject separation based on the radar antenna beam-width.

This thesis proposes a hybrid method consisting of an SNR-based intelligent decision algorithm which integrates two different approaches to isolate respiratory signatures of two-subjects within the radar antenna beamwidth separated by less than 1-m. A 24-GHz phase

comparison Monopulse radar module (K-MC4) has been used to estimate the Direction of Arrival (DOA) for the physiological motion signals of well-spaced subjects at the edge of the beamwidth of the transceiver. DOA is inherently limited to the main beamwidth of the transceiver so when the subjects get closer, crossing the edge of the beamwidth, an additional independent component analysis with the JADE algorithm (ICA-JADE) process is employed to isolate individual respiratory signatures. Experimental results demonstrated that, this proposed SNR-based decision algorithm works with an accuracy of above 93%. In addition, angular location of each subject is estimated by phase-comparison monopulse and an integrated beam switching capability is also demonstrated to optimally extract respiratory information. Additionally, we also conducted a medium scale experiment with twenty participants and collected Doppler radar signals containing the combined respiration mixtures of every pair of participants, over the course of about one month. We then used our proposed SNR-based decision algorithm to separate respiratory signatures from the combined mixtures.

From the separated respiratory signatures, we extracted highly distinguishable breathing dynamics-related hyper-features from the respiratory signatures including breathing rate, heart rate, inhale/exhale rate and inhale/exhale area for identity verification. We evaluated the hyper-feature sets with two different classifiers, k-nearest neighbor (KNN) and support vector machine (SVM), and achieved an accuracy 97.5%. We also analyzed the empirical entropy of the hyper-feature set and found that intrinsic entropy of the hyper-feature set is approximately 3-bits which is insufficient for secure identity verification. To improve the security of the proposed system, we also combined fuzzy extractors with linear coding to transform the breathing dynamic related feature into strong biometric keys compatible with machine learning classifiers. We also integrated this proposed radio-based identity verification system with in-home sleep apnea test scenarios. A compliance tracking switching protocol has been developed to integrate the radio-based identity verification system with OSA test. To the best of our knowledge this is the first attempt to achieve secure radio-based multi-subject identity verification by combining the Doppler radar and Fuzzy extractor.

Table of Contents

List of Tables

List of Figures

Chapter 1

Introduction

Vital signs sensing using microwave Doppler radar has shown great promises in healthcare applications and has become an active area of research and study for about four decades with proof of concepts demonstrated for various applications [1][2][3][4]. In addition, microwave Doppler radar has been used to capture the tiny movement of the chest surface due to cardio-respiratory activities since the early 1970s [1][2][5]. There are several potential advantages of this technique. It is a non-contact and unobtrusive form of monitoring cardiopulmonary activity through clothing and bedding which can lead to potential applications in sleep monitoring and home healthcare applications [4][6][7][8]. Regular respiratory rate and pattern are indicator of good health whereas, rich rate variation in a particular range is healthy. This non-contact and noninvasive form of respiratory motion sensing technology increased its area has expanded to include occupancy detection [9], energy management in smart homes, and baby monitoring has also opened the door to many indoor applications only limited by one's imaginations [6][7][10]. Recently,interest in using microwave Doppler radar respiration sensing to develop a non-contact, continuous and unobtrusive identity authentication system [11][12] [13] [14]. It has been proven in various investigations that different people breathe in different ways in terms of their tidal volume, air flow profile, breathing depth, energy and breathing dynamics related features [15].

Identity theft continues to pose challenges for consumers in their day to day activities and conventional identity authentication system is just a one-pass validation system

[11][16]. Traditional identity authentication system such as fingerprint, password, and facial recognition all require an initial spot check at the start of a user session which potentially allows subsequent theft of personal information like bank account, social security number, credit card and social account details [11] [16]. In 2018, the number of consumers who were victim of identity fraud was approximately 14.4 million in the United states [11][16]. Identity fraud can be significantly reduced by implementing a multi-factor authentication system that integrates of unobtrusive respiration sensing technology with the traditional methods. There are several advantages of this proposed technique as it is non-contact and unobtrusive so users need not to intentionally engage themselves with the authentication system and it can increase the security of the system by monitoring the respiration of human being unobtrusively over the entire course of interaction.

The work presented is concentrated on developing a new, innovative, unobtrusive and continuous identity authentication system for multi-subject scenarios by integrating new signal processing techniques with the microwave Doppler radar [17][18][19][20][21][22]. Highly distinguishable breathing dynamic related features were extracted from the respiratory signatures, including breathing rate and heart rate as well as inhale and exhale area in order to verify identity for twenty different participants for long term studied over a period of two months [19][23][24]. The proposed system also integrated intelligent machine learning classifiers for recognizing people automatically from their radar captured respiration patterns. We also investigated the feasibility of separating independent respiratory signatures of closely spaced subjects and extracting cryptographically secure identities from their breathing pattern using microwave Doppler radar and Fuzzy extractors. We conducted a medium scale experiment with twenty participants and collected Doppler radar signals containing the combined respiration mixtures of every pair of participants. Respiration monitoring for multi-subject scenarios using microwave Doppler radar or any kind of RF sensors remains a significant technological challenge because, when multiple subjects are present in front of the radar, their breathing pattern interference occurs [17][18][21][24][25]. In this work, we also utilized a Independent component analysis

(ICA) with the JADE algorithm for separating independent respiratory signatures from their combined mixtures [17][18][21][24][25]. We also employed 24-GHz phase-comparison Monopulse radar for estimating the angular location of the subject/target [17][24][18], and tested the feasibility of beam switching capabilities to track respiratory patterns for subjects outside the beamwidth [26]. DOA performs well when subjects are well-spaced or at the edge of the beamwidth of the radar [17][18][24]. On the other hand, ICA-JADE performs well when subjects are closely spaced which provides better signal-to-noise ratio (SNR) to the radar captured respiration signal [17][25]. We proposed an intelligent SNR-based decision algorithm to integrate both techniques (ICA-JADE and DOA) coherently so that our proposed system can be much more robust to make possible ubiquitous respiration monitoring [26].

This chapter will provide a clear concept of the basics of Doppler radar for physiological sensing and the scope of this dissertation. The first part covers the basics of Doppler radar for physiological sensing, different Doppler radar topologies, and radar range equations. The next part describes application areas for CW Doppler radar especially in cardio-respiratory monitoring, search and rescue operations, and identity authentication. The following part describes about the existing challenges in Doppler radar identity authentication.

1.0.1 Basics of Radar

Radar stands for Radio Detection and Ranging, which basically transmits an electromagnetic signal and receives the echo reflected from an object/target. Thus, it can capture information about a target. The time delay between the received signal and transmitted signal provides information about distance of the target, the frequency shift of the reflected echoes provides information about velocity of the object and the strength of the signal provides information about target's radar cross section (RCS). One of the potential benefits of microwave radar is that these waves can penetrate through some objects, like walls and clothing, that light cannot penetrate which allows detection of objects that cannot be seen. Radar systems developed for different applications may have different frequency

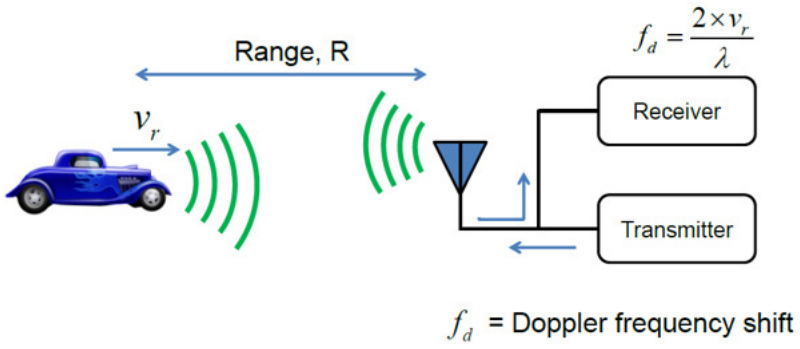

Figure 1.1 Illustration of Doppler effect of a transceiver when a car is moving towards a radar with a constant radial velocity. Taken from [7].

ranges [27]. Fig. 1 above illustrates the block diagram of a radar system which basically consists of transmitter, a receiver, and signal processing hardware/software. Fig. 1 shows a car is moving at a constant radial velocity, V_r and the associated frequency shift of the transmitted signal that represented as, $f_d = 2 \times \frac{V_r}{\lambda}$; where V_r is the radial velocity. From the frequency shift the velocity of the car can be determined. A typical Doppler radar consists of transmitter which may have directional antenna or omnidirectional antenna. The receiver converts the signal from the transmission frequency to an intermediate frequency or baseband, then separates the signal from noise or interference and then amplifies it for digitization and/ or display. Depending on the radar system hardware and the type of signal sent, a radar can be classified into three different categories. A pure continuous wave (CW) radar sends a continuous electromagnetic signal to detect the velocity of a moving target. CW radar cannot detect range. Frequency modulated continuous wave (FMCW) radar can detect range and velocity of the moving target because it sends a frequency modulated signal. Pulsed radar allows transmission and reception of a signal at different times intervals. Table 1.1 illustrates the different topologies of radar, sensing technologies and sensing information. The description of different topology radars is described in next section.

Table 1.1 Sensing Information from Different Topologies Radar Transceivers [10].

Information	**Method of determination**	**Required Topology**
Range	Time delay	Any;CW needs significant range resolution
Velocity	Doppler shift	Any; pulsed needs significant velocity resolution
Angle	Direction of Reflection	Any, requires antenna arrays
Size and shape	Received power	Any but CW, must be high resolution
Radial Velocity	Doppler shift and time delay	CW

1.0.2 Continuous-wave (CW), Frequency modulated continuous wave (FMCW), Pulse Wave Radar

CW radar transmits an unmodulated signal with a known stable frequency and then received reflected signal after striking to the target/subject. From the theory of Doppler effect reflected signal frequency shift occurs due to the velocity of the target, so by analyzing the frequency shift of the target velocity information can be extracted. shift the velocity of the car can be determined. The main advantage of this radar system is it requires simple circuitry to manufacture and operate. The Doppler frequency change is represented as:

$$f_r = \frac{f_t\left(1+\frac{v}{c}\right)}{\left(1-\frac{v}{c}\right)} \tag{1.1}$$

Where, f_r is the reflected signal frequency, f_t is the transmission signal frequency, v is the velocity of the target and c is the velocity of light. The Doppler frequency can be illustrated in below equations (the speed of a target is much smaller than velocity of light, c)

$$f_d = f_r - f_t = \frac{2vf_t}{c-v} \approx \frac{2vf_t}{c} \tag{1.2}$$

CW waves radar without frequency modulation only detects a moving target as stationary targets will not cause a Doppler shift. CW radars are mostly used in radio-altimeters, proximity sensors and sport accessories that operate from a few dozen feet to several kilometers.

FMCW radar transmits frequency modulated signal. In other words, FMCW radar can change its frequency during the measurement. Simple continuous wave radar without frequency modulation have the disadvantage that it cannot determine target range because it lacks the timing mark necessary to allow the system to time accurately the transmit and receive cycle and convert this into range. FMCW radar transmits a signal called "chirp". A chirp is a sinusoid whose frequency increases linearly with time. When the signal is being returned from target it is multiplied with transmitted signal and the resulting signal is called intermediate frequency (IF) signal. The received signal is time delayed version of the transmitted signal and from that time delay information range information of the target can be extracted. FMCW radar can detect the range and velocity of the target [27]. Altimeters and Doppler navigation devices use this type of radar.

On the other hand, pulse radar switches between transmitting and receiving and has a wider bandwidth than CW radar [7][10]. A pulse radar transmits a narrow pulse having a large power with a constant pulse-repetition frequency and analyzes the time delayed version of the reflected echoes from target [10]. Pulse radar that employs the principle of doppler shift for detecting the moving object is known as MTI (moving tracking indicator) radar. Pulse modulator is used to turn on and off the transmitter to generate a pulse waveform. Pulse Radar can also be used to measure range and velocity.

1.0.3 Radar Range Equations

Radar transmits electromagnetic signal with different frequencies based on different applications. Electromagnetic signals travel at the speed of light and when it returns from the target, returning echoes time delays occurs [10]. The time delay of the returning signal is represented as:

$$\tau = \frac{2R}{c} \tag{1.3}$$

Where, R is the range between target and radar, c is the velocity of light and τ is the round-trip time delay between the transmitted signal and received signal. Doppler radar

utilizes the Doppler shift concept of the return signal to track the motion of the moving objects. Doppler shift can be illustrated by the following equation:

$$f_d = -\frac{v}{c} \tag{1.4}$$

Where, v is the target's speed, c is the velocity of the light and f_d is the Doppler frequency shift of the returning signal. If the object or target is in line of sight of the radar transmitter then the reflected signal power can be calculated based on below equation:

$$P_r = \frac{P_t G A_e \sigma}{(4\pi)^2 R^4} \tag{1.5}$$

Where, P_r is the received signal power, P_t is the transmitted signal power, G is the antenna gain, A_e is the receiving antenna effective aperture, σ is the radar cross section (RCS) of the target and R is the radial distance between radar and target. From eqn. (1.5) we can see that the power of the received signal is inverse fourth power of the transceiver and the target. Radar cross section (RCS) is an important term which illustrates how much energy is absorbed by the reflector or in other words, how much energy is being reflected from the transmitted signal. It depends on the size, shape and composition of the object/target. RCS can be illustrated based on the following equation:

$$\sigma = \frac{\frac{Power\ reflected\ toward\ source}{unit\ solid\ angle}}{\frac{Incident\ power\ density}{4\pi}} \tag{1.6}$$

1.1 Application Areas of CW Radar

1.1.1 Non-Contact Cardio-respiratory Monitoring

Doppler radar sends an electromagnetic signal (sometimes it may be frequency modulated) which is reflected back from a target and them demodulated in the receiver [4][7]10]. According to Doppler theory, a subject/target with time varying displacement but no net velocity will reflect the signal, modulating its phase in proportion to the time varying

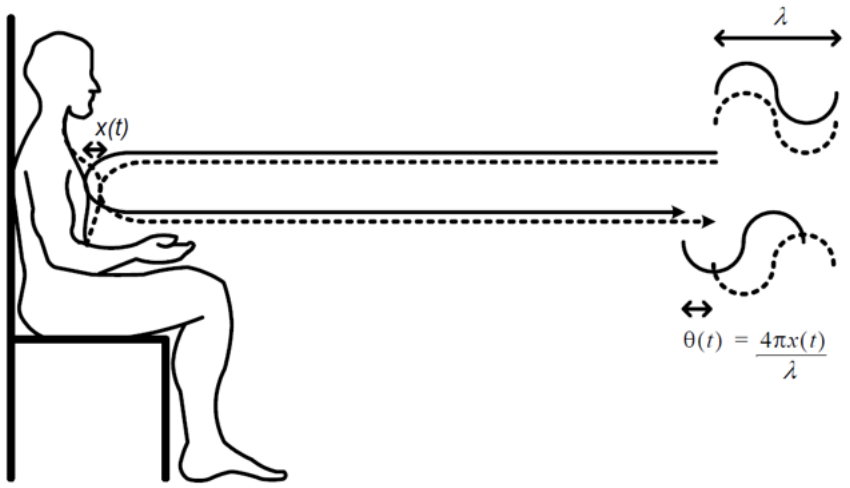

Figure 1.2 Basics of Doppler Radar physiological sensing. The phase of the reflected signal, $\theta(t)$ is directly proportional to the tiny movement of the chest surface due to cardio-respiratory activity. From [10].

displacement of the target [4][28]. A stationary human subject's chest has a periodic tiny movement with no velocity and when the signal is being reflected from the chest surface the reflected signal phase changes [10]. The phase change of the reflected signal is directly proportional to the tiny movement of the chest surface due to cardio-respiratory activities (expansion and contraction of heart) [10]. Demodulating the phase will provide information about movement of the chest surface due to cardio-respiratory activities, which contains information about breathing rate and heart rate [7]. The peak to peak chest motion for an adult range from 4 mm to 12 mm and amplitude of motion due to heartbeat is 0.5 mm [3]. When the wavelength is greater than twice the peak to peak motion the signal can be demodulated by multiplying the signal with an unmodulated signal from the same source [10]. In this work we used 24-GHz phase comparison Monopulse radar which has wavelength of 12.5 mm which is less than twice the peak to peak motion of the signal [7]. So, an advanced signal processing must be utilized to demodulate the signal for extracting breathing rate and heart rate. Microwave Doppler radar was employed for non-contact

detection of cardio-respiratory activities by tracking the chest displacement information in early 1970's [1][4][29]. Based on the above information of tracking chest displacement information also opened the new door of monitoring vital signs such as respiration rate, arterial wall movement and heart rate [1]7][21]. The traditional screening method for cardiopulmonary monitoring is electrocardiogram (ECG) which requires acrefully applied electrodes. Another popular method is pulse oximetry which provides the level of oxygen saturation in the blood but does not provide any information about breathing and heart rate activity and gives a very late indication of a problem. Another technique is spirometry which basically measures the air flow profile which is used for respiratory rate and tidal volume but interfere with typical respiration. Among all of the technique ECG is the most popular which measures electrical activity of the heart over time by measuring the electrical signals passing through the body using electrodes attached to the skin but usually requires trained personnel. Long term respiratory monitoring of subject requires spending a lot of time in a hospital strapped to various wires. Microwave Doppler radar based non-contact respiratory sensing has several potential advantages. No wiring or sensor is required on the chest surface of human so this technique has proved its efficacy for long term sleep monitoring, health monitoring at a home, baby monitoring and assessment of cardiovascular health of a burn victims.

1.1.2 Search, Rescue and Military Applications

Another potential application of microwave Doppler radar is search and rescue operations for military and post-disaster environments. The potential advantage of Radar is it can penetrate through smoke, wall and darkness so it can track life signs under rubble. Doppler radar was demonstrated to extract vital sign information under bricks in [30] and successful measurement of human respiration and heartbeat was also possible under bricks [3]. The experiment performed by chen et al. also demonstrated that, 450 MHz electromagnetic signal can penetrate rubble without any metal for extracting vital signs and 1150 MHz signal has been used to extract vital sign from rubble with metallic wires [3]. Use of

unobtrusive radar vital signs sensing can help to track the victims in post-disaster search and rescue operation which can potentially reduce the sufferings of the victims.

1.1.3 Continuous Identity Authentication Using Radar

Identity authentication using microwave Doppler radar is also gaining a lot of interest as another emerging potential field because camera and fingerprint based biometric systems have several continuous operation and privacy issues [25]. Existing biometric based authentication systems only offer one pass operation and far from being fully satisfactory and trustworthy [11]. People need to intentionally engage themselves with such system such as scanning their fingerprints or entering passwords in a particular time frame. With a view to replacing traditional biometric systems or introducing continuous authentication as a multi-factor authentication scheme, researchers have tried using different physiological traits such as fingerprint, palmprint [31] and iris [32], all which basically depends on high quality and short range sensors resolutions. Recent advancements in wearable sensors and pattern recognition have emerged for physiological monitoring including unique identification sensors, such as electroencephalogram (EEG) [33], finger-vein [31], and gait [34] feature acquisition devices. However, solutions are completely dependent on contact sensors and controlled environments which basically reduce the system's usability and practical range of applications [35][36]. Some of the research efforts are also attempted in terms of non-contact sensors where physiological and behavioral traits are collected far away from the body. Various optical, and thermal cameras are employed for acquisition of face and gait features [37]. Face identification systems can also recognize and verify person [38]. Gait recognition which basically recognizes temporal patterns of walking have also received a great deal of attention for unique identifications [39]. However, these facial and gait features recognition approaches have several disadvantages including insufficient resolution which limits the pattern recognition and unique identification [40] [41]. Considering all these limitations, unobtrusive radar measurement of cardiac motion-based identity authentication is gaining popularity and many research efforts are exploring on this new way of biometric recognition.

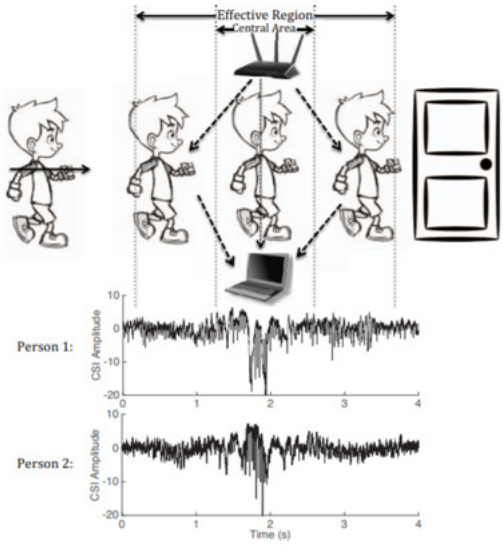

Figure 1.3 Recognizing people from their walking pattern using WiFi signals. One of the major limitations of this proposed method is that it cannot recognize people when multiple people are in view of the WiFi router. From [45].

Doppler radar based non-contact cardio-respiratory identity authentication systems can open a new door for this technology by replacing traditional biometric authentication systems this new unobtrusive method [42][43][44][45]. Prior research attempt have also focused on recognizing people from their gait patterns using WiFi signals [45] which is an unobtrusive way to recognize an isolated person because when multiple people are in view of WiFi router, this signal combines as a mixture of respiration which is hard to separate. Radar based identity authentication system is gaining attention due to its unobtrusive and non-contact form of respiration measurement [11][12][14]. Radar-based identity authentication is focused on extracting unique respiratory features and integrating machine learning classifiers with the unique features [11]12][14]. None of the attempts in literature have focused on utilizing this unobtrusive sensing technology in multi-subject scenarios. In addition, during identity authentication back-scattered RF signals might be corrupted, so extensive security analysis is required to bring this identity authentication system into real world of applications.

1.2 Existing challenges in Doppler radar identity authentication system

This section will focus on describing existing challenges in reported Doppler Radar based identity authentication. Here, I will focus on three important existing challenges in Doppler radar-based identity authentication systems to elucidate the goal of this dissertation. The first challenge is respiration measurement when multi-subjects are in the radar field of view to implement this sensor technology in real world applications. Second is the breathing related unique dynamic feature extraction challenges for different post-physiological activities. Another challenge is security system development for making radar-based identity authentication much more secure.

1.2.1 Multiple subjects in Radar field of view

One of the limitations of Continuous wave (CW) radar system is that it detects all motions in its field of view, not just the motion of interest. When there are multiple subjects present in front of the radar, their reflected radar signal combines as mixture of breathing patterns which basically form an interference respiration pattern [17]. Depending on applications, these problems may or may not affect the utility. For an example in a hospital environment for long term sleep studies the torso respiratory movement may be affected by the presence of medical practitioner in the same room for small amount of time. Also, in a home-environment subjects may share their bed with partners and in that case it is not possible to track the breathing pattern of the subject of interest due to the combination of the breathing pattern for the subjects [18]. Similarly, In an office environment there is the probability of presence of multiple subjects in front of the radar system. Thus, extracting independent respiratory signatures from combined mixtures also remains a significant technological challenge. However, most of the reported results focus on utilizing single subject experiment excluding the scenario of multiple subjects [17][25]. Fig 1.4(a) illustrates a scenarios where two subjects are in a hospital environment and Fig. 1.4(b) illustrates how CW radar is

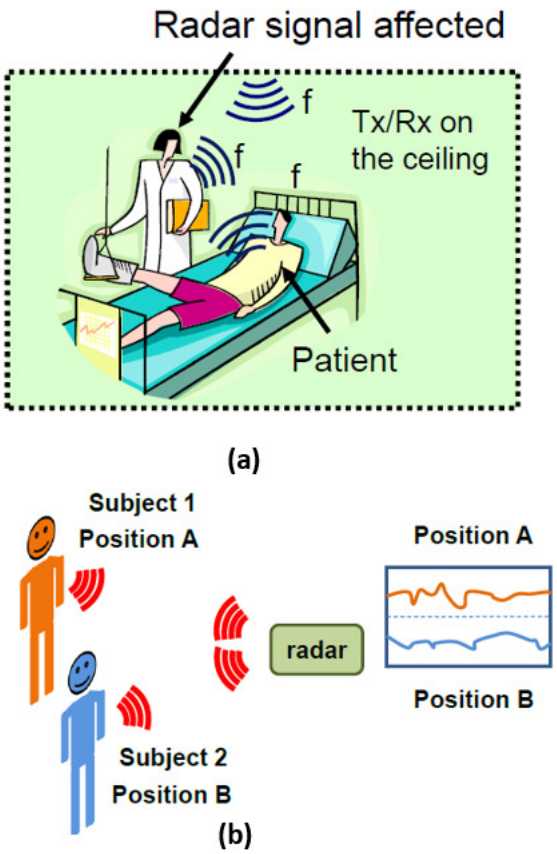

Figure 1.4 (a) Source of undesired motion by the presence of another medical practitioner during sleep study, and (b) schematic illustrating the inability of MIMO CW radar to identify the source motion. From [28].

incapable of estimating the position of two subjects in view of the radar. Previous attempts also focused on utilizing frequency domain analysis for isolating independent signals from the mixtures [17][24]. Prior research focused on solving this issue through integrating a multiple input and multiple output (MIMO) antenna system in CW radar to isolate independent respiratory signatures by utilizing Direction of arrival (DOA) technique [21]. One initial attempt evaluated the efficacy of MIMO technique for physiological motion sensing [46]. However, due to limited antenna array spacing, MIMO technique is not very effective when subjects becomes very close [17]. Thus, integration of MIMO technique helps to extract the breathing related information when subjects are well-spaced [46]. In another attempt,

real analytical constant modulus algorithm (RACMA) was integrated with Doppler radar to separate ceratin motions from breathing [47]. However, in this attempt used different motion signals were used like hand movement for which bandwidth is different than respiratory information and if moving target becomes much more closer the algorithm will not work properly [17][24]. Previous attempts also focused on separating respiratory signatures using the Independent Component Analysis (ICA) algorithm [25][46]. However, this work utilized separate antennas or transceivers for each different participants which is not very practical in realistic scenarios. Thus considering all this prior research, a new method for ubiquitous monitoring must be sought to overcome the existing challenges of multi-subject scenarios.

1.2.2 Respiration based continuous identity authentication

Breathing is a complicated anatomical process due to intra-pulmonary pressure and it is controlled by a central neural mechanism involving coordination of the diaphragm and respiratory muscles [15] [22]. It has been proven in various investigations that different people breathe in different ways in terms of their tidal volume, air flow profile, breathing depth, and energy [15]. Breathing related diversity occurs due to the anatomical variations including how different people have different heart shapes [15].The complete cardiac motion consists of five different stages including: (1) ventricular filling (VF), 2) atrial systole (AS), 3) isovolumetric ventricular contraction (IC), 4) ventricular ejection (VE), and 5) isovolumetric ventricular relaxation (IR). Heart based geometry changes from person to person due to change in size, position and anatomy of the heart, chest configuration and various other factors [11]. Due to having different heart based dynamics people might have different air flow profiles, breathing depth, energy and other unique patterns associated with these anatomical differences [48]. Prior attempts also focused on recognizing people from radar captured signals in situations is mostly limited to single subject experiments [12]14]. Thus, most reported results utilize single subject scenarios for recognizing people from radar captured respiration patterns [11][12]. Fig 1.5 illustrates the identity authentication system for a single subject scenario. The main reason for excluding multi-subject scenarios is due

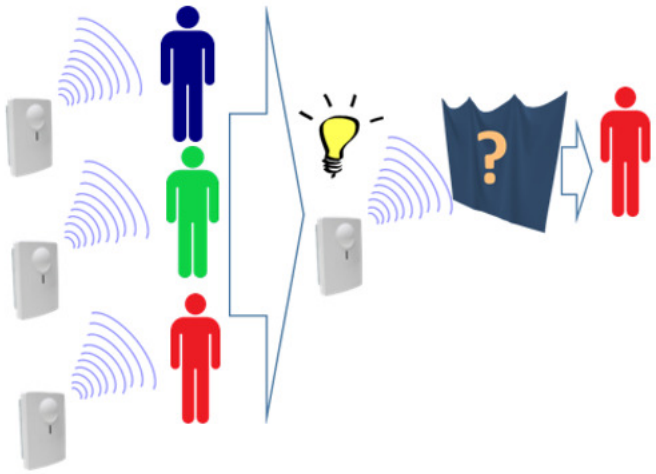

Figure 1.5 Radar-based continuous identity authentication system for single subject scenario.

to the interference caused by multiple subjects' combined signals at the transceiver [17]. So, having multiple subjects in view of the radar creates challenges for extracting unique respiratory features from respiration patterns. In real life, especially in home environments or office environments there is higher probability of the presence of multiple subjects in front of the radar. For these case extracting unique breathing dynamics related features from combined mixture remains a critical challenge. Thus, research questions for exploring multi-subject scenario are as follows:

1. Identity matching: From the combined mixture breathing pattern, can we extract unique breathing dynamics related features for different subjects?

2. Signal separation technique: We need to have a ubiquitous continuous separation technique for implementing this system in a multi-subject environment. Can we find an intelligent decision algorithm for separating independent respiratory signatures from combined mixtures?

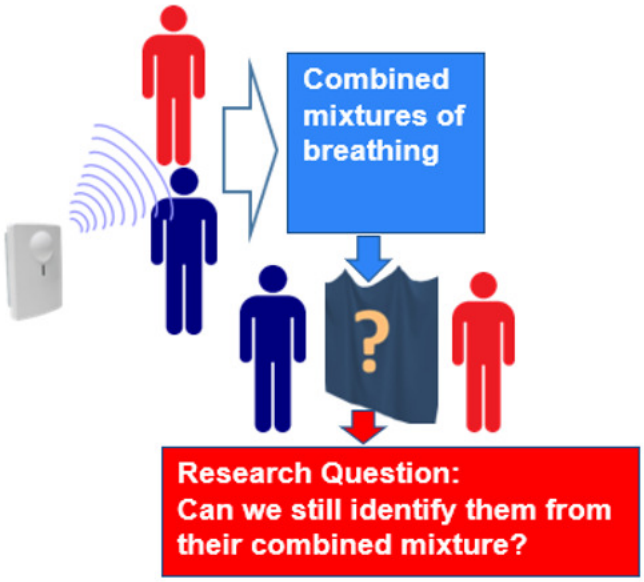

Figure 1.6 Radar based continuous identity authentication system for multiple subjects within the view of Radar scenario.

3. Swapping identity: In a multi-subject environment there is probability of swapping identity or mixing up subjects in the authentication process. Can we propose some reliable security protocol for identity authentication ?

Thus, all these challenges need to be addressed to bring this unobtrusive identity authentication technology into the real world.

1.2.3 Radar authentication data security

Radar based identity authentication mainly focuses on extracting unique features from radar-captured respiration patterns and then integrating machine learning classifiers with the extracted features to recognize different people [11]. Implementing the proposed authentication system in any home-environment, especially for sleep apnea diagnostics which lacks professional supervision, is also subject to unexpected events [49]. For our

project we mostly consider the scenario of an at-home obstructive sleep apnea (OSA) screening system. Existing identity authentication systems provide far from satisfactory level of security. To identify a patient using a radar based approach is inherently difficult as it is an RF-based approach which is vulnerable to noise [50]. Furthermore, integrating this technology with a wireless communication which makes the system vulnerable to attack over the air. So, we divide this data security problems to four categories described below.

1. Mix-up: In case of unobtrusive sleep apnea screening, patient may share the bed with another person during the test. For an example, a couple sharing a bed or a mother sleeping with a new born baby. The identity authentication system needs to separate the individual respiration patterns from the combined mixture as well as the background noise.

2. Surrogate: The patient may substitute another human for the test, perhaps to game a test for a job requirement. The patient may also use breathing phantom mover to replicate the chest movement and replace him entirely. The system needs to identify a person swap.

3. Eavesdrop: The patient may eavesdrop in between the wireless communications and OSA screening system so that he can get the recorded data before the doctor. There is a probability of significant discrepancy that may establish false excuses and convince the doctor to accept the test results.

4. Spoof: The patient may inject false data and manipulate the identity verification outcome. During identity authentication modality switching between the tracker and the OSA screening system is required. For instance, the patient may hijack data and falsify the test results.

Considering all these data authentication discrepancies we have designed a secure non-contact continuous identity authentication system. To the author's knowledge, this work is the first attempt to achieve a secure radar-based non-contact continuous identity

authentication for multiple subjects by integrating the combined power of Doppler radar and Fuzzy key extractors.

References

[1] J. Lin, "Noninvasive microwave measurement of respiration," *Proceedings of the IEEE*, vol. 63, no. 10, pp. 1530–1530, 1975.

[2] K.-M. Chen, D. Misra, H. Wang, H.-R. Chuang, and E. Postow, "An X-Band Microwave Life-Detection System," *IEEE Transactions on Biomedical Engineering*, vol. BME-33, pp. 697–701, July 1986.

[3] Kun-Mu Chen, Yong Huang, Jianping Zhang, and A. Norman, "Microwave life-detection systems for searching human subjects under earthquake rubble or behind barrier," *IEEE Transactions on Biomedical Engineering*, vol. 47, pp. 105–114, Jan. 2000.

[4] J. C. Lin, "Microwave sensing of physiological movement and volume change: A review," *Bioelectromagnetics*, vol. 13, no. 6, pp. 557–565, 1992.

[5] E. Greneker, "Radar sensing of heartbeat and respiration at a distance with applications of the technology," in *Radar Systems (RADAR 97)*, vol. 1997, (Edinburgh, UK), pp. 150–154, IEE, 1997.

[6] M. Baboli, A. Singh, B. Soll, O. Boric-Lubecke, and V. M. Lubecke, "Wireless Sleep Apnea Detection Using Continuous Wave Quadrature Doppler Radar," *IEEE Sensors Journal*, vol. 20, pp. 538–545, Jan. 2020.

[7] A. Droitcour, T. Seto, Byung-Kwon Park, S. Yamada, A. Vergara, C. El Hourani, T. Shing, A. Yuen, V. Lubecke, and O. Boric-Lubecke, "Non-contact respiratory

rate measurement validation for hospitalized patients," in *2009 Annual International Conference of the IEEE Engineering in Medicine and Biology Society*, (Minneapolis, MN), pp. 4812–4815, IEEE, Sept. 2009.

[8] M. Baboli, A. Singh, B. Soll, O. Boric-Lubecke, and V. M. Lubecke, "Good Night: Sleep Monitoring Using a Physiological Radar Monitoring System Integrated with a Polysomnography System," *IEEE Microwave Magazine*, vol. 16, pp. 34–41, July 2015.

[9] E. Yavari, C. Song, V. Lubecke, and O. Boric-Lubecke, "Is There Anybody in There?: Intelligent Radar Occupancy Sensors," *IEEE Microwave Magazine*, vol. 15, pp. 57–64, Mar. 2014.

[10] A. Droitcour, V. Lubecke, Jenshan Lin, and O. Boric-Lubecke, "A microwave radio for Doppler radar sensing of vital signs," in *2001 IEEE MTT-S International Microwave Sympsoium Digest (Cat. No.01CH37157)*, vol. 1, (Phoenix, AZ, USA), pp. 175–178, IEEE, 2001.

[11] F. Lin, C. Song, Y. Zhuang, W. Xu, C. Li, and K. Ren, "Cardiac Scan: A Non-contact and Continuous Heart-based User Authentication System," in *Proceedings of the 23rd Annual International Conference on Mobile Computing and Networking - MobiCom '17*, (Snowbird, Utah, USA), pp. 315–328, ACM Press, 2017.

[12] K. Shi, C. Will, R. Weigel, and A. Koelpin, "Contactless person identification using cardiac radar signals," in *2018 IEEE International Instrumentation and Measurement Technology Conference (I2MTC)*, (Houston, TX), pp. 1–6, IEEE, May 2018.

[13] Z. Yang, P. H. Pathak, Y. Zeng, X. Liran, and P. Mohapatra, "Vital Sign and Sleep Monitoring Using Millimeter Wave," *ACM Transactions on Sensor Networks*, vol. 13, pp. 1–32, Apr. 2017.

[14] A. Rahman, V. M. Lubecke, O. Boric-Lubecke, J. H. Prins, and T. Sakamoto, "Doppler Radar Techniques for Accurate Respiration Characterization and Subject

Identification," *IEEE Journal on Emerging and Selected Topics in Circuits and Systems*, vol. 8, pp. 350–359, June 2018.

[15] G. Benchetrit, "Breathing pattern in humans: diversity and individuality," *Respiration Physiology*, vol. 122, pp. 123–129, Sept. 2000.

[16] "https://www.iii.org/fact-statistic/facts-statistics-identity-theft-and-cybercrime."

[17] S. M. M. Islam, E. Yavari, A. Rahman, V. M. Lubecke, and O. Boric-Lubecke, "Separation of Respiratory Signatures for Multiple Subjects Using Independent Component Analysis with the JADE Algorithm," in *2018 40th Annual International Conference of the IEEE Engineering in Medicine and Biology Society (EMBC)*, (Honolulu, HI), pp. 1234–1237, IEEE, July 2018.

[18] S. M. M. Islam, E. Yavari, A. Rahman, V. M. Lubecke, and O. Boric-Lubecke, "Multiple Subject Respiratory Pattern Recognition and Estimation of Direction of Arrival using Phase-Comparison Monopulse Radar," in *2019 IEEE Radio and Wireless Symposium (RWS)*, (Orlando, FL, USA), pp. 1–4, IEEE, Jan. 2019.

[19] S. M. M. Islam, A. Rahman, E. Yavari, M. Baboli, O. Boric-Lubecke, and V. M. Lubecke, "Identity Authentication of OSA Patients Using Microwave Doppler radar and Machine Learning Classifiers," in *2020 IEEE Radio and Wireless Symposium (RWS)*, (San Antonio, TX, USA), pp. 251–254, IEEE, Jan. 2020.

[20] S. M. M. Islam, A. Sylvester, G. Orpilla, and V. M. Lubecke, "Respiratory Feature Extraction for Radar-Based Continuous Identity Authentication," in *2020 IEEE Radio and Wireless Symposium (RWS)*, (San Antonio, TX, USA), pp. 119–122, IEEE, Jan. 2020.

[21] O. Boric-Lubecke, V. Lubecke, A. Host-Madsen, D. Samardzija, and K. Cheung, "Doppler Radar Sensing of Multiple Subjects in Single and Multiple Antenna Systems," in *TELSIKS 2005 - 2005 uth International Conference on Telecommunication in*

ModernSatellite, Cable and Broadcasting Services, vol. 1, (Nis, Serbia and Montenegro), pp. 7–11, IEEE, 2005.

[22] S. Yue, H. He, H. Wang, H. Rahul, and D. Katabi, "Extracting Multi-Person Respiration from Entangled RF Signals," *Proceedings of the ACM on Interactive, Mobile, Wearable and Ubiquitous Technologies*, vol. 2, pp. 1–22, July 2018.

[23] S. M. M. Islam, B. Tomota, A. Sylvester, and V. M. Lubecke, "A Programmable Robotic Phantom to Simulate the Dynamic Respiratory Motions of Humans for Continuous Identity Authentication," in *2019 IEEE Asia-Pacific Microwave Conference (APMC)*, (Singapore, Singapore), pp. 1408–1410, IEEE, Dec. 2019.

[24] S. M. M. Islam, E. Yavari, A. Rahman, V. M. Lubecke, and O. Boric-Lubecke, "Direction of Arrival Estimation of Physiological Signals of Multiple Subjects Using Phase Comparison Monopulse Radar," in *2018 Asia-Pacific Microwave Conference (APMC)*, (Kyoto), pp. 411–413, IEEE, Nov. 2018.

[25] Y. S. Lee, P. N. Pathirana, R. J. Evans, and C. L. Steinfort, "Separation of Doppler radar-based respiratory signatures," *Medical & Biological Engineering & Computing*, vol. 54, pp. 1169–1179, Aug. 2016.

[26] S. M. M. Islam, O. Boric-Lubecke, and V. M. Lubekce, "Concurrent Respiration Monitoring of Multiple Subjects by Phase-Comparison Monopulse Radar Using Independent Component Analysis (ICA) With JADE Algorithm and Direction of Arrival (DOA)," *IEEE Access*, vol. 8, pp. 73558–73569, 2020.

[27] M. I. Skolink, *Introduction to Radar System.*

[28] A. Singh, X. Gao, E. Yavari, M. Zakrzewski, X. H. Cao, V. M. Lubecke, and O. Boric-Lubecke, "Data-Based Quadrature Imbalance Compensation for a CW Doppler Radar System," *IEEE Transactions on Microwave Theory and Techniques*, vol. 61, pp. 1718–1724, Apr. 2013.

[29] B.-K. Park, O. Boric-Lubecke, and V. M. Lubecke, "Arctangent Demodulation With DC Offset Compensation in Quadrature Doppler Radar Receiver Systems," *IEEE Transactions on Microwave Theory and Techniques*, vol. 55, pp. 1073–1079, May 2007.

[30] I. Arai, "Survivor search radar system for persons trapped under earthquake rubble," in *APMC 2001. 2001 Asia-Pacific Microwave Conference (Cat. No.01TH8577)*, vol. 2, (Taipei, Taiwan), pp. 663–668, IEEE, 2001.

[31] N. A. Fox, R. Gross, J. F. Cohn, and R. B. Reilly, "Robust Automatic Human Identification Using Face, Mouth, and Acoustic Information," in *Analysis and Modelling of Faces and Gestures* (D. Hutchison, T. Kanade, J. Kittler, J. M. Kleinberg, F. Mattern, J. C. Mitchell, M. Naor, O. Nierstrasz, C. Pandu Rangan, B. Steffen, M. Sudan, D. Terzopoulos, D. Tygar, M. Y. Vardi, G. Weikum, W. Zhao, S. Gong, and X. Tang, eds.), vol. 3723, pp. 264–278, Berlin, Heidelberg: Springer Berlin Heidelberg, 2005.

[32] K. Nguyen, C. Fookes, R. Jillela, S. Sridharan, and A. Ross, "Long range iris recognition: A survey," *Pattern Recognition*, vol. 72, pp. 123–143, Dec. 2017.

[33] K. P. Thomas and A. Vinod, "Toward EEG-Based Biometric Systems: The Great Potential of Brain-Wave-Based Biometrics," *IEEE Systems, Man, and Cybernetics Magazine*, vol. 3, pp. 6–15, Oct. 2017.

[34] S. Chen, J. Lach, B. Lo, and G.-Z. Yang, "Toward Pervasive Gait Analysis With Wearable Sensors: A Systematic Review," *IEEE Journal of Biomedical and Health Informatics*, vol. 20, pp. 1521–1537, Nov. 2016.

[35] K. Ricanek, M. Savvides, D. L. Woodard, and G. Dozier, "Unconstrained Biometric Identification: Emerging Technologies," *Computer*, vol. 43, pp. 56–62, Feb. 2010.

[36] T. Liu and Z.-q. Liang, "Lightweight Biometric Sensing for Walker Classification Using Narrowband RF Links," *Sensors*, vol. 17, p. 2815, Dec. 2017.

[37] D. Vivet, A. Derbel, and B. Emile, "Access control based on gait analysis and face recognition," *Electronics Letters*, vol. 51, pp. 751–752, May 2015.

[38] M. Balazia and K. N. Plataniotis, "Human gait recognition from motion capture data in signature poses," *IET Biometrics*, vol. 6, pp. 129–137, Mar. 2017.

[39] S. Springer and G. Yogev Seligmann, "Validity of the Kinect for Gait Assessment: A Focused Review," *Sensors*, vol. 16, p. 194, Feb. 2016.

[40] J. Tang, J. Luo, T. Tjahjadi, and Y. Gao, "2.5D Multi-View Gait Recognition Based on Point Cloud Registration," *Sensors*, vol. 14, pp. 6124–6143, Mar. 2014.

[41] P. van Dorp and F. Groen, "Feature-based human motion parameter estimation with radar," *IET Radar, Sonar & Navigation*, vol. 2, pp. 135–145, Apr. 2008.

[42] V. Chen, "Doppler signatures of radar backscattering from objects with micro-motions," *IET Signal Processing*, vol. 2, no. 3, p. 291, 2008.

[43] J. Geisheimer, W. Marshall, and E. Greneker, "A continuous-wave (CW) radar for gait analysis," in *Conference Record of Thirty-Fifth Asilomar Conference on Signals, Systems and Computers (Cat.No.01CH37256)*, (Pacific Grove, CA, USA), pp. 834–838 vol.1, IEEE, 2001.

[44] A. Rahman, E. Yavari, V. M. Lubecke, and O.-B. Lubecke, "Noncontact Doppler radar unique identification system using neural network classifier on life signs," in *2016 IEEE Topical Conference on Biomedical Wireless Technologies, Networks, and Sensing Systems (BioWireleSS)*, (Austin, TX, USA), pp. 46–48, IEEE, Jan. 2016.

[45] J. Zhang, B. Wei, W. Hu, and S. S. Kanhere, "WiFi-ID: Human Identification Using WiFi Signal," in *2016 International Conference on Distributed Computing in Sensor Systems (DCOSS)*, (Washington, DC, USA), pp. 75–82, IEEE, May 2016.

[46] N. Petrochilos, M. Rezk, A. Host-Madsen, V. Lubecke, and O. Boric-Lubecke, "Blind Separation of Human Heartbeats and Breathing by the use of a Doppler Radar Remote

Sensing," in *2007 IEEE International Conference on Acoustics, Speech and Signal Processing - ICASSP '07*, (Honolulu, HI), pp. I–333–I–336, IEEE, Apr. 2007.

[47] A. Vergara, N. Petrochilos, O. Boric-Lubecke, A. Host-Madsen, and V. Lubecke, "Blind Source Separation of Human Body Motion using Direct Conversion Doppler Radar," in *2008 IEEE MTT-S International Microwave Symposium Digest*, (Atlanta, GA, USA), pp. 1321–1324, IEEE, June 2008.

[48] J. Lin and C. Li, "Wireless Non-Contact Detection of Heartbeat and Respiration Using Low-Power Microwave Radar Sensor," in *2007 Asia-Pacific Microwave Conference*, (Bangkok, Thailand), pp. 1–4, IEEE, Dec. 2007.

[49] "https://www.nhlbi.nih.gov/health-topics/sleep-deprivation-and-deficiency."

[50] "https://patents.google.com/patent/US8679012B1/en."

Chapter 2

Hardware Architecture and Signal Processing for Doppler Radar Physiological Sensing

In this work, we mostly utilized Continuous wave (CW) radar for extracting physiological information. The frequency band we used for CW radar is 2.4 GHz and 24 GHz. CW radars have several advantages than FMCW radar due to its simpler architecture, simple filter requirements due to having narrow signal bandwidth and unambiguous velocity determination capability at any range in heavy stationary clutters [1]. Over the last four decades there has been significant improvement in the area of Doppler radar physiological sensing especially in hardware architecture and baseband signal processing algorithms [2]. Extensive research is also performed by different research groups for the improvement of Doppler radar based physiological sensing [3][4][5]. In the first chapter boarder scope of non-contact identity authentication and its associated challenges have been discussed. So, before discussing the proposed solutions of the associated challenges we need to understand Doppler radar system thoroughly.The following sections will describe in details about the basic theory of Doppler radar physiological sensing, different receivers topology, baseband signal processing and data acquisition system. It will also discuss about the demodulation algorithm and signal processing techniques. Finally, a recent advances in frequency modulated continuous wave radar system will also be highlighted for further development and paradigm shift towards industry oriented FMCW radar for helathcare applications.

2.1 Theory of Doppler Radar for Physiological Sensing

A Continuous-wave (CW) radar topology is simpler architecture than FMCW radar for two reasons. First of all, a same oscillator can be used for transmitter and receiver [1]. Secondly, CW uses narrow-band signal which also helps to avoid interference and eases filtering requirements [6].For physiological sensing the goal is to measure the tiny movement of the chest surface due to cardio-respiratory activities rather than ranges of the target, in that case CW system is ideal [1]. A CW radar system have the capability of measuring velocity at any ranges without any ambiguities, unlike pulsed or modulated radar system that have limited velocity resoultions.

For physiological sensing or other applications radars uses Doppler principle. According to Doppler theory, a subject/target with time varying displacement produces phase changes of the reflected signal and the phase-change of the reflected signal is directly proportional to the tiny movement of the chest surface due to cardio-respiratory activities [7]. When the CW signal is targeted, it is reflected and frequency modulated by the target motion. If the target motion is moving ate velocity v(t) in m/s, the frequency of the reflected signal is shifted by an amount known as the Doppler shift [3]. The frequency of the Doppler shift can be expressed as:

$$f_d\ (t) = 2f/c\ v(t) = 2v(t)/\lambda \tag{2.1}$$

where, f_d is the Doppler shift frequency in Hz, f is the transmitted signal in Hz and λ is the wavelength of the transmitted signal in meter. When the target undergoes a periodic movement with no net velocity then Doppler shift can be better described as phase modulation. The phase modulation $\theta(t)$ can be described as:

$$\theta(t) = 2f/c\ (2\pi x(t)) = 4\pi x(t)/\lambda \tag{2.2}$$

where, x(t) is the periodic movement of the chest surface due to cardio-respiratory activities. When person's phase is target the phase change of the reflected signal occurs. The

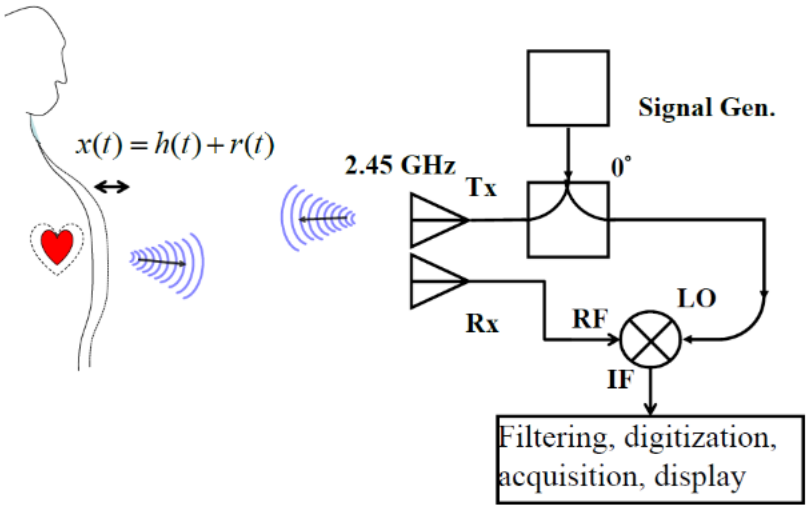

Figure 2.1 A typical block diagram of radar transceiver which is capturing respiratory information from the tiny movement of the chest surface due to cardio-respiratory activities.From [8]

phase change of the reflected signal is directly proportional to the chest surface. After demodulating the signal, breathing rate and heart rate can be extracted. A CW radar typically transmits a single tone signal. The signal is expressed as:

$$T(t) = A\cos(2\pi f(t) + \phi(t)) \tag{2.3}$$

where, A is the amplitude of the signal, f is the frequency of the oscillator, $\phi(t)$ is the phase noise of the oscillator. The reflected signal at the receiver is expressed as:

$$R(t) = A_R\cos[2\pi f(t - t_d\ ) + \phi(t - t_d\ ) + \theta_0] \tag{2.4}$$

where, A_R is the amplitude of the reflected signal, θ_0 is the phase shift at reflection surface and t_d is the time delayed version of the reflected signal. The time delayed version of the signal is represented as:

$$t_d = 2d(t - d(t)/c)/c \tag{2.5}$$

The time delay between the transmitter and the target is the distance travelled by the signal, d(t), divided by the signal's propagation velocity, c. Since the chest moves while the signal is travelling, the distance between the antenna and the chest at the time of reflection is $d(t - d(t)/c$. To detect the motion signature, the phase need to be demodulated or otherwise detected in the receiver to detect the motion.

2.1.1 Receiver Architecture

The basic principle of phase detector is mixing the received signal with the transmitted signal at the same frequency as it is transmitted to convert RF frequency directly into baseband signal [9]. Receiver architecture can be classified into two different categories. One is homodyne receiver architecture and another one is heterodyne receiver architecture [3].In homodyne architecture, the reflected signal is mixed up with the transmitted signal at the same frequency. On the other hand, a heterodyne receiver mixes the received signal with local oscillator (LO) signal at a different frequency, so the information signal is modulated at non-zero intermediate frequency (IF) rather than being directly converted to baseband signal [3].The heterodyne receiver architecture is mostly used in radio transmission as tuning can be accomplished by varying frequency at the LO.

In homodyne receiver shown in Fig. 2.2, typically the received signal is band-pass filtered to remove noise and amplified with low noise amplifier (LNA) to decrease the receiver noise figure. Then the signal is mixed with the LO signal at the same frequency of the transmitted signal. After down conversion signal remains in the same frequency band that's why we called it baesband signal. A homodyne receiver is used for this application as it is simpler in architecture and due to its straightforward use as phase detector.

In heterodyne receiver architecture shown in Fig. 2.2, the input signal is amplified, filtered at RF, then mixed with an intermediate frequency (IF) where it is amplified, tuned in a IF stage and filtered with band pass filter before the signal is detected. After band pass filtering the signal is passed into low noise amplifier (LNA) to reduce the receiver noise figure by increasing the signal power at the input. Then the signal is being multiplied with LO to

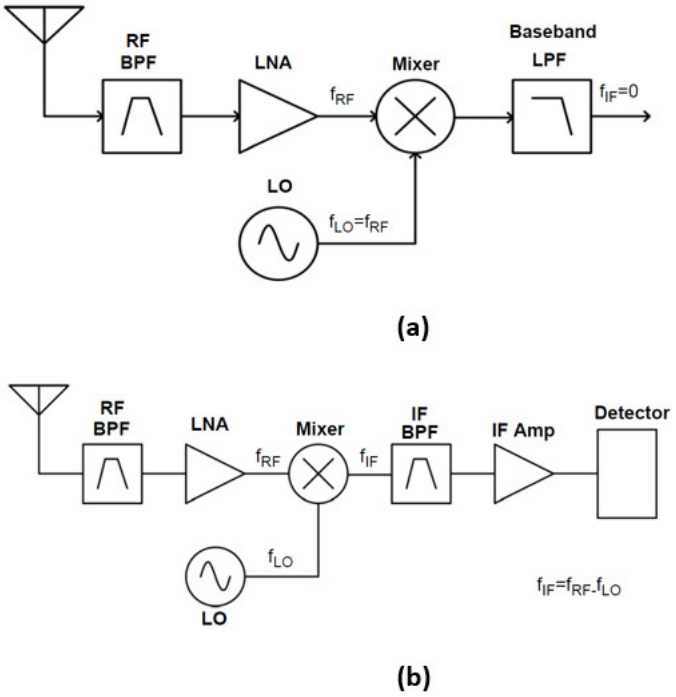

Figure 2.2 (a) Typical homodyne receiver architecture. (b) a heterodyne receiver architecture where RF signal is down converted into IF signal. From [3]

down-convert it into intermediate frequency (IF). After converting it into IF signal, it passes through IF band-pass filter which is used to isolate the neighboring channel. In general, the IF amplifier is often a gain controlled amplifier that adjusts the signal to the appropriate amplitude for the detector. The detector also varies depending on the modulation scheme and the type of information that is modulated. Fig. 2.2 (a) illustrates the schematic diagram of the homodyne receiver architecture and (b) represents the heterodyne receiver architecture.

A homodyne receiver architecture with frequency of 2.4 GHz and 24 GHz was employed in this research work due to its simplicity and straightforward use as phase detector. The information about the periodic motion of the target can be demodulated if this signal is

multiplied by local oscillator (LO) with same frequency. Because of the phase noise of the received signal is correlated with that of the LO signal, the received signal can be expressed as without amplitude variations.

$$L(t) = \cos(2\pi f t + \phi(t)) \tag{2.6}$$

When the received signal is mixed up with LO signal then the baseband signal is expressed as:

$$B(t) = A_B \cos[\theta + 4\pi x(t)/\lambda + \delta\phi(t)] \tag{2.7}$$

where

$$A_B = A_R\sqrt{(}G_R\ G_C) \tag{2.8}$$

is the baseband amplitude with G_R is the receiver gain and G_C is the mixer conversion gain.

$$\delta\phi(t) = \phi(t) - \phi(t - (2d_0)/c) \tag{2.9}$$

is the residual phase noise and

$$\theta = (4\pi d_0)/\lambda - \theta_0 \tag{2.10}$$

is the constant phase shift depends on the nominal distance to the target, d_0. Fig 2.3 below shows the simplified block diagram and signal flow used to detect the tiny movement of the chest surface using microwave Doppler radar. If $x(t) << \lambda$ and θ in equation 2.12 is an odd multiple of $\pi/2$, the small angle approximation is valid and the baseband output is approximately:

$$B(t) \approx A_B\ (4\pi x(t)/\lambda + \delta\phi(t)) \tag{2.11}$$

In this case, the optimum phase demodulation selectivity is achieved, the baseband output is proportional to the periodic chest displacement, x(t). When θ is an integer multiple of π

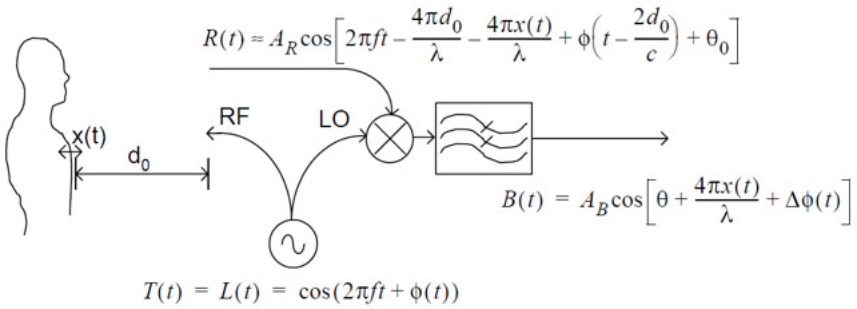

Figure 2.3 Simplified Doppler radar system with signal flow. The baseband output signal is proportional to the cosine of a constant phase shift determined by the distance of the target and receiver which is also summed up with phase shift which is directly proportional to the tiny movement of the chest surface [3]

then the output is approximately.

$$B(t) \approx A_B\ (1 - [4\pi x(t)/\lambda + \delta\phi(t)]^2) \tag{2.12}$$

In this point, the baseband signal is no more directly proportional to the tiny movement of the chest displacement. This null point occurs when the LO and the received signal are either in phase or 180^0 out of phase. Since the variable part θ is only dependent on the distance of the target so there is a null point every quarter wavelength of the radar. At a frequency of 2.4 GHz this null point occurs every quarter wavelength of the radar and therefore difficult to avoid due to the position of the transceiver and the subject. This problem can be avoided using quadrature receiver which is described below in the subsection.

2.1.2 Single Channel and Quadrature Receiver

Single channel transceiver has null point problem that makes heart rate detection less accurate at some ranges. On the other hand, quadrature receivers requires two receiver chains to avoid this problem which increases power consumption. Fig 2.4 below illustrates the block diagram of single channel and quadrature channel transceiver. The main

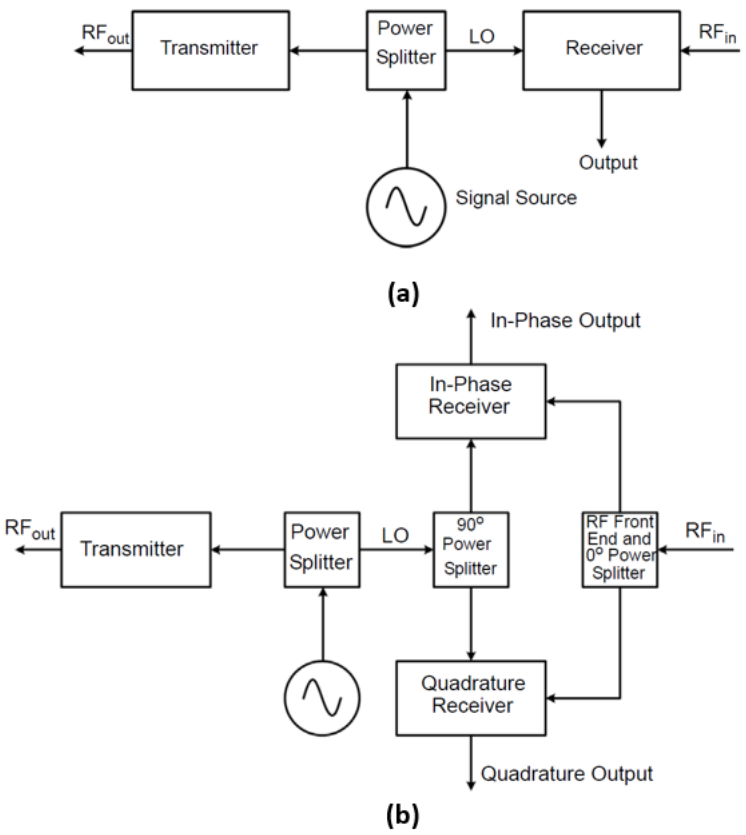

Figure 2.4 (a) Block diagram of single channel CW radar transceiver (b) block diagram of quadrature channel CW radar transceiver. From [3]

challenges associated with single channel transceiver for phase demodulation accuracy varies with the range to the target. From the previous section, it is clear that the phase change of the signal is directly proportional to the tiny movement of the chest surface due to cardio-respiratory activities and at the phase demodulation points the baseband signal is proportional to the square of the motion [10]. A quadrature receiver offers the opportunity to avoid phase demodulation null points by integrating receiver chains. One is in-phase channel signal and another one is quadrature-phase channel signal.

A quadrature receiver block diagram is shown in Figure 2.4 which has two receiver chains with LO phases 90^0 apart to ensure that at least one output is not in null points. The two

LO signal has phase difference by $\pi/2$:

$$L_I\ (t) = \cos(2\pi ft + \delta\phi(t) + \pi/4) \tag{2.13}$$

$$L_Q\,(t) = \cos\left(2\pi ft + \delta\phi\,(t) - \frac{\pi}{4}\right) = \sin(2\pi ft + \delta\phi\,(t) + \frac{\pi}{4}) \tag{2.14}$$

Therefore, the output of the quadrature receiver channel will be:

$$B_I\ (t) = A_B \cos[\theta + \pi/4 + 4\pi x(t)/\lambda + \delta\phi(t)] \tag{2.15}$$

$$B_Q\ (t) = A_B \cos[\theta - \pi/4 + 4\pi x(t)/\lambda + \delta\phi(t)] = A_B \sin[\theta + \pi/4 + 4\pi x(t)/\lambda + \delta\phi(t)] \tag{2.16}$$

When $\theta + \pi/4$ is an integer multiple of π, the I signal will be at null point. When $\theta - \pi/4$ is an odd multiple of $\pi/2$, the Q signal will be optimum phase demodulation points. As long as $x(t) << \lambda$ is the chest motion signal can be accurately detected.

2.1.3 Base-band Signal Conditioning and Data Acquisition

Base-band noise is significant factor in determining the sensitivity and specificity of the microwave Doppler radar in physiological sensing [5]. Before acquiring baseband signal digitally low noise amplifier and filters are utilized to condition the baseband signal. There are three dominant source of error for signal conditioning such as phase noise, flicker noise and thermal noise [7]. Flicker noise occurs due to LO self mixing problem characterized by homodyne receivers [11]. This large DC offset cause saturation in the low noise amplifier, limits the dynamic range [12]. DC offset can be compensated in hardware by using ac coupling or by dc offset compensating [5].AC coupling is simple but it increases the distortion of the signal whereas, dc offset compensation requires careful tuning manually [13]. AC coupling which is basically high pass filter results in slower response of the system [13].

After signal conditioning, the signal is acquired by Data Acquisition System (DAQ). The bandwidth requirement for DAQ in physiological sensing is not that much high because the respiratory information of the signal remains within 0.2 Hz- 0.8 Hz and cardiac related

information remains within 0.6 Hz-2 Hz [14]. Typically the bandwidth of the physiological signal is within 0-8 Hz. According to nyquist theorem, for reconstructing the signal sampling frequency needs to be more than twice of the highest frequency content of the signal [1]. As the physiological signal maximum bandwidth is 8 Hz, so for reconstructing the signal the sampling frequency of DAQ needs to be 16 Hz. In our system, we used sampling frequency of the DAQ is within 100 Hz which is almost more than ten times of the highest frequency content of the signal.

The length of the arc in I/Q transcribed in the plane depends on the frequency content of the signal. If the operating frequency increases then the length of the arc also increases.

2.2 Demodulation and Signal Processing

The obtained baseband signal can be further processed using demodulation technique to extract respiratory rate and heart rate related information. The various methods that have been used for combining I/Q channel signal include linear demodulation [15] and arc-tangent demodulation [5].In the following subsection we will describe in details about two most popular demodulation techniques.

2.2.1 Linear Demodulation (Principal Component Analysis (PCA))

Linear demodulation is also known as principal component analysis (PCA). The basis idea of PCA technique is to combine the two dimensional data space into single dimension by maximizing their variances and suppressing redundant information [15]. It is also applicable to multidimensional data-set. To perform linear demodulation, we remove the DC offset by removing the mean form the original signal. Then a covarinace matrix of I and Q channel signal is formed and eigenvalue and eigenvector is calculated using eigenvalue decomposition method. After multiplying the eigenvectors matrix with data we can get the data with maximum variance [16]. Since we are utilizing linear demodulation technique so basically

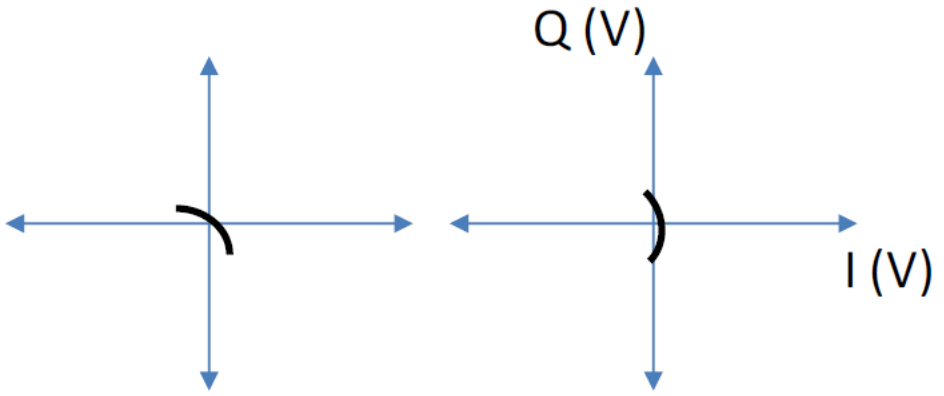

Figure 2.5 Graphical representation of the linear demodulation of I/Q plot

we are approximating line instead of arc. With the approximation of small arc, PCA method can accurately determine the line of the small arc.

2.2.2 Nonlinear Demodulation (Arc-tangent Demodulation)

Non-linear demodulation considers that I/Q channels form an circular arc in complex plane. In general, the phase of the signal can be expressed as [5]:

$$\theta(t) = \arctan((B_Q\ (t))/(B_I\ (t)\ )) \tag{2.17}$$

By considering the dc offset of the signal we can express it as:

$$\theta(t) = \arctan((V_Q + A_B \sin(\theta + 4\pi x(t)/\lambda + \delta\phi(t)))/(V_I + A_B \cos(\theta + 4\pi x(t)/\lambda + \delta\phi(t)) \tag{2.18}$$

Let us consider that V_Q and V_I are negligible.

$$\theta(t) \approx 4\pi x(t)/\lambda \tag{2.19}$$

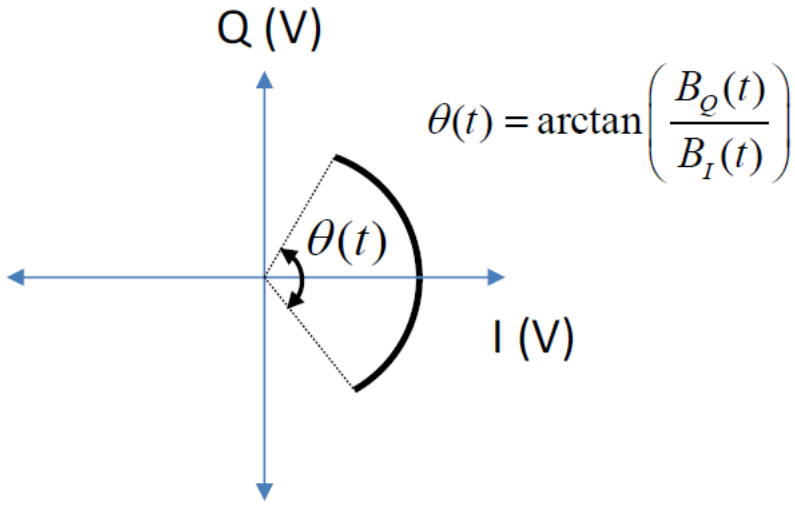

Figure 2.6 (a) Graphical representation of arc-tangent demodulation. From [5]

In other words,

$$x(t) \approx \theta(t)\lambda/4\pi \tag{2.20}$$

Arc-tangent demodulation provides the chest displacement information which is one of the biggest advantage of this technique.

Another demodulation technique is used to represent I/Q data as complex plane and perform signal processing on the complex signal itself. One of the advantage of complex technique is that many signal processing algorithms can be directly applied to the complex signal and it can be transformed into exponential form. After demodulating the signal various signal processing techniques can be integrated for breathing rate and heart rate estimation.

2.2.3 Filtering Approaches for Respiratory and Heart Rate Extraction

After demodulating the signal we need to extract the breathing rate and heart rate related information. For converting time domain signal into frequency domain signal we typically use Fast Fourier transform (FFT) of the time domain signal to find the spectrum [17].After

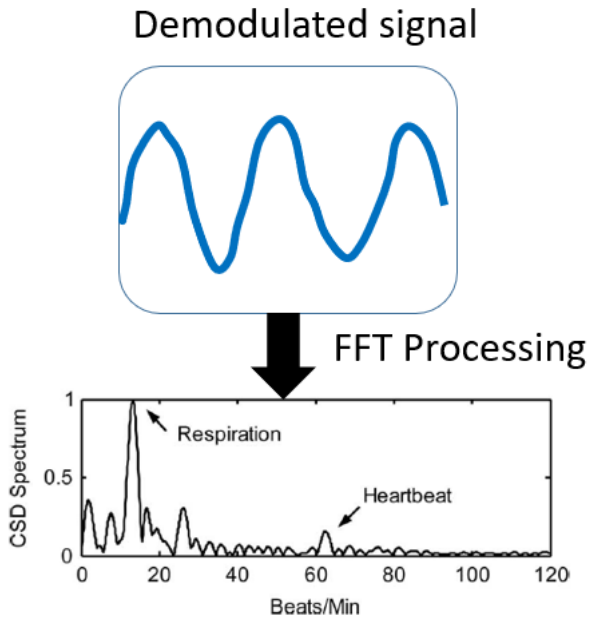

Figure 2.7 From the FFT processing of the demodulated signal provides us two dominant peak points on is breathing rate and another one is heartbeat

utilizing FFT we can see the spectrum of the signal where the highest peak shows the breathing as breathing is superimposed over heartbeat [18]. From Fig 2.7, it is clear that the badnwidth of the respiration signal is within 0-0.6 Hz whereas, for heart rate it lies within 0.8-2 Hz. Thus, utilizing bandpass filter with different frequency bandwidth helps us to extract breathing rate and heart rate more accurately. Apart from bandpass filter we can also utilize finite impulse response low pass filter and gernally its order is selected about 10 times of the sampling frequency of the transmitted signal. So, for extracting physiological related information we need to use filtering to isolate the respiratory and heart related information. Low noise amplifier filtering is mostly used to eliminate the baseband noise of the signal. LNA is also used to strengthen the signal by increasing their amplitude level. On the other hand, the purpose of post-processing filtering of the signal helps to isolate the respiratory and heart rate related information.

2.2.4 Fast Fourier Transform (FFT) for Respiratory and Heart Rate Extraction

Fourier transform is mostly used in transforming a time domain signal into frequency domain signal [17]. Generally a data is divided into chunk based on the window length and then FFT is applied to find a rate of the signal. FFT is calculated on the windows length of the signal to extract breathing rate. FFT is very efficient algorithm for calculating the Fourier transform for discrete signal. The peak of the specific window represents the rate within that segmented window of the signal. Then the window moves to the next chunk of the data based on step size. The window length is determined by FFT resolution. A typical window size for heart signal is around 6- 10 second. Respiratory signal has lower frequencies around .2 Hz. Consequently larger window size around 10-18 second should be selected for extracting heart rate information. Usually Hamming, Hanning, and Kaiser windows are mostly used instead of rectangular window to shape the data in the time domain to control the side-lobe in the spectral domain. Windowing function reduce the leakage of the signal so that side-lobe can be minimized properly to represent the spectra better.

2.3 Recent Advances in Doppler Radar Physiological Sensing

In the previous section, we described the basics of CW Doppler radar physiological sensing and its signal processing techniques to extract respiratory information. Over the last four decades, there has been significant advances in Doppler radar physiological sensing as many researchers are working on developing the new signal processing algorithms and improving the hardware circuitry [2]. Due to the advancement of semiconductor technologies, frequency modulated continuous wave (FMCW) radar is also manufactured in mass scale for automotive industry. In addition to that, FMCW radar is also utilized for this type of healthcare applications. It has been investigated by different researchers about the feasibility of this high frequency FMCW radar technology for extracting vital sign information (breathing rate and heart rate). FMCW radar sends a frequency range

of signal in a modulated version of the signal and when the signal is being reflected it is converted into intermediate frequency (IF) signal [1]. In this subsection, we will describe about the basic principle of FMCW radar for physiological sensing. Chirp parameter design and signal processing approach for extracting breathing rate and heart rate information will be described in separate subsections.

2.3.1 Basic Principle of FMCW Radar for Physiological Sensing

The basic principle for physiological sensing for any kind of radar is related to the Doppler principle [3]. According to Doppler principle, A subject/target with time varying velocity produces a phase change in the reflected signal and the phase change of the reflected signal is directly proportional to the tiny movement of the chest surface due to cardio-respiratory activity [7]. The basic difference between CW and FMCW radar is it changes a frequency in a certain range to modulate the transmitted signal [18][19]. In FMCW, signal is modulated in a frequency to produce linear chirp which is radiated towards target [20]. The frequency modulated signal can be represented as [21]:

$$x_T\ (t) = A_T \cos(2\pi f_c\ t + \pi B/T_c\ \ t^2 + \phi(t)) \tag{2.21}$$

where, A_T is the chirp amplitude, f_c is the chirp starting frequency, B is the Bandwidth of the chirp and T_c is the chirp duration. When the signal is reflected its phase changes and the phase change of the reflected signal is directly proportional to the tiny movement of the chest surface due to cardio-respiratory activities. The received signal is then represented as [20]:

$$x_R\ (t) = \alpha A_T\ \cos\ (2\pi f_c\ (t - t_d\ ) + \pi B/T_c\ \ (t - t_d\ )^2 + \phi(t - t_d\ )) \tag{2.22}$$

where, t_d is the time delayed version of the reflected signal and it is represented as:

$$t_d = 2R(t)/c \tag{2.23}$$

R is the radial range of the target and c is the velocity of light. After receiving the signal, the received signal is mixed with transmitted signal and after mixing it produces a single channel signal (In phase (I)) channel signal. After simplification the in-phase channel signal is represented as:

$$y(t) = A_R \cos\left(2\pi f_b\ t + \phi_b\ (t) + \delta\phi(t)\right) \tag{2.24}$$

where, A_R is the received signal amplitude, f_b is the beat frequency and it is represented as:

$$f_b = 2BR(t)/(cT_c\ ) \tag{2.25}$$

The phase of the beat signal ϕ_b can be represented as:

$$\phi_b = 2\pi f_c\ t_d + \pi B/T_c\ \ t_d^2 \tag{2.26}$$

The residual phase noise can be reflected for short range radar application. The beat signal after the nth ADC sample for the mth chirp can be represented as:

$$y[n\ m] = A_R \cos(2\pi f_b n T_f + 4\pi/\lambda R(nT_f + mT_s)) \tag{2.27}$$

Here, T_f is the first time axis after ADC sampling interval, T_s is the slow time axis (successive time between two chirps). As the chest movement has very small amplitude (¿10 mm) and low vibrational frequency (¡4 Hz), so concentrating on extracting phase changes in the slow time axis is sufficient to extract respiration and heart related information.

There are some advantages of millimeter wave FMCW radar in physiological sensing as tiny movement of chest surface is in millimeter range and it closely matches with millimeter wavelength [21]. In this particular application, we are concentrated on extracting phase information of the received signal in the slow time axis, so phase change of the beat signal is represented as:

$$\phi_b = 4\pi RNT_f/\lambda \tag{2.28}$$

Here, $R(t) = R_0 + x(t)$ where R_0 is the radial distance from the target and $x(t)$ is the tiny movement of the chest surface due to cardio-respiratory activities. Wireless localization or range information is another important feature of millimeter wave FMCW radar. In other words, CW radar receives all echoes which is vulnerable to multi path fading.

2.3.2 Chirp Parameter Design for Respiration Sensing

In this section, I will describe about chirp parameter design for respiration sensing. The design of chirp parameter is bit different than car velocity movement so, the basic idea of designing chirp parameters are below.

1. Frame Periodicity,T_f: For tiny periodic vibration monitoring, FMCW radar uses interferometry theory [1]. According to radar interferometry theory, the vibration frequency of the tiny displacement measurement (maximum 10 Hz) must be matched with the frame repetition time. So, for extracting phase information of the received signal the frame repetition time must be matched with the vibration frequency. The frame periodicity is represented as[18]:

$$T_f = 1/f_vibration \tag{2.29}$$

   where $f_vibration$ is the maximum vibration frequency.

2. ADC Sampling rate and chirp slope: According to the Nyquist theorem, the ADC sampling rate should be greater than the twice the IF bandwidth. For extracting vital signs our frequency of interest is within 0.1-4 Hz so a sampling rate of 20 Hz was chosen to ensure sufficient sampling of the signal [14]. The IF sampling frequency can be expressed as:

$$f_IF = Sd_m/c \tag{2.30}$$

   where, S is the chirp slope and d_m is the highest range of the target from Radar.

3. Chirp duration and bandwidth: The chirp duration is related to the SNR of the received signal [22]. The bandwidth of the chirp is related to the range resolution of the transceiver.

2.3.3 Signal Processing Approach for FMCW Radar

Signal processing technique for FMCW radar is quite different than CW radar. After chirp design in a specified manner for extracting physiological information, FFT is performed on the captured signal which basically provides the range information of the target. After that, second FFT is performed on the range FFT phase information to extract the breathing rate and heart rate information. We conducted experiment with FMCW radar in an industry collaboration. Figure 2.8 illustrates the experimental setup where multiple subject was present in front of the FMCW radar system for extracting respiratory information [18].

Figure 2.8 Multiple subject presence in front of the radar system. The equidistant subjects are in seated position in front of the radar at 0.5 m from radar. From [18]
.

The study was performed on normal healthy people in an office environment (table, chair, desk and cell phone were present) to test the feasibility of the system design. The raw data was captured in a database using a USB port with a software interface. After capturing the waveform a range FFT was calculated to find the spatial position of the subject from radar. Fig. 2.9 represents the range FFT of the radar captured signal with

only phase information considered. Phase information of range FFT was unwrapped, and another FFT was performed on the phase information as the phase of the received signal is directly proportional to the tiny movement of the chest surface. For extracting respiration rate we used a 6th order Butterworth band-pass filter with cut off frequencies of .001 Hz-.05 Hz and for heart rate, cut off frequencies of 0.8-2 Hz were used. Figure 2.10 illustrates that the respiration rate and heart rate of a particular subject is .39 Hz (23 breaths per min) and heart rate is 1.179 Hz (70.314 beats per minute). [18]. Figure 2.10 illustrates that the

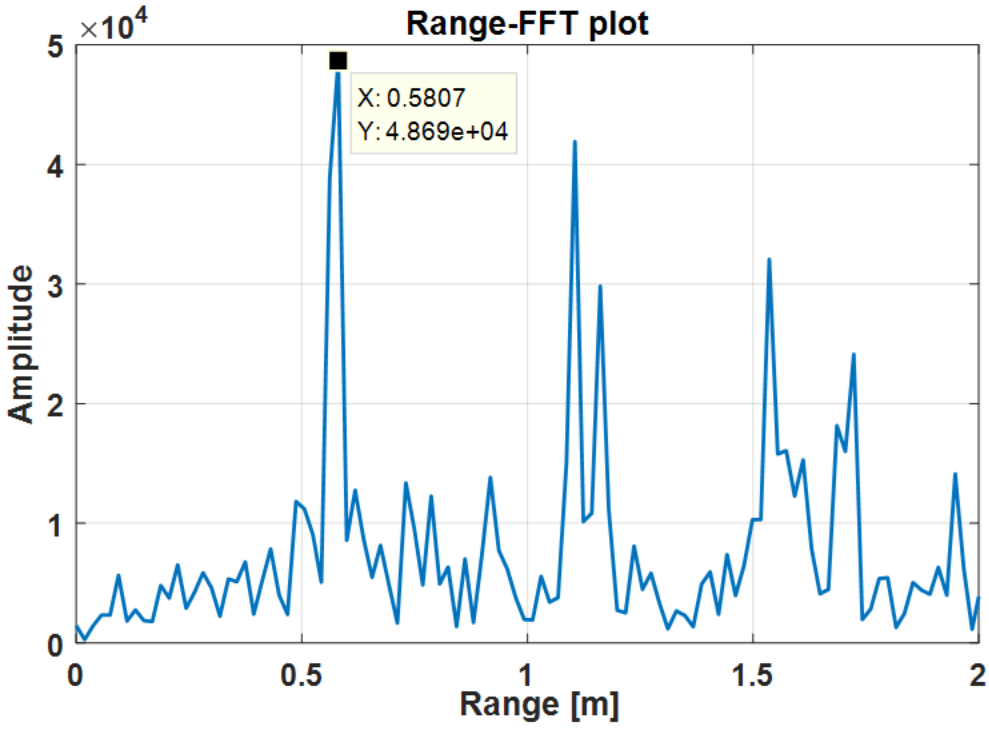

Figure 2.9 Range FFT plot of Radar-captured respiration pattern. The maximum peak is around .58 meter which also illustrates the presence of subject within that range. Apart from there are other dominant peaks which shows the static clutter like wall and cube in an office environment, From [18]

.

radar captured respiration pattern within one chirp averaged in a frame (overall 256 frames were sent). After range-FFT we unwrapped phase and then applied FFT on the unwrapped

phase to extract breathing rate and heart rate. This experiment was performed for single subject scenario to test the feasibility of extracting vital sign.

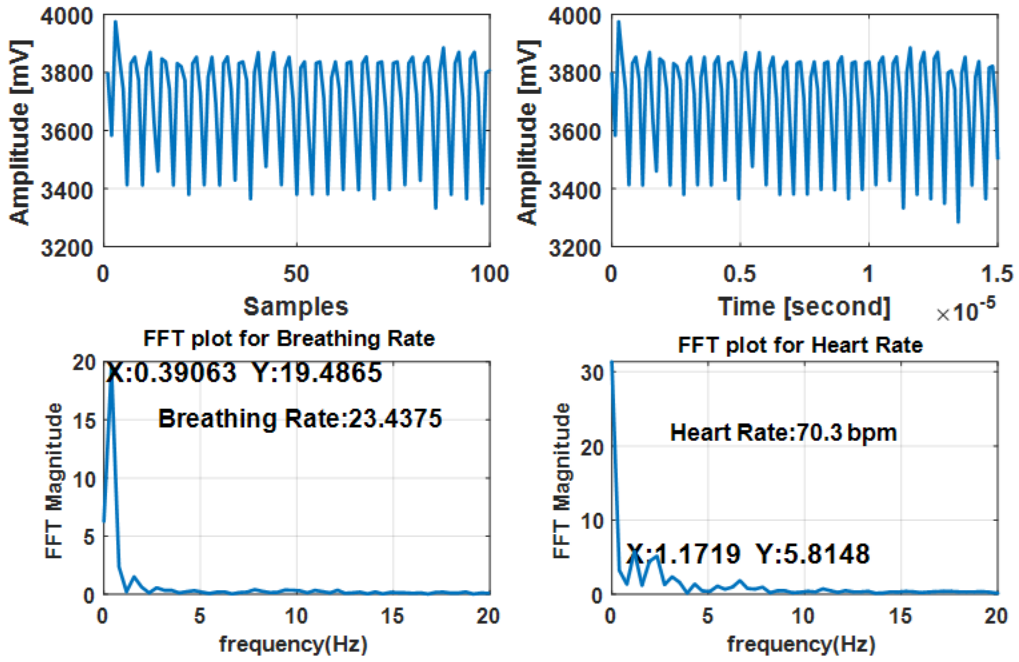

Figure 2.10 Radar-captured received signal 256 samples in one chirp, time domain received signal of the chirp within one frame of the chirp. Breathing rate and heart rate is .39 Hz and 1.179 Hz respectively. From [18]

.

References

[1] M. I. Skolink, *Introduction to Radar System.*

[2] C. Li, V. M. Lubecke, O. Boric-Lubecke, and J. Lin, "A Review on Recent Advances in Doppler Radar Sensors for Noncontact Healthcare Monitoring," *IEEE Transactions on Microwave Theory and Techniques*, vol. 61, pp. 2046–2060, May 2013.

[3] A. Droitcour, *NON-CONTACT MEASUREMENT OF HEART AND RESPIRATION RATES WITH A SINGLE-CHIP MICROWAVE DOPPLER RADAR.* PhD thesis.

[4] W. Massagram, V. Lubecke, and O. Boric-Lubecke, "Microwave non-invasive sensing of respiratory tidal volume," in *2009 Annual International Conference of the IEEE Engineering in Medicine and Biology Society*, (Minneapolis, MN), pp. 4832–4835, IEEE, Sept. 2009.

[5] B.-K. Park, O. Boric-Lubecke, and V. M. Lubecke, "Arctangent Demodulation With DC Offset Compensation in Quadrature Doppler Radar Receiver Systems," *IEEE Transactions on Microwave Theory and Techniques*, vol. 55, pp. 1073–1079, May 2007.

[6] S. M. M. Islam, E. Yavari, A. Rahman, V. M. Lubecke, and O. Boric-Lubecke, "Direction of Arrival Estimation of Physiological Signals of Multiple Subjects Using Phase Comparison Monopulse Radar," in *2018 Asia-Pacific Microwave Conference (APMC)*, (Kyoto), pp. 411–413, IEEE, Nov. 2018.

[7] A. Droitcour, T. Seto, Byung-Kwon Park, S. Yamada, A. Vergara, C. El Hourani, T. Shing, A. Yuen, V. Lubecke, and O. Boric-Lubecke, "Non-contact respiratory

rate measurement validation for hospitalized patients," in *2009 Annual International Conference of the IEEE Engineering in Medicine and Biology Society*, (Minneapolis, MN), pp. 4812–4815, IEEE, Sept. 2009.

[8] A. Singh, "ELECTRICAL ENGINEERING DECEMBER 2012," p. 190.

[9] S. M. M. Islam, E. Yavari, A. Rahman, V. M. Lubecke, and O. Boric-Lubecke, "Multiple Subject Respiratory Pattern Recognition and Estimation of Direction of Arrival using Phase-Comparison Monopulse Radar," in *2019 IEEE Radio and Wireless Symposium (RWS)*, (Orlando, FL, USA), pp. 1–4, IEEE, Jan. 2019.

[10] E. Yavari, C. Song, V. Lubecke, and O. Boric-Lubecke, "Is There Anybody in There?: Intelligent Radar Occupancy Sensors," *IEEE Microwave Magazine*, vol. 15, pp. 57–64, Mar. 2014.

[11] S. M. M. Islam, E. Yavari, A. Rahman, V. M. Lubecke, and O. Boric-Lubecke, "Separation of Respiratory Signatures for Multiple Subjects Using Independent Component Analysis with the JADE Algorithm," in *2018 40th Annual International Conference of the IEEE Engineering in Medicine and Biology Society (EMBC)*, (Honolulu, HI), pp. 1234–1237, IEEE, July 2018.

[12] J. Lin and C. Li, "Wireless Non-Contact Detection of Heartbeat and Respiration Using Low-Power Microwave Radar Sensor," in *2007 Asia-Pacific Microwave Conference*, (Bangkok, Thailand), pp. 1–4, IEEE, Dec. 2007.

[13] A. M. Vergara and V. M. Lubecke, "Data Acquisition System for Doppler Radar Vital-Sign Monitor," in *2007 29th Annual International Conference of the IEEE Engineering in Medicine and Biology Society*, (Lyon, France), pp. 2269–2272, IEEE, Aug. 2007.

[14] S. M. M. Islam, O. Boric-Lubecke, and V. M. Lubekce, "Concurrent Respiration Monitoring of Multiple Subjects by Phase-Comparison Monopulse Radar Using Independent Component Analysis (ICA) With JADE Algorithm and Direction of Arrival (DOA)," *IEEE Access*, vol. 8, pp. 73558–73569, 2020.

[15] O. Boric-Lubecke, W. Massagram, V. M. Lubecke, A. Host-Madsen, and B. Jokanovic, "Heart Rate Variability Assessment Using Doppler Radar with Linear Demodulation," in *2008 38th European Microwave Conference*, (Amsterdam, Netherlands), pp. 420–423, IEEE, Oct. 2008.

[16] S. M. M. Islam, A. Rahman, E. Yavari, M. Baboli, O. Boric-Lubecke, and V. M. Lubecke, "Identity Authentication of OSA Patients Using Microwave Doppler radar and Machine Learning Classifiers," in *2020 IEEE Radio and Wireless Symposium (RWS)*, (San Antonio, TX, USA), pp. 251–254, IEEE, Jan. 2020.

[17] S. M. M. Islam, A. Rahman, N. Prasad, O. Boric-Lubecke, and V. M. Lubecke, "Identity Authentication System using a Support Vector Machine (SVM) on Radar Respiration Measurements," in *2019 93rd ARFTG Microwave Measurement Conference (ARFTG)*, (Boston, MA, USA), pp. 1–5, IEEE, June 2019.

[18] S. M. M. Islam, N. Motoyama, S. Pacheco, and V. M. Lubecke, "Non-Contact Vital Signs Monitoring for Multiple Subjects Using a Millimeter Wave FMCW Automotive Radar," *Los Angeles*, p. 4.

[19] A. Droitcour, V. Lubecke, Jenshan Lin, and O. Boric-Lubecke, "A microwave radio for Doppler radar sensing of vital signs," in *2001 IEEE MTT-S International Microwave Sympsoium Digest (Cat. No.01CH37157)*, vol. 1, (Phoenix, AZ, USA), pp. 175–178, IEEE, 2001.

[20] G. M. Brooker, "Understanding Millimetre Wave FMCW Radars," *New Zealand*, p. 7, 2005.

[21] F. Adib, Z. Kabelac, H. Mao, D. Katabi, and R. C. Miller, "Demo: real-time breath monitoring using wireless signals," in *Proceedings of the 20th annual international conference on Mobile computing and networking - MobiCom '14*, (Maui, Hawaii, USA), pp. 261–262, ACM Press, 2014.

[22] A. Ahmad, J. C. Roh, D. Wang, and A. Dubey, "Vital signs monitoring of multiple people using a FMCW millimeter-wave sensor," in *2018 IEEE Radar Conference (RadarConf18)*, (Oklahoma City, OK), pp. 1450–1455, IEEE, Apr. 2018.

Chapter 3

Literature Review for Separation and Identity Authentication

Here in this chapter we have reviewed the recent progress at introducing this non-contact identity authentication technology in practical applications. One of the goal of this research work is to implement this sensor technology into multiple-subject scenarios. So, we reviewed the recent advances in identity authentication in multiple subject scenarios. First we will describe about the recent progress of vital sign monitoring of multiple subjects using contact-less Radar based sensor.It includes an evaluation of the applicability of different research efforts in isolating respiratory signatures from combined mixture of respiration pattern. In the next subsection we will highlight the recent progress of identity authentication using radar-based sensor and also identify the future research required to address remaining challenges in applying this system into real world of application.

3.1 Literature Review on Subject Separation

One of the potential challenge of this non-contact vital sign detection was the concurrent measurement of respiration monitoring of multiple subjects.When two subjects are present in front of the radar sensor, basically it gets combined mixture of breathing pattern. When the two signals are mixed it is hard to distinguish respiratory signatures from the combined mixtures . Researchers also explored different radar operation modes, namely

the continuous wave (CW) radar, frequency modulated continuous wave (FMCW) radar and ultra-wideband (UWB) radar for extracting vital sign information (breathing rate and heart rate) [1]. Different mode of operation for single subject scenario is represented in Figure 3.1. CW radar transmits a single tone frequency continuously and it can measure the velocity of the target due to the phase shift of the reflected signal. Thus, CW radar can distinguish between stationary and moving target independently of their distances. FMCW radar can measure the distance of target as it transmits varying frequency ranges where frequency modulation is performed usually with a triangular waveform in order to increase and decrease frequency linearly over time. UWB radar is a special application of pulsed radar. Pulsed radar transmits pulsed bursts and then listens to the resultant echoes. In contrast to other radar mode of operation, transmission and receptions are not done simultaneously. The transceiver operation mode (CW, FMCW and UWB) has several advantages for different applications. For an example, when there are multiple subjects to monitor FMCW radar can locate the subject location due to its capability of range estimation [1]. Additionally, for rescue applications UWB radar mode is preferred as electromagnetic waves cross obstacles. And if the goal is to monitor vital signs of bedridden patients, CW is mostly preferred as the hardware architecture and signal processing are less complex. By utilizing range correlation, selecting carrier frequency optimally and utilizing different radar mode of operations, researchers have built the Doppler radar vital sign detection system for numerous applications [2]. Researchers also found with different experimentation is that other major problem with Doppler non-contact vital sign detection are the noise caused by motion artifacts and presence of multiple subjects shown in Figure 3.1(b). When there are multiple subjects presents in front of the radar sensor, it receives a combined mixture of reparation pattern which in interference and hard to separate respiratory signatures from combine mixture of breathing patterns [2]. In the next few subsections we review the recently reported research efforts in separating respiratory signatures from combined mixtures using different radar mode of operations (CW, FMCW

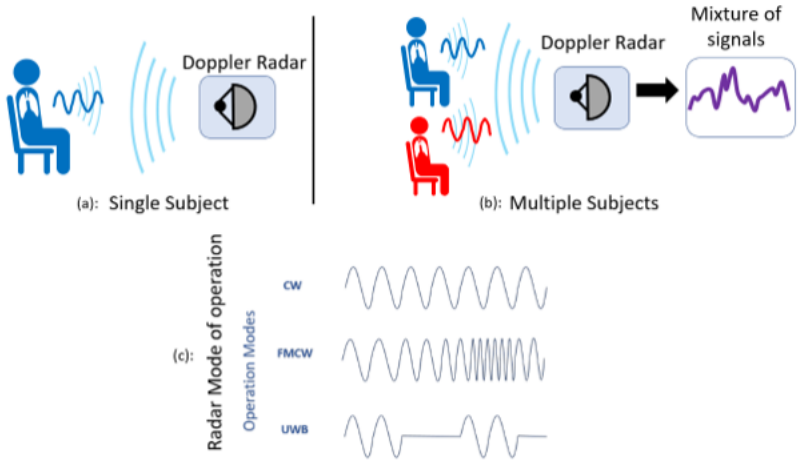

Figure 3.1 Single subject present in front of the radar to extract breathing rate and heart rate (a), and when there is multiple subjects present in front of the radar, it receives an interference of respiration pattern which is hard to separate (b). Different radar mode of operations (CW, FMCW and UWB) has been utilized in literature for vital sign sensing.

and UWB). In the next section we categorized the research efforts in three different ways, based on radar mode of operations.

3.1.1 Separation Of Respiratory Signatures Using CW Radar

One of the first attempts to solve this problem was proposed by Boric-Lubecke et al [3].They proposed multiple-input-multiple-output (MIMO) technique to solve the challenge of multi-subject respiration sensing [3][4].In their subsequent approach, they also investigated the feasibility of utilizing single-input-multiple output (SIMO) technique for isolating respiratory signatures from combined mixtures [5]. In their first attempt, they built a Doppler radar life sensing MIMO system using commercially available components Agilent CW signal source, Mini circuits ZFM-4212 mixer and ZFSC-2-25000 coupler, Narda 4923 circulator and Antenna specialist with patch antenna with beamwidth of 80 degree and demonstrated the feasibility MIMO technique for separating the respiratory signatures from combined mixtures. MIMO technique helps to estimate the spatial position of the subjects which is known as direction of arrival (DOA). Additionally, in spectral domain, they utilized

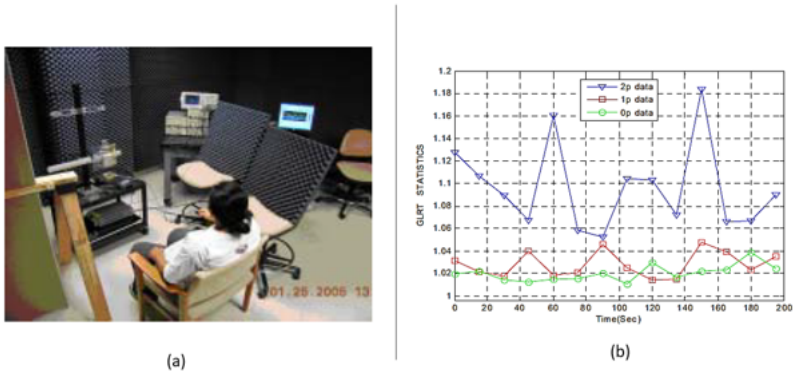

Figure 3.2 Experimental setup of a MIMO Doppler radar system (a), GLRT test statistics when two subjects, one subject, or zero subject was detected by a single antenna system. From [5].

fast Fourier transform (FFT) technique. The proposed solution has some limitation as subjects need to be well-spaced to isolate them as the beamwidth of the antenna was not that narrow (around 80 degree) and FFT technique cannot isolate respiratory signatures when there is mixture of different respiratory patterns. Additionally, with the increase number of subjects it requires separate discrete receivers to isolate the respiratory signatures which is not scalable technique. Although, it showed the efficacy of the MIMO technique for isolation respiratory signatures from combined mixtures. In their next attempt they developed a generalized likelihood test ratio (GLTR) based on a model of the heartbeat, to show that the technique can be utilized to distinguish between the presence of subjects even with a single antenna [5]. Furthermore, it also found that the technique can be used to detect up to 2N-1 subjects using N antennas [5]. In their attempt, they experimented with single antenna and simulated for multiple antennas. Fig. 3 shows the experimental scenario and GLRT can determine the number of people based on statistics by using threshold 1.25. One of the limitations of the proposed GLRT technique is when there is heavy multi-path the proposed technique will not work and need to integrate blind source (BSS) separation technique [3][5][6]. BSS is a technique which is used to extract the independent source signals from the combined mixture of the signal without knowing the information of the source signal. Independent component analysis (ICA) is one of the popular techniques of BSS.

One of the first attempt on integrating BSS techniques with Doppler radar multi-subject respiration technique was reported in 2007 [6]. In their attempt, they also investigated the feasibility of real analytical constant modulus algorithm (RACMA) and ICA for isolating respiratory signatures from combined mixtures [6]. Their investigation showed that, ICA outperformed than RACMA in terms of isolating the heartbeat signals more accurately even when the signal-to-noise ratio (SNR) of the received signal less than 20 dB [6]. Clearly, this study showed the new path of integrating ICA with the Doppler radar system. However, one of the limitations of the above study was mostly evaluated in semi experimental setup where the mixing of the signal was performed on integrating a predefined matrix. For further investigation, Lee et al. demonstrated that, fast-ICA algorithm can separate two distinct respiratory signatures from two subjects adjacent to each other with multiple transceiver configuration [7]. Figure 3.3 illustrates the experimental setup and signal processing flow for separating respiratory signatures. Additionally, they also investigated the feasibility of isolating respiratory signatures when one person has apnea or stoppage of breathing and showed that it is possible to extract independent respiratory patterns even in the presence of apnea events. One of the fundamental limitations of this technique with the increase of number of subjects they need to utilize separate discrete receivers for each different subject which makes the system not scalable in practical applications. Although, the proposed method showed the efficacy of fast-ICA technique in isolating independent respiratory pattern from the experimental dataset which also encourages other researchers for further exploration. In another attempt, single antenna CW radar channel is also utilized by changing the phase shift of the transmitted signal and inspecting the optimum/null points in helps to different between two moving targets [8][9]. However, further exploration and experimentation is required to test the efficacy of the proposed single antenna CW radar system. Having dealt with the different approaches to solve the challenges of respiration monitoring of multiple subjects, researchers also turned their attention towards phased-array CW radar which can also estimate the spatial positions of the human subjects by DOA. Additionally, researchers also investigated hybrid method where they can combine DOA and

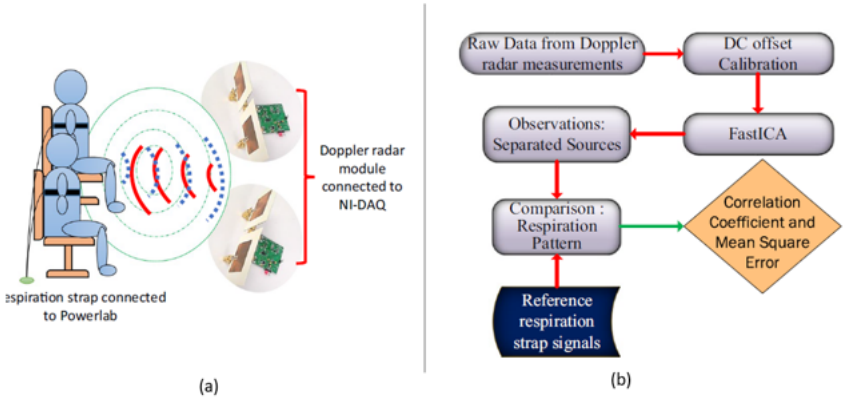

Figure 3.3 Experimental setup for multiple-subject respiration sensing concurrently (a), signal processing flow for isolating the respiratory signatures from combined mixtures of breathing (b). From [7].

ICA together as DOA has certain resolution limit which depends on antenna array elements spacing's. In the next subsection we will describe about the recent advancements on utilizing phased array CW radar for respiration monitoring of multiple subjects concurrently.

3.1.2 Separation Of Respiratory Signatures Using Phased-Array CW Radar

One of the inherent advantages of phased array CW radar is its capability of beamforming and beam steering which helps to estimate the spatial position of the human 1. Phased array CW radar can steer beams to different angles if the adjacent antenna array elements are fed with different phase signals by using phase shifters 1. In a recent attempt, an on-shelf 24-GHz phase-comparison monopulse radar has been utilized to track the spatial position of the target 10 and tested the efficacy of the estimation of the angle of arrival for different breathing patterns also 11. In their investigation, they found that, DOA estimation is possible when the subjects are within the edge of beamwidth of the radar and if the participant crosses the boundary of the edge then the DOA technique fails to estimate the angle due to antenna array spacing limits [10][11]. In addition to that, they also integrated ICA with joint approximate diagonalization of the eignematrices (JADE)

technique for closely spaced subjects [12]. They also developed an intelligent SNR-based decision algorithm to coherently combine two different approaches for concurrent respiration monitoring and their experimental scenario is shown in Figure 3.4(a) [13]. One of the inherent advantages of this technique is it can track both closely spaced and well-spaced subjects. On the other hand, the proposed technique may be computationally intensive as it needs to switch between two different approaches. In another recent attempt, phased-array 2.4-GHz CW Doppler radar is fabricated and implemented using a hybrid beamforming network [14][15]. Figure 3.4(b) illustrates the fabricated radar system integrated with the

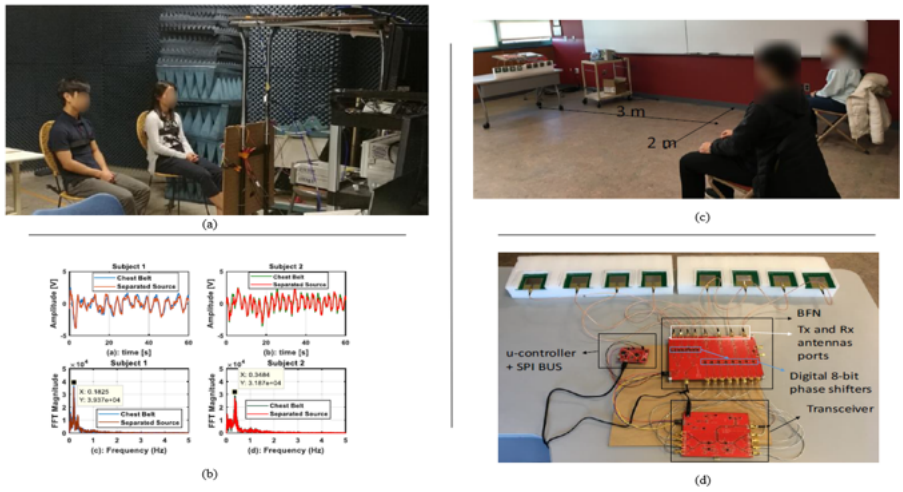

Figure 3.4 Experimental setup showing two-well spaced subjects in front of 24-GHz K-MC4 monopulse radar [13], separated respiratory signatures from the combined mixtures, and compared with chest belt respiration pattern (a), (b). Experimental set up for 2.4 GHz phased array CW radar and fabricated radar system with beamforming network for real-time beam steering (c) and (d).

beamforming network. In their research effort, they can distinguish the subject by switching the beam in a certain direction and isolating the human subjects [15]. Another attempt also investigated the feasibility of beamforming for isolating the respiratory signatures [16]. However, the proposed systems have a minimum resolution limit and it can isolate subjects when the minimum angular resolution limit between them is 1 meter [15][16]. When the

subject becomes much closer intrabeam interference occurs which makes it harder to isolate respiratory signatures.

3.1.3 Separation of Respiratory Signatures Using FMCW and UWB Radar

FMCW radar can estimate the range information of the target and on the other hand, CW radar is limited mainly by its inability to obtain range information form the target. In this subsection, we will describe the recent research efforts on isolating respiratory signatures using FMCW radar by academia and industry. We will categorize them. FMCW radar is the heart of the automotive industry and many researchers are trying to employ high-frequency automotive radar in driver's healthcare monitoring purposes. In the next subsection, we will describe the research efforts for multiple people respiration monitoring by utilizing UWB radar

The first attempt on utilizing FMCW radar on multiple subject scenarios was reported by Wang et al. [17]. FMCW modulates CW carrier frequency with a triangular waveform, so range information can be extracted. However, the range correlation of phase noise for cancellation purposes is less satisfactory with a larger frequency differences between transmitted and reflected echoes [18][19]. Therefore, it requires an integer phase-locked loop (PLL) referencing a direct digital frequency synthesizer to achieve low phase noise, fast settling time, and precise frequency control [20]. Utilizing FMCW radar mode for vital sign sensing signal generator is complex and power consumption is high. To solve this issue, a 2.3-2.8 GHz self-injection locked (SIL) radar is designed which contains a differential voltage-controlled oscillator (VCO) with an injection input, low-noise amplifier shown in Figure 3.5(a) [17]. Additionally, a transmit (TX) antenna, a power amplifier (PA) with a power gain of 8 dB, a receive (RX) antenna array consisting of two elements, a phase shifter, a combiner to synthesize sum different pattern for azimuth angle detection [17]. By utilizing their designed SIL radar they were able to detect the range information by utilizing background subtraction of the spectra. Additionally, radar uses CW mode to

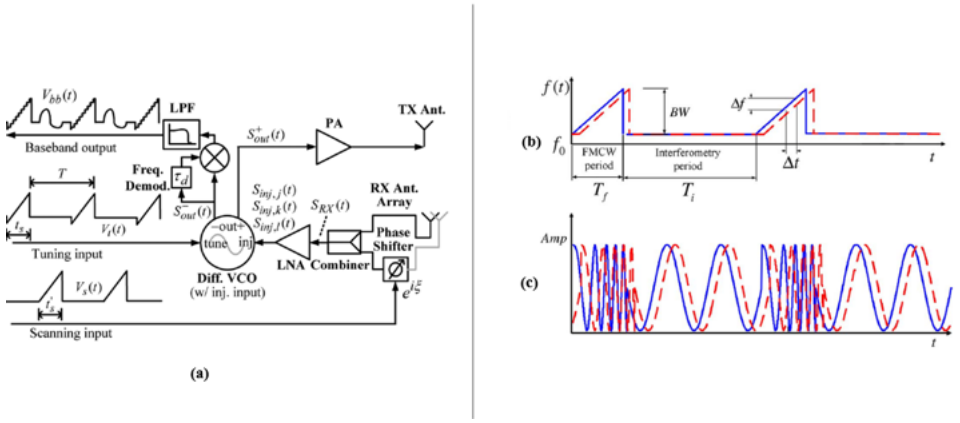

Figure 3.5 (a) Functional block diagram of the proposed SIL radar for isolating respiratory signatures [18]. Proposed hybrid radar mode where a solid line represents the transmitted signal and dashed line represents the received signal in the (b) frequency domain and (c) time domain [18].

monitor the azimuth angle of the subject. However, one of the limitation of the proposed system is for equidistant subjects the method cannot distinguish individual subjects. Prior attempt utilized the hybrid mode of operation which consists of a time division system that switches between FMCW mode and interferometry mode shown in Figure 3.5(b) and (c) [18]. FMCW mode provides range information and interferometry mode is advantageous in relative displacement (e.g. physiological motion) detection. FMCW signal uses an up-ramp linear frequency modulated signal while the interferometry mode has a fixed operating frequency. By mixing a local copy of the transmitted with the received signal back-scattered by the target, the baseband signal contains a series of FMCW baseband signal and interferometry baseband signal. In other words, in their proposed technique a sequence of chirp is embedded into the single tone interferometry signal [18]. Clearly, both SIL and hybrid methods showed the feasibility of utilizing FMCW radar for vital sign monitoring in multiple subject scenarios. However, each technique was not able to utilize FMCW mode directly because the need to modify the radar mode of operation either in SIL or interferometry mode to isolate the interference of the respiration pattern from combined mixtures. In another attempt, 24 GHz FMCW radar mode was directly

employed to distinguish the vital signs from a combined mixture of respiration patterns by using the path loss compensation method [20]. Since FMCW radar can detect the range and velocity of the target so, a signal amplitude differences from the polarity of the target is utilized by using the path loss equation of the transmitted radar signal [19]. One of the limitations of the technique is that it cannot isolate the respiratory signatures when the subjects are within the beamwidth and if their position is at the same distance from the radar. To solve this limitation in their prior research effort they proposed an efficient spectral estimation-based algorithm which helps to overcome the ambiguity of the range detection based on the conventional FFT method [20]. They employed multiple signal classification (MUSIC) algorithm for spectral position estimation instead of FFT and that helped to cross the resolution limit of the antenna array spacing. However, the reported results just focused on the subjects having different distances within the beamwidth of the radar. Recently another research group utilized 5.5-7.2 GHz FMCW radar module in multi-shift mode (five TX and five RX) to isolate reflections from each of the antenna [21]. In their attempt, they utilized time of flight information which is measured from different receivers and static reflectors (e.g. table and chairs) reflected echoes can be removed by background subtraction. Additionally, they mapped the time of flight information to distance to localize multiple people in the view of radar [21]. The result shows significantly it can differentiate between static and moving human subject from the time of flight information. One of the limitations of the proposed technique is the scalability issue as the proposed system can track a maximum of five people simultaneously and if the number of people increases then number of receiver antennas needs to be increased. In another latest attempt utilized a 7.03-8.05 GHz FMCW radar system to isolate respiratory signatures from combined mixtures by proposing an intelligent multi-people tracking algorithm [22]. Figure 3.6 illustrates the experimental setup and radar system utilized by them. Their utilized radar system consists of a digital signal processor/field programmable gate array (DSP/FPGA) board, an analog-to-digital converter (ADC) and a laptop. The radar waveform is generated by a PLL that is configured by the DSP/FPGA board. The signal is fed into the power divider that is

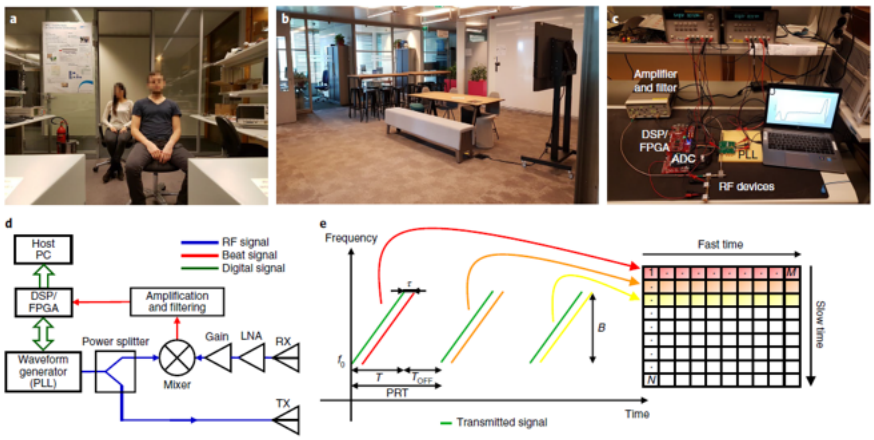

Figure 3.6 (a) Experimental setup (b) experiments conducted in the environment (c) FMCW radar sensor (d) typical block diagram of the radar sensor module (e) series of N chirps that are transmitted by FMCW radar module and it is represented in a matrix format. From [22].

splits into two branches. The first output is connected to the transmitter antenna and when the signal is being reflected it's also multiplied with the transmitted copy of the signal [22]. In their multiple people tracking algorithm, they worked on the FMCW mode of operation, especially on the received data frame format. After receiving the FMCW data matrix, generally, FFT is performed for extracting range information which is known as range-FFT. Following the range information, Doppler information can be achieved by taking the FFT of the phase information [21]. For example, for a certain target range bin, the object is moving if there is a target moving towards radar at a constant speed then the phase of the range bin will change with a ramp trend. On the other hand, if there is no moving target in that range bin then the phase information of the range bin will experience a small and random change due to noise. Thus, if the range bin has a moving target, then it will produce a phase change whose dominant peak in the frequency domain will not be DC. The above procedure will be continued over the whole received data matrix. Then they multiplied the speed matrix by the magnitude of the range profile matrix to get the new matrix called range speed matrix (RSM. RSM still contains the information of the static objects (e.g. chair, tables). Then a peak detection algorithm is employed in every slow time

instances to find local maxima and then compared to the time domain threshold to extract the number of participants. The proposed method can easily distinguish between multiple subjects in a static and moving environment. However, hardware scalability and antenna resolution limit remain a challenge for this multiple people tracking.

3.1.4 Industry Efforts on FMCW Radar and Research Efforts on UWB Radar

Industry efforts on utilizing millimeter-wave FMCW automotive radar for multiple subject scenarios is also gaining attention as most of them are focused on employing W-band (76-110 GHz) radar for in-cabin monitoring in the automotive environment [23][**?**]. Two giant semiconductor companies, Texas Instrument, and ON Semiconductor reported their research investigations on utilizing FCMW radar for isolating respiratory signatures from combined mixtures of respiration patterns. Texas Instrument utilized 76-81 GHz FMCW radar modules for this purpose. Initially, they investigated the feasibility of utilizing this high- frequency band for extracting vital sign information and they integrated a beamforming technique based on estimating the angular location of the target [23]. Additionally, ON Semiconductor investigated the feasibility of utilizing beam steering technique based on the angular location of the driver front seat and passenger side seat locations [**?**]. Both, beamforming, and beam steering technique showed the efficacy of isolating respiratory signatures especially in the automotive environment two persons are in a seated position in a well-spaced manner. However, none of the attempts investigated the scenario if there is a presence of more than two persons the method will be able to distinguish vital signs from different subjects.

One of the attempts for utilizing UWB radar in this purpose was reported by T. Sakamato et al [24]. In their attempt, they employed 8.4 GHz UWB radar for adaptive array processing to estimate the spatial position of the target. For estimating the spatial position of angle of arrival they used the capon beamforming method and then directionally constrained minimization of power algorithm (DCMP) is applied to the received signal to

Table 3.1 Systematic review on vital sign monitoring in multi-subject scenario

Reference Year of Publication and Radar Mode	**Methods**
O. Boric-Lubecke et al. 2005, CW	D0A
Q. Zhou et al. 2006, CW	GLRT
N. Petrochilos et al. 2007, CW	ICA
Y. S. Lee et al. 2016, CW	ICA
S. M. M. Islam et al. 2020, phased-array CW	ICA, DOA
M. Nosrati et al. 2020	DOA
J. Xiong et al. 2020, CW	DOA
F. K. Wang et al. 2013, FMCW	SIL
G. Wang et al. 2014, FMCW	Interferometry mode
H. Lee et al. 2018, FMCW	Path loss compensation
H. Lee et al. 2019, FMCW	Parametric spectral estimation
F. Adib et al. 2015, FMCW	TOF)
M. mercuri et al. 2016, FMCW	spatial tracking algorithm
A. Ahmed et al. 2018, FMCW	Digital beamforming
S. M. M. Islam et al. 2020, FMCW	Digital beamforming
T. Sakamato et al. 2018, FMCW	DCMP

extract the heart rate information [24]. The proposed method works well when subjects are symmetrical positions and equidistant positions with a certain resolution limits around 1 m. Table 3.2 provides a summary of published work on radar-based non-contact vital sign sensing in a multiple-subjects environment.

3.2 Literature Review on Identity Authentication Using Radar

Existing traditional identity authentication methods (e.g. Fingerprint, password and facial recognition) predominately employ a one-off, interrupting approach, which authenticates only at the start of a user session with users actively engaging an input device or biometric reader [25] [26]. This type of traditional authentication systems are vulnerable to open session exploitation and may interfere with user activity.There are lot of ongoing research which focuses on designing continuous identity authentication system. Many researchers explored different sensing technologies to acquire different physiological traits, such as fingerprint [27], palm print [28], and iris [29], used to monitor and authenticate users

throughout a session. Recent advancement of sensor technologies also enable to collect subtle physiological patterns, such as those associated with electroencephalogram (EEG) [30], finger-vein [31], and gait [32], to authenticate people continuously.

Compared to these contact-based solutions, non-contact and unobtrusive identity authentication using microwave Doppler radar can improve the system usability in practice and increase the range of applications which can privacy invasive also [33][34]. For example, various visible and thermal-based cameras are employed to acquire face and gait features for user identity authentication [35][36][37].Image based approcah has several limitations including lack of privacy and degrades performances under a low light ambient condition [34]. Additionally, a solution leveraging unobtrusive radar measurement of cardiopulmonary motion can be immune to such deficiencies and it can achieve reliable recognition under privacy sensitive conditions [38][39].

3.2.1 Cradiopulmonary Diversity and Physiological Motion Measurement

Doppler radar can track tiny movement of the chest surface due to physiological events, including heartbeat, arterial pulsation, and breathing [40]. This physiological motion is concentrated mostly in the thorax, where the heart and lung lie, but it also includes the abdomen, which moves with respiration, and superficial pulses, which are present at any points in the body [41]. Tiny movement of the chest surface due to respiratory effort is a complex and three dimensional pattern and it varies with emotional stress and physiological activities [40][42].Respiratory effort motion can come from one of two regions: chest or abdomen, known as thoracic and diaphragmatic breathing, respectively [43]. When the heart contracts generally it drives blood flow which moves within the chest cavity, hitting the chest wall, and creating a measurement minute movement of the chest surface due to cardio-respiratory activities [26][40].Non-contact microwave Doppler radar can operate at frequencies where primarily minute movement of the chest surface can be detected [39].Thus,

microwave Doppler radar systems can sense respiratory related information as well as cardiac related patterns.

Various clinical investigations demonstrated that sedentary adult human subjects exhibit a diversity in respiratory pattern while awake, not only in terms of tidal volume and inspiratory and expiratory duration, but also in terms of air flow profile [40].Additionally, each individual selects to exhibit one unique pattern among the infinite number of possible ventilatory variables and air flow profiles [40][41][42]. These variabilities are non-random and may be explained by either central neural mechanisms or chemical feedback loops [41][42].Each individual has a different physical size and shape of lungs, as well as different rib cage and abdominal muscle strength that contributes to the variations in breathing patterns [42]. In addition to variations in respiratory features, there is also significant variation in heart-based geometry [41][42]. In general, the human heart contains two upper cavities (atria) and two bottom chambers (ventricles) [44][45]. The successive contraction (systole) and relaxation (diastole) of both atria and ventricles circulate the oxygen-rich blood throughout the whole human body [44][45] .A diagrammatic section of the heart is shown in Figure 3(a). The heart drives blood through the lungs and to tissues throughout the body [40]. Cardiac motion consists of contraction and relaxation of both atria and ventricles [26]. In one cardiac cycle, ventricles relax and passively fill with blood to seventy percentage of the total volume from atria through the open mitral valve [26]. At the same time, the atria contract with heart muscles and pump blood. Figure 3.7(b) shows the motion of the heart through the phases of the cardiac cycle [26][46].Generally, the cardiac motion cycle consists of five distinct stages including: (1) ventricular filling (VF), (2) atrial systole (AS), (3) isovolumetric ventricular contraction (IC), (4) ventricular ejection (VE), and (5) isovolumetric ventricular relaxation (IR) [44][45]. These cycles are significantly unique because of the different volumes, surface shape, and moving dynamics (speed, acceleration, etc.), and also deformation of the heart [26][46]. These stages or cycles are different for each person because of variations in size, position, anatomy of the heart and chest configuration, and various other factors [44][45]. It has also been demonstrated in

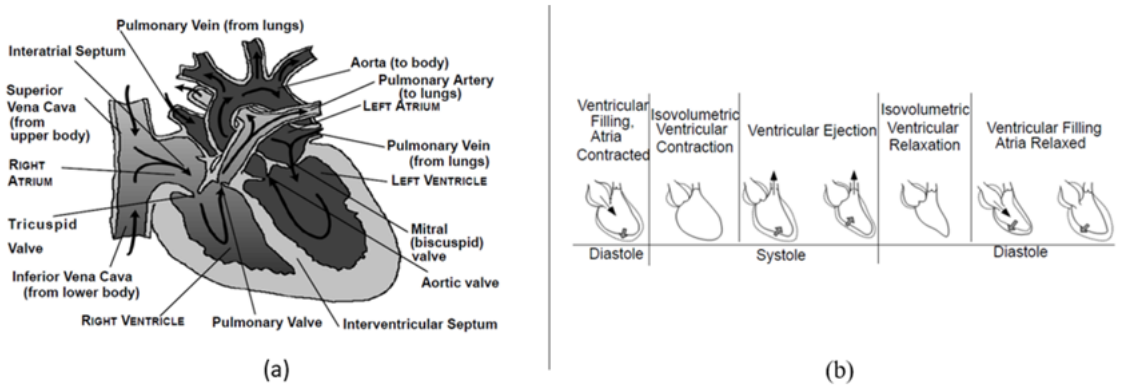

Figure 3.7 Diagrammatic section of the heart, (a), [16] and motion of the heart through the phases of the cardiac cycle, (b) [18]. The arrows indicate direction of blood flow.

various clinical investigations that no two persons have the same cardiac blood circulation [45][46]. Thus, cardiopulmonary motion which basically consists of respiratory and heart-based dynamic pattern can be a unique identity marker for everyone, due to differences in their physical organ size, shape and muscle strength [44]. Additionally, breathing related motion is controlled by central neural mechanisms or chemical feedback, which makes it extremely difficult to counterfeit or hide a living individual's motion signatures [39].

3.2.2 Radar-Based Continuous Identity Authentication Research

Traditional identity authentication system is vulnerable in terms of security as it is one pass validation approach (e.g., fingerprint, password, and facial/iris)[26]. Radar based identity authentication can add an extra layer of security to the vulnerable traditional one-pass validation approach as it is non-contact, unobtrusive and continuous[26][46].Radar-based identity authentication system and its basic principle us shown in Figure 3.7.Pattern recognition is always challenging in this continuous identity authentication research as human breathing pattern changes due to physical activities and emotional stresses [40]. With the advancement of machine learning, Doppler radar-based physiological signals can be turned into useful data and knowledge [26]. In addition to that, diverse respiratory motion patterns have good potential to be used as biometric identifiers [26][46][47]. In this section,

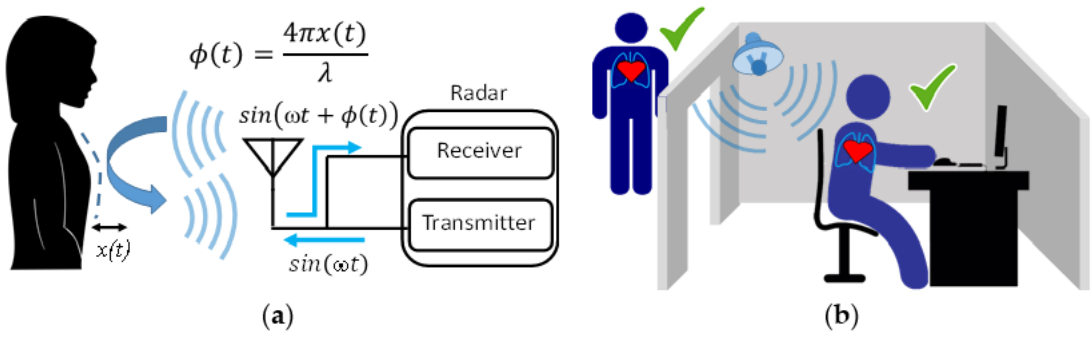

Figure 3.8 Basic principle of Doppler radar physiological sensing (a), and non-contact continuous identity authentication concept (b). A radar system typically consists of a transmitter and a receiver. When a transmitted signal of frequency f is reflected its phase changes, $\omega\ x(t)$, in direct proportion to the subtle motion.From [22]

radar-based sensing authentication is categorized in two different ways, based either on breathing-related features, or heart-based features. Breathing motion is generally periodic, and respiratory-related features can be extracted from the time domain signature of the reflected phase signal and rate information extracted by performing an FFT [47]. Heartbeat motion is modulated on top of respiratory motion and the larger resulting breathing signal is dominant over the heartbeat signal [26]. This leads to a classical problem in FFT, where the stronger signal at given frequency leaks into other frequencies and can mask a weaker signal at nearby frequencies [47]. Generally, the radar captured signal is filtered outside the 0.005–0.5-Hz frequency band for extracting respiration information and 0.8–2 Hz for extracting heartbeat-related information. All the radar authentication research is focused on extracting two separate distinguishable features, based on either respiration or heartbeat [46]. Extracting both simultaneously has the potential for stronger authentication. however, such a process may increase computational complexity. Table 3.2 provides a summary of published work on radar-based non-contact continuous identity authentication considered in this paper. In the next two subsections, details are provided on these two different unique features (breathing and heart, respectively), including related identification demonstrations along with associated challenges for further development. There have also been attempts to

Table 3.2 Systematic review on radar-based non-contact continuous identity authentication.

Reference Year of Publication	Identification Features
A. Rahman et al. 2016	Respiration-based: power spectral density, inspiratory time
F. Lin et al. 2017	Heart-based dynamics: cardiac-motion cycle
A. Rahman et al. 2018	Respiration-based dynamics:inhale-exhale area ratio
S. M. M. Islam et al. 2019	Respiration-based dynamics:FFT features
S. M. M. Islam et al. 2020	Respiration-based: exhale area and breathing depth
S. M. M. Islam et al. 2020	Respiration-bases OSA pateints (peak power spectral density)
S. M. M. Islam et al. 2020	Respiration-based: exhale area and breathing depth
D. Rissacher et al. 2015	Heart-based: cardiac motion
K. Shi et al. 2018	Heart-based: heartbeat signal complexity
T. Okano et al. 2017	Heart-based: power spectral density
P. Cao et al. 2017	Heart-based: heartbeat, energy and bandiwdth
J. Zhang et al. 2016	Channel state information: gait pattern
J. Liu et al. 2016	Respiration-based morphologic pattern

use Doppler modulation of WiFi signals to authenticate people and this research is described in the next subsection.

3.2.3 Radar-Based Identity Authentication through Respiration Related Features

One of the first attempts at radar-based identity authentication using breathing pattern was reported by a research group at the University of Hawaii, where they integrated a neural network classifier to recognize individual human beings 39. In this work they extracted three different respiratory features (peak power spectral density, linear envelop error, and packing density) from respiratory motion measurements, as illustrated in Figure 3.9. A 2.4 GHz quadrature direct conversion is shown in figure. Doppler radar system was used for this experiment, assembled from coaxial components. A data acquisition system recorded the data and post processing was performed in MATLAB. Three subjects with similar breathing rates were selected and various features were investigated, such as power spectral density, linear envelop error, and packing density, which convey the breathing energy and air flow profile related phenomena. The research concentrated on using the

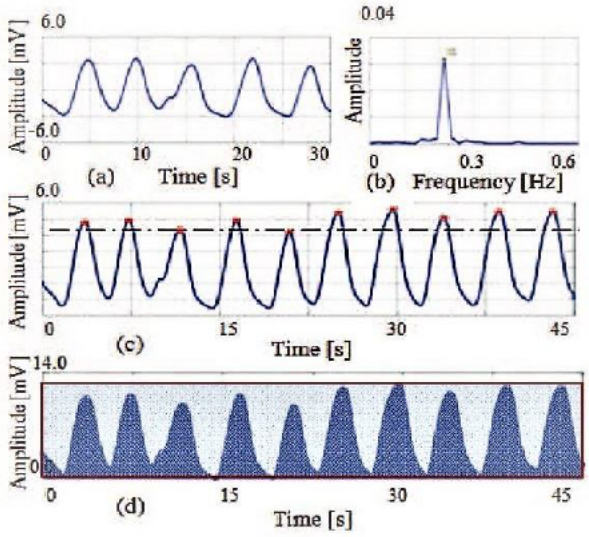

Figure 3.9 Radar-measured respiratory features from 30 second epochs. Pioneering efforts at recognizing subject identity from radar measured respiratory signals (a) involved extraction of three different features: breathing rate (b), linear envelop error (c), and packing density (d). Linear envelop error shows the peak distribution differences and packing density illustrates the differences in air flow profile with the inhale and exhale area episodes. Taken from [52]. Taken from [15]

Levenberg–Marquadrt back propagation algorithm to perform classification [52]. Figure 3.10 illustrates the experimental setup and reported results for training and applying a neural network classifier to recognition of the Doppler radar physiological measurements [52]. The overall classification accuracy was above 90%, which clearly illustrates that the proposed technique can be effective for this application. However, this work was limited to identifying only three participants. Another issue is that the experiment was entirely focused on measuring a single subject at a time. Subsequent research by the same group reported on continuous authentication based on dynamic segmentation where they used inhale and exhale area ratios of the captured respiratory pattern as unique features for six different participants [48]. Dynamic segmentation evaluates the displacement and identifying points in the range of 30%–70% of both exhale and inhale episodes, which defines four boundary points of a trapezium [48]. The ratio of these two areas provides a useful feature which indicates how quickly the next cycle of inhalation begins [68]. Figure 3.11 illustrates

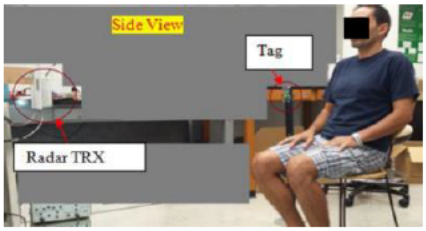

(a)

TABLE II
TESTING RESULTS CONFUSION MATRIX

	Person 1	Person 2	Person 3	Success
Person 1	7	0	0	100 %
Person 2	0	13	4	76.4%
Person 3	0	0	17	100%

(b)

Figure 3.10 Human identification experiment using a radar system. The test set-up is shown, (a), along with the neural network recognition results, (b). From [15].

the inhale/exhale area ratio features for two different subjects, which differ significantly. Based on extracted unique features, a K-nearest algorithm was integrated to identify each person, which showed a classification accuracy of almost 90% [48]. In order to increase the accuracy of the proposed method, minor component analysis was performed on subject data sets which showed overlapping inhale/exhale area ratios. For minor-component analysis, a linear demodulation technique was employed [48].The variation in minor component shows the radar cross section and high frequency component of respiration and heart signal modulation. Higuchi fractal dimension analysis was performed on minor components of the radar captured signals to identify overlapped inhale/exhale area ratios of subjects, which increased the classification accuracy to 95% [48].The proposed method clearly shows efficacy. However, the number of subjects of tested was small and further investigation is required to establish larger data set functionality. Another limitation of this approach is the reliance on two different parameters (inhale/exhale area ratio and minor component analysis). Further investigations also demonstrated that, as inhale/exhale ratio become more similar, false classification may occur [47]. To increase performance further, an FFT based feature extraction approach was applied with an integrated SVM classifier using

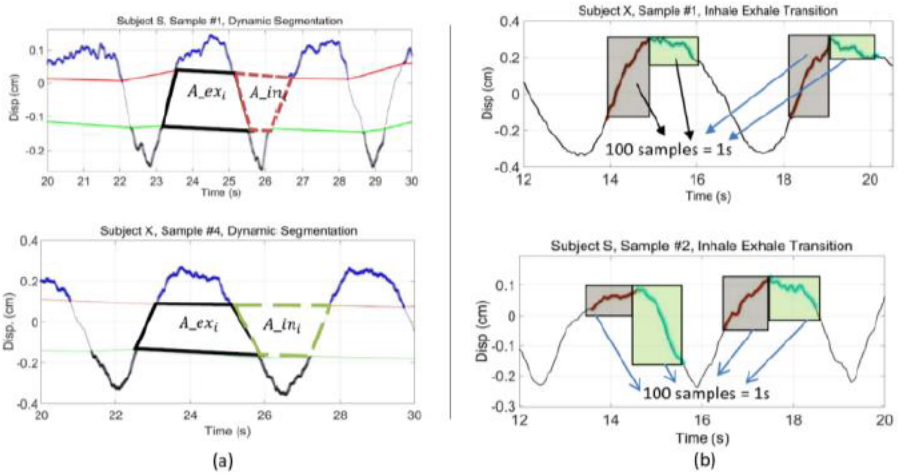

Figure 3.11 Respiratory pattern classifiers used for subject recognition. Dynamically segmented inhale/exhale area ratios of two subjects significantly differs, (a), as do signal patterns relating to the dynamics of breathing near the points where the inhale and exhale transition occurs,(b). From [24].

a radial basis function [47]. The performance of the proposed system increased as the FFT based feature extraction approach contains all breathing dynamics related features (breathing rate, breathing depth, inhale rate, exhale rate and airflow profile). Figure 3.12 illustrates the FFT based feature extraction approach used for six different participants. As the data set and number of participants was small, continued experimentation remains needed to verify the efficacy of the FFT-based feature extraction approach. For further investigation, the feasibility of the FFT-based approach for extracting identifying features from radar respiratory traces for sedentary subjects was tested, along with measurements of the subjects just after performing physiological activities (walking upstairs) [49]. It was found that subject recognition still worked but was not as effective after performing short exertions as it was for sedentary subjects [49]. Experimental results demonstrated that, after short exertion, the dynamically segmented exhale area and breathing depth increased by more than 1.4 times for all participants, which made evident the uniqueness of the residual heart volume after expiration for recognizing each subject, even after short exertions [49]. They also integrated a machine learning classifier support vector machine (SVM), with

a radial basis function kernel which resulted in an accuracy of 98.55% for subjects in a sedentary condition and almost 92% for a combined mixture of conditions (sedentary and after short exertions) [49].Furthermore, they also investigated identity authentication of patients with obstructive sleep apnea (OSA) symptoms based on extracting respiratory

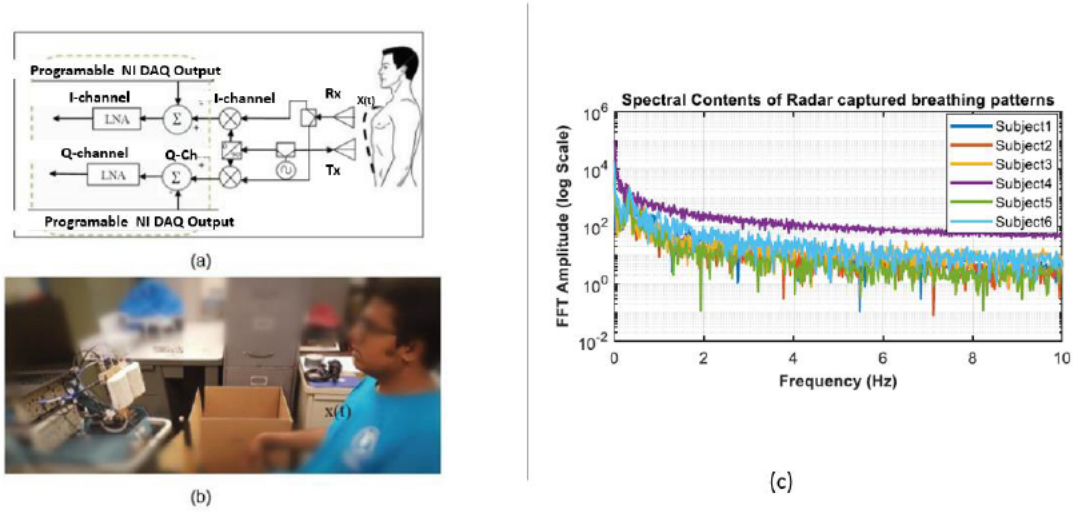

Figure 3.12 Respiratory pattern classifiers used for subject recognition. Dynamically segmented inhale/exhale area ratios of two subjects significantly differs, (a), as do signal patterns relating to the dynamics of breathing near the points where the inhale and exhale transition occurs,(b). From [24].

features (peak power spectral density, packing density, and linear envelop error) for radar captured paradoxical breathing patterns, in a small-scale clinical sleep study integrating three different machine learning classifiers (support vector machine (SVM), k-nearest neighbor (KNN), and random forest). Their proposed OSA-based authentication method was tested and validated for five OSA patients with 93.75% accuracy, using a KNN classifier which outperformed other classifiers [50]. This study was limited to only six supine subjects in the controlled environment of a sleep center.

3.2.4 Radar based Identity Authentication through Heart based Features

One of the first attempts at recognizing people from their heart-based features (cardiac cycle) from Doppler radar was reported on by a research group at Clarkson University [51]. They used a 2.4-GHz heterodyne radar system from which cardiac data was extracted, and an ensemble average was computed using ECG as time reference [51]. A continuous wavelet transform was integrated to provide time-frequency analysis of the average radar-measured cardiac cycle and a k-nearest neighbor algorithm was used to recognize people with an accuracy of 82%. This was the first reported attempt for applying cardiac-based features using a cardiac-radar system as biometric identification tool [51]. The low classification accuracy occurred as there was overlap in the ensemble average of the cardiac cycle; therefore, further investigation and experimentation is required to demonstrate efficacy for more reliable recognition of subjects from radar captured signals.

A study conducted by a research group at the University of Buffalo [26] proposed a continuous identity authentication system named "Cardiac Scan". This system used a 2.4-GHz Doppler radar transceiver with two antennas (one for transmit and another for receive functions) each having a beam width of . The radar power consumption was 650 mW with a 5V-volt source and 130 mA of current [26]. The customized Doppler radar was placed in front of the subject at 1 meter [26]. Figure 3.13 shows the experimental set up of the proposed cardiac scan system, from which five different points were extracted from the radar captured respiration patterns which were hypothesized to fully represent cardiac motion. Based on the hypothesis the experiment illustrated that these heart-based geometry measures differ from person to person due to difference in size, position and anatomy of the heart, chest configuration, and various other factors [26].From their experimental results, it was also clear that no two subjects had the same heart, tissue, and blood circulation system, as there were significant differences in their cardiac cycle points measured in the radar data set [26]. Figure 3.14 illustrates the cardiac motion marker for one segment captured from the radar respiration measurement. In this work, the user's cardiac-motion related features were stored in the system. A support vector machine (SVM) with

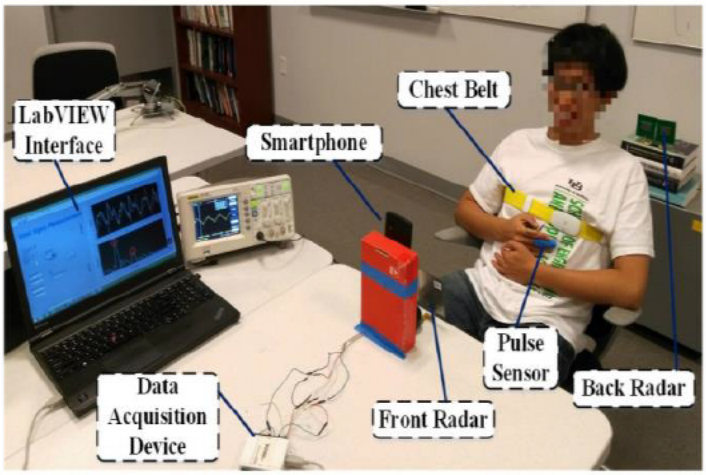

Figure 3.13 Experimental setup for cardiac scan continuous authentication system using microwave Doppler radar. A data acquisition device and LABVIEW interfaces were used to capture signals. A pulse sensor and chest belt were used for reference measurements. From [2].

a radial basis function (RBF) kernel classifier was employed to uniquely identify different participants. A study of a 78 subject data set was reported, and the proposed system achieved an accuracy of 98.61% and a 4.42% equal error rate [26]. One of the limitations of the above proposed technique is that the complete study was performed with healthy sedentary persons and only for single-subject measurements. If subjects have cardiovascular diseases, unique identification may be problematic as the cardiac cycle would be affected. Further study is also required to verify that the proposed heart-based cardiac cycle points remain consistent after subjects perform varying degrees of physiological activity. In another reported study, cardiac measurement of different persons was used to uniquely identify each using a 24-GHz continuous wave radar system employing six-port measurement technology [52]. Figure 3.15 represents the hardware setup used for this experiment. A six-port measurement system consists of two input ports and four output ports. The two input signals are superimposed to extract phase shift information due to chest displacement. This particular work focused on extracting heartbeat signal information for each participant, as the exact position and angle of the heart in the thorax, as well as the anatomy of the

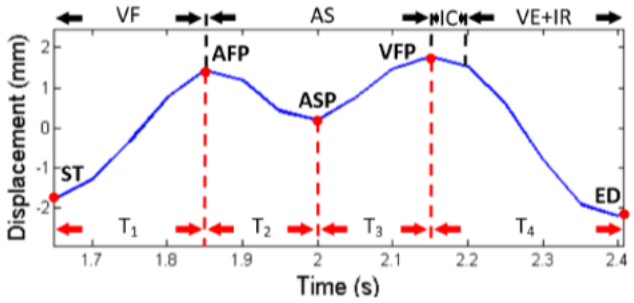

Figure 3.14 Cardiac motion marker. The cardiac motion cycle defined by five different points (red dots) within five different points of displacement and timing was calculated as a unique feature for recognizing people. From [2].

thorax itself, is a little different for every person due to varying tissue and muscle/fat components [52]. Due to these differences, the radar-captured heartbeat signal involved different propagation and attenuation characteristics. As each person has a different heart position and dimensions, dominant features exist in the heartbeat signal which form a complex and unique pattern. Figure 3.16 illustrates the heartbeat signal variation for each participant. Initially a 5-second heartbeat signal was used for identifying unique features for each participant. Integrated machine learning classifiers were also used to recognize people. A quadratic support vector machine (SVM) outperformed other classifiers, with an accuracy of 74.2%. To increase the accuracy, a 7-second heartbeat segment was used, which increased the classification accuracy to 94.6%. The study provides a clear indication that heart-based geometry can be used as a unique feature to identify people. However, validation for this study only included four different participants. Thus, further investigation is required for larger data sets having varying conditions, especially those involving measurements made after physical activities. Another study used a 24-GHz radar system to extract heartbeat related unique features to recognize eleven different participants [53]. An autoregressive (AR) model-based frequency analysis was introduced, which is superior to FFT, having a window length of 100 milliseconds, from which power spectral density could be calculated [53]. Each peak in this analysis represents the contraction and extraction of the heart.

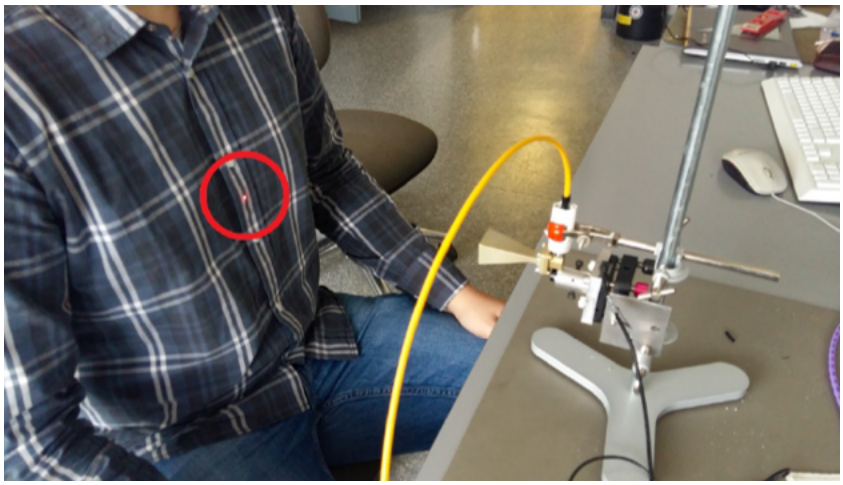

Figure 3.15 Experimental setup for unique identification of a human from radar captured respiration pattern which includes six-port technology. From [28].

The first peak was used as a reference and then a period of 0.2 s before and after, 0.4 s, was used as a template. Template matching was used to detect all heartbeats. The average of the power spectral density was used as a unique identification number for each participant. Figure 3.17 illustrates the power spectral density features extracted from the radar respiration signal and PSD profile for eleven different participants. The success rate was 92.8%. The proposed method clearly demonstrates heart-based PSD feature extraction efficacy for recognizing people. However, if the position between the radar and human subject changes or the heart rate fluctuates greatly then the proposed method produces false classification. Motion artifacts and multi-subject scenarios were not considered and remain a significant challenge for this approach.Recently, another study demonstrated the efficacy of radar-based identity authentication using a short-time Fourier Transform (STFT) [54]. Each person sat a 1.5 m distance and physiological signatures were recorded for about 6 seconds of the breathing pattern, using a 24-GHz continuous wave radar. An STFT was used to characterize the micro-Doppler signature of ten different participants, followed by basic image transformation methods like translation, rotation, zoom, mirror, and cropping. The STFT image was used to represent heart-based features for each different subject. A

deep convolutional neural network (DCNN) was used to classify subjects based on their radar captured micro-Doppler signatures.

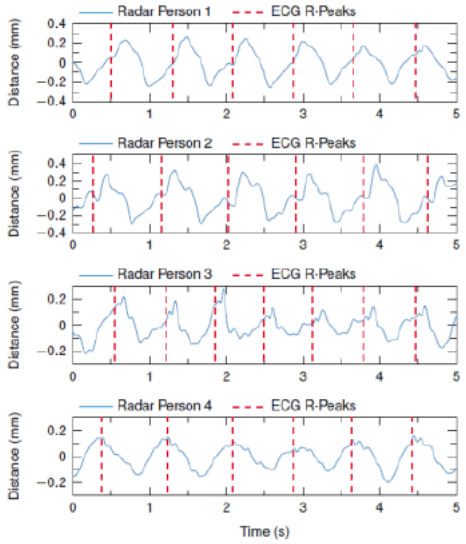

Figure 3.16 Heartbeat curves recorded by a 24-GHz radar for four subjects. Each signal is periodic but for each subject the pattern is a bit different which serves as a unique feature for recognition of identity. From [28].

Figure 3.16 illustrates the STFT images for four participants which are significantly different for each subject and include unique features for identification. From the spectrogram, three different heart-based features were extracted, such as the period of the heartbeat, the energy of the heartbeat, and the bandwidth of the signal. A deep convolutional neural network was then trained, and the resulting classification accuracy was almost 98.5%. To extract heart-based or respiratory information, data segmentation generally plays an important role. Segments correspond to the FFT window size and should contain at least one full respiration cycle and multiple cardiac cycles [26][47]. The number of segments used for a data set also plays an important role for authentication time and accuracy [26].Increasing the FFT window size will bring a benefit in resolution as a higher number of samples are included in the operation, but this will also increase the time delay and complexity of authentication and is not generally justified for real-time operation.

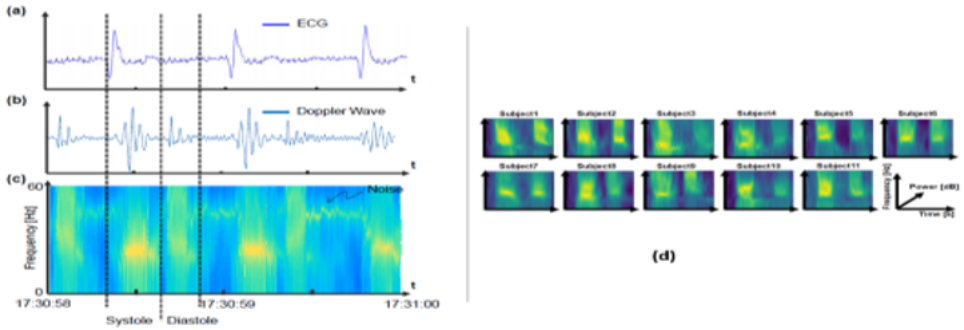

Figure 3.17 Short time Fourier transform (STFT) of four different participants for extracting micro-Doppler signatures. The images for four different participants clearly have significantly different spectral content. From [30].

3.2.5 WiFi-ID: Non-Contact Human Identification Using WiFi Signals

Several studies in parallel seek to achieve non-intrusive continuous identity verification using off-the-shelf WiFi devices [55][56][57][58][59]. These methods leverage the fact that the majority of IEEE 802.11 WiFi protocols have the access point (AP) explicitly sending out known pilot symbols,prior to the data communication, which allows the receiver(s) to measure the wireless channel effect in terms of signal attenuation, e.g., receive signal strength (RSS), plus phase offset, e.g., channel state information (CSI), and cancel the channel effect for better reception. Since the wireless channel effect is the combined result of scattering, fading, and power decay with distance, it is also correlated to body movement if human subjects are present within the environment. These studies on WiFi sensing aim to distill the physiological patterns from the channel measurements via various signal processing algorithms and utilize the patterns for continuous identification and authentication, which are briefly surveyed below.

In [57], Abdelnasser et al. proposed a non-invasive RSS based WiFi breathing estimator shown in Fig. 3.13. The design leverages the fact that inhalation and exhalation can cause a perceivable periodic pattern in the RSS observed by a device positioned on the chest surface [55]. The pattern can be analyzed to characterize various breathing-related physical factors

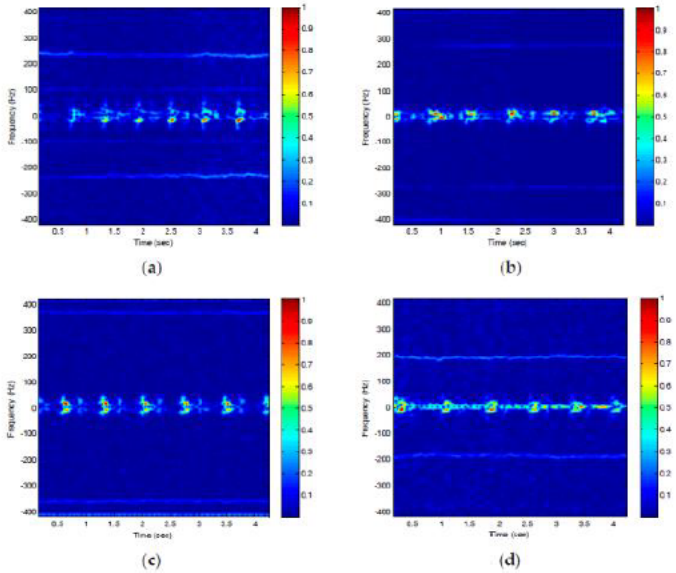

Figure 3.18 Measured 24-GHz heartbeat patterns for autoregressive PSD analysis based subject recognition. Measurement of heartbeats are shown for electrocardiogram (reference) (a), Doppler radar (b), PSD of Doppler sensor output (c), and PSD for 15-s Doppler radar for eleven participants [29].

[55]. For instance, the authors examine the RSS with bandpass filtering and fast Fourier transform (FFT) to obtain the subject's breathing rate and heart rate. This effect extends to scenarios when the subject obstructs the line-of-sight (LOS) between the transmitter and the device.

In [55], Zhang et al. analyzed the CSI to identify people within the environment. In their experiments, the OFDM pilot signal exchanged between a WiFi router and a receiver node (e.g., laptop) are exploited to extract the CSI, which can be regarded as the aggregated result of the multipath fading. A person walking within the environment would affect the multipath reflections with the particular gait pattern, thus creating unique perturbations in the CSI, allowing the system to differentiate individuals via the received WiFi signal [57].

Similarly, in [56], Liu et al. extracted fine-grained channel state information (CSI) of individual OFDM subcarriers from off-the-shelf WiFi devices to detect minute movements and provide accurate breathing (inhalation and exhalation) and heartbeat (diastole and

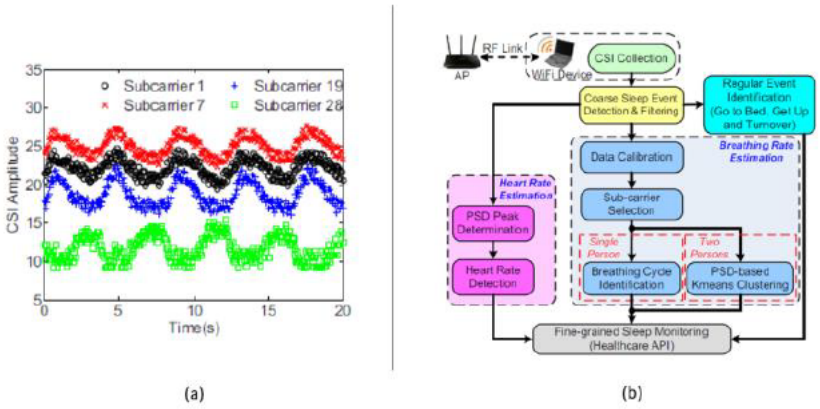

Figure 3.19 Wi-Fi sensing of cardiopulmonary motion. Channel state information of four different subcarriers over time during sleep study are shown (a), along with an overview of the system design used to capture respiratory biometrics (b) [33].

systole) estimation, concurrently. The system, shown in Figure 3.19, utilizes multiple CSIs captured at different OFDM subcarriers to differentiate the small body movement of breathing and heartbeat. Their experiment shows that the CSI granularity in commercial devices is sufficient to track the cardiopulmonary vital signs of one isolated person, as well as two-people in a bed, which covers typical in-home scenarios.

In [56], Liu et al. combined the CSI-based approach with a deep neural network to achieve continuous, non-intrusive, user verification, as illustrated in Figures 3.20 and 3.21. The design collects respiratory-related patterns in CSI by applying an empirical mode decomposition (EMD)-based adaptive filter, which mitigates immanent radio interference and other irrelevant body movement [59]. The resulting patterns are further processed through waveform morphology analysis and fuzzy wavelet packet transforms (FWPT) to construct unique respiratory biometrics, which are input to a two-hidden-layer neural network for user classification. [57].

Fundamentally, WiFi setups for human identification can be regarded as bistatic or multistatic radar systems, in which the transmitter(s) and receiver(s) are separated. Comparing to monostatic radar systems, such as CW radar, the transmitter(s) and

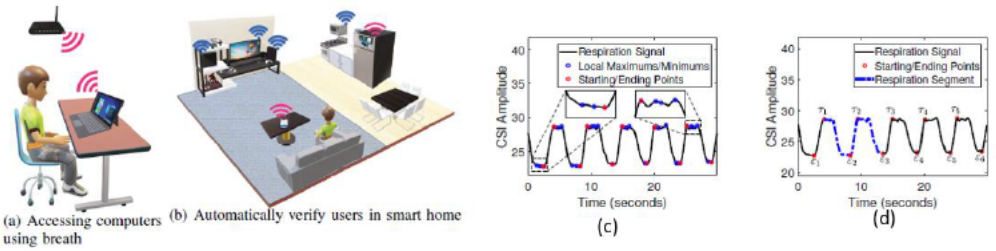

Figure 3.20 Example of continuous user verification using WiFi signals leveraging respiratory pattern. The concept is illustrated, (a) and (b), along with morphological respiratory features of captured waveforms using WiFi signals, (c) and (d). From [32].

receiver(s) in these configurations operate independently and lack coherency, which limits radar sensitivity and resolution. The issue is partially compensated by the packet synchronization mechanism of the WiFi protocol, which, however, introduces latency in target detection. Methods using RSS are generally less sensitive to subtle body movement, compared to CSI-based approaches, due to the lack of phase information. In contrast, the latter exhibits less tolerance to background noise and synchronization errors. Current research to improve the reliability of WiFi-based identity verification engages the problem using a two-pronged approach. The data analytic approach aims to extract more distinguishable and consistent features from the WiFi signals using state-of the-art machine learning or statistical learning algorithms. The device-and-spectrum approach aims to suppress the irrelevant signal and directly capture the physiological signatures by exploiting the frequency and bandwidth advantages of new 802.11 protocol family members, such as 802.11ad. [57].

3.3 Conclusion

The section 3.1 reviews the research related to the vital sign monitoring on multiple subject environments. Over the four decades, there has been significant advancements

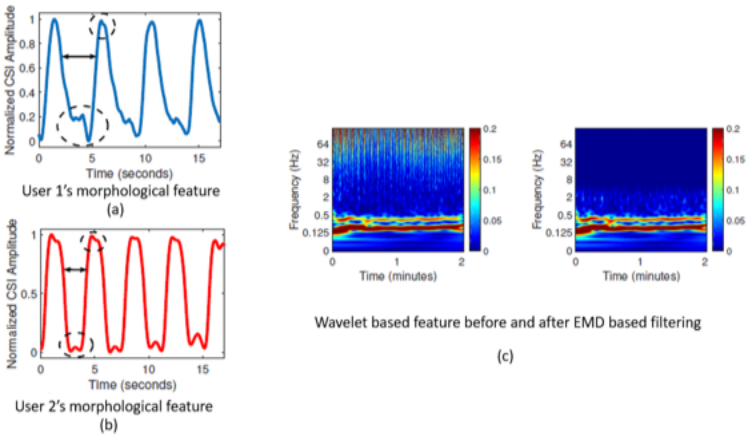

Figure 3.21 Waveform morphology analysis with EMD. Morphological features representing the respiratory pattern of two different participants in an experiment are shown, (a) and (b), along with fuzzy wavelet-based features which represent the frequency domain components of the respiratory pattern (c). After EMD filtering much of the noise and interference is removed. From [32].

both in hardware level and signal processing part in the Doppler radar sensor for healthcare monitoring in multi-subject scenarios. However, ongoing work should focus on the below challenges that are still unresolved by the reported researches:

1. Antenna resolution limit and beamwidth: There is a certain antenna resolution limit which also affects the minimum resolution limit for two subjects for separating their respiratory patterns. Beamforming and beam steering is gaining attention for solving this problem but there are unresolved questions, for example in a typical beamwidth 30 degree how many people can be accommodated for isolation their life signatures.

2. Breathing diversity:Breathing pattern changes with emotional stress and physiological activities. With the change of breathing pattern, the efficacy of the proposed methods needs to be tested for the robustness of the system.

3. Random body movement: Random body movement is another fundamental challenge that needs to be addressed as well. For separating respiratory signatures during

random body movement how to design an efficient algorithm is remains an unexplored area.

This area of continuing investigation has already made a significant advancement. With the help of new hardware architecture and signal processing algorithms, Doppler radar sensor will be able to overcome this fundamental challenge to become common devices for healthcare monitoring.

The section 3.2.3 reviews principles and research relating to the identification of people from radar captured cardiopulmonary patterns. Over four decades, there have been significant advancements in theory and engineering directed to enable biomedical Doppler radar for healthcare monitoring. However, achieving persistent and reliable measurements and recognition of multiple targets remains the primary obstacle toward a practical implementation. On this front, there are several promising results attained under controlled laboratory environments. However, large-scale studies for varying physiological conditions are yet to be conducted, and solution spaces yet to be explored. With recent advances in machine learning and artificial intelligence, human identification based on breathing patterns and heart-based dynamics demand further investigation for the potential to form a sound alternative to traditional biometric systems. By overcoming this fundamental challenge, microwave Doppler radar sensors can become common devices for daily activities monitoring. Continued experimentation and further exploration are required to bring this unobtrusive form of identity authentication system into real-world application.

References

[1] C. Gouveia, C. Loss, P. Pinho, and J. Vieira, "Different Antenna Designs for Non-Contact Vital Signs Measurement: A Review," *Electronics*, vol. 8, p. 1294, Nov. 2019.

[2] C. Li, V. M. Lubecke, O. Boric-Lubecke, and J. Lin, "A Review on Recent Advances in Doppler Radar Sensors for Noncontact Healthcare Monitoring," *IEEE Transactions on Microwave Theory and Techniques*, vol. 61, pp. 2046–2060, May 2013.

[3] O. Boric-Lubecke, V. Lubecke, A. Host-Madsen, D. Samardzija, and K. Cheung, "Doppler Radar Sensing of Multiple Subjects in Single and Multiple Antenna Systems," in *TELSIKS 2005 - 2005 uth International Conference on Telecommunication in ModernSatellite, Cable and Broadcasting Services*, vol. 1, (Nis, Serbia and Montenegro), pp. 7–11, IEEE, 2005.

[4] D. Samardzija, B.-K. Park, O. Boric-Lubecke, V. Lubecke, A. Host-Madsen, and T. Sizer, "Experimental Evaluation of Multiple Antenna Techniques for Remote Sensing of Physiological Motion," in *2007 IEEE/MTT-S International Microwave Symposium*, (Honolulu, HI, USA), pp. 1735–1738, IEEE, June 2007.

[5] Qin Zhou, Jianhan Liu, A. Host-Madsen, O. Boric-Lubecke, and V. Lubecke, "Detection of Multiple Heartbeats Using Doppler Radar," in *2006 IEEE International Conference on Acoustics Speed and Signal Processing Proceedings*, vol. 2, (Toulouse, France), pp. II–1160–II–1163, IEEE, 2006.

[6] N. Petrochilos, M. Rezk, A. Høst-Madsen, V. Lubecke, and O. Boric-Lubecke, "Blind separation of Human Heartbeats and Respiration by the use of a Doppler Radar Remote Sensing," p. 4.

[7] Y. S. Lee, P. N. Pathirana, R. J. Evans, and C. L. Steinfort, "Separation of Doppler radar-based respiratory signatures," *Medical & Biological Engineering & Computing*, vol. 54, pp. 1169–1179, Aug. 2016.

[8] K. Ishmael, A. Whitworth, E. Yavari, and O. Boric-Lubecke, "Single Antenna Continuous Wave Doppler Radar Detection for Multiple Moving Targets," in *2019 IEEE Radio and Wireless Symposium (RWS)*, (Orlando, FL, USA), pp. 1–4, IEEE, Jan. 2019.

[9] S. M. M. Islam, B. Tomota, A. Sylvester, and V. M. Lubecke, "A Programmable Robotic Phantom to Simulate the Dynamic Respiratory Motions of Humans for Continuous Identity Authentication," in *2019 IEEE Asia-Pacific Microwave Conference (APMC)*, (Singapore, Singapore), pp. 1408–1410, IEEE, Dec. 2019.

[10] S. M. M. Islam, E. Yavari, A. Rahman, V. M. Lubecke, and O. Boric-Lubecke, "Direction of Arrival Estimation of Physiological Signals of Multiple Subjects Using Phase Comparison Monopulse Radar," in *2018 Asia-Pacific Microwave Conference (APMC)*, (Kyoto), pp. 411–413, IEEE, Nov. 2018.

[11] S. M. M. Islam, E. Yavari, A. Rahman, V. M. Lubecke, and O. Boric-Lubecke, "Multiple Subject Respiratory Pattern Recognition and Estimation of Direction of Arrival using Phase-Comparison Monopulse Radar," in *2019 IEEE Radio and Wireless Symposium (RWS)*, (Orlando, FL, USA), pp. 1–4, IEEE, Jan. 2019.

[12] S. M. M. Islam, E. Yavari, A. Rahman, V. M. Lubecke, and O. Boric-Lubecke, "Separation of Respiratory Signatures for Multiple Subjects Using Independent Component Analysis with the JADE Algorithm," in *2018 40th Annual International*

Conference of the IEEE Engineering in Medicine and Biology Society (EMBC), (Honolulu, HI), pp. 1234–1237, IEEE, July 2018.

[13] S. M. M. Islam, O. Boric-Lubecke, and V. M. Lubekce, "Concurrent Respiration Monitoring of Multiple Subjects by Phase-Comparison Monopulse Radar Using Independent Component Analysis (ICA) With JADE Algorithm and Direction of Arrival (DOA)," *IEEE Access*, vol. 8, pp. 73558–73569, 2020.

[14] M. Nosrati, S. Shahsavari, and N. Tavassolian, "Multi-Target Vital-Signs Monitoring Using a Dual-Beam Hybrid Doppler Radar," in *2018 IEEE International Microwave Biomedical Conference (IMBioC)*, (Philadelphia, PA), pp. 58–60, IEEE, June 2018.

[15] M. Nosrati, S. Shahsavari, S. Lee, H. Wang, and N. Tavassolian, "A Concurrent Dual-Beam Phased-Array Doppler Radar Using MIMO Beamforming Techniques for Short-Range Vital-Signs Monitoring," *IEEE Transactions on Antennas and Propagation*, vol. 67, pp. 2390–2404, Apr. 2019.

[16] J. Xiong, H. Zhang, H. Hong, H. Zhao, X. Zhu, and C. Li, "Multi-target Vital Signs Detection Using SIMO Continuous-wave Radar with DBF Technique," in *2020 IEEE Radio and Wireless Symposium (RWS)*, (San Antonio, TX, USA), pp. 194–196, IEEE, Jan. 2020.

[17] F.-K. Wang, T.-S. Horng, K.-C. Peng, J.-K. Jau, J.-Y. Li, and C.-C. Chen, "Detection of Concealed Individuals Based on Their Vital Signs by Using a See-Through-Wall Imaging System With a Self-Injection-Locked Radar," *IEEE Transactions on Microwave Theory and Techniques*, vol. 61, pp. 696–704, Jan. 2013.

[18] G. Wang, C. Gu, T. Inoue, and C. Li, "A Hybrid FMCW-Interferometry Radar for Indoor Precise Positioning and Versatile Life Activity Monitoring," *IEEE Transactions on Microwave Theory and Techniques*, vol. 62, pp. 2812–2822, Nov. 2014.

[19] H. Lee, B.-H. Kim, and J.-G. Yook, "Path Loss Compensation Method for Multiple Target Vital Sign Detection with 24-GHz FMCW Radar," in *2018 IEEE Asia-Pacific*

Conference on Antennas and Propagation (APCAP), (Auckland), pp. 100–101, IEEE, Aug. 2018.

[20] H. Lee, B.-H. Kim, J.-K. Park, and J.-G. Yook, "A Novel Vital-Sign Sensing Algorithm for Multiple Subjects Based on 24-GHz FMCW Doppler Radar," *Remote Sensing*, vol. 11, p. 1237, May 2019.

[21] F. Adib, H. Mao, Z. Kabelac, D. Katabi, and R. C. Miller, "Smart Homes that Monitor Breathing and Heart Rate," in *Proceedings of the 33rd Annual ACM Conference on Human Factors in Computing Systems - CHI '15*, (Seoul, Republic of Korea), pp. 837–846, ACM Press, 2015.

[22] M. Mercuri, I. R. Lorato, Y.-H. Liu, F. Wieringa, C. V. Hoof, and T. Torfs, "Vital-sign monitoring and spatial tracking of multiple people using a contactless radar-based sensor," *Nature Electronics*, vol. 2, pp. 252–262, June 2019.

[23] A. Ahmad, J. C. Roh, D. Wang, and A. Dubey, "Vital signs monitoring of multiple people using a FMCW millimeter-wave sensor," in *2018 IEEE Radar Conference (RadarConf18)*, (Oklahoma City, OK), pp. 1450–1455, IEEE, Apr. 2018.

[24] T. Sakamoto, P. J. Aubry, S. Okumura, H. Taki, T. Sato, and A. G. Yarovoy, "Noncontact Measurement of the Instantaneous Heart Rate in a Multi-Person Scenario Using ${X}$ -Band Array Radar and Adaptive Array Processing," *IEEE Journal on Emerging and Selected Topics in Circuits and Systems*, vol. 8, pp. 280–293, June 2018.

[25] G. Gennarelli, L. Crocco, and F. Soldovieri, "Doppler Radar for Real-Time Surveillance," in *2018 18th Mediterranean Microwave Symposium (MMS)*, (Istanbul), pp. 387–390, IEEE, Oct. 2018.

[26] F. Lin, C. Song, Y. Zhuang, W. Xu, C. Li, and K. Ren, "Cardiac Scan: A Non-contact and Continuous Heart-based User Authentication System," in *Proceedings of the 23rd Annual International Conference on Mobile Computing and Networking*, (Snowbird Utah USA), pp. 315–328, ACM, Oct. 2017.

[27] S. C. Dass and A. K. Jain, "Fingerprint-Based Recognition," *Technometrics*, vol. 49, pp. 262–276, Aug. 2007.

[28] A. Maceo, M. Carter, and B. Stromback, "Palm Prints," in *Encyclopedia of Forensic Sciences*, pp. 29–36, Elsevier, 2013.

[29] K. Nguyen, C. Fookes, R. Jillela, S. Sridharan, and A. Ross, "Long range iris recognition: A survey," *Pattern Recognition*, vol. 72, pp. 123–143, Dec. 2017.

[30] K. P. Thomas and A. Vinod, "Toward EEG-Based Biometric Systems: The Great Potential of Brain-Wave-Based Biometrics," *IEEE Systems, Man, and Cybernetics Magazine*, vol. 3, pp. 6–15, Oct. 2017.

[31] K. Shaheed, H. Liu, G. Yang, I. Qureshi, J. Gou, and Y. Yin, "A Systematic Review of Finger Vein Recognition Techniques," *Information*, vol. 9, p. 213, Aug. 2018.

[32] S. Chen, J. Lach, B. Lo, and G.-Z. Yang, "Toward Pervasive Gait Analysis With Wearable Sensors: A Systematic Review," *IEEE Journal of Biomedical and Health Informatics*, vol. 20, pp. 1521–1537, Nov. 2016.

[33] K. Ricanek, M. Savvides, D. L. Woodard, and G. Dozier, "Unconstrained Biometric Identification: Emerging Technologies," *Computer*, vol. 43, pp. 56–62, Feb. 2010.

[34] P. van Dorp and F. Groen, "Feature-based human motion parameter estimation with radar," *IET Radar, Sonar & Navigation*, vol. 2, pp. 135–145, Apr. 2008.

[35] D. Vivet, A. Derbel, and B. Emile, "Access control based on gait analysis and face recognition," *Electronics Letters*, vol. 51, pp. 751–752, May 2015.

[36] M. Balazia and K. N. Plataniotis, "Human gait recognition from motion capture data in signature poses," *IET Biometrics*, vol. 6, pp. 129–137, Mar. 2017.

[37] S. Springer and G. Yogev Seligmann, "Validity of the Kinect for Gait Assessment: A Focused Review," *Sensors*, vol. 16, p. 194, Feb. 2016.

[38] V. C. Chen, "Micro-Doppler effect of micromotion dynamics: a review," (Orlando, FL), p. 240, Apr. 2003.

[39] A. Rahman, E. Yavari, V. M. Lubecke, and O.-B. Lubecke, "Noncontact Doppler radar unique identification system using neural network classifier on life signs," in *2016 IEEE Topical Conference on Biomedical Wireless Technologies, Networks, and Sensing Systems (BioWireleSS)*, (Austin, TX, USA), pp. 46–48, IEEE, Jan. 2016.

[40] G. Benchetrit, "Breathing pattern in humans: diversity and individuality," *Respiration Physiology*, vol. 122, pp. 123–129, Sept. 2000.

[41] E. W. Raff, Hershel, *Vander's Human Physiology: The Mechanisms of Body Function.*

[42] Douglas P. Zipes, *Braunwald's Heart Disease: A Textbook of Cardiovascular Medicine Single Volume.*

[43] P. Hung, S. Bonnet, R. Guillemaud, E. Castelli, and P. T. N. Yen, "Estimation of respiratory waveform using an accelerometer," in *2008 5th IEEE International Symposium on Biomedical Imaging: From Nano to Macro*, (Paris, France), pp. 1493–1496, IEEE, May 2008.

[44] J. E. Hall, *Gayton and Hall Textbook of Medical Physiology.* Elsevier Health Sciences: Amsterdam, The Netherlands.

[45] K. E. Barrett, *S. Ganong's Review of Medical Physiology.* McGraw Hill: New Delhi, India,, 2010.

[46] S. M. M. Islam, O. Borić-Lubecke, Y. Zheng, and V. M. Lubecke, "Radar-Based Non-Contact Continuous Identity Authentication," *Remote Sensing*, vol. 12, p. 2279, July 2020.

[47] S. M. M. Islam, A. Rahman, N. Prasad, O. Boric-Lubecke, and V. M. Lubecke, "Identity Authentication System using a Support Vector Machine (SVM) on

Radar Respiration Measurements," in *2019 93rd ARFTG Microwave Measurement Conference (ARFTG)*, (Boston, MA, USA), pp. 1–5, IEEE, June 2019.

[48] A. Rahman, V. M. Lubecke, O. Boric-Lubecke, J. H. Prins, and T. Sakamoto, "Doppler Radar Techniques for Accurate Respiration Characterization and Subject Identification," *IEEE Journal on Emerging and Selected Topics in Circuits and Systems*, vol. 8, pp. 350–359, June 2018.

[49] S. M. M. Islam, A. Sylvester, G. Orpilla, and V. M. Lubecke, "Respiratory Feature Extraction for Radar-Based Continuous Identity Authentication," in *2020 IEEE Radio and Wireless Symposium (RWS)*, (San Antonio, TX, USA), pp. 119–122, IEEE, Jan. 2020.

[50] S. M. M. Islam, A. Rahman, E. Yavari, M. Baboli, O. Boric-Lubecke, and V. M. Lubecke, "Identity Authentication of OSA Patients Using Microwave Doppler radar and Machine Learning Classifiers," in *2020 IEEE Radio and Wireless Symposium (RWS)*, (San Antonio, TX, USA), pp. 251–254, IEEE, Jan. 2020.

[51] D. Rissacher and D. Galy, "Cardiac radar for biometric identification using nearest neighbour of continuous wavelet transform peaks," in *IEEE International Conference on Identity, Security and Behavior Analysis (ISBA 2015)*, (Hong Kong), pp. 1–6, IEEE, Mar. 2015.

[52] K. Shi, C. Will, R. Weigel, and A. Koelpin, "Contactless person identification using cardiac radar signals," in *2018 IEEE International Instrumentation and Measurement Technology Conference (I2MTC)*, (Houston, TX), pp. 1–6, IEEE, May 2018.

[53] T. Okano, S. Izumi, H. Kawaguchi, and M. Yoshimoto, "Non-contact biometric identification and authentication using microwave Doppler sensor," in *2017 IEEE Biomedical Circuits and Systems Conference (BioCAS)*, (Torino), pp. 1–4, IEEE, Oct. 2017.

[54] P. Cao, W. Xia, and Y. Li, "Heart ID: Human Identification Based on Radar Micro-Doppler Signatures of the Heart Using Deep Learning," *Remote Sensing*, vol. 11, p. 1220, May 2019.

[55] J. Zhang, B. Wei, W. Hu, and S. S. Kanhere, "WiFi-ID: Human Identification Using WiFi Signal," in *2016 International Conference on Distributed Computing in Sensor Systems (DCOSS)*, (Washington, DC, USA), pp. 75–82, IEEE, May 2016.

[56] J. Liu, Y. Chen, Y. Dong, Y. Wang, T. Zhao, and Y.-D. Yao, "Continuous User Verification via Respiratory Biometrics," p. 10.

[57] H. Abdelnasser, K. A. Harras, and M. Youssef, "UbiBreathe: A Ubiquitous non-Invasive WiFi-based Breathing Estimator," in *Proceedings of the 16th ACM International Symposium on Mobile Ad Hoc Networking and Computing - MobiHoc '15*, (Hangzhou, China), pp. 277–286, ACM Press, 2015.

[58] J. Liu, Y. Wang, Y. Chen, J. Yang, X. Chen, and J. Cheng, "Tracking Vital Signs During Sleep Leveraging Off-the-shelf WiFi," in *Proceedings of the 16th ACM International Symposium on Mobile Ad Hoc Networking and Computing - MobiHoc '15*, (Hangzhou, China), pp. 267–276, ACM Press, 2015.

[59] N. E. Huang, Z. Shen, S. R. Long, M. C. Wu, H. H. Shih, Q. Zheng, N.-C. Yen, C. C. Tung, and H. H. Liu, "The empirical mode decomposition and the Hilbert spectrum for nonlinear and non-stationary time series analysis," *Proceedings of the Royal Society of London. Series A: Mathematical, Physical and Engineering Sciences*, vol. 454, pp. 903–995, Mar. 1998.

Chapter 4

Subject Separation Proposed Techniques

Doppler radar life sensing has shown its efficacy in medical and security applications, however, the presence of multiple subjects limit the usefulness of this technique [1]. When there is presence of multiple subjects in front of the radar sensor it gets combined mixture of breathing pattern which is hard to separate independent respiratory signatures from the combined mixtures [2]. This chapter discusses about proposed techniques to overcome the challenges of multi-subject. We proposed two different approaches to overcome this challenge, one is direction of arrival (DOA) and another one is Independent component analysis with joint approximation of diagonalization of Eigematrices (ICA-JADE). We will describe in details about two different approaches in the next subsections. 24-GHz phase-comparison monopulse radar has been employed in all the experimental scenarios because of its inherent capability of estimating the direction of arrival of the target. Finally, an intelligent signal-to-noise ratio (SNR-based) decision algorithm has been developed by combining two different approaches which will be described in the next subsection.

4.1 Theoretical Background:Respiration Monitoring of Multiple-Subject Using Microwave Doppler Radar

In a homodyne CW Doppler radar system a monotonic source of electromagnetic wave is transmitted continuously and can be represented as:

$$T\left(t\right) = Acos(2\pi ft + \phi(t)) \tag{4.1}$$

Where, A, f_0 are the amplitude and frequency of the transmitted signal. $\phi(t)$ is the arbitrary phase noise of the signal source. In a single subject measurement, the phase modulated signal at quadrature receiver is given by,

$$B_I(t) = A_B I\cos[4\pi d(t)/\lambda + 4\pi x(t)/\lambda + \delta\phi(t)] \tag{4.2}$$

$$B_Q(t) = A_B Q\sin[4\pi d(t)/\lambda + 4\pi x(t)/\lambda + \delta\phi(t)] \tag{4.3}$$

Where, θ,λ,$\delta\phi(t)$,d,x(t) represents the constant phase shift, wavelength, residual phase noise of the oscillator, distance from the receiver end and abdomen displacement respectively. When multiple subjects are present within the range of Doppler radar,each receiver receives a mixture of signals from all subjects shown below in Fig 4.1.

$$B_I1\ (t) = A_B I\cos((4\pi d_o)/\lambda + (4\pi x_1\ (t))/\lambda + \delta\phi(t)) \tag{4.4}$$

$$B_I2\ (t) = A_B I\cos((4\pi d_o)/\lambda + (4\pi x_2\ (t))/\lambda + \delta\phi(t)) \tag{4.5}$$

$$B_I3\ (t) = A_B I\cos((4\pi d_o)/\lambda + (4\pi x_3\ (t))/\lambda + \delta\phi(t)) \tag{4.6}$$

$$B_IN\ (t) = A_B I\cos((4\pi d_o)/\lambda + (4\pi x_N\ (t))/\lambda + \delta\phi(t)) \tag{4.7}$$

Similarly, quadrature signals are,

$$B_Q1\ (t) = A_B Q\sin((4\pi d_o)/\lambda + (4\pi x_1\ (t))/\lambda + \delta\phi(t)) \tag{4.8}$$

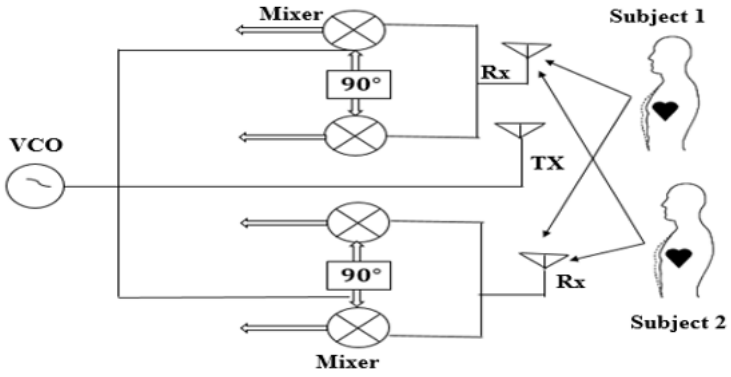

Figure 4.1 Multiple subject measurement with Doppler radar quadrature receivers. Due to the presence of two subjects each receiver is receiving a combined mixtures of breathing pattern from two subjects.

$$B_Q 2\ (t) = A_B Q \sin((4\pi d_o)/\lambda + (4\pi x_2\ (t))/\lambda + \delta\phi(t)) \tag{4.9}$$

$$B_Q 3\ (t) = A_B Q \sin((4\pi d_o)/\lambda + (4\pi x_3\ (t))/\lambda + \delta\phi(t)) \tag{4.10}$$

$$B_Q N\ (t) = A_B I \sin((4\pi d_o)/\lambda + (4\pi x_N\ (t))/\lambda + \delta\phi(t)) \tag{4.11}$$

Suppose there is one K-MC4 transceiver (one transmitter and two receivers) and two subjects present; so N=M=2 where, N is the number of subjects and M is the number of receivers, the received signal can be represented by: mixture of signals from all subjects shown below in Figure 4.1. Where, a_{ij} are the mixing parameters, in general N=M=X,

$$\begin{bmatrix}\text{Receiver}_1\\ \text{Receiver}_2\end{bmatrix} = \begin{bmatrix}a_{11} & a_{12}\\ a_{21} & a_{22}\end{bmatrix}\begin{bmatrix}B_{I1}(t)\\ B_{I2}(t)\end{bmatrix} + j\begin{bmatrix}a_{11} & a_{12}\\ a_{21} & a_{22}\end{bmatrix}\begin{bmatrix}B_{Q1}(t)\\ B_{Q2}(t)\end{bmatrix}$$

$$\begin{bmatrix}\text{Receiver}_1(t)\\ \text{Receiver}_2(t)\\ .\\ .\\ \text{Receiver}_N(t)\end{bmatrix} = \begin{bmatrix}a_{11} & \cdots & a_{1N}\\ \vdots & \ddots & \vdots\\ a_{N1} & \cdots & a_{NN}\end{bmatrix}\begin{bmatrix}B_{I1}(t)\\ B_{I2}(t)\\ .\\ .\\ B_{IN}(t)\end{bmatrix} + j\begin{bmatrix}a_{11} & \cdots & a_{1N}\\ \vdots & \ddots & \vdots\\ a_{N1} & \cdots & a_{NN}\end{bmatrix}\begin{bmatrix}B_{Q1}(t)\\ B_{Q2}(t)\\ .\\ .\\ B_{QN}(t)\end{bmatrix}$$

where X=1, 2, 3, .N.

4.2 Phased Array Monopulse Radar Architecture

K-MC4 module contains two coherent receivers with each receiver provides in phase (I) and quadrature phase (Q) channels [3]. The receiver antenna array has two receivers separated by 13.7 mm each with an independent receivers. Table 4.1 shows the important features of the module.We used this on shelf radar module as it can estimate the angular location of the target due to the antenna array elements. Figure 4.2 shows the K-MC4 radar transceiver module.

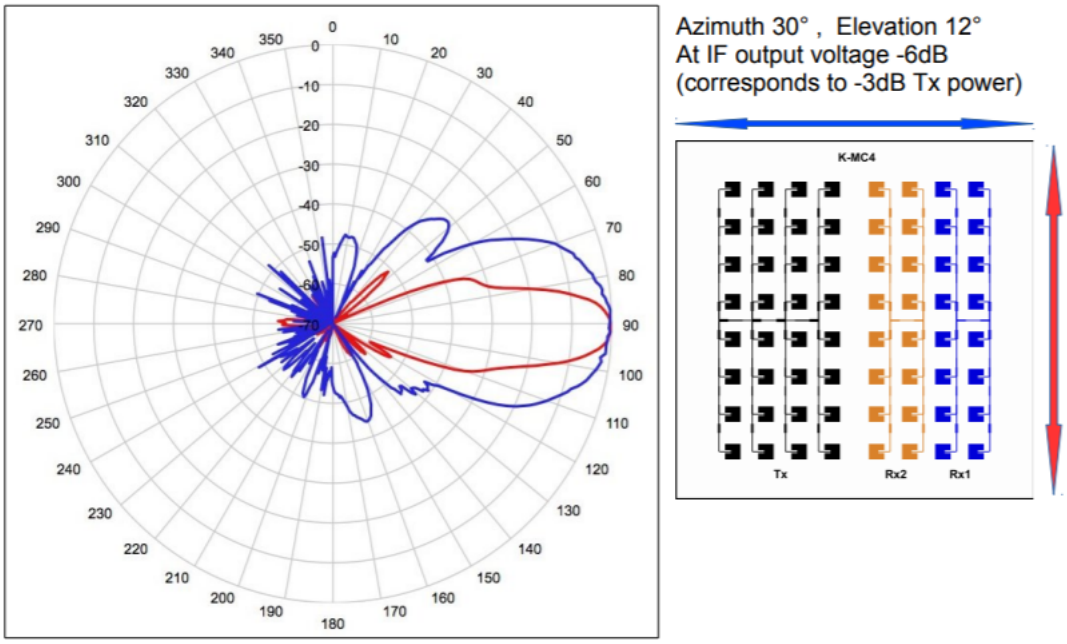

Figure 4.2 24-GHz K-MC4 radar transceiver antenna system diagram

4.2.1 Angular discrimination and radiation pattern

Angular discrimination of a radar is the minimum distance between two equal targets at the same range in which a radar can distinguish and separate each other [4].Figure 4.2 illustrates the schematic of angular discrimination and locations.The angular discrimination S_A from

Table 4.1 K-MC4 transceiver architecture

Properties	**Features**
Antenna array size	Transmitter: 4×8 patch, Receiver:2×8 patch
Antenna gain	13.0 dBi
Output power	18 dBm
Beam-width	30°
Distance between antenna elements	$\lambda/2$

sensors between two targets/subjects can be calculated as follows:

$$S_A \geq 2Rsin(\theta/2) \tag{4.12}$$

Where, R= Slant range of targets/subjects from sensor, θ=Beamwidth of the transmitting array, S_A= angular discrimination specified as distances between two subjects.Suppose if slant range of two subjects from radar is 1 meter then using K-MC4 radar transceiver module we can separate two subjects within their angular discrimination will be 0.52 meter. If subjects become closer less than angular discrimination limit of K-MC4 transceiver

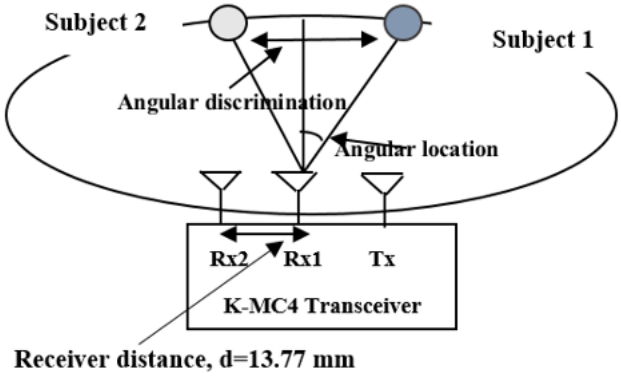

Figure 4.3 Appearance of measurement setup with the relationship between angular discrimination and angular locations. Here in the picture it clearly illustrates that the angular discrimination is the minimum separation distance between subjects where angular location can be determined.

then it is not possible to estimate the spatial position of subjects/targets [5][6][7].The radar transceiver angular discrimination is determined by the transmitting antenna -3 dB

beamwidth. Smaller the beamwidth higher the directivity of the radar transmitting antenna array pattern but at the same time it also increases the associated hardware cost [6][7].We have also utilized phased array system toolbox to explore K-MC4 transceiver radiation pattern. It has 8 array elements in its transmitter and 16 array elements in its receiver section. Figure 4.3 shows the transmitter and receiver array pattern (one transmitter and two receivers). From our simulation it is clear that the horizontal -3 dB beamwidth is approximately 30°.From the above analysis, we have also calculated the relationship between slant ranges with angular discrimination to estimate DOA perfectly within its main beamwidth of the transceiver Table 4.1 represents the experimental radial distances

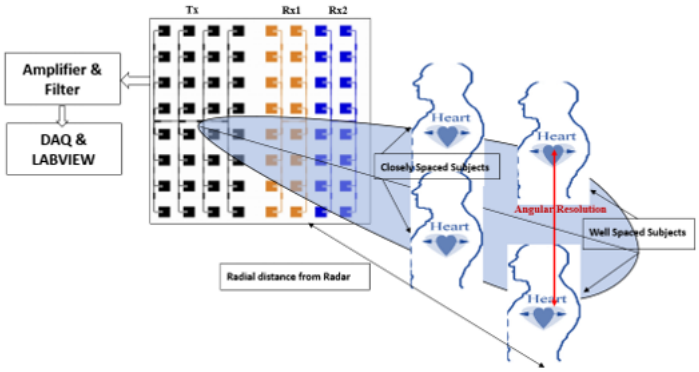

Figure 4.4 Schematic diagram of K-MC4 transceiver main beamwidth where subjects are located at the edge of the beamwidth and within the beamwidth. When subjects are located at the edge of the beamwidth they are well-spaced subjects as DOA estimation is possible. When subjects are within the beamwidth they are closely spaced subjects as DOA estimation is not possible when subjects become closely spaced.

and angular discrimination of transceiver what we have considered for the experiment. In our experiment, we have considered radial distances from 1 meter to 3 meter with two subjects and for each of the radial distances we have selected two different angular positions. One is within minimum angular discrimination limit for DOA estimation and another one is lesser than angular discrimination limit of that radial distances to test our hypothesis.

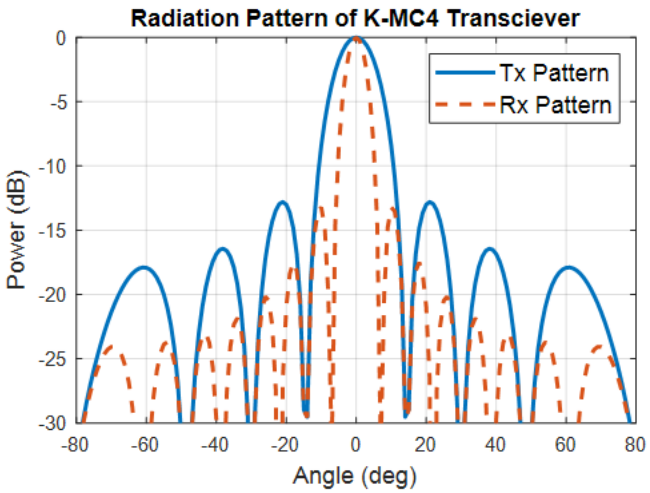

Figure 4.5 Radiation Pattern of K-MC4 transceiver (blue line indicates TX pattern and red line indicates Rx pattern).

Table 4.2 Relationship between radial distance, angular discrimination limit and selected angular discrimination limit

Slant ranges (m)	**Angular discrimination limit**	**Experimental dsicrimination limit**
R=1	0.52 m	0.52m(edge),0.4m(within)
R=1.5	0.78 m	0.78m(edge),0.5m(within)
R=2	1.04 m	1.04m(edge),0.7m(within)
R=2.5	1.294 m	1.29m(edge),1m(within)
R=3	1.55 m	1.55m(edge),1.22m(within)

4.3 Direction of Arrival (DOA) techniques

In signal processing, DOA is a technique which estimates the direction of propagating arrives at the receiver where multiple sensors are located [8].The set of sensor in the receiver section is called sensor array [9].In radar transceiver, there is another associated technique which is called beamforming, pointing the antenna radiation patterns in a given direction [8].We used two different approaches which is quite common and popular in the literature.As we used 24-GHz phased array radar whcih can estimate the angular location based on phase-comparison monopulse technique [10]. Another popular technique is multiple signal

classification (MUSIC) algorithm [9].We also compared their performances for estimating the spatial position of the target. In the next subsection we will describe about the basic principle of this techniques and our exploration on integrating them with the Doppler radar system.

4.3.1 Phased comparison Monopulse DOA technique

Monopulse is a technique where information concerning the spatial position of a target is estimated by comparing the signal properties (amplitude and phase) received simultaneously by two receivers [3][10].In this work we utilized an off-the-shelf K-MC4 module which is a 24-GHz phase comparison monopulse radar [14]. The K-MC4 is a Doppler transceiver with a 4×8 patch antenna array for the transmitter and two 2×8 patch antenna arrays for the receiver [3], as shown in Figure 4.6 (a). Figure 4.6 (b) shows the basic principle of the DOA estimation technique, where antenna arrays are separated by a distance d, with a wave front incident at an angle θ. Due to the path difference between the antenna array elements, incoming wave fronts experience a a phase difference of $\delta\phi$. The relationship between phase difference and path difference is:

$$kdsin(\theta) = \delta\phi \tag{4.13}$$

where, k is the wavelength of the transceiver. With a distance between two receiver elements

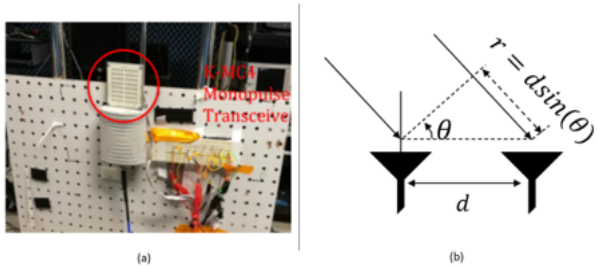

Figure 4.6 K-MC4 radar transceiver used in this experiment (a) and the principle of the phase-comparison monopulse technique to estimate the angular location of the target. The monopulse radar transceiver had a 4×8 patch antenna array for the transmitter and the two-receiver used 2×8 patch antenna arrays.

of 13.77 mm, the DOA can be calculated by simplifying the equation to:

$$6.7\theta = \delta\phi \tag{4.14}$$

where, $\delta\phi$ is the phase difference between the I channels (I1 and I2) and Q channels (Q1 and Q2). As the transceiver has a fixed number of antennas and beamwidth, it has a limited angular resolution [5][6][7].

4.3.2 Multiple signal classification (MUSIC)

The classic MUSIC algorithm is the most common approach for estimating DOA, basically using a peak search to estimate the arrival angle [9][11]. This algorithm uses Eigen value decomposition of the received signal covariance matrix. Using this algorithm, the pseudo spectrum of the received signal is calculated to derive the frequency content of the signal [3] [9][11].The peaks of the pseudo spectrum represent the Angle of Arrival (AOA) i.e. DOA, and higher estimation accuracy can be achieved at the expense of more extensive computational cost [5].

4.3.3 Experiments for DOA estimation of well-spaced subjects

In our first attempt, we mounted a 24 GHz KMC4 Monopulse radar with four channels (I1,I2,Q1 and Q2) connected to four LNA's (Stanford Research System Model SR650); All the LNA's were ac-coupled with a gain of 200, and low-pass filtered with cut-off frequency of 30 Hz. The four channel outputs were connected to a DAQ (NI-6009). Finally, a customized LABVIEW interface captured the signals.Two different experiments were performed using the above setup. In the first experiment, one subject sits at 2.89 m from the mounted radar transceiver and subject changes positions (7.5°,-15°,15°) at three different angular positions and in the next, two subjects two meters apart and each sat 2.89 meters away from the sensor with 30° angle from each other [6]. We have manually measured the relative angle

of subject from the sensor using a protractor. Figure 4.7 illustrates the presence of two subjects in front the radar.

After capturing data from the system, we filtered the signal using an FIR filter of order of thousand with cut off frequency of 10 Hz. Figure 4.8 and 4.9 show the filtered I and Q channel signal, FFT spectrum and I/Q plot for the experiment-2. From the FFT spectrum plot in Figure 4.8 there were two dominant breathing frequencies 0.2 Hz and 0.4 Hz which indicates the presence of two subjects in front of sensor. The phase difference measurement is based on discrete Fourier transform and maximum likelihood estimation of the signal properties and their initial phases [12] and phase difference between I_1 and I_2 channels is calculated as 79.50°. Using phase comparison technique equation 4.3, we have calculated DOA as 11.86° We have also compared the DOA estimation accuracy between single subject

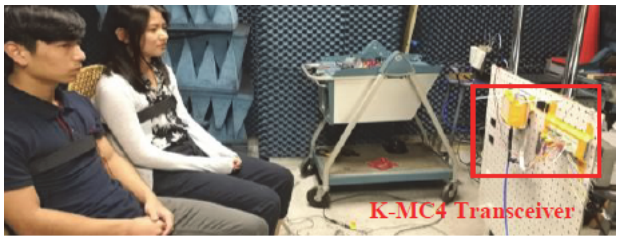

Figure 4.7 K-MC4 radar transceiver used in this experiment and two subjects were in seated position in font of the radar sensor and they also used chest belt for reference measurement

measurement and multiple subject's measurement. The experimental setup for estimating DOA is shown Figure 4.7. In single subject measurement we have three different angular positions and based on our experimental data we have calculated the estimation accuracy as almost 95% for single subject measurement and result is shown in Figure 4.10.In case of multiple subject measurement we have considered two different angular positions (15°,-15°) as the subjects are 30° form each other and the estimation accuracy is found to be 80% and the result is illustrated in Figure 4.11.The accuracy is not as good in multiple subject measurement due to the increased amount of multi-path for the presence of two subjects which usually becomes a dominant source of error for estimating the angular locations with the monopulse technique[10].Another significant factor reducing the estimation accuracy is

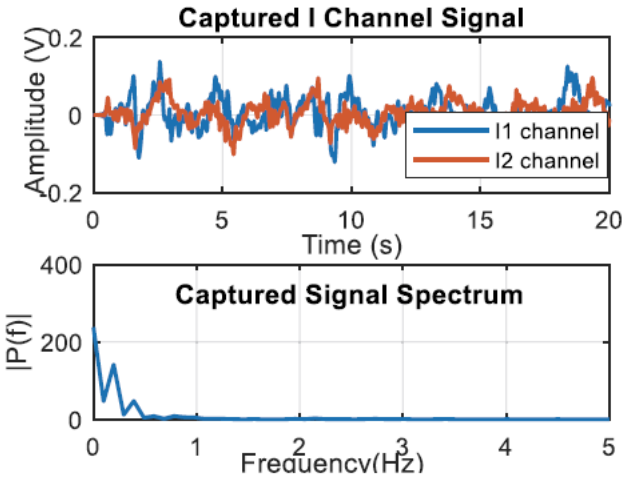

Figure 4.8 Measured I channel signals of two subjects at the distance of 2.89 meter with angular resolution of 30° and FFT of the combined mixture.

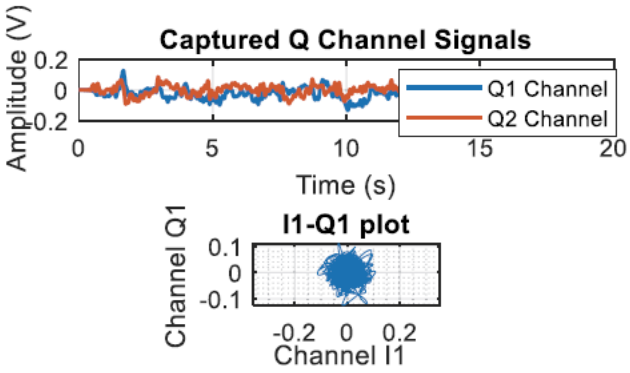

Figure 4.9 Measured Q channel signals of two subjects and I/Q plot

the grating lobe which arises if the antenna element spacing (13.77 mm) is greater than half of the operating wavelength (6.25 mm) then it also affects the overall estimation accuracy [10]. The estimation accuracy can be increased by using more precise model of the antenna array [3] but such low cost scalable system can be used for monitoring multiple subjects as it can estimate the angular location of subjects quite closely.

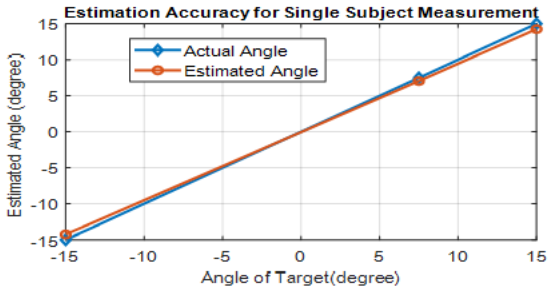

Figure 4.10 Comparative analysis of estimation accuracy of angle measurement for singe subject.Blue line represents actual angle and red line illustrates the estimated angle

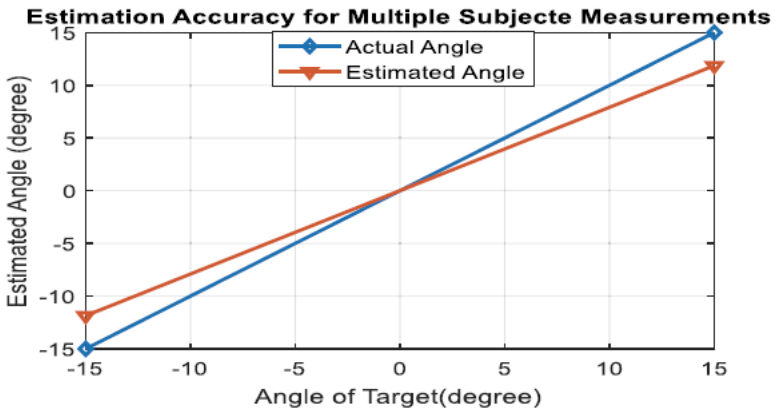

Figure 4.11 Estimation accuracy for multiple subject measurement

4.3.4 Experiments for DOA estimation using MUSIC algorithm

In this experiment we used a 24-GHz K-MC4 monopulse radar transceiver with four channels ac-coupled to four Low-noise amplifiers (LNA) (SR560), each with a cut-off frequency of 30 Hz and with gain of 200. The four outputs were connected to a DAQ (National Instrument) with a customized LABVIEW interface used to capture the respiration patterns[13].We used similar setup of the phase-comparison monopulse experiment. Two subjects were placed within the beamwidth of the transceiver, which for the K-MC4 radar was within a 12.5° azimuth angle from each other [3]. The subjects were seated 2.89 meters away from the radar keeping a 1.5-m angular discrimination limit between them. The relative angle

between the subject and the sensor was measured using a protractor.Figure 4.7 illustrates the experimental setup.

The captured signal was processed with an FIR filter of order 1000 with a cut off frequency of 10 Hz. The filter order was selected based on the sampling frequency of DAQ which was around 100 Hz. The selection of the10 Hz cut off frequency was based on the physiological motion signal bandwidth. Physiological motion signals from respiration and heartbeat lie within 0.01-2 Hz and a cut off frequency of almost five times of the highest frequency content of the signal was used. Post processing was performed in MATLAB [13]. illustrates the radar captured respiration patterns for a combined mixture of two different

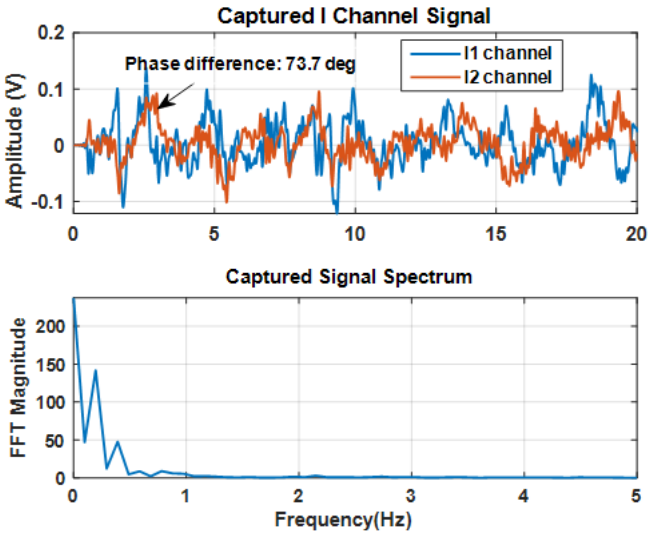

Figure 4.12 Radar captured respiration pattern for the combined mixture of two different channel signals (I1 and I2). An FFT of the signal shows two dominant peaks which illustrates the presence of two subjects in front of the radar.

subjects seated in front of the sensor. The phase difference was measured between the two corresponding channel signals (I1, I2 or Q1, Q2), and measured based using a fast Fourier transform (FFT) with a maximum likelihood estimation of the signal properties and their initial phases [12]. An FFT analysis of the mixed signal was performed to show the two dominant peaks which illustrate the presence of the two subjects in front of the sensor [6]

[12].The phase difference between the two channel signals is around 73.7°.To estimate the direction of arrival (DOA) we used equation 4.14 as in our previous work [5][6][7],which basically divides the phase difference by 6.7.So,the estimated direction of arrival of the physiological signal was approximately 11°.One potential advantage of this technique is that it is computationally fast as it requires only a single snapshot [6][7].The estimation accuracy is limited due to the grating lobe effect which occurs when the antenna element spacing (13.77 mm) is less than the half of the operating wavelength (6.25 mm) [6][7]. When multiple subjects are present there is unaccommodating multi-path which results in some error when estimating the phase from the FFT [10].However,the off the shelf system is adequate for proof of concept.

To increase the accuracy of estimating the angle of arrival (AOA) the MUSIC algorithm was also incorporated. To implement the MUSIC algorithm the received data from the Doppler radar system is taken in the form:

$$x\,[k] = [x_1, x_2, \ldots\ldots..x_n] \tag{4.15}$$

where,

$$x_n = x_{in} + jx_{Qn} \tag{4.16}$$

is the complex baseband signal comprised of the I and Q channels, N=4 is the number of demultiplexed IQ channels(I1,I2,Q1,Q2), and k=1... K is the total number of samples or snapshots required. The peaks of the pseudo spectrum are the estimated angle of arrival. Figure 4.13 illustrates the pseudospectrum of the signal utilizing the experimental data set. The pseudospectrum represents the two dominant peaks at the azimuth angle of 12° and -12° which also illustrates the presence of two subject in front of the radar.For simulating the above estimated DOA in MUSIC algorithm, we have used 1024 snapshots.Computational time for DOA estimation in MUSIC algorithm requires higher number of snapshots and it increases the computational cost also [9][11] whereas, phase comparison technique requires just one snapshot or sample point [9].Table 4.3 demonstrates the estimated

Table 4.3 Computational timing requirement for MUSIC. From [14]

Snapshots	Floating points	Vertex 7 FPGA
Nb=128 samples	97,000	0.61 μs
Nb=1024 samples	550,000	3.44μs

computational time for MUSIC algorithm using Virtex-7 FPGA [12]. We also compared the DOA estimation accuracy between two different techniques using our experimental data. Estimation accuracy is computed based on the following equation:

$$Accuracy \ = \mid Estimated\ DOA - measured\ DOA \mid / (measured\ DOA) * 100 \qquad (4.17)$$

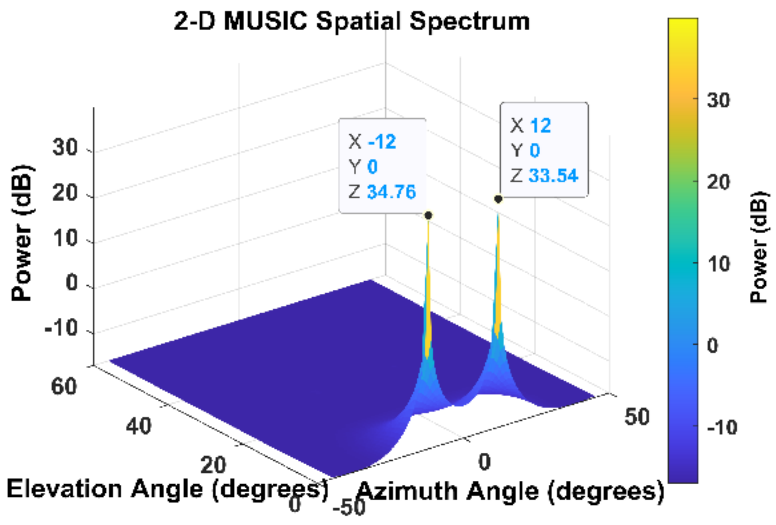

Figure 4.13 Radar captured combined signal pseudospectrum of MUSIC algorithm.The peak of the signal in the x-axis represents the angle of arrival which is around 12 °. The presence of two subjects in front of the radar sensor was measured around 12.5 ° azimuth angle.We did not consider the elevation angle as we used protractor for measuring the angle.

For estimating the accuracy, we also repeated the experiments for single subject at different angles and two subjects within the beamwidth of the transceiver. Estimation

accuracy for phase comparison technique is 88% whereas, MUSIC has 95% accuracy. Figure 4.14 represents the comparative analysis in estimation accuracy. Higher accuracy indicates the system has much more robustness with respect to noise and interference. The details of this comparative analysis provide a basis for understanding the benefits and trade offs for both DOA algorithms to develop a method for practical implementation. After estimating the angular location of subject more precisely we can switch the beam in certain direction by using mechanical rotator to isolate respiratory signatures from being mixed up with another respiratory pattern.

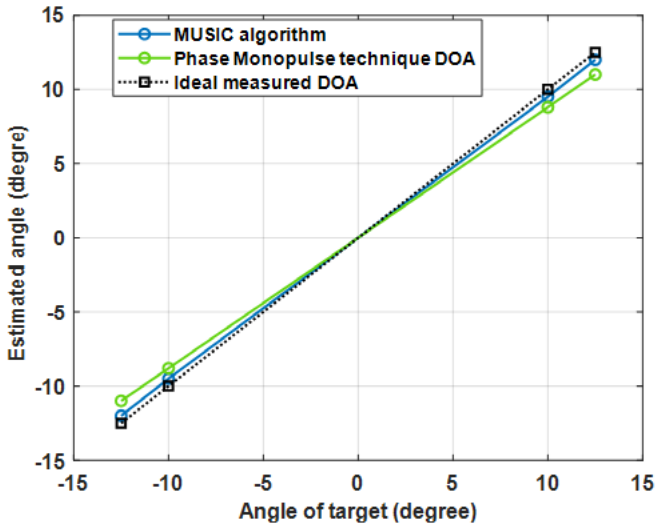

Figure 4.14 Comparative Analysis of estimation accuracy for different DOA methods. The blue line illustrates MUSIC estimated DOA and the green line represents phase comparison based DOA, while the black line illustrates the ideal measured DOA.

4.3.5 Experiments for DOA estimation of well-spaced subjects with varied breathing patterns

In this experiment, we used a 24-GHz K-MC4 Monopulse radar system with four channels (I1, I2, Q1, Q2), connected to four LNA's (Stanford Research System Model SR650); All the LNA's were ac-coupled with the gain of 200, and low-pass filtered with a cut-

off frequency of 30 Hz. The four output channels were connected to DAQ (NI-6009).A customized LABVIEW interface was used to capture all the signals. In this experiment, three different respiratory motions (normal, fast, and slow) of three different subjects within the main beamwidth (30°) of the transceiver at different angles (10°,15°,20°,25°), and at 1 meter away from the sensor. We also used a chest belt (UFI Model 1132 Pneumotrace II) as reference measurement for each subject, for each of the three different respiratory motion patterns. Similarly, we repeated the experiment for the simultaneous measurement of two subjects' and positioned at the edge of the beamwidth (30°) of the transceiver which is also the angular discrimination limit for two subjects to estimate DOA accurately. The goal of this experiments was to test the feasibility of DOA estimation accuracy for varied breathing patterns (normal, fast and slow).

After capturing the data from the system, we filtered the signal using an FIR filter with an order of one thousand with cut off frequency of 10 Hz. In the first experiment, we captured three different breathing motions (normal, fast and slow) of single subject at 1 meter away from the sensor. The purpose of this experiment was to test the efficacy of our system to capture different breathing patterns. Figure 4.15 represents the captured different breathing motions from a single subject at the angular location of 10° from Doppler radar sensor. The chest belt measurement closely correlate with the captured respiratory motion for normal and fast breathing whereas for slow breathing the peak of the respiration pattern from radar measurement does not closely correlates because of the distortion caused by ac-coupling of the LNA. The un-distorted results closely correlates with the chest belt respiration patterns which validates the efficacy of our proposed system to capture the three different respiratory motion patterns. We then performed similar experiments for two subjects within the angular discrimination limit of the transceiver for three different breathing patterns (normal, fast and slow).Figure 4.16 represents the filtered signal of two subjects I2 and Q2 signal of fast breathing and the constellation diagram. From the FFT spectrum two dominant breathing frequencies 1.953 Hz and 2.06 Hz which clearly indicates the presence of two subjects in front of the sensor. After that we measured the phase

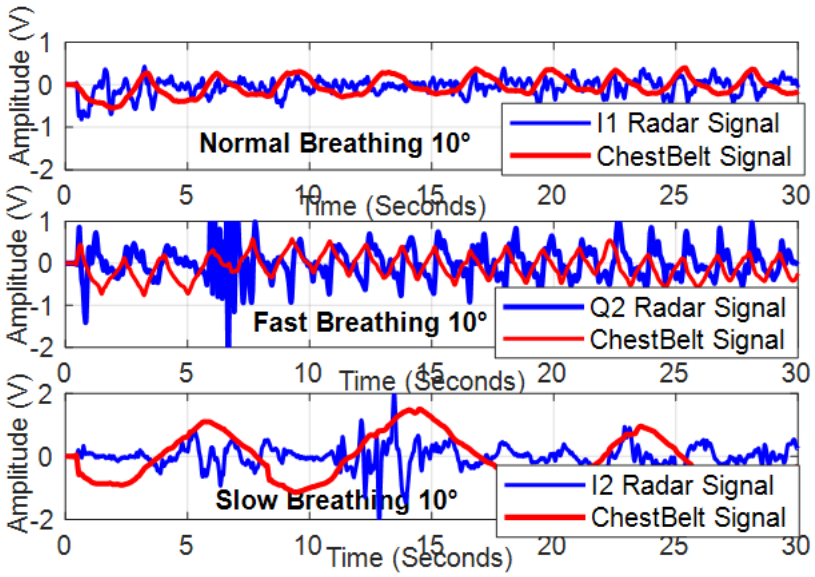

Figure 4.15 Captured three different breathing motions of a single subject at angular location of 10° and 1 meter away from radar.

Table 4.4 Summary of breathing pattern for single subject[7].

Breathing type	**Breathing cycles (60s)**	**Breathing rate**	**MSE**	**Accuracy**
Normal	19	0.32 Hz	.0171	84%
Slow	10	0.17 Hz	.1214	79%
Fast	76	1.26 Hz	.2692	56%

difference between I1,I2 and Q1,Q2 channels for single subject measurement and multiple subject signals for three different respiratory patterns. The phase difference measurement is based on discrete Fourier transform and maximum likelihood estimation of the signal properties and their initial phases [6][7].Using equation 4.14 we estimated the angle of arrival of physiological signal.For a single subject measurement, we used four different angular positions with three different breathing patterns.Table 4.4 represents the corresponding breathing cycle and rate for three different breathing patterns for a single subject.

Based on analysis of our experimental result, "normal breathing" rate is .32 Hz which indicates good estimation accuracy (84%) and with a low mean square error with respect to

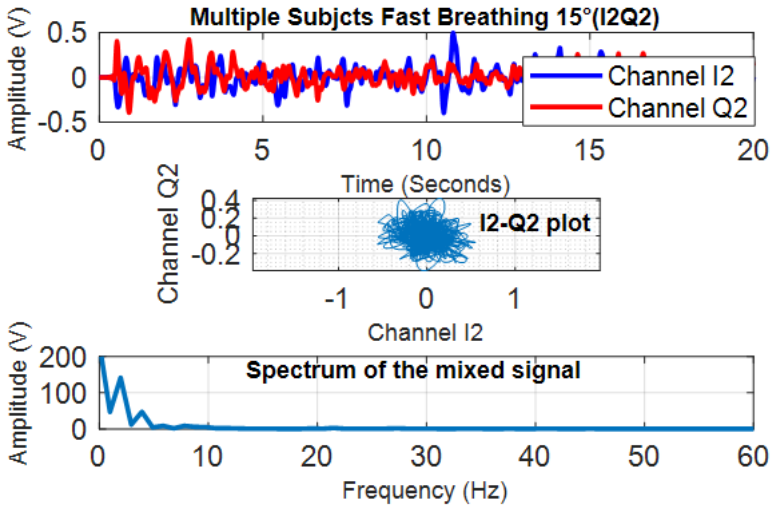

Figure 4.16 Captured fast breathing motions of multiple subjects 1 m away from the sensor, constellation plot (I2,Q2) and FFT.

reference measurement. The estimation accuracy graph is shown in Figure 4.16. In general, the DOA estimation error for the "fast breathing" case is higher than that of the "normal" and "slow" breathing case, due to difficulty test subjects had breathing at this rate without creating extraneous motion artifacts and with reproducing breathing pattern across tests. There is also increased error in the averaging effect for the increased number of breaths per sample window. In the case of normal and slow breathing patterns, there are less chest motion artifacts and a more manageable number of breathing cycles, results in smooth and consistent repetitive arc pattern provides higher SNR than for fast breathing thus more accurate phase measurement. Similarly, simultaneous and concurrent measurement of two subjects at two different angular locations (15°,-15°) was carried out, with three different breathing patterns. Table 4.5 represents the recorded corresponding breathing cycles and rates for two subjects. The dual subject measurement accuracy is not as good as the single subject measurement because of the increased amount of multipath in the presence of two subjects especially in the case of irregular breathing patterns (fast, slow).The motion artifacts for fast breathing cause the same SNR reduction and angle estimation problem as in

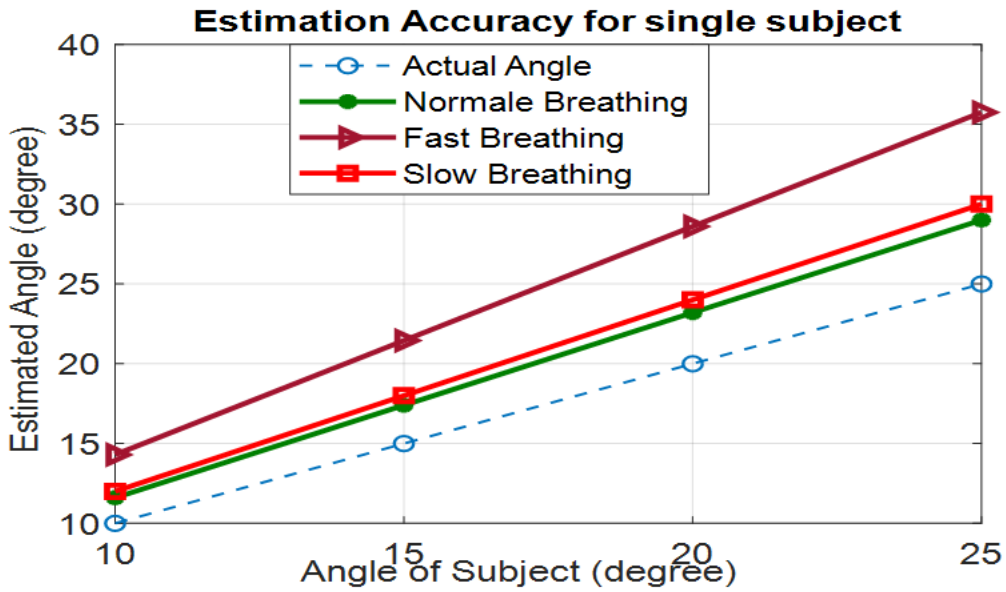

Figure 4.17 Estimation accuracy for single subject measurement

the single subject case, which becomes the dominant source of error for estimating angular location [6][7][8]. In case of normal breathing the accuracy was 78% having a repetitive pattern and an acceptable limit in the number of breathing cycles (12 to 20 breathing cycle per minutes) and rate. We could not obtain an accurate rate for the slow breathing case with two subjects present. We believe this is due to the ac-coupling distortion which increases as respiration rate slow down. While tolerable on the single subject measurements, the combined signal of two slow breathing subject's changes more slowly and thus results in greater distortion. The rate and angle estimation accuracy for all cases can be increased by using a precise model of the antenna array [7][8][9]. The overall results provide a convincing indication that such low-cost scalable systems can be used for monitoring multiple subjects as they can estimate the angular location of subjects with reasonable accuracy and also that such systems are robust to variations in respiratory pattern as long as the breathing cycle or rate remains within the specified limits.

Table 4.5 Summary of breathing pattern for multiple subject[7].

Breathing type	**Breathing cycles (60s)**	**Breathing rate**	**Accuracy**
Normal	sub1:11,sub2:23	sub1:.19,sub2:.39	78%
Slow	sub1:9,sub2:5	sub1:.15,sub2:.083	33%
Fast	sub1:118,sub2:234	sub1:1.96,sub2:2.06	1%

4.4 Independent Component Analysis (ICA)

Blind source separation (BSS) consists of recovering unobserved independent signal sources from several mixtures. The term blind signifies the fact that only prior knowledge of the source signal is their statistical independence. Basically the term "blind" illustrates the fact that (1) the sensors are unaware of the source signals (2) no other information is available about the source signal is immediately just beforehand [14]. Promising application of BSS are in the processing of communication signals [15], in biomedical signal like ECG and EEG. ICA is another important tool for performing BSS [16].

ICA is a powerful statistical method that recovers the independent source signals from combined mixture signals and generally uses higher order statistics [16].Several different algorithms are available among which Fast-ICA [15], Infomax and JADE [16]. We will be only focusing on JADE algorithm for this application.The major advantage for choosing JADE algorithm in this work is that it is based on matrix computation involving matrix diagonalization whereas other algorithm depends on an optimization procedure and hence variable results might occur. Suppose that two mixture signals x1 and x2 are linear combinations of two source signals. The linear mixture can be represented as:

$$x_1 = a_{11}s_1 + a_{12}s_2 \tag{4.18}$$

$$x_2 = a_{21}s_1 + a_{22}s_2 \tag{4.19}$$

In other words, it can be represented as: $X(t) = AS$; where, $X(t) = [x_1(t), x_2(t), \ldots\ldots, x_m(t)]^T$ is the linear combination of combined mixtures and

whose components are assumed to be statistically independent and $s(t) = [s_1(t), s_2(t), \ldots..s_n(t)]^T$ where, A is the full rank $m \times n$ mixing matrix. Then a separating or de-mixing matrix must be estimated under certain assumption and constraints [14] with a view to extracting independent source signals from mixtures. According to central limit theorem, if there is a combination of different independent sources then combined mixture is "more Gaussian" than independent sources. The objective of ICA is to find the least Gaussian possible sources. ICA aims to extract the pure source signals from combined mixtures by maximizing their non-gaussianity [15].

4.4.1 Joint Approximate Diagonalization of Eigenmatrices (JADE) Algorithm Basics

There are several different ways to find out the non-gaussianity of the source signals. One of them is the kurtosis of the signals [16]. In summary, ICA-JADE method attempts to recover separating matrix or demixing matrix, W based on non-gaussianity or independence of the signal sources from their combined mixtures. JADE algorithms is based on the fourth order cumulants or higher order statistics computation method. Several steps of JADE algorithm are [16]: Step 1: Whitening of X: Whitening is basically the preprocessing step where the

Algorithm 1: Joint Approximate Diagonalization of Eignematrices

Step 1: Whitening Data Matrix
Step 2: Cumulants Computation
Step 3: Eigen value Decomposition of cumulants tensor
Step 4: Diagonalization of Eignematrices
Step 5: Obtaining the Vectors of Proportions

data matrix is transformed into orthonormal column by removing the mean.

$$X_c = x - E[x]. \tag{4.20}$$

Then it is being multiplied with whitening matrix, B which is the transpose of differently scored scaled matrix.

$$B \times X_c = P_w^T \tag{4.21}$$

So, it consists of applying a linear transformation to the observation that its components are uncorrelated and have unit variance which is the fundamental difference between principal component analyses (PCA) which aims finding direction of high sample of dispersion.

Step 2: Cumulants Computation: The next step is to find out the fourth order cumulants which is kurtosis of the data set. After whitening we get P_w in which its column vectors are uncorrelated. If the signal vectors are independent the fourth order cumulants can be calculated as follows:

$$cum_4 \{P_w, P_W, P_w, P_w\} = E \{P_w\}^4 - 3E^2 \{P_w\}^2 \tag{4.22}$$

In this step, the fourth order cumulants tensor is being formed which is variance-covariance (statistics of 2nd order) matrix. The main diagonal element of this matrix is auto-cumulants whereas no diagonal elements are cross-cumulants. Two independent vectors are led to null cross cumulants while the auto cumulants are maximal that's why JADE algorithm tries to find out the rotation matrix to initialize so that the independent vectors are figured out.

Step 3: Decompose the cumulants tensor: In this step, a diagonal matrix can be obtained by Eigen value decomposition of the above covariance matrix.After this step set of symmetrical orthogonal diagonal matrix is being created.

Step 4: Joint diagonalization of the Eignematrices: After eigenvalue decomposition the diagonalization of eignematrices is done based on Jacobi algorithm which aims at minimizing the sum-of-squares of the off-diagonal elements. The rotation matrix obtained in this transformation produces independent vectors. Finally the pure source signal can be obtained by multiplying this rotation matrix which is separating or de-mixing matrix.

$$s(t) = Wx(t) \tag{4.23}$$

Step 5: Obtaining the Vectors of proportions: from the above equation X=AS, A can be obtained by projecting X onto S:

$$A = X_0 S^T \left(SS^T\right)^{-1} \tag{4.24}$$

Independent Components (ICs) are independent which means the correlation between different ICs are null.

4.4.2 Experiments for separating independent respiratory patterns for closely spaced subjects using ICA-JADE algorithm

In this experiment (Figure 4.18), two subjects each sat 2.89 m away from the sensor with 30° angle from each other[17]. Apart from four transceiver channels, chest belts were used for reference measurement in this trial. We have chosen 2.89 m as nominal distance because K-MC4 radar transceiver in Doppler mode operation, it has no range resolution bindings but for estimating DOA it has limited angular resolution capabilities [6].Angular resolution of a phase-comparison Monopulse radar is the minimum distance between two equal targets/subjects at the same range in which radar can distinguish and separate each other [3].When subjects become closer especially more than angular resolution limit then estimating DOA becomes difficult in our system [5].In this experiment, angular resolution is 1 meter between two subjects and at that time DOA fails to separate due to its fixed number of antenna arrays and beam width. So, by integrating ICA-JADE method can help to make our system more robust and ubiquitous and overcome the angular resolution limit of K-MC4 radar transceiver. This will be interesting to see the error curve with relation distance and angular separation of subjects between the sensor but remains as our future work to be explored.The experimental procedures involving human subjects described in this paper were approved by the Institutional Review Board.The Institution's Ethical Review Board approved all experimental procedures involving human subjects. After data acquisition of observed mixtures for two subjects, raw data was linearly demodulated and then mixed

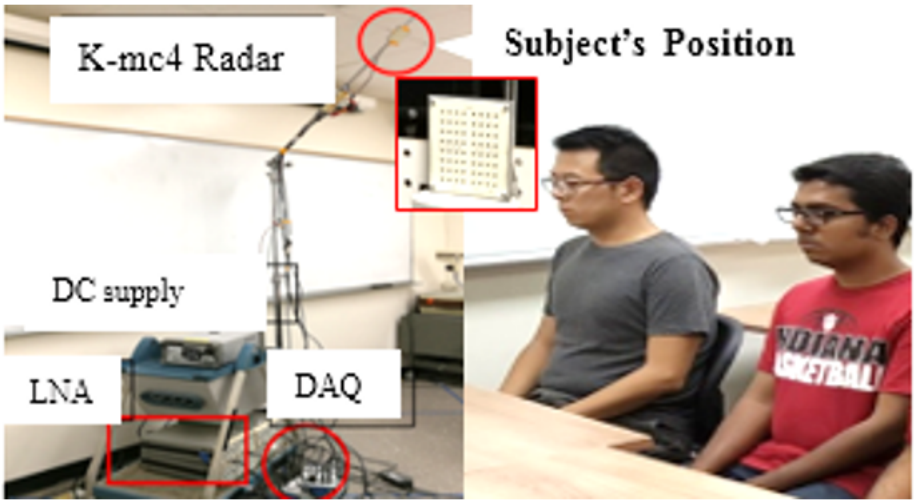

Figure 4.18 Experiment setup with 24-GHz K-MC4 radar transceiver. The complete setup is shown on the left, and on the right the two subjects are shown one meter apart from each other with an angle 30° and a 2.89 m away from Doppler radar sensor

with random noise and mixing matrix. In this case we used random numbers as mixing matrix. Finally, applying the JADE algorithm we tried to separate the observed mixtures. Separated sources are compared with the chest belt respiration pattern and finally the mean square error was calculated between separated sources and chest belt respiration pattern.

Figure 4.19, 4.20, 4.21 and 4.22 depicts the process flow of the JADE algorithm for separating two respiration signals respectively. The mean square error between separated sources and chest belt respiration pattern is found to be 11.5846% which demonstrates practical efficacy using the JADE algorithm.Then we have linearly demodulated two channels signals. The linearly demodulated signal is shown in Figure 4.19.After that linear demodulated signal is being mixed with random noise and mixing matrix. The observed mixture is shown in Figure 4.20. Separated sources are shown in Figure 4.21. The separated sources closely correlate with chest belt respiration pattern which evaluates the efficacy of ICA-JADE method.In this experiment, the feasibility of using the ICA-JADE method for separating multiple subject's respiratory vital signs was evaluated. From the experimental results it was demonstrated that by incorporating the JADE algorithm in a Doppler radar

physiological monitoring system; simultaneous multiple subject measurement is possible for two subjects in close proximity.

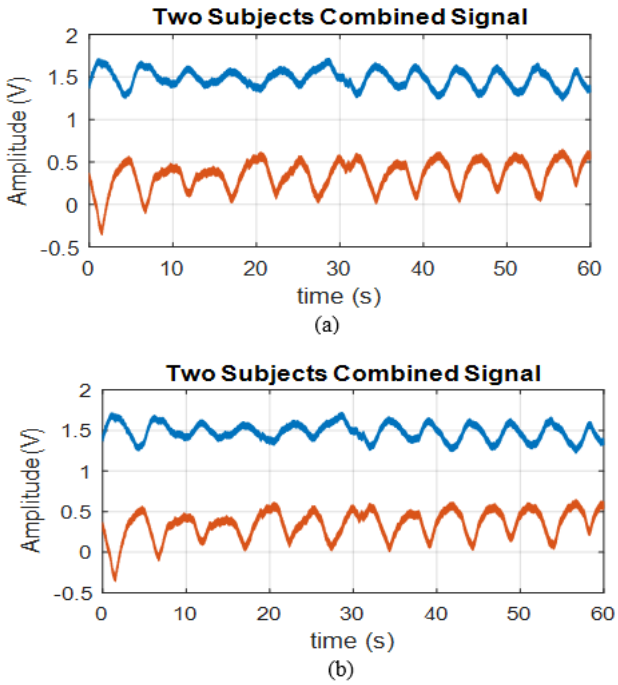

Figure 4.19 Two-Subject measurement from Doppler radar sensor at 2.89 meters with an angle of 30° channel I_1 and Q_1 captured signals (a), and channel I_2 and Q_2 captured signals (b) are shown versus time.

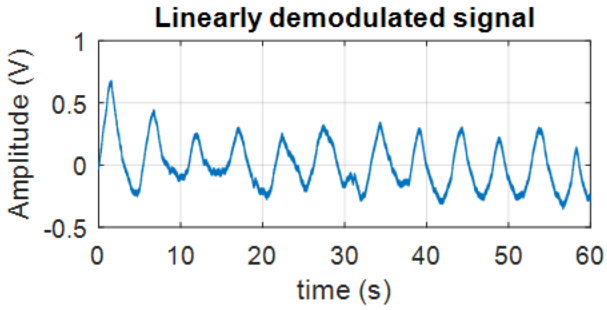

Figure 4.20 Linearly demodulated signal of channel I_1 and Q_1.

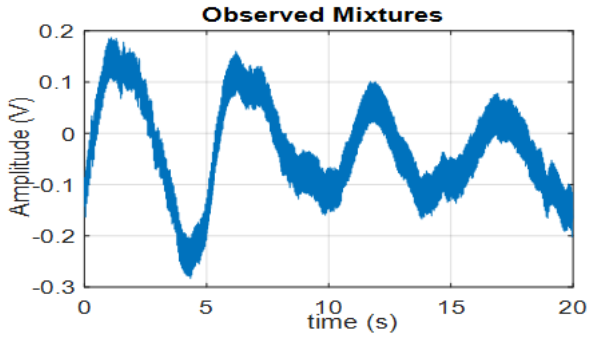

Figure 4.21 Observed mixture of linearly demodulated signal of I_1 and Q_1 signal

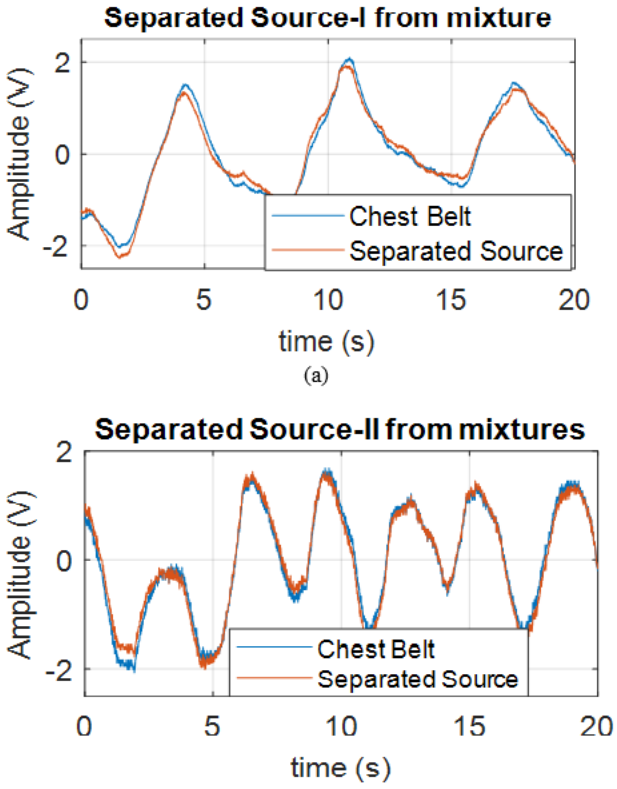

Figure 4.22 Comparison of separated sources with chest belt reference signal Separated source-I (a) Separated source-II (b) are shown in red.

4.4.3 Experiments for separating independent respiratory pattern for closely-spaced subject with varied breathing pattern

After collecting combined reflection data for varied breathing patterns, the data was linearly demodulated and mixed with random noise in a mixing matrix.After applying the JADE

algorithm, independent respiratory signatures were separated from from the combined mixtures. The mean square error and cross correlation coefficient of the separated sources were calculated with respect to a chest belt measured reference respiration pattern.A Fast Fourier transform (FFT) of the separated source and reference chest belt respiration pattern was performed to find determine the accuracy of the proposed method for all three breathing patterns (normal, fast and slow) [18].

Figure 4.23 illustrates the radar captured respiration patterns for a combined mixture of normal and fast breathing patterns for two subjects in front of the radar system. It was observed that when both subjects exhibited faster breathing patterns breathing depth increases illustrates in Figure 4.24, the three different combined mixtures of respiratory patterns and corresponding I/Q plots. The linearly demodulated signals were mixed with random noise and a mixing matrix, and the output was used in the JADE algorithm to isolate independent respiratory patterns from the combined mixtures of the signals.The combined and separated sources for normal and fast breathing are shown in Figure 4.25 where it is clear that the separated source for normal breathing closely correlate with the chest belt reference. On the other hand, for the fast breathing case the separated source

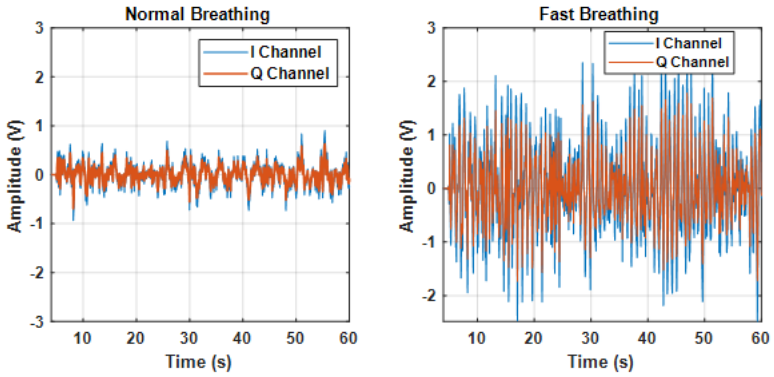

Figure 4.23 Radar measurement of combined mixtures of breathing patterns. When people exhibit fast breathing pattern, they produce some extraneous motion artifacts which increases breathing depth.

does not correlate as closely. The mean square error and cross correlation coefficient of

the separated source signals was calculated with respect to the reference measurement. It was observed that, when subjects exhibited fast breathing patterns, they had difficulty breathing at this rate without creating extraneous motion artifacts. Extraneous motion artifacts also appear in the I/Q plots where averaging was effected by the increased number of breath cycles per window. This also affected the phase measurement accuracy for the irregular signal due to the lower signal to noise ratio for this situation. For slow breathing

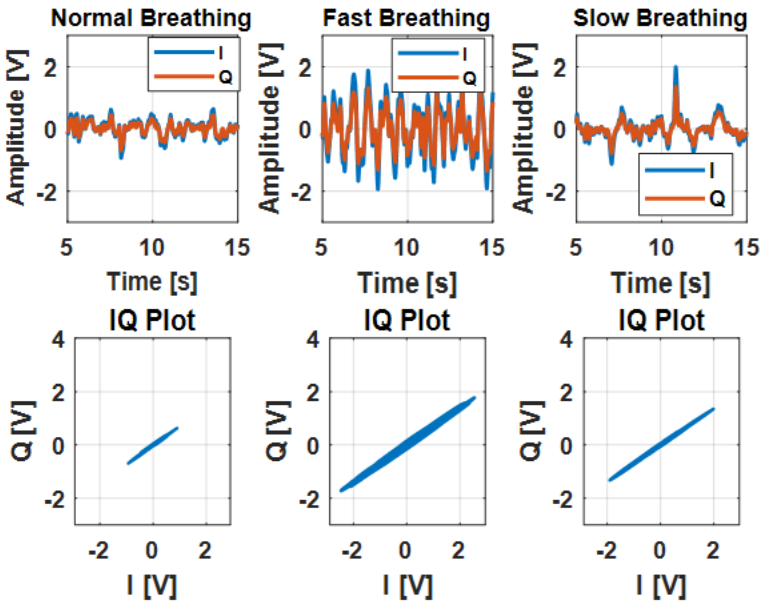

Figure 4.24 Radar captured respiratory patterns for combined mixtures where subjects exhibited normal, fast and slow breathing patterns. Fast breathing pattern has a higher number of cycles and I/Q plot indicates a less clearly retraced arc pattern.

a distortion occurs due to the LNA's ac coupling which resulted in larger error with respect to the reference measurement. The cross correlation coefficients of the separated source with the corresponding chest belt signal for normal, slow and fast breathing patterns were 0.9971, 0.9335 and 0.8634 respectively. An FFT was also used to compare rates for the radar and reference measurements.Figure 4.26 illustrates the separated source for normal breathing and fast breathing and an FFT error analysis for the separated signal and chest

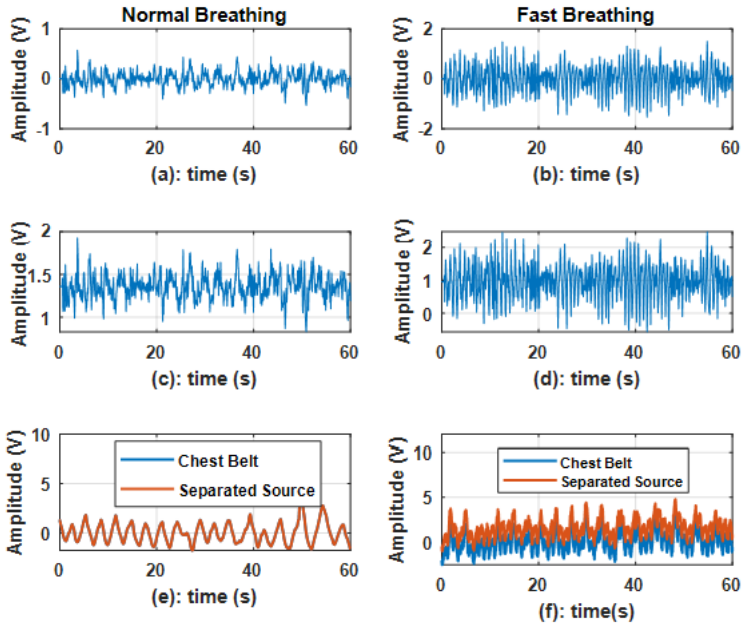

Figure 4.25 (a) Linearly demodulated signal for normal breathing pattern (c) combined mixture of breathing pattern (e) separated source from combined mixture for normal breathing pattern. Similarly (b), (d) and (f) are for fast breathing pattern.

belt signal. The accuracy was calculated by following equation:

$$accuracy = ((|chest\ belt\ - separated\ )breathing\ rate|)/(chest\ belt\ signal\ breathing\ rate) \tag{4.25}$$

Table 4.6 summarizes the performance of the JADE algorithm for extracting breathing rates from combined mixtures for three different breathing patterns (normal, fast and slow). The accuracy decreased for fast breathing due to low signal to noise ratio. SNR also degraded due to motion artifacts associated with exhibiting fast breathing patterns.

In this experiment, we investigated the feasibility of separating respiratory signatures for combined mixtures of varied breathing patterns using the ICA-JADE algorithm. While the study indicated usefully accurate measurement of separated signals, the results were affected by the decrease in SNR for the extreme breathing cases. This study illustrates the

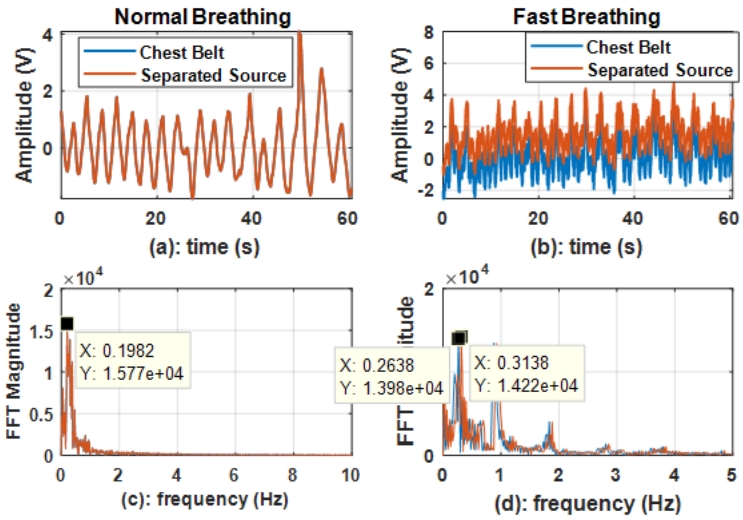

Figure 4.26 Radar captured separated respiratory pattern with chest belt signal for normal breathing (a) and fast breathing (b). From FFT of the signal the breathing rate for (c) normal breathing is .19 Hz and for fast breathing is .31 Hz whereas chest belt signal is .26 Hz.

Table 4.6 Summary of accuracy for breathing patterns.

Breathing type	**Breathing rate**	**MSE**	**Cross-correlation coefficient**	**Accuracy**
Normal	.2	.055%	.9971	100%
Slow	.13	7.2354%	.9335	92.30%
Fast	.3	24.5%	.8634	83.87%

challenges associated with tracking respiratory patterns which significantly deviate from normal. The proposed system has several potential applications especially for in-home sleep monitoring, automotive in-cabin monitoring, and security/surveillance applications.

4.5 Decision Algorithm Development

By combing two different approaches (ICA-JADE and DOA) we developed a decision algorithm. In order to understand the efficacy of the proposed hybrid-system, the isolation of respiratory signatures for three different practical scenarios are considered. First considered

is a scenario where two well-spaced equidistant subjects are positioned [Figure 4.27(a)] and a CW radar is used to isolate independent respiratory signatures using DOA and switching the beam in corresponding directions. Prior work has demonstrated the feasibility of DOA for isolating well spaced subjects [6][7] and our proposed method can also isolate respiratory signatures using a phase comparison monopulse DOA technique under these

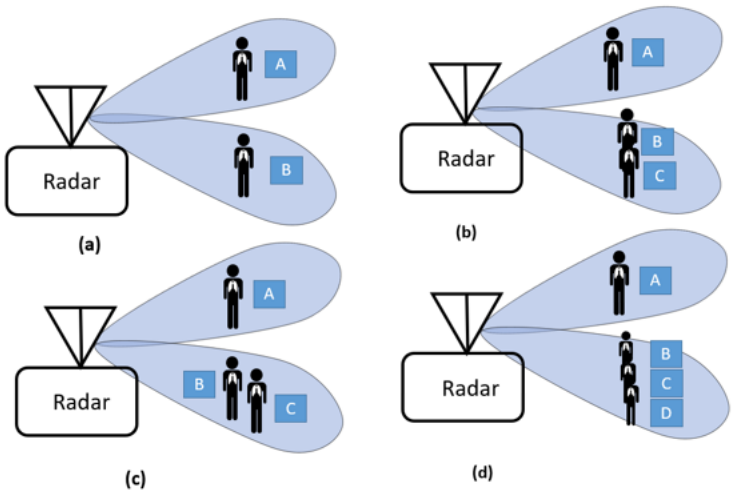

Figure 4.27 Practical subject separation scenarios considered for two radar beam positions. These include (a) two well-spaced subjects (one per beamwidth), (b) two equidistant subjects within one beamwidth, (c) two subjects at different distances within one beamwidth, and (d) three equidistant subjects within one beamwidth.

conditions. The second scenario [Figure 4.27(b)] involves two subjects closely spaced within the beamwidth, and one subject well-spaced outside the beam. In this case our proposed technique can separate respiratory signatures using DOA for the well-spaced subject and ICA-JADE for the subjects closely spaced within the beamwidth. When subjects are at the edge of the beamwidth of the transceiver our proposed method can estimate the angular location of the target and mechanically switch the beam in the appropriate directions to isolate respiratory signatures.We also developed an algorithm to switch between these two methods (ICA-JADE and DOA) for extracting respiratory signatures when the subjects

are within the beamwidth of the radar. To the best of the authors' knowledge, none of the work in prior literature has solved this critical problem which is illustrated in Figure 4.27(b).For the next scenario,it might happen that two subjects are at different distances within the beamwidth and this has been previously addressed using FMCW radar with wireless localization technique.Our proposed SNR-based decision algorithm can also isolate respiratory signatures for subjects at different ranges within the beamwidth. An additional scenario may also be considered where three closely spaced subjects are positioned within the beamwidth of the radar (Figure 4.27(d)), and the research reported here provides a basis on which to solve this problem in future extensions of this scalable work.

4.5.1 Estimation of signal-to-noise ratio (SNR) at different azimuth discrimination ranges within the beamwidth

The signal to noise ratio (SNR) for the received signal at a certain range within the beamwidth can be calculated using the radar range equation shown in Eqn. below. SNR is the ratio of the signal power at the receiver, PS, and noise power at the receiver, P_N, G_T, G_R is the directive gain of transmit and receive antenna, λ is the wavelength, σ is the radar cross section (RCS), and R is the range of the target. K is Boltzmann's constant, so SNR is calculated as:

$$SNR = \quad P_S/P_N \ = (P_T\ G_T\ G_R\ \lambda^2\ \sigma)/((4\pi)^3\ R^4\ KT_0\ BF_n\ L) \tag{4.26}$$

where B is the effective noise bandwidth, F_n is the noise figure, and L accounts for path loss. The path loss is Friss propagation loss [19][20].

$$.L = (4\pi d/\lambda)^2 \tag{4.27}$$

where, d is the distance from the subject to the antenna, and λ is the wavelength of the transceiver. For analyzing the SNR of the received signal from equidistant subjects at a particular range we used equation 4.26 and 4.27. We considered two extreme positions

where subjects were at a certain range at the angular decimation limit both at the edge and well within the beamwidth. Table-4.7 shows the relationship between threshold angular discrimination limit and radial distances. At 1-meter radial distance, when the subjects are at an angular discrimination limit of 0.52 meters, their angular spatial position is at the edge of the beamwidth. Once they cross the boundary of 0.4 m their position is within the beamwidth. We examined two situations, with subjects placed very closely at a maximum 0° angular position within the beam, and at a maximum 15° angular position at the edge of the beamwidth of the radar.Figure 4.28 illustrates the spatial position scenarios considered. When equidistant subjects are at the edge of the beamwidth we can isolate them by estimating their location but as they get much closer, we cannot. Instead we investigated the SNR differences between these two locations. For simulation we considered the radar antenna array parameters from the data sheet and estimated SNR considering the Friss propagation formula [19].We also used a human subject radar cross section parameter of 1.22 m^2. In addition to simulations we also analyzed the measured radar reflections in an anechoic chamber experiment for two subjects present within the beamwidth having different angular resolutions Table-4.7 represents the SNR at two different locations where

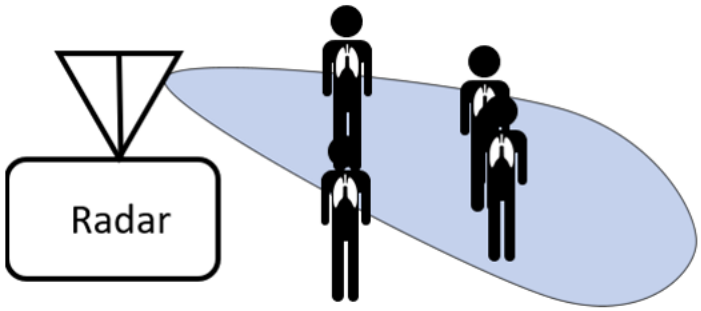

Figure 4.28 Diagram of subjects located at the edge and within the transceiver main beamwidth. Subjects located at the edge are well-spaced and DOA estimation is possible. When subjects are within the beamwidth (closely spaced) DOA estimation is not possible.

we can switch between two methods. From the simulation and experimental results, it is

Table 4.7 Simulated SNR at different radial distances within beamwidth.

Range	SNR within beamwidth	SNR at the edge beamwidth
1 m	26.141 dB	20.14 dB
2 m	20.12 dB	14.12 dB
3 m	13.19 dB	7.19 dB

Table 4.8 Experimental Radar captured SNR at different radial distances

Range	SNR within beamwidth	SNR at the edge beamwidth
1 m	24.12 dB	18.13 dB
2 m	17.12 dB	11.15 dB
3 m	9.19 dB	3.17 dB

clear that the SNR difference between two different boundaries (edge and within beam) is almost 6 dB. This SNR difference occurs due to antenna array gain differences at the corresponding locations [3] [3].From analysis of the SNR look up table we can easily detect the spatial positions of two subjects, either within or at the edge of the beamwidth.

4.5.2 Experimental results for SNR-based decision algorithm

Three different experiments were carried out to evaluate the integration and algorithm development for coherently combining two different separation techniques (ICA, DOA) for the Doppler radar measurements.

1. In experiment one, two well-spaced equidistant subjects were positioned at different angular discrimination ranges from 1 meter to 3 meters. This experiment was performed to test the effectiveness of DOA technique and integrating the beam switching to isolate breathing rate of a single subject. Figure 3 illustrates the experimental scenario for well-spaced subjects in front of the radar module.

2. In second experiment, two equidistant subjects within the beamwidth of the radar each sat at different slant ranges (1, 1.5, 2, 2.5 and 3 m) at two different angular discrimination ranges (shown in Table-II) for developing an algorithm to switch

between the two separation methods. We also tested the feasibility of estimating DOA when one subject was outside the beam.

3. In the third experiment, we placed two subjects at different distances within the beamwidth of the radar.

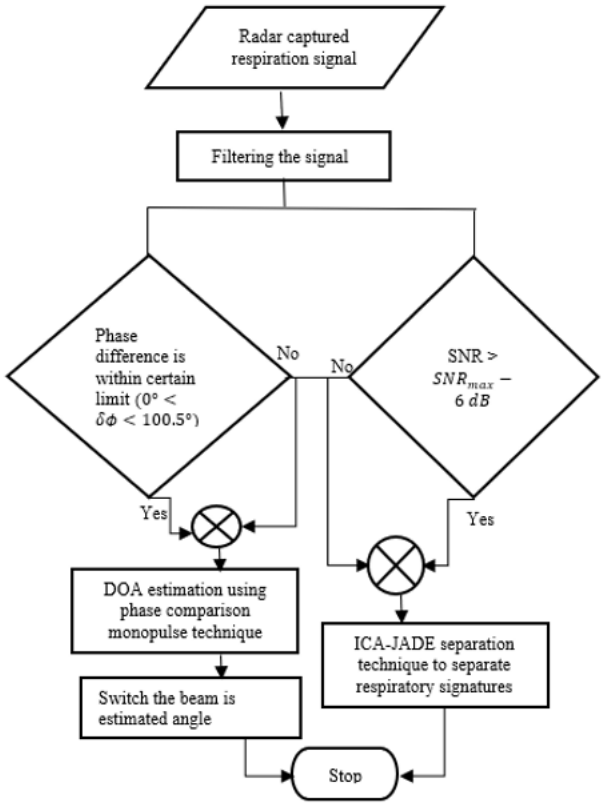

Figure 4.29 Proposed decision algorithm for selecting appropriate approach (ICA-JADE or DOA) when two subjects are within the beamwidth of the radar.

The decision algorithm developed to switch between two different techniques (ICA-JADE, DOA) is shown in Figure 4.29. After capturing and filtering the radar respiration signal, we found the phase difference and SNR of the received signal. Based on our simulation and experimental setup we created an SNR lookup table for equidistant subjects at different slant ranges (1 m to 3 m).If the SNR of the received signal at a particular distance is less than 6

dB and phase difference between two received signals is higher than 100.5°, then the ICA-JADE algorithm is employed to separate the respiratory signatures.If instead the SNR of the received signal is less than the threshold limit ($SNR > SNR_{max} - 6dB$) the phase difference between two receivers remains within the limit.Thus, DOA can isolate two subjects based on their spatial positions by switching the beam in the direction corresponding to each subject.

4.5.3 Scenario-I: two subjects are well-spaced

In the first experiment we considered two well-spaced subjects with an angular discrimination limit of at least 1 to 3 meters. The captured signal for each single subject was filtered using a Finite Impulse response filter (FIR) of an order of 1000 with a cut off frequency of 10 Hz. Then we measured the phase-difference between two receiver channels using a Fats Fourier Transform (FFT) and maximum likelihood estimation [12]. From the phase difference information, we can estimate the angular location of a subject by using Eqn. 4.13. From Figure 4.30 (a) the phase difference between the received two-channel signals is 83.75°. Using Eqn. 4.14 we can estimate the angular location of one subject from the radar azimuth angle as 12.5°. After estimating the angular locations, we can switch the beam in the corresponding direction to isolate the respiratory pattern of a single subject. Figure 4.30 (b) illustrates that the FFT of the switched beam in a certain direction is around 0.31 Hz. It is also clear from the figure the chest belt respiration rate is 0.29 Hz. Similarly, by rotating the beam in another direction we also extracted the respiration rate of the signal subject after determining the angular location from the azimuth plane view of the radar. Then we measured the estimation accuracy of the isolated respiratory rate with a chest belt reference respiratory rate using:

$$Accuracy = (|(\ chest\ belt - radar\ signal)\ extracted\ rate|)/(chest\ belt\ extracted\ \ rate) * 100 \tag{4.28}$$

The percentage accuracy of the system using this beam switching technique is around

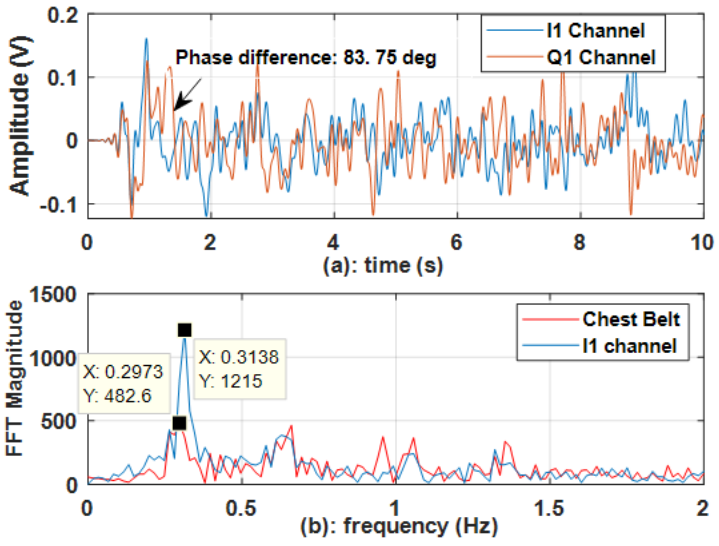

Figure 4.30 (a)Phase difference between receivers for a well-spaced subject (3-m from second subject) and (b) spectrum for isolated subject's respiration signal.Chest belt measured reference signal closely matches the radar-measured respiration rate.

94.45% with an angular discrimination of 3 meters. Accuracy of the system also depends on DOA estimation accuracy which determines the direction in which the beam is switched.

4.5.4 Scenario II: two subjects are closely-spaced within the beam and one subject is outside the beam

If two subjects are within the beamwidth and one subject is outside the beam, then we can extract respiratory rate for the outside subject by switching the beam. Here we will concentrate on the two subjects within the beam to test the effectiveness of our proposed separation algorithm. Two subjects were positioned at 1-meter slant ranges from the Doppler radar and with an angular discrimination of 0.4 meters between them within the main beamwidth (30°) of the K-MC4 transceiver. Figure 4.31 depicts the filtered captured signal of two subjects and their corresponding constellation (IQ) plots. In one of the mixed signal spectrum plots, there were two dominant breathing frequencies of 0.19 Hz and 0.39 Hz. Two different respiration frequencies were clearly observed form the FFT of

the mixed signal which demonstrated the presence of two subjects in front of the sensor. Figure 4.32 represents the SNR of the radar measured signal at this particular position

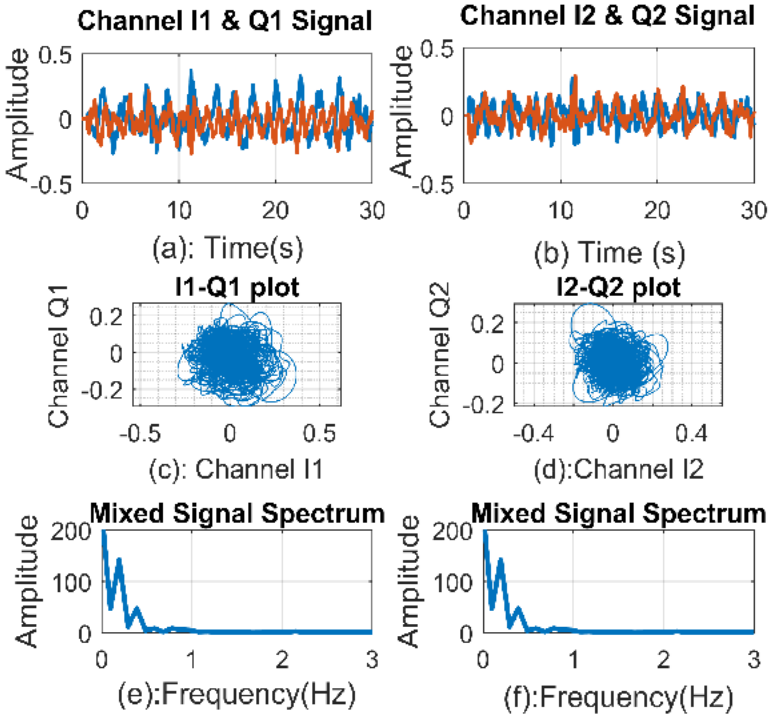

Figure 4.31 Two-subject radar measurement captured at a slant range of 1 m with an angular discrimination of 0.4 m at an angle of 30°. Plots of measured (a) I1 and Q1 signals, (b) I2 and Q2 signals, (c)I1 vs Q1, and (d) I2 vs Q2 are reproduced from [17].

which is around 22.40 dB. By looking at the SNR lookup table it is clear that subject position is within the beamwidth of the transceiver. We also measured the phase difference between two receivers to be around 110 °, which is beyond the functional phase difference range of the monopulse radar transceiver. Thus, for this case we used the ICA-JADE algorithm technique to separate respiratory signatures based on our proposed intelligent decision algorithm. Then we linearly demodulated the two-channel signals as shown in Figure 4.33 and mixed the signals with random noise with a mixing matrix. The ICA-JADE method was then used to separate the individual respiratory signatures from their combined mixtures. From Figure 4.34 it can be seen that the mixed signals were successfully

separated from their combined mixtures, and the separated sources closely correlated with

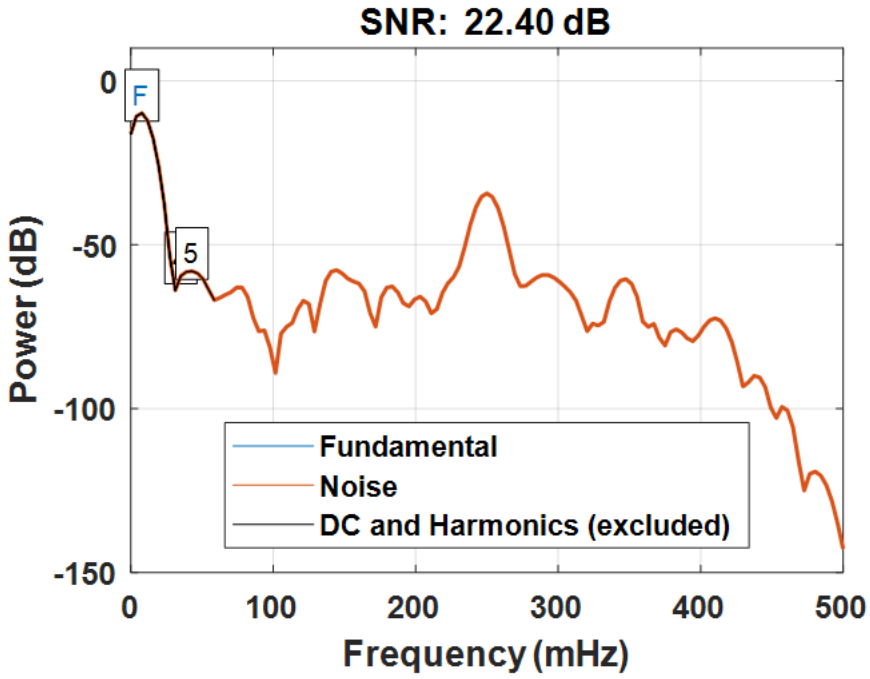

Figure 4.32 SNR of radar captured respiration signal with two equidistant subjects at 1 m with angular discrimination limit of 0.4 m.

reference chest belt respiration pattern. The mean square error (MSE) between separated sources with corresponding reference chest belt respiration pattern was found to be 0.06% and the corresponding cross-correlation coefficient was 0.99. Now we consider another scenario where the equidistant subjects are located at 3-meters distance with an angular discrimination limit of 1.55 m. Figure 4.34 shows the I1 ,I2, Q1 and Q2 signals FIR filtered using a filter with an order of 1000 and measured with the subject located at slant ranges of 3 m with an angular discrimination limit of 1.55 m. The SNR of the filtered received signal was 3.17 dB. From the SNR lookup table, the SNR was less than 6 dB of the estimated maximum SNR. Thus, the phase-comparison monopulse technique should be employed in this scenario. The phase difference at that location (3 m) between I1 and I2 was found to be 80.4°. Using the phase-the comparison technique of Eqn 4.14 we have calculated DOA as 12 °. Figure 4.35 illustrates the SNR of the associated received signals Figures 4.36 (a) and (b)

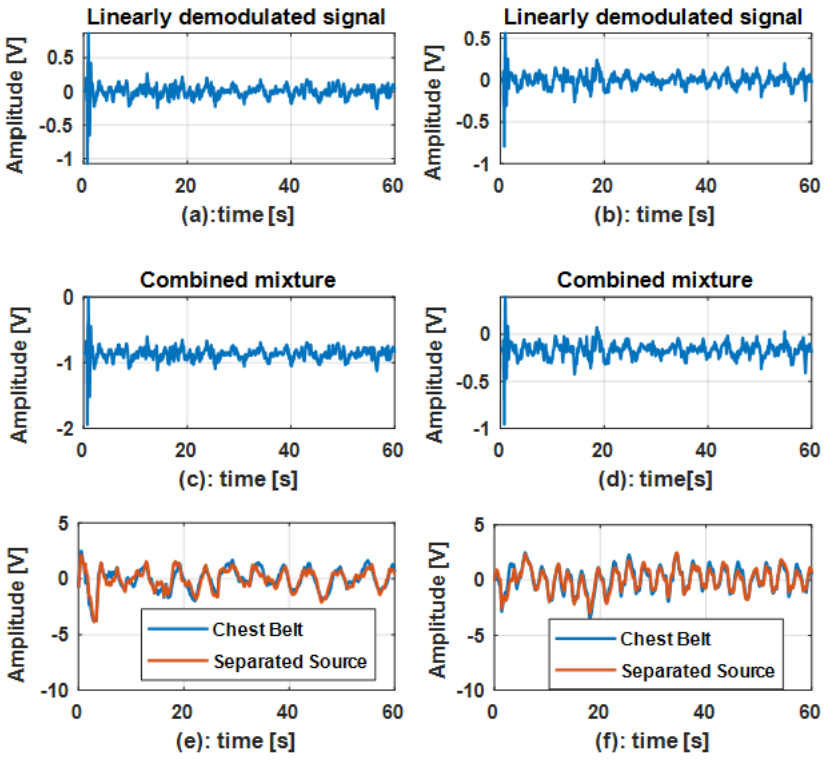

Figure 4.33 Signals for 2-receiver ICA-Jade separation of respiratory signatures. Shown are linear demodulated signals for (a) I1 and Q1 and (b) I2 and Q2, along with corresponding combined mixtures for receivers (c) 1 and (d) 2. Separated sources are also shown in comparison with chest-belt reference signals for receivers (e) 1 and (f) 2.

depict the separated sources from the combined mixture of the two subjects at slant ranges of 1.5 meters within an angular discrimination of 0.78 meters. Figures 4.36 (c) and (d) represent the separated sources from the combined mixtures of two subjects at slant ranges of 2 meters with angular discrimination of 1.04 meters. The mean square error Corr for two different slant ranges (1.5m, 2m) are 12.86 % and 0.93 and 21.34 % and 0.88, respectively. In addition to decomposition of the signals from the combined mixtures, we have also calculated the mean square error (MSE) and cross-correlation coefficient (Corr) for the separated sources compared with chest belt reference respiration signals. We selected two different angular discrimination within the same slant ranges as one angular discrimination is less than the acceptable limit for DOA estimation.Table 4.9 illustrates the performance

of separated sources compared with reference respiration strap signals. From Table-4.9, it was shown that when subjects are closer to the radar and within the main beamwidth (30°) of the transceiver, thus having an angular discrimination limit within the beamwidth of the transceiver, the mean square error between the separated sources and chest belt reference signals increases and cross correlation coefficient decreases

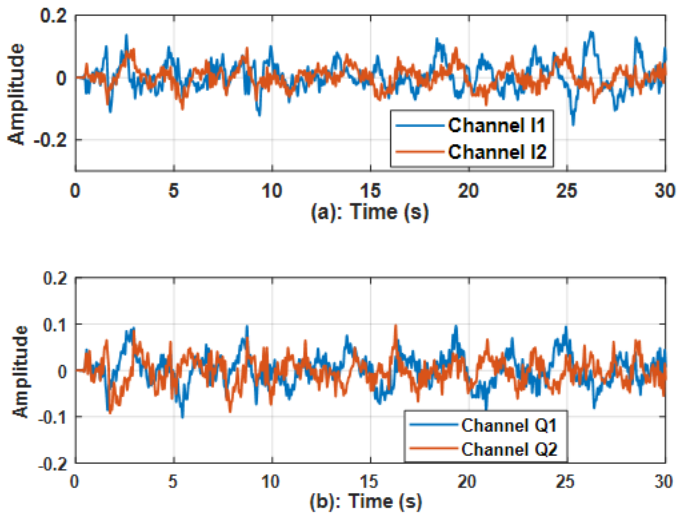

Figure 4.34 Signals for monopulse separation of respiratory signatures. Shown are linear demodulated signals for (a) I1 and Q1 and (b) I2 and Q2.

This occurs because when the subjects are closer and the angular position is within the main beamwidth of the directional antenna pattern of the transceiver, the SNR level of the received signal is higher than that for subjects at the edge of the main beamwidth of the Doppler radar transceiver due to the directional antenna radiation pattern [3]. The efficacy of the ICA-JADE method is well suited for separating subjects that are closer to the radar sensor and within the main beamwidth of the directional antenna pattern of the for separating subjects that are closer to the radar sensor and within the main beamwidth of the directional antenna pattern of the transceiver as the probability of the received signal being degraded is less than it is for larger distances [5]. Previous research has demonstrated that the failure rate for detecting heartbeat from a combined mixture increases as the

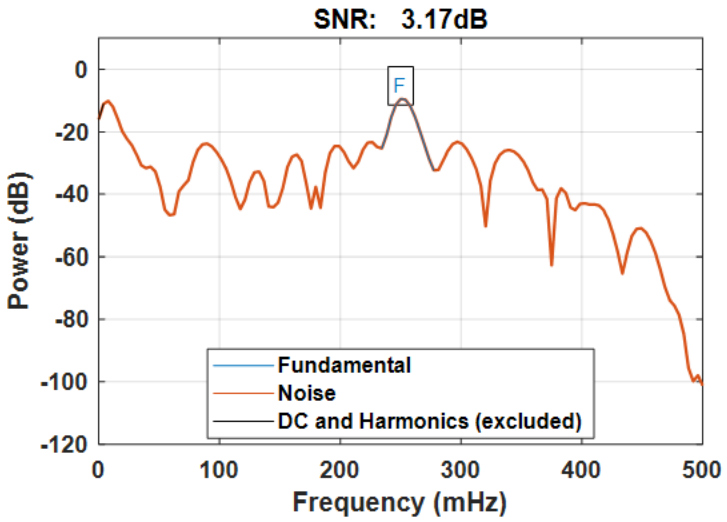

Figure 4.35 SNR of radar captured respiration pattern for two equidistant subjects at 3 m with angular discrimination limit of 1.55 m.

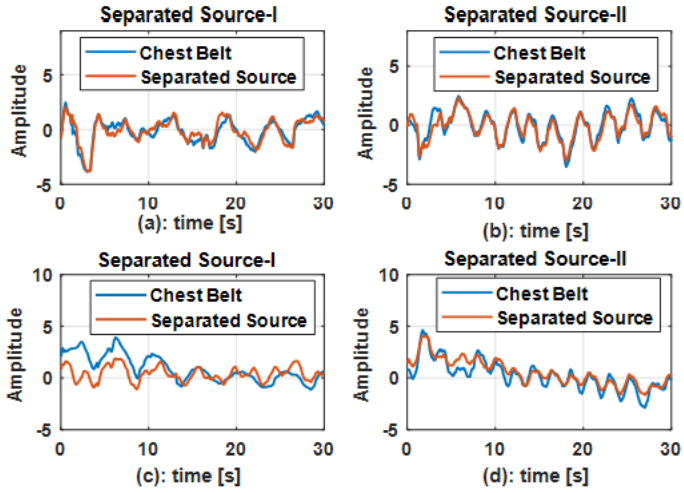

Figure 4.36 Demodulated respiration signatures for sources separated from combined mixtures for two subjects. Shown are signatures for (a) subject I and (b) II at slant ranges within 1.5 m from the radar and angular discrimination limit of 0.78 m, and (c) subject I and (d) II with slant ranges of 2 m and angular discrimination limit of 1.04 m.

SNR of the received signal deteriorates [5]. The SNR of the received signal degrades as the distance of subjects from the transceiver increases which also affects the performance of ICA-JADE algorithm in separating two independent respiration patterns.Figure 4.37

Table 4.9 Performance evaluation of separated sources with reference respiration strap signal patterns at slant ranges (1 meter to 3 meters) at two different angular discrimination [5].

Slant Ranges	Angular discrimination	MSE	cross-correlation coefficient
R=1 m	0.4 m (within), 0.52 m (edge)	.055%, 5.53%	.99, .94
R=1.5 m	0.5 m (within), 0.78 m (edge)	7.23%, 12.86%	.95, .93
R=2 m	0.7 m (within), 1.04 m (edge)	15.86%, 21.34%	.94, .93
R=2.5 m	1 m (within), 1.29 m (edge)	24.04%, 30.52%	.86, .82
R=3 m	1.25 m (within), 1.55 m (edge)	32.22%, 38.69%	.81, .77

represents the MSE of separated sources compared with chest belt respiration signals for two different angular discrimination limits. When two subjects are positioned within the angular discrimination limit of the beamwidth the mean square error (MSE) is reduced. In addition, when the subjects are positioned at further slant ranges from the radar the MSE is higher, as signal quality is being degraded with increased distance.For each 0.5-meter slant range increase in subject position from the radar, the MSE degrades by about 7.18% and if the subject's angular discrimination is within the beamwidth of the transceiver then the MSE is approximately 5.478% higher than for the case with the angular discrimination at the edge of the transceiver, due to reduced SNR at the edge of the beamwidth.

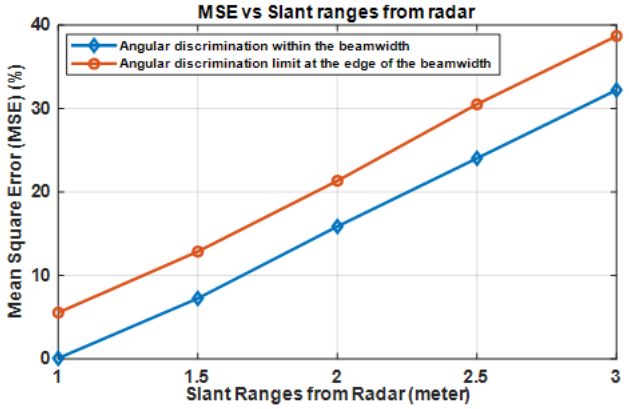

Figure 4.37 Mean Square Error (MSE) versus slant ranges from Doppler radar transceiver. Blue line represents angular discrimination limit within the main beamwidth of the transceiver, and red line represents the angular discrimination limit at the edge of the beamwidth of the transceiver.

When the subjects are well-spaced at the edge of the main beamwidth of the radiation pattern then we can employ phase-comparison monopulse to estimate DOA [6][7] compared the accuracy of our estimated angle with the actual angle measured using a protractor. The estimation accuracy was calculated using the below formula:

$$Estimation\ Accuracy\ (DOA) = (|actual\ angle - estimated\ angle|)/(actual\ angle) * 100 \tag{4.29}$$

In the case of measurements for multiple subjects we considered angular locations of the subjects from the radar as 15° so they are within the edge of the main [10]. horizontal

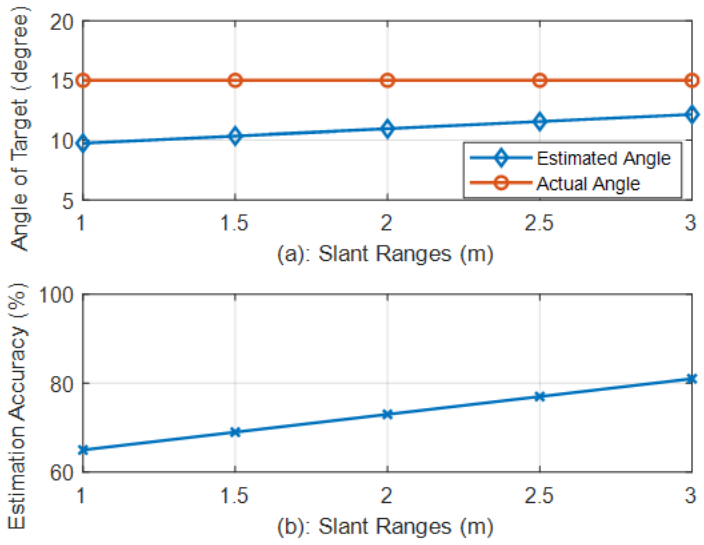

Figure 4.38 (a) Estimated angle of subjects at different slant ranges (1m, 1.5m, 2m, 2.5m and 3m), and (b) estimation accuracy for different slant ranges. As the slant ranges increase, the estimation accuracy also increases.

beamwidth of the transceiver at different slant ranges. We also measured estimation accuracy for different slant ranges. Fig. 4.38 (a) represents the estimated angle using the phase-comparison monopulse technique at different subject ranges and Fig. 4.38 (b) shows the variation of the estimation accuracy with different slant ranges or positions of the subjects. Fig. 4.38 shows that the estimation accuracy increases when subjects are

well-spaced in terms of angular discrimination and slant ranges from the Doppler radar. The estimation accuracy at slant ranges of 3 meters is 81%, while at slant ranges of 2 meters the accuracy falls to 73%. Multipath and grating lobes are two dominant sources of error affecting the estimation accuracy of monopulse radar. When two subjects are closer to the sensor the probability of experiencing multipath is higher than when subjects are well-spaced [5]. Another dominant source of error in using the monopulse technique comes from grating lobes generated when the antenna element spacing (13.77 mm) of transceiver is greater than half of the operating wavelength (6.25mm) [3].As the spacing, d, between the array phase centers of the antenna elements is greater than that of the antenna diameter, high side lobes are produced at the edge of the beamwidth for closer ranges (1m to 2m) and ambiguities occur in the angle measurement for closer ranges at the edge of the beamwidth, due to side lobes produced closer to main beamwidth. At the same time, the minimum angular discrimination limit to separate reflections for the 24-GHz KMC4 radar transceiver is 0.4 m due to the antenna array element spacing limit [5].Since, the K-MC4 transceiver has this grating lobe effect when subjects are closely spaced, and slant range is small, grating lobes affect the phase measurement of the received signal. Thus, the side lobes produced at the edge of the main beamwidth in small ranges also affects the overall estimation accuracy. While the estimation accuracy can be increased by using a more precise model of the antenna array, the low-cost scalable system described here can be used for monitoring well-spaced multiple subjects as it can estimate the angular location of subjects quite well.In practice, the separation between the two receiver antenna elements should be less than the antenna diameter to reduce angle measurement ambiguities [6][7].If the subjects are oriented at different distances within the beamwidth we can still isolate them by utilizing the SNR distribution of different distances and using the ICA-JADE, we can isolate independent breathing patterns. For comparing the accuracy of our proposed SNR based decision algorithm for subjects within the beamwidth, we also performed an FFT after separating respiratory signatures for extracting breathing rate information and compared it with the chest belt respiration reference. Figure 4.39 illustrates that the extracted breathing rates

from separated respiratory signatures (angular discrimination 0.4 m) closely match with chest belt captured breathing rates.

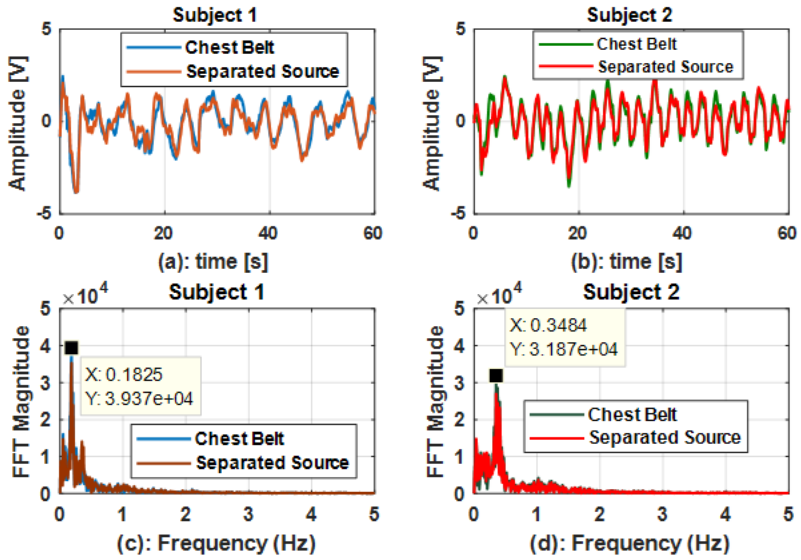

Figure 4.39 Separated respiratory signatures and chest belt signals (blue) shown for (a) subject-1 and (b) subject-2, along with corresponding FFTs used to extract breathing rates for (c) subject-1 and (d) subject-2. Measured rates are 0.18Hz for subject-1 and 0.38Hz for subject-2, which, match closely to chest belt reference measurements.

4.5.5 Comparative analysis with the proposed method with existing literature

The proposed hybrid method (ICA-JADE and DOA) helps to resolve this antenna array element resolution limit because it uses DOA estimates only for subjects at the edge of the beamwidth and not when subjects are within beamwidth where DOA breaks down [6] [7] [4]. To achieve an accurate measurement, we consider how closely isolated respiratory rates match with chest belt extracted respiratory rates using Eqn. 4.28.Figure 4.40 illustrates the improved accuracy attained by switching intelligently between two different techniques, where it is clear that the ICA-JADE method performs well up to an angular resolution limit of 1 meter (having higher SNR within the beamwidth of the radar), and when subjects are

much more well-spaced and within the boundary of the beamwidth estimation of angular location is possible with DOA. We developed an efficient algorithm which efficiently switched the beam in the appropriate direction so beyond the angular discrimination limit of 1 meter, DOA could isolate respiratory patterns as verified by chest belt measurements. Thus, the overall accuracy of the system always remains above 93%. We also performed an accuracy comparison between our proposed hybrid method and the existing literature results. To the

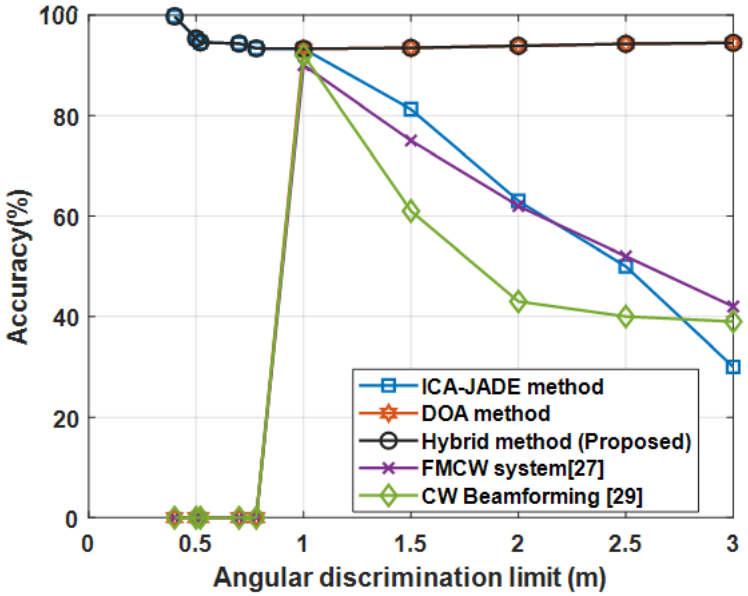

Figure 4.40 Comparative accuracy analysis of proposed method with other reported results. ICA-JADE method accuracy remains above 93% until angular discrimination limit reaches 1 meter, at which point DOA accuracy increases to maintain a hybrid system accuracy at or above 93%.

best of author's knowledge this is the first reported result where a two-subject respiratory signature can be isolated using CW radar when the separation distance between them is less than 1 meter, and the system can also isolate three subjects when two subjects are within the beam and one is outside the beam. Previous research [21] solely focused on designing a dual beam phased array CW radar to isolate respiratory signatures, with a minimum angular resolution limit between two subjects of at least 1 meter, with a reported

Table 4.10 Comparison of this work with other recent relevant work.From [5].

Ref year	**Radar type**	**Angular discrimination (m)**	**No of subjects**	**Accuracy (%)**
[22] 2015	FMCW	1	2	90%
[21] 2019	CW	1	2	92%
[17] 2018	CW	1	2	93.25%
[6] 2018	CW	1.5	2	72%
[7] 2019	CW	2	2	74%
[5] 2020	CW	0.4	3	99.71%

accuracy of 92%. However, for more well-spaced subjects, e.g. 1.5 meters, the accuracy of the system dropped to 75% due to a systemic intra-beam interference issue [21]. Previous FMCW radar work focused on multiple subjects at different distances [22].For equidistant subjects the minimum angular resolution limit was 1 meter as FMCW can separate two equidistant subjects at least c/2B apart, where c is the speed of the light and B is the bandwidth of the radar system. The reported accuracy was 90% when the subject's angular resolution limit was 1 meter, and the system could not isolate independent respiratory signatures when the subjects were closely spaced (angular resolution limit less than 1 m). The accuracy of our proposed hybrid method compared with the existing literature reported results is illustrated in Fig. 4.40. A comparative analysis with relevant research efforts shown in Table-4.10.

By combining two techniques using our proposed SNR based decision algorithm, practical monitoring of multiple subjects becomes possible. Our proposed system can be effectively applied to find a human target with respect to azimuth angle within the radar transceiver beamwidth and also separate breathing patterns of closely spaced subjects. If there are three subjects within the beam, our proposed SNR based decision algorithm can switch between two different techniques to isolate respiratory patterns. SNR based analysis and threshold limit for different numbers of subjects remains future work for which this research establishes a basis.

4.6 Conclusion

The feasibility of combining two different techniques (ICA-JADE, DOA) to isolate radar measured respiration is examined. An integrated decision algorithm has been proposed to efficiently separate the respiratory signatures of multiple subjects using a 24-GHz phase comparison monopulse radar, applying ICA-JADE when the subjects within the beamwidth, and DOA when they are not. The need to separate individual respiratory signatures for combined mixtures is essential, especially in home-based sleep monitoring environments. From source separation results it was shown that the ICA-JADE method can separate independent respiratory patterns more accurately when subjects are closely spaced.We also employed a phase-comparison monopulse technique to accurately estimate the angular location of subjects. When subjects are well-spaced, this allows the radar beam to be steered toward the subject of interest allowing for accurate DOA based subject isolation. This research demonstrates that an effective combination of two approaches (ICA-JADE, DOA) can maintain accurate and efficient monitor multiple subjects across a broad range of subject separation scenarios.

References

[1] O. Boric-Lubecke, V. Lubecke, A. Host-Madsen, D. Samardzija, and K. Cheung, "Doppler Radar Sensing of Multiple Subjects in Single and Multiple Antenna Systems," in *TELSIKS 2005 - 2005 uth International Conference on Telecommunication in ModernSatellite, Cable and Broadcasting Services*, vol. 1, (Nis, Serbia and Montenegro), pp. 7–11, IEEE, 2005.

[2] Y. S. Lee, P. N. Pathirana, R. J. Evans, and C. L. Steinfort, "Separation of Doppler radar-based respiratory signatures," *Medical & Biological Engineering & Computing*, vol. 54, pp. 1169–1179, Aug. 2016.

[3] "[online] https://www.rfbeam.ch/product?id=18."

[4] "[online] http://www.radartutorial.eu/01.basics/Angular%20Resolution.en.htlml."

[5] S. M. M. Islam, O. Boric-Lubecke, and V. M. Lubekce, "Concurrent Respiration Monitoring of Multiple Subjects by Phase-Comparison Monopulse Radar Using Independent Component Analysis (ICA) With JADE Algorithm and Direction of Arrival (DOA)," *IEEE Access*, vol. 8, pp. 73558–73569, 2020.

[6] S. M. M. Islam, E. Yavari, A. Rahman, V. M. Lubecke, and O. Boric-Lubecke, "Direction of Arrival Estimation of Physiological Signals of Multiple Subjects Using Phase Comparison Monopulse Radar," in *2018 Asia-Pacific Microwave Conference (APMC)*, (Kyoto), pp. 411–413, IEEE, Nov. 2018.

[7] S. M. M. Islam, E. Yavari, A. Rahman, V. M. Lubecke, and O. Boric-Lubecke, "Multiple Subject Respiratory Pattern Recognition and Estimation of Direction of Arrival using Phase-Comparison Monopulse Radar," in *2019 IEEE Radio and Wireless Symposium (RWS)*, (Orlando, FL, USA), pp. 1–4, IEEE, Jan. 2019.

[8] Q. Zhang, H. Abeida, M. Xue, W. Rowe, and J. Li, "Fast implementation of sparse iterative covariance-based estimation for source localization," *The Journal of the Acoustical Society of America*, vol. 131, pp. 1249–1259, Feb. 2012.

[9] R. DeGroat, E. Dowling, and D. Linebarger, "The constrained MUSIC problem," *IEEE Transactions on Signal Processing*, vol. 41, pp. 1445–1449, Mar. 1993.

[10] S. M. Sherman, *Monopulse Principle and Techniques.* Artech House: Boston, MA, USA, 2012 ed.

[11] R. Schmidt, "Multiple emitter location and signal parameter estimation," *IEEE Transactions on Antennas and Propagation*, vol. 34, pp. 276–280, Mar. 1986.

[12] J. Villanueva, S. Catunda, and R. Tanscheit, "Maximum-Likelihood Data Fusion of Phase-Difference and Threshold-Detection Techniques for Wind-Speed Measurement," *IEEE Transactions on Instrumentation and Measurement*, vol. 58, pp. 2189–2195, July 2009.

[13] S. M. M. Islam and O. Bori, "Comparative Analysis of Phase-Comparison Monopulse and MUSIC Algorithm Methods for Direction of Arrival (DOA) Estimation of Multiple-Subject Respiration Measured with Doppler Radar," p. 4.

[14] J.-F. Cardoso, "Blind signal separation: statistical principles," *Proceedings of the IEEE*, vol. 86, pp. 2009–2025, Oct. 1998.

[15] E. Chaumette, P. Comon, and D. Muller, "ICA-based technique for radiating sources estimation: application to airport surveillance," *IEE Proceedings F Radar and Signal Processing*, vol. 140, no. 6, p. 395, 1993.

[16] D. Rutledge and D. Jouan-Rimbaud Bouveresse, "Corrigendum to 'Independent Components Analysis with the JADE algorithm'," *TrAC Trends in Analytical Chemistry*, vol. 67, p. 220, Apr. 2015.

[17] S. M. M. Islam, E. Yavari, A. Rahman, V. M. Lubecke, and O. Boric-Lubecke, "Separation of Respiratory Signatures for Multiple Subjects Using Independent Component Analysis with the JADE Algorithm," in *2018 40th Annual International Conference of the IEEE Engineering in Medicine and Biology Society (EMBC)*, (Honolulu, HI), pp. 1234–1237, IEEE, July 2018.

[18] S. M. M. Islam and O. Bori, "Extracting Individual Respiratory Signatures from Combined Multi-Subject Mixtures with Varied Breathing Pattern Using Independent Component Analysis with the JADE Algorithm," p. 4.

[19] S. M. M. Islam, F. A. Qazi, M. F. Iskander, Z. Yun, and G. Sasaki, "Advanced directional networking: LTE vs WiFi radios," in *2017 IEEE International Symposium on Antennas and Propagation & USNC/URSI National Radio Science Meeting*, (San Diego, CA, USA), pp. 189–190, IEEE, July 2017.

[20] F. A. Qazi, M. F. Iskander, Z. Yun, G. Sasaki, and S. M. M. Islam, "Smart physical layer based directional communication networking," in *2017 XXXIInd General Assembly and Scientific Symposium of the International Union of Radio Science (URSI GASS)*, (Montreal, QC), pp. 1–2, IEEE, Aug. 2017.

[21] M. Nosrati, S. Shahsavari, S. Lee, H. Wang, and N. Tavassolian, "A Concurrent Dual-Beam Phased-Array Doppler Radar Using MIMO Beamforming Techniques for Short-Range Vital-Signs Monitoring," *IEEE Transactions on Antennas and Propagation*, vol. 67, pp. 2390–2404, Apr. 2019.

[22] F. Adib, H. Mao, Z. Kabelac, D. Katabi, and R. C. Miller, "Smart Homes that Monitor Breathing and Heart Rate," in *Proceedings of the 33rd Annual ACM Conference on*

Human Factors in Computing Systems - CHI '15, (Seoul, Republic of Korea), pp. 837–846, ACM Press, 2015.

Chapter 5

Proposed Continuous Unobtrusive Identity Authentication System

Identity authentication using microwave Doppler radar is based on recognizing people from radar-captured cardiopulmonary pattern [1].This chapter focuses on highlighting the proposed radar-based identity authentication system in multi-subject environment.We will describe in details of extracting respiratory features from radar-captured cardiopulmonary signals.In our proposed method, machine learning classifiers are integrated with the Doppler radar system for recognizing people.So, a brief introduction of different classifiers will also be described in the next subsections. Initially, we attempted different approaches for recognizing people in single subject experimental scenarios and tried to test the feasibility of different approaches.

5.1 Unobtrusive Identity Authentication Basics

Breathing is a complicated anatomical process that takes place by the control of the central neural mechanism in the coordination of lung, diaphragm, and respiratory muscles [2].In general, the breathing mechanism has three different stages: inhale, exhale, and in between there is a pause.Different clinical investigations proved that adult awake human subjects at rest, there exists diversity in the breathing pattern not only in terms of tidal volume, inspiratory, and expiratory duration but also in the airflow profile [2][3]. Everyone selects

to have one pattern among the number of infinite possible ventilatory variables and airflow profile [4].This variability is non-random and may be explained by either central neural mechanism or by the instability in the chemical feedback loops. In addition to that, heart-based geometry is different for different subjects and clinical investigation also suggests that cardiac cycle variations occur based on different shapes of the heart [4].Radar can detect respiratory motions and it is also possible to extract unique features based on diversity in the breathing dynamics.

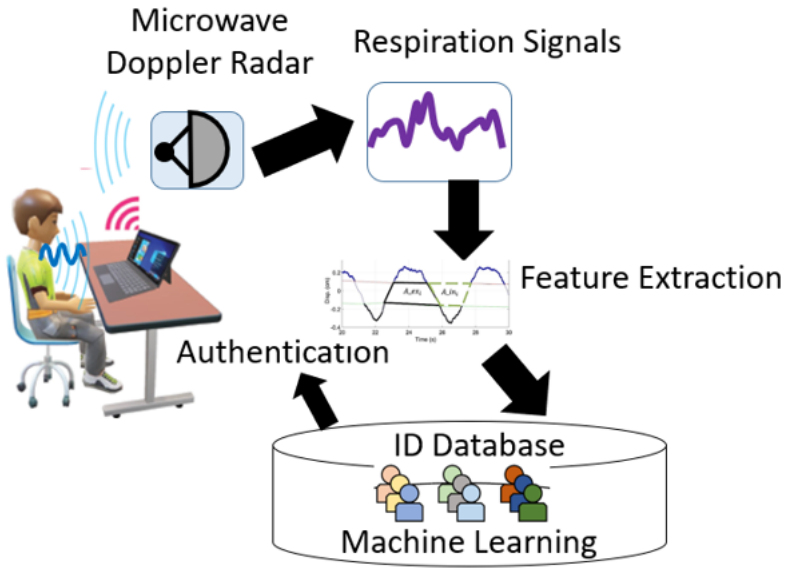

Figure 5.1 Proposed Doppler-radar based non-contact continuous identity authentication system. Human respiration signal pattern is captured by Radar.Then feature extraction is performed using unique identification algorithm and machine learning classifiers are utilized to recognize different participants based on their respiratory features.

Based on reported results researcher focused on extracting two different features one is respiratory- based and another one is heart-based [1].Our proposed unobtrusive identity authentication system is respiration-based shown in in Fig. 5.1 and thus the methodology can be broken down into five different parts:

1. Signal acquisition

2. Preprocessing

3. Feature extraction

4. Machine learning classifier integration

5. Security protocol

We will describe about each of the components of our proposed non-contact continuous identity authentication system in the next subsections.

5.2 Machine Learning (ML) Classifiers

Classification is the process of distinguishing between different classes of data points[5]. In ML terminology, classes are sometimes called as targets/labels of categories. The basic task of classification predictive modeling is the approximating a mapping function (f) from input variable (X) to discrete output variables (y) [5].Classification belongs to the category of supervised learning where targets are provided with the input data and model is trained based on extracted attributes or features of the data set of that particular class. There are many applications in classification in many fields especially in health and security/surveillance areas.

In ML literature, there are lot of established and popular classification algorithms but it is hard to conclude which particular algorithm is Superior to others [6]. The performance of the classification algorithm varies with the data set as they are mostly data driven algorithm. We employed two popular classification algorithms one is K-nearest neighbor (KNN) and support vector machine (SVM). We will describe briefly about their basics in the next subsection.

5.2.1 K-nearest neighbor (KNN) algorithm

The KNN algorithm is a simple, easy-to-implement supervised machine learning algorithm that can be used both for classification and regression [5]. A supervised machine learning

algorithm is dependent on training the model with some input data set and then test the performance of the model with new data set of the same class [5].A classification problem has a discrete value as its output.

The KNN algorithm assumes that the similar things exist in close proximity [5].In KNN learning process it stores all instances correspond to the training data points in n-dimensional space.When an unknown data is received, it analyzes the closest k number instances and calculates its euclidean distance from other data points of different classes and based on the closest distance data-set it gets classified [5].

The potential advantage of KNN is easy to implement and versatility of the algorithm as it can be used for regression and classification as well. One of the major bottleneck of this method is computational time and it is very slow as it need to do some iterative calculations to estimate the closest neighbors of the target.

5.2.2 Support vector machine (SVM) algortihm

SVM is a discriminative classifier which works by utilizing a separating hyperplane [6]. It constructs a set of hyperplane which can be used for classification between classes. Hyperplane performs well for linear classification problem. When non-linear problem is solved using SVM basically it uses kernel trick. In machine learning, a "kernel" is usually used to refer to the kernel trick, a method of using a linear classifier to solve a non-linear problem. The kernel function entails transforming non-linearly inseparable data to linearly separable ones [6]. In this work, we have utilized Radial Basis Function (RBF) as SVM kernel as it is most popular and used in various learning algorithms [6]. The RBF kernel on two samples x1 and x2 represented as feature vectors in some input

$$K(x_1, x_2\ ) = \exp(-(|x|_1 - |x|_2)^2)/2\sigma^2) \tag{5.1}$$

$$|(|x_1 - x_2|)|^2 = squaredEuclideandistance \tag{5.2}$$

σ is a free parameter. The value of RBF kernel decreases with distance and ranges which is used for similarity measure between two features [6].

5.3 Feature Extraction for Identity Authentication

Here in this section we highlighted different efforts we made to propose an unique identification algorithm for multi-subject measured data. As the goal of this research work is to implement this non-contact identity authentication technology in real-world environment especially in multiple-subject scenarios. For finding an unique breathing-related feature we started exploring with single subject data and modifying the previous algorithm developed by our research group [3]. Eventually, we utilized this algorithm for the ICA-JADE separated respiratory patterns for the presence of two subjects in front of the radar. Prior research [3] demonstrated the efficacy of using dynamic segmentation

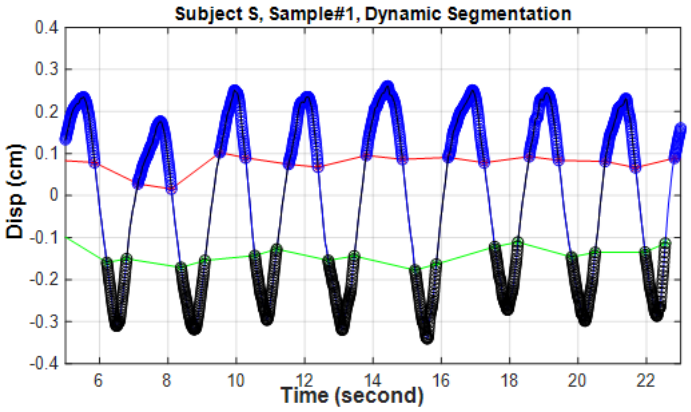

Figure 5.2 Dynamic segmentation of [30%-70%] displacement in each breathing cycle where inhale to exhale area ratio is being calculated for a segment. From [3]

approach to recognize human subjects based on their breathing patterns. The idea of dynamic segmentation is that it considers 30%-70% of both inhale and exhale episode and then calculating the area ratio of inhale and exhales.The method is represented in Fig. 5.2. However, when the inhale and exhale area ratio becomes closer among subjects this

method cannot accurately identify human subjects and creates ambiguity in the system. It was demonstrated in [3] that two subjects having very close area ratio resulted in some ambiguity during observations recorded over few weeks [3].In practice, it might happen that under certain circumstances two subjects may have identical inhale/exhale area ratios which would lead to false identification. Thus, we started on investigating for improving the dynamic segmentation algorithm by testing the feasibility of algorithm for large number of participants and with different physiological activities as well.

5.3.1 FFT based feature extraction and limitations for single subject experimental scenario

In this experiment, we used a 2.4 GHz quadrature Radar system which has two channels (I and Q) connected to Low-noise-amplifier (LNA) (SR560). All the LNA's were dc-coupled with 200 gain and with a cut-off frequency of 30 Hz. The two channels outputs were connected to DAQ (NI-6009). Finally, a customized LABVIEW interface captures all the signals. Major components of the antenna part are (Antenna Specialist ASPPT2988), two 0° power splitter (Mini-circuits ZFC-2-2500) and two mixers (Minicircuits ZFM-4212). The local oscillator utilizes a quadrature power divider, providing in-phase and quadrature version of the signal.The radar system and human experiment setup is shown in Fig. 5.3. We collected the data set for six different participants for sedentary condition. The Datasets shown are respiration traces collected from the Doppler radar setup for six subjects, using 50 sets of respiration traces with 100 Hz, 60 second sampling.The breathing pattern captured in the I/Q channels for the first participant is shown in Fig 5.4. After capturing the signals DC offset was removed as it is produced by system imperfections, internal DC offset. Fig. 5.4 depicts the captured breathing pattern from in phase and quadrature phase channel of the radar system. In order to find accurate displacement we employed arctangent demodulation [7]. Since the quadrature outputs have 90° phase difference, and each signal can be expressed as sine and cosine functions, the phase information can be obtained by taking the ratio between two outputs and applying arctangent function. This demodulation

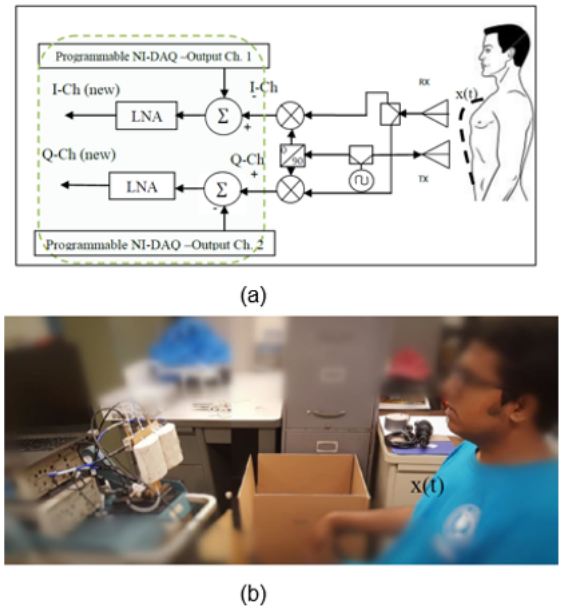

Figure 5.3 (a) 2.4 GHz quadrature Radar system and (b) human experiment setup, where subjects are in seated position in front of the radar system in a controlled environment.

process can be expressed as:

$$\phi(t) = \arctan(B_Q/B_I\ ) \tag{5.3}$$

FFT of single subject respiration pattern contains a peak which basically represents the breathing rate of the subject. We have analysed the six subjects breathing rate from their captured breathing pattern using FFT. The breathing rate of six participants are as follows: .2973 Hz, .2662 Hz, .3135 Hz, .5475 Hz, .3161 Hz and .3306 Hz.Figure 5.6 illustrates the demodulated signal of third participant's chest displacement in meter and his corresponding breathing rate .3135 Hz. As each individual breathing pattern is different in terms of tidal volume, air flow profile and other unique features. Feature extraction from breathing signal always remains a challenging and time consuming task. However, FFT based feature extraction contains all the unique breathing features in that captured pattern samples as it contains the spectral characteristic of the signal. FFT spectrum elucidates the spectral characteristics of that respiration signal as it consists of breathing

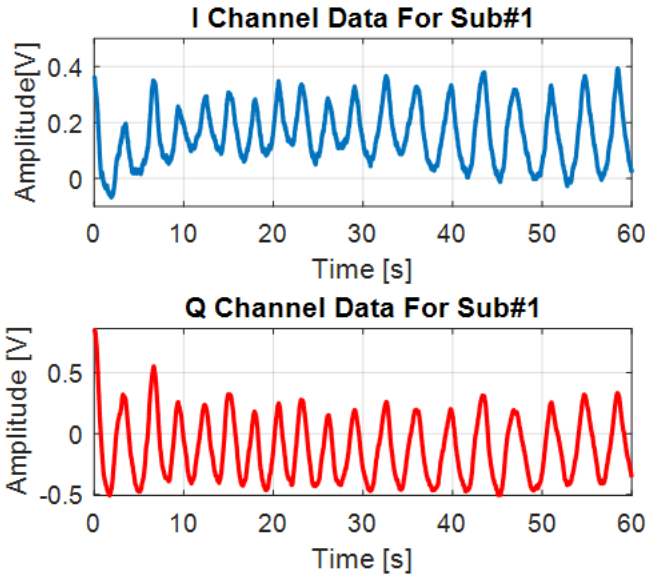

Figure 5.4 Radar output I (blue) channel and Q (red) channel captured signals with DC offset removed.From [7]

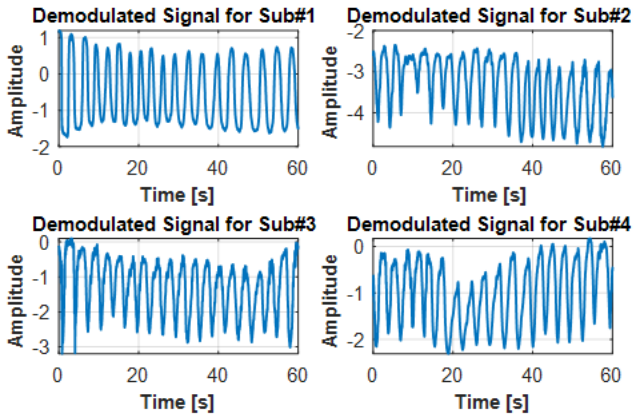

Figure 5.5 Demodulated signal for four different subjects.Arc-tangent demodulation technique is used to find chest wall displacement from captured I and Q channel signal.From [7]

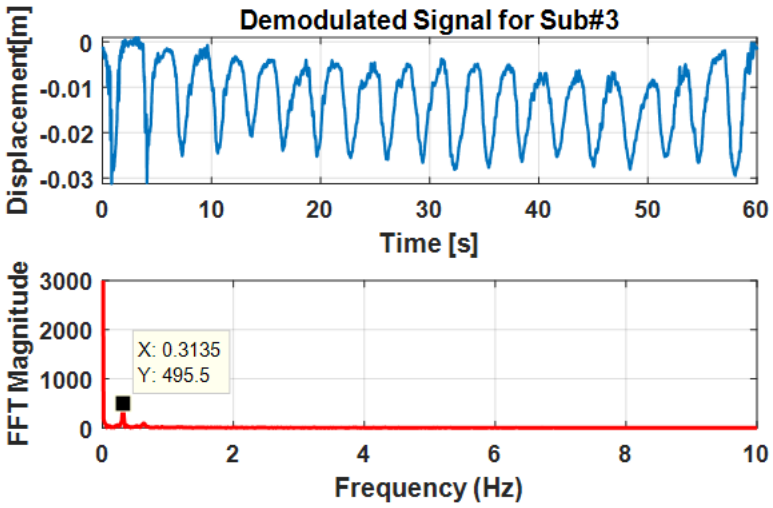

Figure 5.6 Demodulated signal of subject 3 and FFT of the respiration signal. FFT peak demonstrates the breathing rate of .3135 Hz.

rate, energy, and peaks distribution. So, analysing the FFT spectrum of the recorded first hundred samples for six subjects provides us unique features of that corresponding respiration pattern. Figure 5.7 represents the FFT magnitude of averaged hundred samples of respiration trace of six participants with 100 Hz sampling of 60 seconds. The FFT spectrum of each respiration trace will act as unique features of respiration patterns. In Fig. 6 shows participant 4 has higher FFT magnitude (logarithmic scale) of fundamental frequency than other participants as we have found that in most of the respiration trace of that participant has higher breathing rate (.5475 Hz) which produces that larger magnitude in FFT spectral contents.

In order to test the performance of our proposed SVM classifier with radial basis function a total of 50 set of data each having 60 second of epoch were collected from six different persons where in Fig 4 showed the patterns has body motion in the data , low frequency sag or level shift on the data. So, having many samples would average out the effect of body motion. 60% of this dataset were used for training the SVM classifier and then 40% of the data set were tested to verify the classification task. The learning curve for

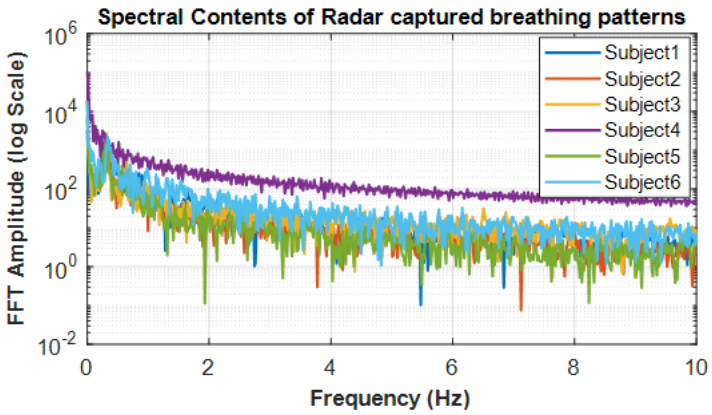

Figure 5.7 FFT spectrum of captured breathing pattern for six different participants, showing variations up to 10 Hz. FFT spectral content was used for providing unique features for each participant to train and test the system.

the training score of RBF kernel for varying number of training sample is shown below in Figure 5.8. Training score and validation score closely converges after 60 training samples which also illustrates the RBF estimator is not suffering from bias or variance error. The confusion matrix for training data set is shown below in Figure 5.9. A confusion matrix for training data set shows the classification performance.Participant-1 was classified accurately 30 times, participant-2 29 times, participant-3 30 times, participant-4 29 times, participant-5 35 times and participant-6 27 times. Overall attempt for classification was 180 times. In each of the attempts it could recognize different participants accurately without any false classification incidence. So, the overall classification training accuracy was 100%. The data set is split into two parts one is training and another one is for testing. The tested data set is not a part of training as it was split before training SVM classifier. Figure 5.10 represents the confusion matrix for test data sets. As test data is less than training data sets so classification attempts was less. In testing overall 60 attempts were made to classify different participants based on their FFT of first hundred samples which is unique features for each participants. Participant-1 was classified 9 times, participant-2 was classified 11 times, participant-3 10 times, participant-4 15 times, participant-5 six times and participant-

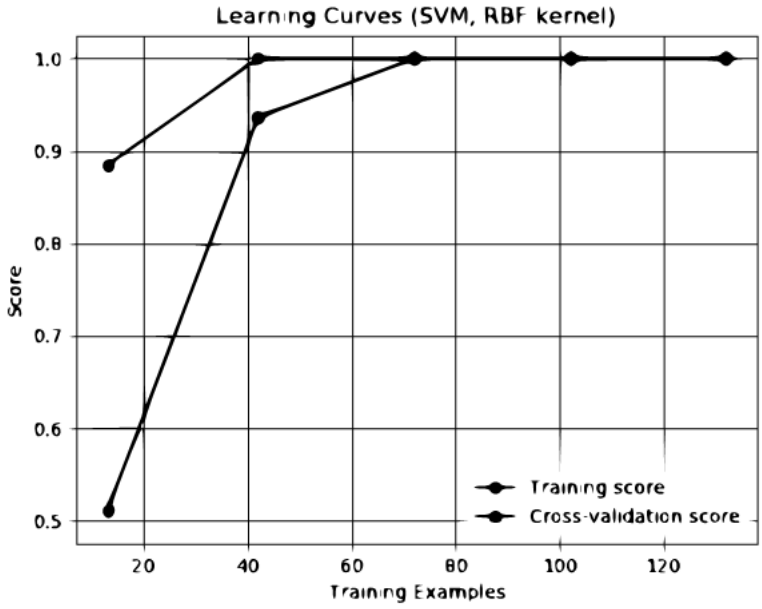

Figure 5.8 Learning curve for training samples of SVM Classifier. The validation score and training score converges after seventy training samples which indicates there is no overfitting or under fitting.

6 9 times accurately. The overall classification accuracy for testing data set is also 100%.

So, the overall success rate of SVM with radial basis function is 100% success rate to recognize individuals based on their FFT coefficients of the sampled respiration pattern collected form Doppler radar. There is no false classification incidence in our proposed system so, SVM radial basis function based classifier system can overcome the existing limitation.

1. Limitation of this work: As the data set and number of participants was small, continued experimentation remains needed to verify the efficacy of the FFT-based feature extraction approach. For further investigation, the feasibility of the FFT-based approach for extracting identifying features from radar respiratory traces for sedentary subjects was tested, along with measurements of the subjects just after performing physiological activities (walking upstairs) [8].It was found that subject recognition still worked but was not as effective after performing short exertions as it

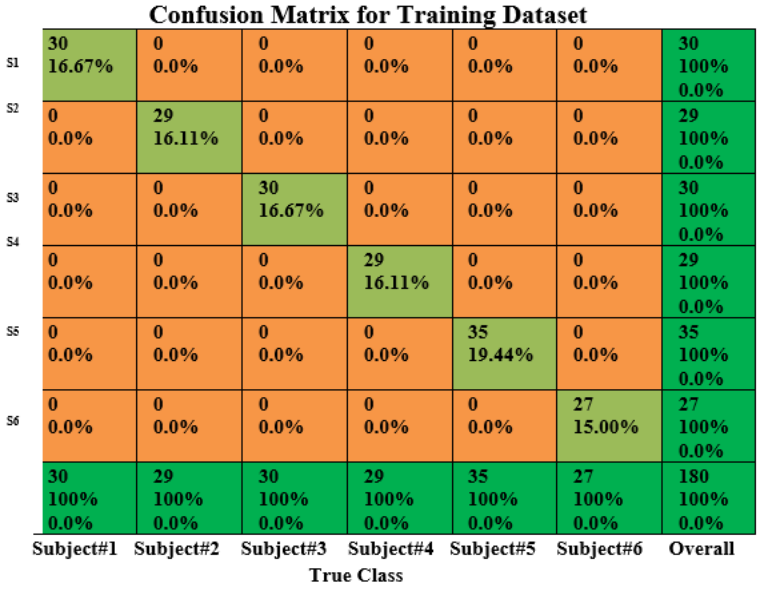

Figure 5.9 Confusion matrix of SVM with radial basis function for training respiration traces. The diagonal position of the matrix represents the number of times of subject classified accurately.

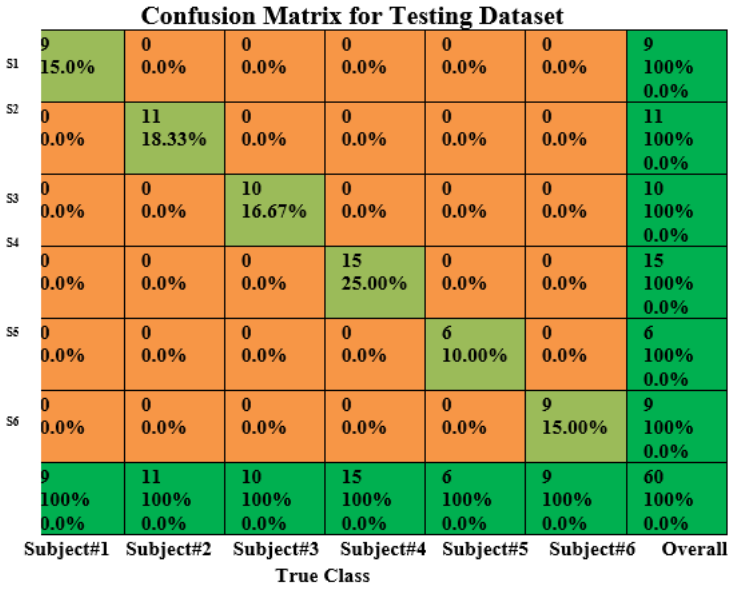

Figure 5.10 Confusion matrix of testing respiration traces. The diagonal matrix represents the successful classification attempt for different participants.

was for sedentary subjects [8]. Figure 5.11 illustrates the FFT spectrum of six different participants after performing post-physiological activities.From the figure it is clear that, participants FFT spectrum gets overlapped. So, from this experiment, we clearly understood that, FFT spectra works well for sedentary breathing condition but for after performing post-physiological activities it didn't remain constant or different for different participants.Thus, we further explored for finding a unique respiratory feature from participants that work similarly both for sedentary and after performing post-physiological activities [8].

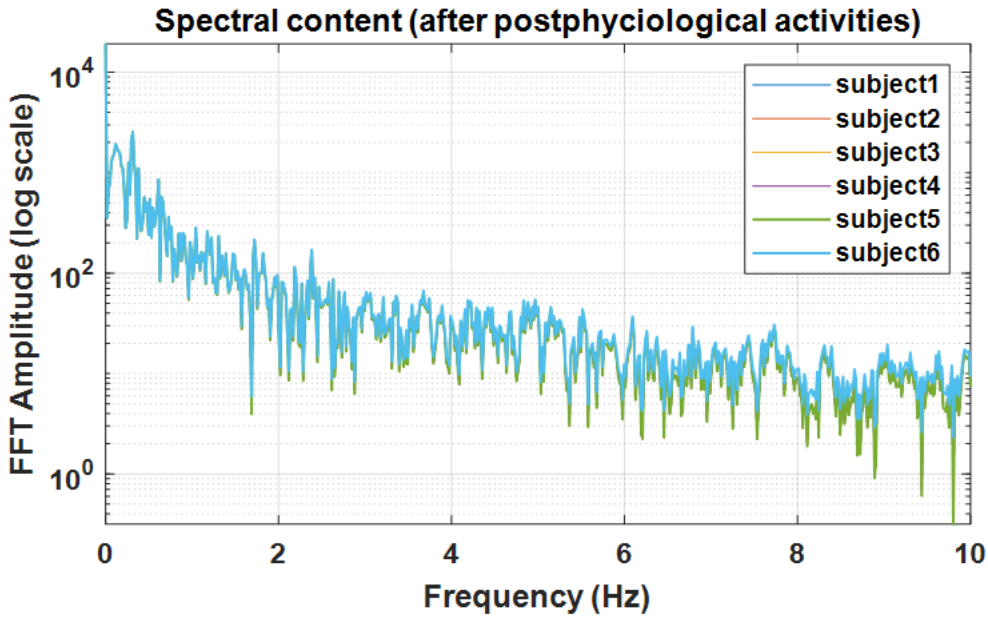

Figure 5.11 FFT spectrum of captured breathing pattern for six different participants after post-physiological activities (walking stairs),showing variations up to 10 Hz. FFT spectral content was overlapping so it is hard to extract unique features from FFT.

5.3.2 Feature extraction for identity authentication for single subject scenario

In this experiment, we collected data set from ten participants for about four weeks both for sedentary and post-physiological activities.Figure 5.12 illustrates different respiratory features of radar captured respiration pattern. The extracted features are described below:

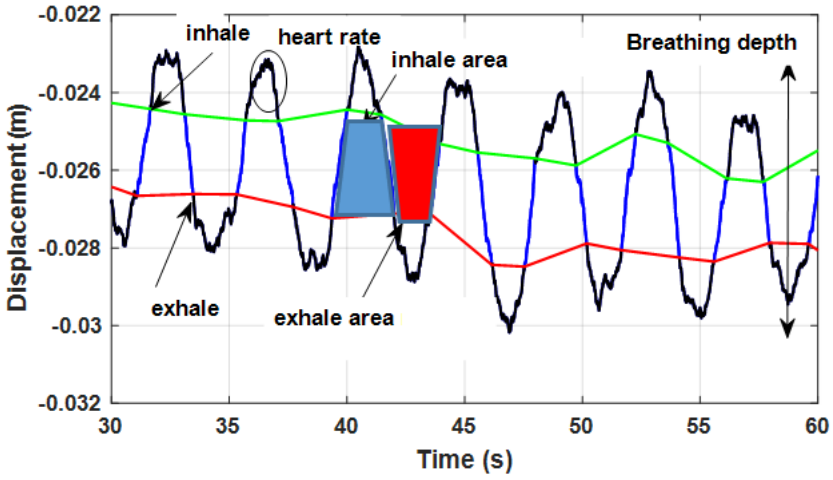

Figure 5.12 Extracted features from Radar captured respiration.Each breathing cycle contains inhale, pause and exhale episode.

1. Breathing/heart rate: Breathing rate can be found by counting the number of breathing cycles in a given amount of time. Generally, we take the Fast Fourier Transform (FFT) of the recorded signal to find the breathing rate [9]. For extracting heart rate, we filtered respiration signal using butter-worth band pass filter within .8-2 Hz and then performing FFT [9].

2. Inhale/exhale speed, average distances and standard deviation of peaks: From the peak search process we can find maximum/ minimum peaks and their time indexes of radar captured signal. From the information of peaks positions and time indexes we can find inhale/exhale rate, average distances, and standard deviation of the peaks [3].

3. Breathing depth: Breathing depth can be calculated by taking into account of the total displacement from minimum peak to maximum peak. Average depth is taken into consideration and calculated as one of the respiratory features.

4. Spectral entropy: Spectral entropy is calculated by taking square of the amplitude of the radar captured signal and by normalizing the number of samples.Spectral entropy represents the breathing energy of the signal.

5. Dynamic Segmentation: Prior research [3] demonstrated the efficacy of this technique. The idea of this technique is that segmenting the 1-minute breathing cycle episode with 30%-70% amplitude and calculating the average area ratio of the inhale and exhale segment. This feature breath ratio, R gives us an idea how fast people initiates the next cycle of breathing [3]. R=inhale area trapezium / exhale area trapezium

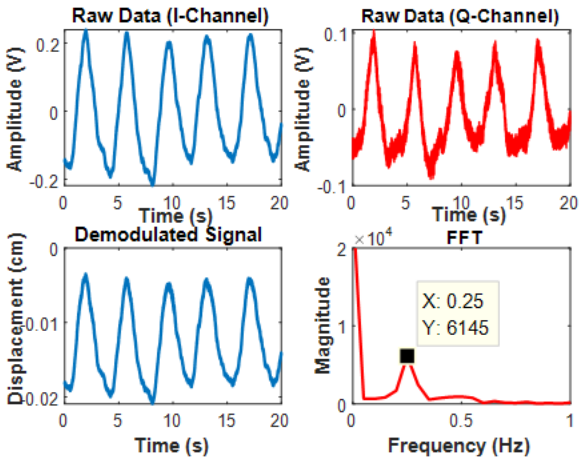

Figure 5.13 Radar captured raw data channel signal (a) In-phase (I) channel signal (b) quadrature phase (Q) signal (c) arc-tangent demodulated signal for finding maximum chest displacement (d) FFT of the signal where peak of the signal illustrates the breathing rate of .25 Hz.

After capturing the respiration signal, we filtered the signal segment for 60 seconds using FIR filter of the order of 1000. The sampling frequency of the data acquisition (DAQ) was 100 Hz. Finally, FFT is employed on arc-tangent demodulated signal to find

the breathing/heart rate [8]. Figure 5.13 illustrates the breathing rate .25 Hz when subject's measurement was taken during normal conditions. Figure 5.14 represents the breathing rate of five participants at sedentary and after short exertion.After analyzing five participants breathing pattern we found that, when people finish any short physiological activities their breathing/heart rate increase occurs a bit as just after short exertions and then they got chance to take rest (seated position) for radar measurement. For sedentary conditions,

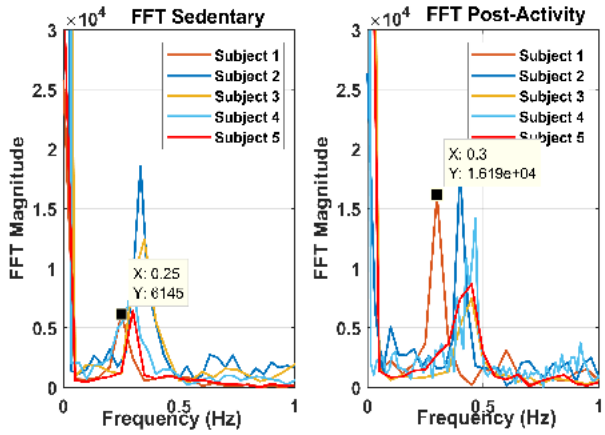

Figure 5.14 FFT magnitude of Radar Captured signal. It illustrates that breathing rate change occurs after exertions.

breath ratio is a unique feature for identifying people [3] but after short exertion, breath ratio changes abruptly due to change in exhale area and there is also overlapping breath ratio for different subjects [10]. However, we found that, their exhale area increases almost more than 1.4 times and breathing depth approximately more than 1.2 times than sedentary condition [8].We believe this is due to aerobic capacity or oxygen flow pattern, which means after finishing a short exertion subjects tend to take a long time to exhale which increases exhale area and breathing depth. It also indicates that the subject bodies try to make sure that more oxygen is absorbed into blood. Figure 5.15 represents the increase in breathing depth and exhale area of participants after short exertions. Further investigation is required to understand better how breathing dynamics changes when people come from long exertion (Gym workout) which remains as future work. Aerobic dynamics related unique features

(exhale area and depth) change in pattern in a consistent manner for individuals and thus help with recognition of people even after short exertion. We also integrated SVM classifier

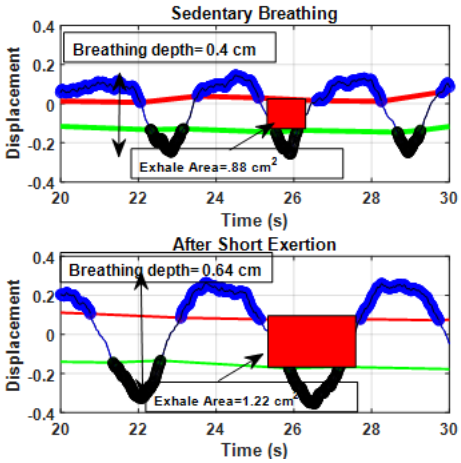

Figure 5.15 Dynamic segmented (10 second) radar captured two different respiratory patterns for one participant. Breathing depth and exhale area increases after short exertions.

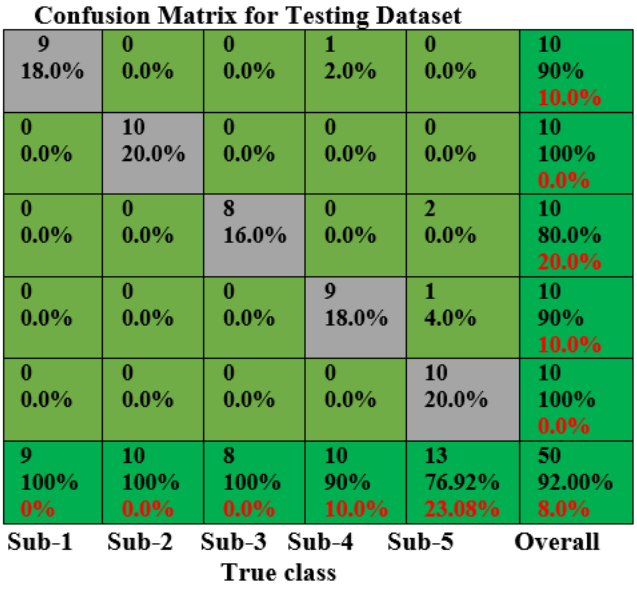

Figure 5.16 Confusion matrix of the testing data set.The diagonal position of the matrix represents the number of times subjects classified accurately.

with radar system in our previous work [7]. In order to test the performance of our integrated

classifier a total of 50 sets of data each having 60s of data were used for five different participants. Figure 5.15 illustrates the confusion matrix for identifying people for having mixed respiratory features (sedentary and exercise). The overall classification accuracy is almost 92% while it is 98.55% for sedentary. Some misclassification is occurred due to overlapping of some of the respiratory features after physiological activities yet including short exertion in training was sufficient to maintain a significantly high success rate.

5.3.3 Hyper features for identity authentication for multi-subject scenarios

From the above two subsections it is clear that air-flow profile related features are much more distinguishable than FFT-based features. In this subsection, we will describe about the feature extraction for multiple subjects in front of the radar.

We conducted experiments on 20 different participants to prove identifiability in their radar captured respiratory signatures. In our experiments, two subjects each sit in front of radar .5 to 1m away with angular discrimination limit between two subjects were .4 m. The experimental procedure involving human subjects described in this paper were approved by the Institutional Review Board (IRB). The institution's ethical review board approved all experimental procedures involving human subjects. Twenty subjects with their age 16-35 participated in the study. Their weights are in between 42-85 kg. None of them have any heart disease. We conducted the experiment for about one month. In each trial we had two different subjects in front of the radar system and we collected data set for about 1 min (60 s) and the collected data set was combined mixture of respiration pattern of two subjects. After separating independent respiratory signatures for extracting features we just considered 10 to 20 second data set which contains at least two to three respiratory cycles. Therefore, in total we collected almost 30,000 cardiac cycle samples for each different participants. A chest belt (UFI 1132 piezo-electric respiration transducer) is also used for capturing reference respiration pattern. One of the advantage of our system is as we are utilizing 24 GHz radar system so there is less probability of interference with Wi-

Fi and Bluetooth module in home environment as they operated in 2.4 GHz so there needs no arrangement for co-existence as the frequency are different bands [4]. The proposed authentication system comprises of 24-GHz radar which has one transmitter two receivers and the main beam width of the transmitter is around 30° [11]. There is no known health hazards attached to the system as the maximum power consumption limit is 750 mW which is almost a thousand time less than the peak power of ordinary global system for mobile communication (GSM) cellphone.

After separating two independent respiratory signatures, we used low pass filtered that signal with cut off frequency 2 Hz because within that frequency band, breathing rate and heart rate exists.Then we performed Fast Fourier transform (FFT) of the signal to extract breathing rate and heart rate. Fig. 5.17 illustrates the breathing rate and heart rate of two subjects from separated respiratory signatures.Breathing rate and heart rate are harmonics of each other.From Figure 5.17 it is shown that the breathing and heart rate of subject 1 and subject 2 is .33 Hz, .98 Hz and .32 Hz and .97 Hz respectively.So, extracting only breathing rate and heart rate cannot be a unique way to recognize individual subject as they may have overlapping respiratory rate. Breathing is controlled by central neural mechanisms which is basically complex interactions between various chemicals in blood and air we breathe [2]. It consists of two different phases: inspiration (inhale) and expiration (exhale). During inspiration, the diaphragm and the intercostal muscle contracts and during expiration they relaxes [2] . It has been proved in other investigations that no two persons can have the exact same heart, blood circulation system and cardiac movement for performing breathing activities [4][3][12].In our previous work, we tested the feasibility of extracting different respiratory features from radar captured single subject measurement [8]. So, we extracted eleven different respiratory features.Respiratory features are listed below:

1. Breathing rate

2. Average maximum peak distances

3. Standard deviation of maximum peak distances

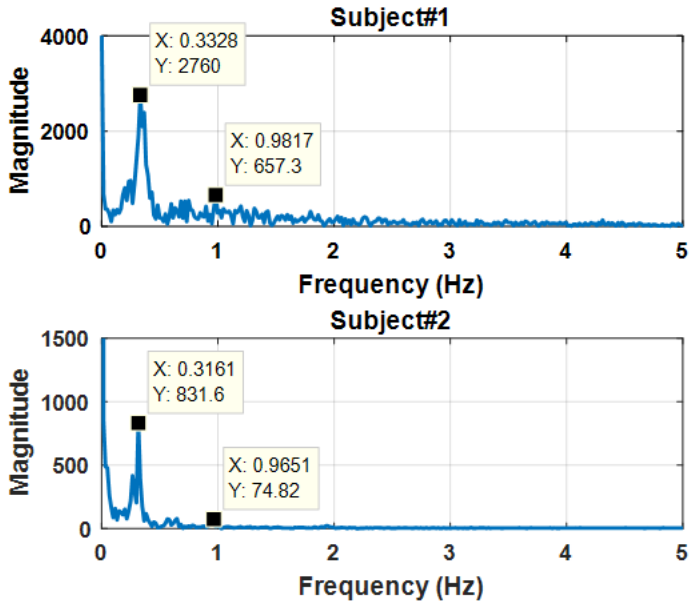

Figure 5.17 Respiratory rate and heart rate of two subjects whereas one participant has respiratory rate of .33 Hz and heart rate of .98 Hz where other participant has very similar breathing rate and heart rate.

4. Average minimum peak distances
5. Standard deviation of minimum peak distances
6. Breathing depth
7. Inhale speed
8. Exhale speed
9. Spectral entropy
10. Inhale area
11. Exhale area

Figure 5.18 illustrates the extracted respiratory features from radar captured respiration pattern. Among all other extracted features we found that, inhale area and exhale area is

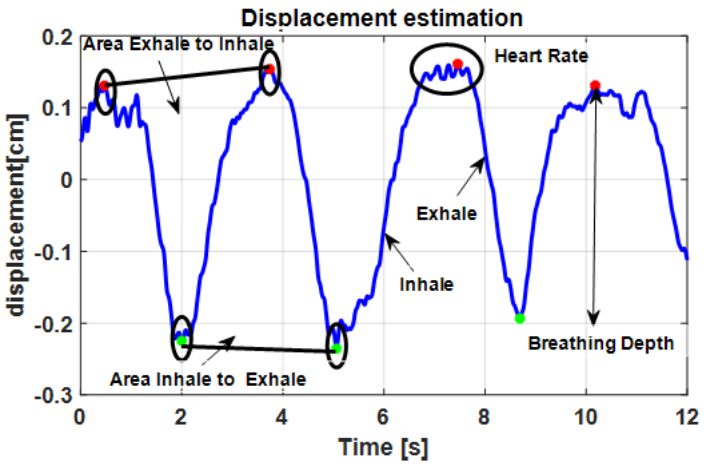

Figure 5.18 Extracted respiratory features from radar captured respiration pattern. The extracted features are breathing rate, heart rate, inhale rate, exhale rate, distribution of the peaks.

significantly different for different participants. After separating independent respiratory signatures, we used peak search method to find local maxima and minima points in the segmented portion (12s) of signal. After finding the peaks of maxima and minima we created an array of two consecutive maxima and in between one minima point and then we constructed triangle within that three points (two maxima and one minima). Before triangulation method we also dynamically evaluated the displacement of each separated signal. Then we calculated area of that triangle. Figure 5.19 illustrates the summary of the algorithm for determining inhale and exhale area. Figure 5.20 represents the peak finding method after separating respiratory signatures.

Peak search process allows to create an array of maximum points and minimum points within that segment of the signal. We also created an array of two consecutive maxima and in between one minima and stored that in the variable. Then we constructed a triangle in between three peaks with its side's tangents to the side of peaks. The inhale and exhale area represent two different cardiac phenomena. Inhale area illustrates the ventricular filling state of heart and exhale area represents ventricular contraction. During that stages

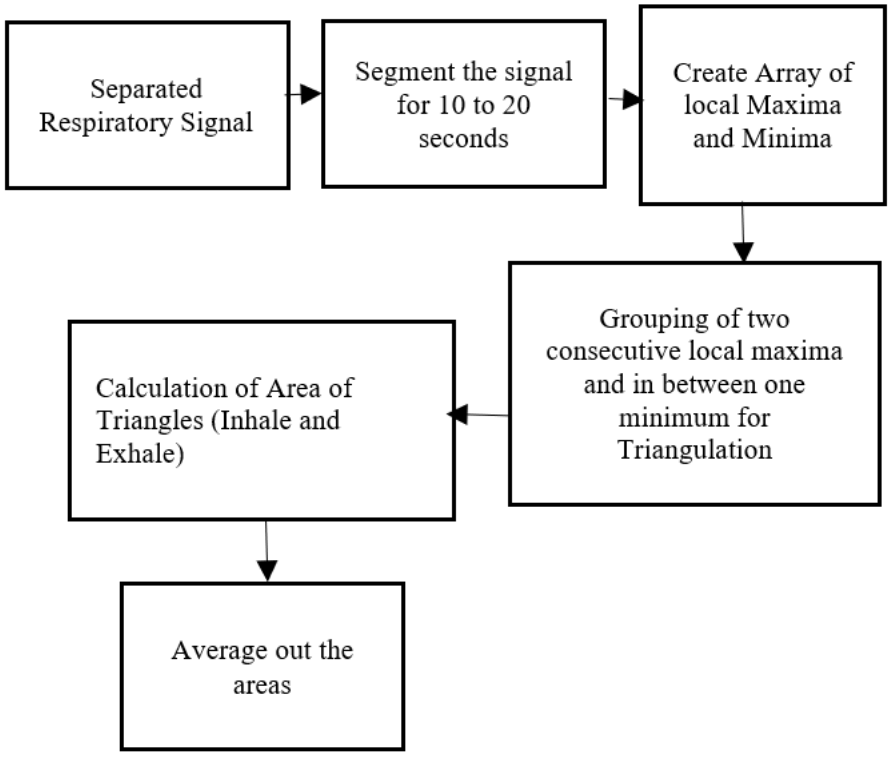

Figure 5.19 The summary of the algorithm (flow chart) determining the inhale and exhale area of the segmented separated-respiratory signal.

different people might have different breathing depth and air flow profile due to variations in cardiac movement which also affect the area of that segment.

Figure 5.21 shows the significant differences between these two area segments for two different subjects. In our earlier attempt, we concentrated on dynamic segmentation which is basically identifying the points in the range of 30%-70% of both inhale and exhale episode and calculating the area ratios between inhale and exhale [3].However, in our later study it has been proved that, inhale/exhale area ratio feature didn't remain constant after post-physiological activities as the method totally ignores the heart related dynamics because it considers 30%-70% of the chest displacement [3]. Table 5.1 illustrates the inhale and exhale area differences between five different participants with triangulation method.

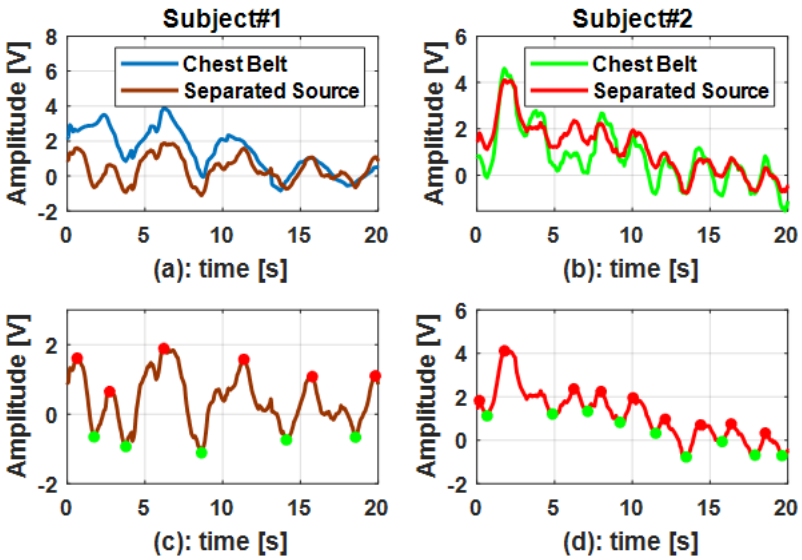

Figure 5.20 Separated Respiratory signatures (a) subject1 (b) subject2 (blue line represents separated signal for subject 1 and red line represents separated signal for subject 2). Peak search method for estimating breathing depth and finding array of maxima and minima for (c) subject1 (d) subject2. (red dots represent maxima and green dotes represent minima).

5.4 Classification Accuracy For Identity Authentication System in Multiple Subject Scenarios

We collected data set for 20 different participants. We also repeated the experiment in different days of months for twenty times.For our analysis, We considered each subject twelve seconds radar captured pattern which contains more than one cycle. Therefore, in total there are 20 set of data for each participants containing almost 5000 cardiac cycles sample

Table 5.1 Inhale areas for five participants. The inhale area shows certain range differences between five different participants.

Area	S1	S2	S3	S4	S5
min (cm^2)	1.49	1.50	0.8	0.95	1.29
max (cm^2)	1.54	1.52	0.95	1.25	1.45

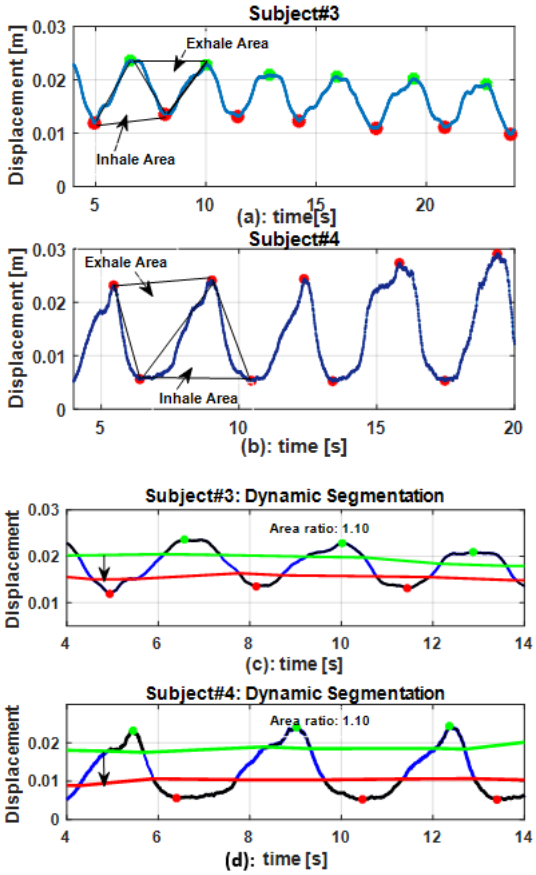

Figure 5.21 The illustration of determining inhale and exhale area of the signal, there is a clear visible difference in between (a) subjects 3 and (b) subject 4. The area appears to be higher for subject4.Dynamically segmented inhale and exhale area ratio for (c) subject 3 and (d) subject 4 where both subjects have the same area ratio.

in the evaluation. We extracted eleven respiratory features described in previous section and then we utilized machine learning classifiers to train and test the accuracy of the proposed system.So we integrated KNN and SVM algorithm to test the accuracy of our proposed system. To evaluate the performance of different classifier algorithms, KNN and SVM with different kernel functions were integrated and tested using the Classification learner app in Matlab.The dataset is split into five parts whereby 3/5 of the data are used for training and 2/5 are used for testing. Figure 5.22 illustrates the hyperparameter optimization curve that seeks to minimize the classification error by utilizing different distance metric for

Table 5.2 Exhale areas for five participants. The exhale area shows certain range differences between five different participants.

Area	S1	S2	S3	S4	S5
min (cm^2)	1.72	1.20	1.40	1.50	1.35
max (cm^2)	1.80	1.30	1.50	1.55	1.40

KNN (Euclidean, hamming, and other), for SVM with different kernel function: (linear, quadratic, gaussian and other) and for decision trees different split criteria (Towing rule, maximum deviance reduction, etc.). Figure 5.22 shows the minimum classification error plot for optimizeable SVM algorithms. Classification learner app uses Bayesian optimizer and it

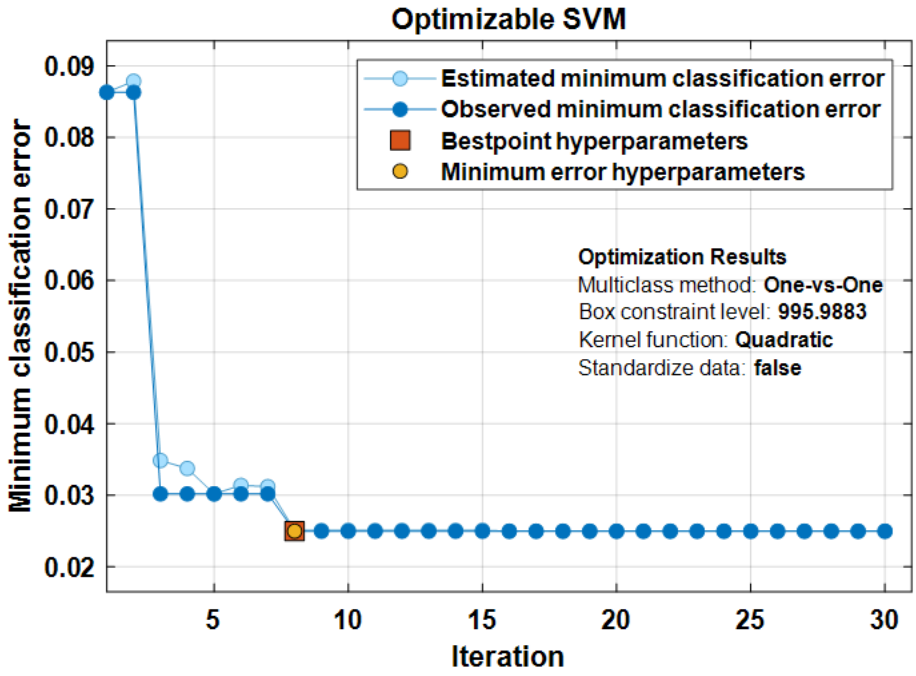

Figure 5.22 Minimum classification error plot for optimizeable SVM, where deep blue line represents the minimum classification error line and the red square represents the best hyperparameter (minimum classification error).SVM with quadratic function outperformed other classifiers.

runs the program for different kernels for thirty times to find out the best optimizer kernel function. At each iteration, the simulation tries to different combination of hyperparameter

Table 5.3 Accuracy of different classifiers for testing data-set.

Classifiers	**Accuracy**
KNN (Cubic)	84.4%
KNN (Cosine)	86.4%
KNN (Medium)	86.9%
SVM (Linear)	95%
SVM (Quadratic)	97.5%
SVM (Fine Gaussian)	93.5%
SVM (Medium Gaussian)	96.5%

values and updates the plot with minimum validation classification error observed up to the iteration indicated in dark blue. After running the program for thirty times with different combination of kernel parameters, SVM with quadratic function outperformed other classifier with minimum classification error of .025, represented as red circle in Figure 5.22. Table 5.23 illustrates the accuracy of different classifiers.

We utilized 5-fold cross validation so 60% data set were used for training and rest of the 40% data set were used for testing. Among all other classifier SVM (Quadratic) outperformed than other classifier with an accuracy of 97.5%. Fig. 15 below illustrates the confusion matrix of SVM classifier with quadratic function to recognize different subjects based on their radar captured respiratory signatures.From the confusion matrix, it is clear that, subject 2 was misclassified 5% as subject 1 as they have some overlapping inhale/exhale area and other features also. Similarly subject 3 and 4 has some misclassification issues due to overlapping area of the inhale and exhale. For other subject study it performs well to recognize subject accurately.Additionally, subject 6 and 7 has misclassification about 12% and 14% respectively.The overall classification accuracy was 97.5% which provides clear indication that the proposed method can be utilized for real world applications as well. Then we also looked into learning curve of the outperformed classifier SVM with quadratic function. Figure 5.24 illustrates the learning curve of SVM with quadratic function. With the increase in training sequences the gap between two learning curve decreases which also clearly illustrates that the training model has quite less variance. After 60 training sequences

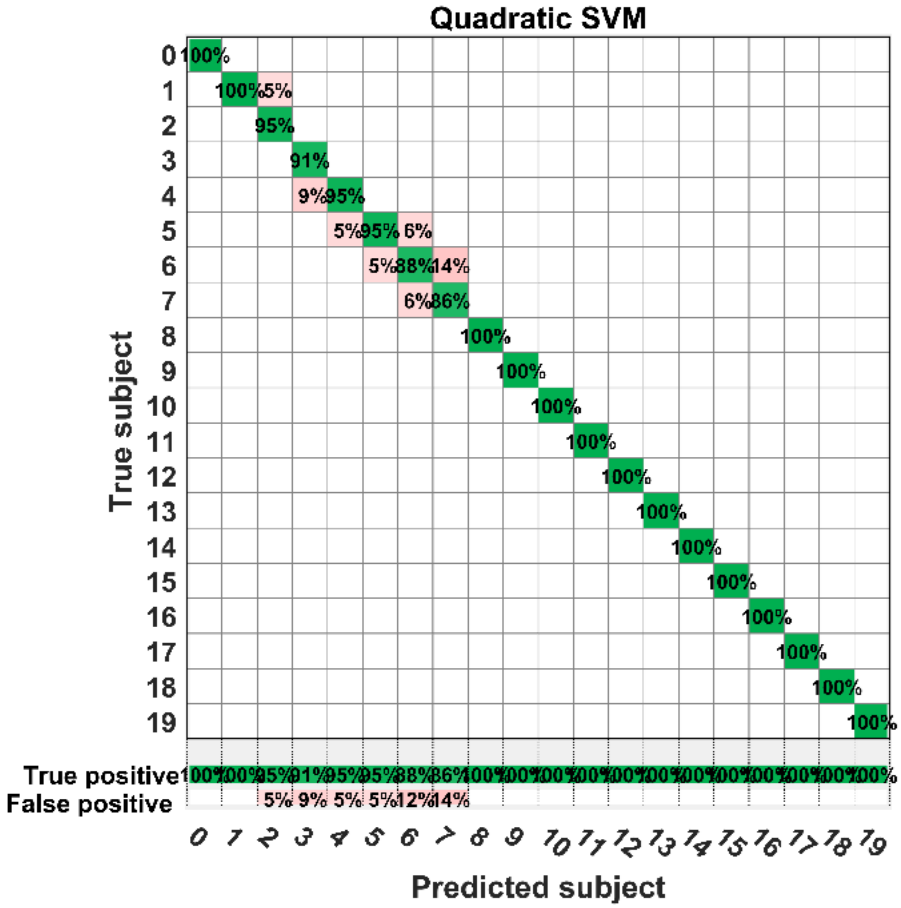

Figure 5.23 Confusion matrix of testing data set of SVM with quadratic function. Subject 2 was misclassified as subject 2 for 5% whereas subject 3 was misclassified as subject 4 for 9% times. Subject 6 and 7 was misclassified 12% and 14% times respectively. So overall classification accuracy was 97.5%.

the two curve closely overlaps with each other which reduces the gap between two graphs. Adding more training instances can increase the training score of learning algorithm but still it shows reasonable accuracy with 97.5%. Classification accuracy of SVM with quadratic kernel outperformed with other clasisfiers with an accuracy of 97.5%. From the learning curve in Figure 5.23 it also illustrates there is not over fitting or under-fitting of the tested data set.

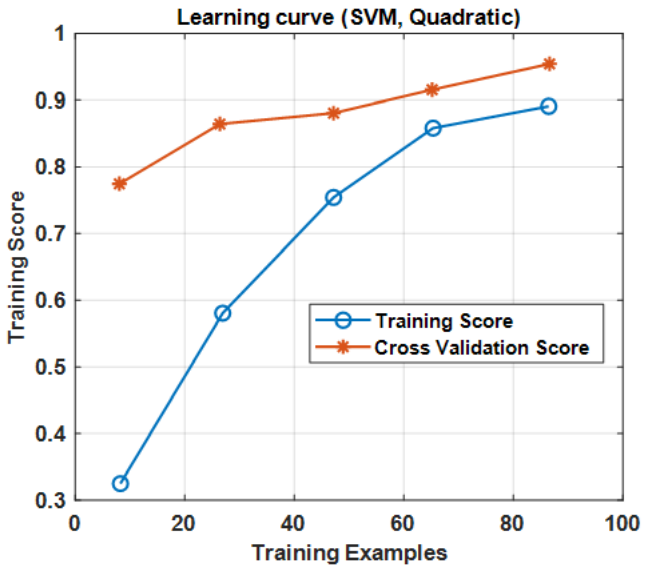

Figure 5.24 Learning curve of SVM with quadratic function.With the increase of training sequences the training score closely matches with cross validation score.The way convergence is occurring so there is no over fitting or under fitting.

5.5 Conclusion

In this chapter, we highlighted the feature extraction process from radar captured respiration pattern. Based on our analysis, we found that, air-flow based profiles shows more unique pattern than FFT-based approach.We also developed an algorithm for hyper feature (inhale and exhale area) extraction from radar echoes. Additionally, different approaches for extracting unique feature has been described in details in this chapter. We also integrated two different machine learning classifiers with the Doppler radar system.Based on our experimental analysis, SVM with quadratic function outperformed other classifiers with an accuracy of 97.5%.

References

[1] S. M. M. Islam, O. Borić-Lubecke, Y. Zheng, and V. M. Lubecke, "Radar-Based Non-Contact Continuous Identity Authentication," *Remote Sensing*, vol. 12, p. 2279, July 2020.

[2] G. Benchetrit, "Breathing pattern in humans: diversity and individuality," *Respiration Physiology*, vol. 122, pp. 123–129, Sept. 2000.

[3] A. Rahman, V. M. Lubecke, O. Boric-Lubecke, J. H. Prins, and T. Sakamoto, "Doppler Radar Techniques for Accurate Respiration Characterization and Subject Identification," *IEEE Journal on Emerging and Selected Topics in Circuits and Systems*, vol. 8, pp. 350–359, June 2018.

[4] F. Lin, C. Song, Y. Zhuang, W. Xu, C. Li, and K. Ren, "Cardiac Scan: A Non-contact and Continuous Heart-based User Authentication System," in *Proceedings of the 23rd Annual International Conference on Mobile Computing and Networking*, (Snowbird Utah USA), pp. 315–328, ACM, Oct. 2017.

[5] "[online] https://towardsdatascience.com/machine-learning-classifiers-a5cc4e1b0623."

[6] C. Cortes and V. Vapnik, "Support-vector networks," *Machine Learning*, vol. 20, pp. 273–297, Sept. 1995.

[7] S. M. M. Islam, A. Rahman, N. Prasad, O. Boric-Lubecke, and V. M. Lubecke, "Identity Authentication System using a Support Vector Machine (SVM) on

Radar Respiration Measurements," in *2019 93rd ARFTG Microwave Measurement Conference (ARFTG)*, (Boston, MA, USA), pp. 1–5, IEEE, June 2019.

[8] S. M. M. Islam, A. Sylvester, G. Orpilla, and V. M. Lubecke, "Respiratory Feature Extraction for Radar-Based Continuous Identity Authentication," in *2020 IEEE Radio and Wireless Symposium (RWS)*, (San Antonio, TX, USA), pp. 119–122, IEEE, Jan. 2020.

[9] S. M. M. Islam, E. Yavari, A. Rahman, V. M. Lubecke, and O. Boric-Lubecke, "Multiple Subject Respiratory Pattern Recognition and Estimation of Direction of Arrival using Phase-Comparison Monopulse Radar," in *2019 IEEE Radio and Wireless Symposium (RWS)*, (Orlando, FL, USA), pp. 1–4, IEEE, Jan. 2019.

[10] S. M. M. Islam, A. Rahman, E. Yavari, M. Baboli, O. Boric-Lubecke, and V. M. Lubecke, "Identity Authentication of OSA Patients Using Microwave Doppler radar and Machine Learning Classifiers," in *2020 IEEE Radio and Wireless Symposium (RWS)*, (San Antonio, TX, USA), pp. 251–254, IEEE, Jan. 2020.

[11] "[online] http://www.radartutorial.eu/01.basics/Angular%20Resolution.en.htlml."

[12] K. Shi, C. Will, R. Weigel, and A. Koelpin, "Contactless person identification using cardiac radar signals," in *2018 IEEE International Instrumentation and Measurement Technology Conference (I2MTC)*, (Houston, TX), pp. 1–6, IEEE, May 2018.

Chapter 6

Security Protocol For Back-scattered RF Signal Based Identity Authentication

Radio-based identity verification has the potential to overcome the limitations of contact-based biometric verification due to its unobtrusive way to sense physiological signal. The feasibility of these approaches has been demonstrated in prior researches [1][2[3][4].It has been proved in various investigations that people breathe in unique ways and breathing pattern variations might occur in terms of tidal volume, air flow profile, breathing depth and energy also [5]. In addition, identity verification using Radar technology has been tested for recognizing individual sleep apnea patients in our prior work [6].

To improve the quality and accessibility of sleep healthcare, non-contact sleep monitoring devices using microwave Doppler radar is proposed for screening OSA [7][8][9]. However, one major area of concern to adopt these devices is the possibility of falsifying sleep test data during unattended sleep studies. Some patients either unintentionally nullify or deliberately use surrogates during their tests, due to underestimation of their level of sleepiness, concerns regarding their job perspectives or insurance premium, or as an effort to obtain restricted stimulant medication [8][9][10]. Prior research to prevent data falsification mostly rely on fingertip sensors to maintain the integrity of the sleep test records [10].Unfortunately, attachment of contact sensors creates extra burden for the patients and affects the quality of sleep [9].

While prior works show great promises in radar based identity verification, the method is mostly evaluated under a controlled sing-subject experiment setting and lack formal analysis regarding their robustness against security threats such as data breach and spoof [1][2][3][4]. In real-world in-home sleep monitoring scenario, the probability to have multiple subject present during the test is high [11][12][13][14].Thus, concurrent measurement or isolation of respiratory signatures from the RF signal is crucial [11][12][13][14].In addition, when there are multiple subjects present in front of radar sensor, separating and extracting unique features from the combined mixture is equally challenging [11][12][13][14].Finally, the extracted breathing dynamics contain limited entropy (randomness) and may subject to impersonation attacks and exhaustive key search if they are stored and use in their naive forms.

In this chapter we described the feasibility to separate closely spaced subjects and extract cryptographically secure identities from their breathing patterns, using microwave Doppler radar, and Fuzzy Extractor. The contributions of our work are listed as the following:

1. We conducted a medium scale experiment with twenty participants and collected Doppler radar signals containing the combined respiration mixtures of every pair of participants. (Described in Chapter 5)

2. We customized Independent Component Analysis (ICA) with Joint Approximation Diagonalization of Eigen-matrices (JADE) algorithm to isolate respiratory signatures from the radar signals. (Described in Chapter 5)

3. We extracted highly distinguishable, breathing dynamic related hyper-features from the respiratory signatures, including breathing rate, heart rate, inhale/exhale rate, inhale/exhale area, etc., for identity verification.(Described in Chapter 5)

4. We evaluated the hyper-feature set with two different popular classifiers, K-nearest neighbor (KNN) and Support Vector Machine (SVM) and achieved promising performance in terms of false acceptance rate and false rejection rate. (Described in Chapter 5)

5. We formally calculated the empirical entropy of breathing related hyper-features, and determined that the intrinsic entropy of the hyper-features sets (approximately 3-bits) is insufficient for secure identity verification.

6. We combined Fuzzy Extractor with linear coding to transform the hyper-feature sets into strong biometric keys compatible with the machine learning classifiers.

To the best of our knowledge, our work is the first attempt to achieve secure radio-based multi-subject identity verification for in-home OSA screening, by harnessing the combined power of Doppler radar and Fuzzy key Extractor.

6.0.1 Related Work

As healthcare providers trend in favor of in-home versus in-lab testing, the recorded data confirming the patient's intention to undergo the test becomes increasingly critical. Within the patient population, members of several professions may be deeply concerned that positive test results or noncompliance with prescribed therapy will jeopardize their careers. As a result, some may choose to commit fraud by having a friend or a family member serve as a substitute for the tests. For this reason, manufacturers and researchers have proposed and incorporated several means of identity verification and compliance tracking into the in-home medical test and diagnostic devices. The following section provides a brief review of Doppler radar and non-contact sleep study, test compliance tracking, as well as related work in radio-based sensing/verification and co-presence authentication.

6.0.2 Test Compliance Tracking

The OSA test compliance tracking works as follows: Prior to the test, the doctor secures a tracker to the identified patient. Once attached, the tracker continuously observes and records the patient's vital signs until the test is finished. During the follow-up visit, the compliance data is compared with the screening data recorded by the OSA test equipment. If there were significant gaps, during which the compliance tracker fails to observe the

patient's vital signs or significant inconsistency between the compliance data and the OSA screening data, the test would be nullified. The initial assessment ensures the patient never removes the tracker, and the subsequent data analysis verifies the identification information between the patient wearing the tracker and subject undergoing the test.

Existing industry solutions utilize skin-contacting sensors to execute test compliance tracking [10][15].These approaches are reliable and have minimal chance of false identifications. However, the patient may feel discomfort due to the attached sensors, which hampers the confidence of the test results. Several relevant experiments achieve identity verification by remotely monitoring and verifying the subject's physiological or behavioral traits. Common methods use imaging or audio sensors to perform facial-based or voice-based recognition [16][17][18] or authenticate the subject through behavioral characteristics, such as tactile dynamics and gait patterns[19][20].Though essential, these methods are not suitable in addressing our problem due to the low-light and low-sound conditions and the subject's state of consciousness during such sleep studies.

6.0.3 Radio-based Identity Verification

Radio-based identity verification is one of among a few promising directions in addressing the aforementioned issues. It obtains unique physiological traits from radio signals reflected from the subject and does not require the subject's active involvement or ambient conditions unsuitable for the sleeping study.Several research works employ Doppler radar measurement of cardiopulmonary motion at decimeter or mmWave band for continuous user authentication. Others utilize the channel measurement protocols inherent to off-the-shelf WiFi devices to extract unique features for individual identification. Recent development further incorporates advanced signal processing algorithms and machine learning techniques to improve the identification accuracy and reliability.

Despite many advances, two fundamental problems associated with our setting remain unsolved. First, the challenges to establish the connection between the radio signature and the subject's identity are largely omitted in existing work. In other words, the initial

enrollment, during which the system captures the subject's physiological measurements to be compared with the traits extracted from radio signals, is contingent upon the assurance of the user's identity, which must be verified in a more reliable method. Second, the results in existing work are mostly obtained through single-subject experiments under controlled settings [1] [2][3][4].The challenges to apply radio-based approaches in complex environments subject to disruptive events and multiple targets, e.g., scenarios mostly encountered for in-home sleep arrangements, remain to be addressed.

6.1 System and Adversary Models

In this section, we describe the system and adversary model of the modality-switch compliance tracker for at-home OSA screening. The focus of the design is to enable continuous tracking and verification of the patient undergoing the sleep test, and allow the operation modalities to shift between a on-body compliance tracker and a mmWave radar. By doing so, the test can adapt to the patient's physical activities and minimize uncomfortable and inconvenient settings, without creating unsupervised periods that render it vulnerable to cheating and data forgery. There are several unique challenges to realize such a design.In the rest of this section, we analyze them through the elaboration of the system and the adversary model.

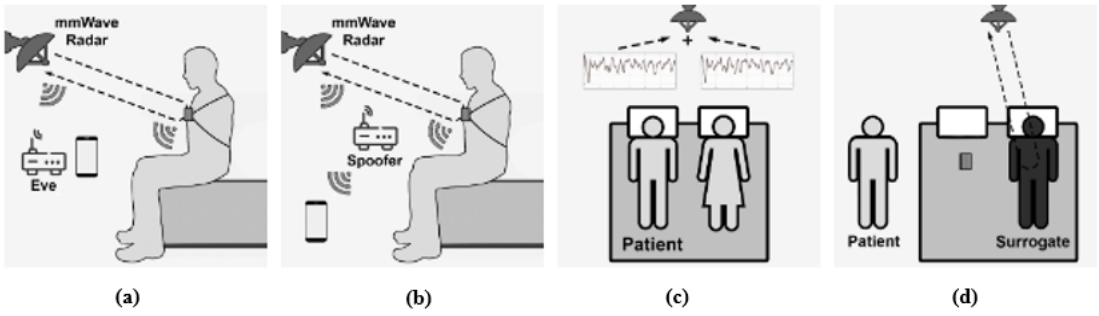

Figure 6.1 Adversary model of the system (a) Eavesdrop (b) spoof (c) mix-up and (d) surrogate

6.1.1 System Model

Consider a typical setting for an in-home unobtrusive OSA screening with a compliance tracking feature. The simplified system model contains three modules: (1) A mobile OSA app that aggregates the test and compliance data records. (2) A mmWave radar capable of remotely measuring the patient vital signs, including heartbeat, arterial pulsation, and breathing, primarily used to conduct the OSA screening. (3) A contact-based compliance tracker, often a chest band sensor or a fingertip sensor, attached by a doctor to monitor the patient's vital signs. For simplicity, we consider the contact-based compliance tracker as a chest band sensor that monitors the patient's breathing. Although our design also works with fingertip sensors due to the variety of vital signs captured by the mmWave radar.

We further make the following assumptions in terms of function, security, computation, and communication. (1) The sensor and radar contains tamper-resistant storage's with limited capacity. Any attempts to physically modify the content within the storage would nullify the test. (2) The circuity of the sensor and radar are capable of performing computational inexpensive cryptographic algorithms, such as SHA-1 hash and AES. (3) The sensor and radar are equipped with radio interfaces such as Bluetooth. However the sensor and radar do not have any prior key agreement.

6.1.2 Adversarial Model

We consider the two categories of adversarial and environmental challenges. First, the wireless communication incurred due to modality switch opens up windows for attacks over the air. Second, the home environment lacks professional supervision and is subject to unexpected events. Identifying and tracking the patient's vital signs under such a environment, especially when using the radar based approach, is inherently difficult [10][21]. We further divide them into four scenarios detailed below.

Eavesdrop. The patient may eavesdrop the wireless communication between the sensor/radar and OSA app, seeking to evaluate the data records before the doctor examines them shown in Fig. 6.1 (a). For instance, the patient may intercept the key exchange

between the sensor/radar and the OSA app, decrypt, and review the data records. If significant discrepancy were detected, the patient would have time to establish false excuses and convince the doctor to accept the test results.

Spoof. The patient may exploit the wireless connection between the sensor/radar and the OSA app to hi-jack, inject false data, and manipulate the identity verification outcome shown in Fig. 6.1 (b). For instance, the patient may launch a man-in-the-middle attack upon the communication between the sensor/radar and the OSA app, by creating a record of his/her normal breathing and replaying it during modality switch, seeking to replace record that shows significant unattendance.

Mix-Up. The patient may follow his/her daily routine and share the bed with his/her spouse or family during the test shown in Fig. 6.1 (c). For instance, two persons, such as a couple or a mother and a newborn, sharing a bed is common in a real-world setup. The system needs to correctly identify the patient among the two/multiple breathing patterns as well as the background noise.

Surrogate. The patient may use a machine or human surrogate to substitute for the test shown in Fig. 6.1 (d).For instance, the patient may use a mechanical plunger to simulate the muscular movements of human breathing. Or the patient may ask another person to replace him/her entirely. The system needs to detect the deliberate impersonation and "person swap.".

A distinct feature of our adversary model compared to continuous and co-presence authentication is that the legitimate user of the system, e.g., the patient, is simultaneously the system's attacker. The objective of the attacks is to either trick the system into accepting false data/identity or eavesdrop the communication between the system modules. The corresponding security assumption to counter the adversary is that the patient's identity is initially verified by a medical technician and unambiguously linked to a breathing signature via the contact-based vital sensor. However, the challenge is that the connection would naturally weaken as the test progresses due to the dynamic of human physiological, signal

differences between modalities, as well as noise present in the environment and need to be restored without interfering with the unobtrusive OSA screening task.

6.1.3 Modality Switch Compliance Tracking System

Here we present our design of MASCOT, the first **M**od**A**lity-**S**witch **CO**mpliance **T**racking system for unobtrusive in-home sleep apnea screening. MASCOT ensures OSA test compliance by consistently linking the patient's identity to one of the breathing signatures among multiple targets; and continuously tracking such a signature throughout the test, with the tracking modalities switching between two sentinels: the contact-based sensor and contactless radar. It leverages the patient's breathing signature to establish and renew a shared security key between the sentinels during each switch, which is used to protect the integrity and certify the authenticity of the compliance tracking records. As a result, MASCOT is more comfortable than solely contact-based compliance trackers, reliable under a complex in-home environment, and most importantly, secure against sleep test fraud.

6.1.4 Overview

The design of MASCOT is based on a simple intuition: the respiratory patterns monitored by skin-contacting compliance trackers can also be detected remotely via the mmWave Doppler radar; they are distinguishable among different persons; and most importantly, may experience small variations but rarely any dramatic changes within a short time, especially when the subject is at rest. The observed consistency allows us to design a protocol to switch the compliance tracking modalities between the sentinels while avoiding the disambiguation and resisting the attacks specified in the previous section, e.g., mix-up, surrogate, eavesdrop, and spoof.

The detailed design of MASCOT is shown in Fig. 6.2. It starts when the patient first visits a doctor to obtain the test authorization. During the visit, the doctor attaches a chest band sensor to the patient and links it to the OSA app to initialize compliance tracking. The sensor continuously records the patient's breathing from the moment it is attached.

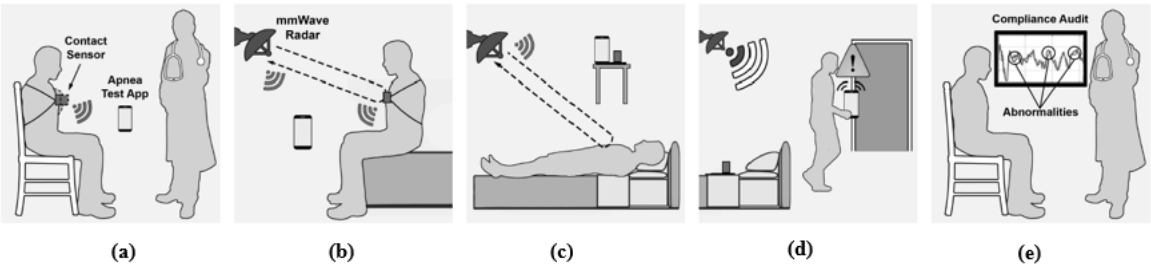

Figure 6.2 Overview and schematic diagram of the proposed modality switch compliance tracking protocol

For each data record, the sensor attaches a timestamp to it and store it in a tamper-proof storage module (Fig. 6.2(a)).

Once arriving at home and being ready for the test, the patient links the mmWave radar to the OSA app and requests a modality switch. The app broadcasts a modality-switch message to both the sensor and the radar, allowing the two to bootstrap a shared key based on the patient's current breathing patterns (detailed in section 6.1.5). The sensor uses the key to compute an HMAC tag of the compliance data, encrypt the data and the HMAC tag, and upload the ciphertext to the OSA app. The OSA app acknowledges and hands over the compliance tracking task to the radar. The radar leverages the key establishment process to identify the patient (detailed in), starts the OSA test by recording multiple OSA related vital signs, including the breathing dynamic for compliance tracking. The patient can take off the skin-contact sensor and sleep in comfort (Fig. 6.2 (b-c)).

Were to move out-of-view from the radar, the patient put on the skin-contact sensor and request another modality switch via the OSA app, which prompts the radar and sensor to update the shared key using the patient's current breathing patterns. The radar uses the key to generate two data packages: one being the encrypted compliance data and the corresponding HMAC tag, and the other being the encrypted OSA screening data and the corresponding HMAC tag. Both data packages are then uploaded to the OSA app, which acknowledges and hands over the compliance tracking task to the sensor. The sensor carries

on the compliance tracking, while the radar continues the OSA screening. Such a modality switch can occur multiple times as needed throughout the test (Fig. 6.2 (d)).

Once the test completes, the patient's doctor retrieves all keys from the skin-contact sensor and all screening and compliance data from the app, decrypts the data, and verifies the data's authenticity using the HMAC tags. Finally, the doctor runs a compliance check and examines whether there were significant gaps or inconsistencies in the compliance data. Based on the compliance check report, the doctor decides whether to accept or reject the OSA screening (Fig. 6.2 (e)).

6.1.5 Key Evolution using Breathing Patterns

The core of MASCOT is a three-party key evolution protocol (Fig.), which allows two sentinels, a and b, to securely evolve a shared key through the OSA app, utilizing the patient's breathing patterns observed by both devices at the moment of the modality switch. The key is then leveraged by the former sentinel to protect the authenticity and integrity of the compliance/screening data being uploaded to the OSA app during modality switch.

The key evolution protocol utilizes a cryptographic device known as a fuzzy commitment scheme, which transforms a secret value s into a into a commitment/opening value tuple (δ, λ) via $(\delta, \lambda) = \textsc{Commit}(s)$, such that δ appears random and devoid of any information about s. And all tuples $(\delta, \hat{\lambda})$ reveals s via $s = \textsc{Open}(\delta, \hat{\lambda})$ if and only if the Hamming distance $\textsc{Ham}(\lambda, \hat{\lambda}) \leq t$, where t is a parameter denoting the maximum allowable Hamming distance between $\hat{\lambda}$ and λ to reveal s.

To initiate the key evolution protocol at the ith modality switch, the OSA app broadcasts a message, $\left(\mathcal{H}(K^{i-1}), t^i_{str}, t^i_{end}\right)$, where $\mathcal{H}(\cdot)$ denotes a cryptographic hash function, K^{i-1} key of the previous iteration [1], t^i_{str} and t^i_{end} the starting and ending timestamps on which the two sentinels to synchronize the generation of the breathing fingerprints.

From breathing patterns $C_a(t^i_{str}, t^i_{end})$ and $C_b(t^i_{str}, t^i_{end})$ captured within the specified time interval, the two sentinels extract breathing fingerprints $F^i_a = \phi\left(C_a(t^i_{str}, t^i_{end})\right)$ and

[1] K^0 can be a random key selected by the OSA app.

$F_b^i = \phi\left(C_b(t_{str}^i, t_{end}^i)\right)$, via a fingerprint extraction function $\phi(\cdot)$ (detailed in Section 6.1.7). In case a sentinel, e.g., the mmWave radar, observes a breathing mixture of multiple subjects, the mixture is first separated into the breathing patterns of individual subjects (detailed in Section 6.1.16), which are processed by $\phi(\cdot)$ to create multiple fingerprints, one for each subject.

Once the breathing fingerprints are generated, the sentinel to be relieved, a, randomly selects a key evolution salt, $\Delta K^i \in \mathbb{F}_{2^k}^m$, and transforms it into a commitment/opening value tuple (δ^i, λ^i), where $\lambda^i \in \mathbb{F}_{2^k}^m$ is the codeword for ΔK^i using the Reed-Solomon (RS) encoding function: $\lambda^i = \mathrm{RS}(2^k, m, n, \Delta K^i)$, and the $\delta^i \in \mathbb{F}_{2^k}^m$ is the difference between λ^i and F_a: $\delta^i = F_a \ominus \lambda^i$, with $\ominus$ denoting subtraction in the finite field $\mathbb{F}_{2^k}^m$. The latter, together with $\mathcal{H}(\Delta K^i)$, are transmitted to the relieving sentinel, b.

Upon receiving δ^i, b computes $\hat{\lambda}^i = F_b^i \ominus \delta^i$ and attempts to retrieve the key evolution salt by decoding $\hat{\lambda}^i$ using the the Reed-Solomon (RS) decoding function: $\Delta\hat{K}^i = \overline{RS}((2^k, m, n, \hat{\lambda}^i)$. Due to the error correction capability of Reed–Solomon codes, $\Delta K^i = \hat{K}^i$ if and only if λ^i and $\hat{\lambda}^i$) differs in at most t bits. And since $\lambda^i = F_a^i \ominus \delta^i$ and $\hat{\lambda}^i = F_b^i \ominus \delta^i$, it is equivalent in saying that F_a^i and F_b^i can only differ in at most t bits for b to retrieve ΔK^i.

To confirm whether the retrieval were successful, b computes $\mathcal{H}(\Delta\hat{K}^i)$ and compares it with $\mathcal{H}(\Delta K^i)$. Depending on whether they were equal, an ACK or a NAK message is transmitted from b to a, with the ACK message initiating the final step of the key evolution protocol and the NAK message initiating the reattempt of the previous steps. In case b has multiple fingerprints, it will try to retrieve ΔK^i with each of them before sending the message.

If an ACK message is received, a and b will identify the previous key, K^{i-1}, through its hash value $\mathcal{H}(K^{i-1})$, which is part of the initial message broadcast by the OSA app, and apply a key derivation function to obtain the new key $K^i = \mathrm{KDF}(\Delta K^i, K^{i-1})$. b sends the hash value of the new key $\mathcal{H}(K^i)$ to the OSA app. The OSA app records it and ends the key evolution. Fig 6.3 illustrates the key evolution protocol using breathing pattern.

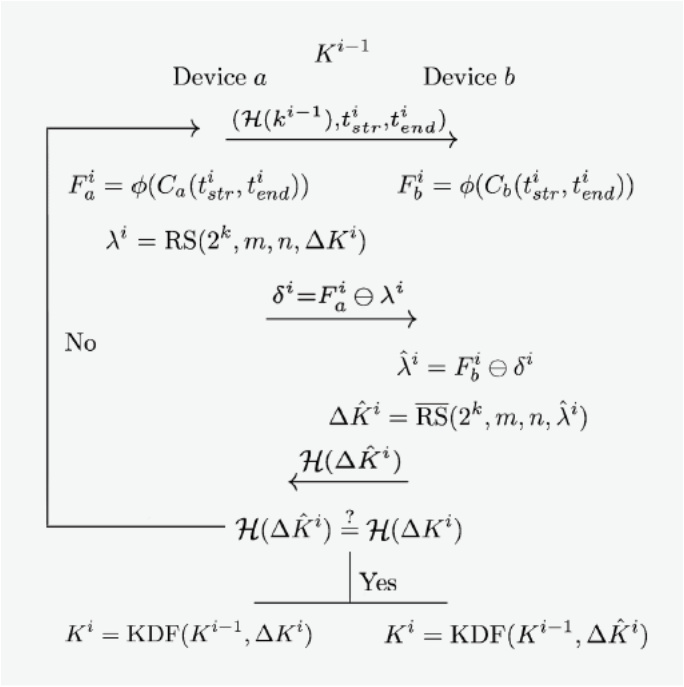

Figure 6.3 Key evolution protocol of breathing pattern

6.1.6 Breathing Separation with ICA-JADE

A home environment is noisy and unpredictable, with the possibility of irrelevant individuals in close vicinity from the patient undergoing the screening procedure.To achieve reliable modality switches in an environment with potentially multiple subjects, MASCOT augments the radar sentinel with a breathing separation module, which reconstructs the breathing signals of multiple co-located individuals to select the correct target.Several works have been proposed to correctly separate and isolate the patient's respiratory signature from the combined signal mixture, all of which fall into the problem domain of blind source separation (BSS) [14].

The goal of BSS is to reconstruct a set of source signals from a set of mixtures, without knowing the properties of the sources and the mixing proportion. If the sources are independent and have non-Gaussian distributions, and the mixing is linear, one can recover the source signals from the mixture and use independent component analysis (ICA), which is

formulated as the following: assume N independent time varying sources $s_i(t),\ i = 1 \ldots N$, and M different observations $x_i(t),\ i = 1 \ldots M$. For T time units ($t = 1 \ldots T$), we can define the source signal as a $N \times\ T$ matrix,

$$\mathbf{S}_{N\times T} = s_{11}s_{12}\ldots \vdots \ddots . s_{N_1}s_{N_T},$$

and the observed mixtures as a $M \times\ T$ matrix,

$$\mathbf{X}_{M\times T} = x_{11}x_{12}\ldots \vdots \ddots . x_{M_1}x_{M_T}.$$

The mixtures are produced as the product of source and a mixing matrix $W_{M\times N}$, e.g.,

$$\mathbf{X}_{M\times T} = \mathbf{W}_{M\times N} \times \mathbf{S}_{N\times T}. \tag{6.1}$$

The goal of ICA is to recover $\mathbf{S}_{N\times T}$ and $\mathbf{W}_{M\times N}$ given only $\mathbf{X}_{M\times T}$, assuming the $s_i(t),\ i = 1 \ldots N$ are independent and non-Gaussian.

We employ the joint approximate diagonalization of eignematrices (JADE) algorithm to perform ICA. The JADE algorithm extract independent non-Gaussian sources $\mathbf{S}_{N\times T}$, e.g., the breathing pattern of individual targets, from signal mixtures with Gaussian noise $\mathbf{X}_{M\times T}$, e.g., the breathing mixture received by the radar sentinel, by constructing a fourth-order cumulants array from $\mathbf{X}_{M\times T}$. Specifically, assuming $T > M, N$, the algorithm first applies PCA to whiten $\mathbf{X}_{M\times T}$, resulting

$$\mathbf{P}^{tr}_{T\times K} = \mathbf{B}_{K\times M} \times \mathbf{X}_{M\times T},$$

where the whitening matrix $\mathbf{B}_{N\times M}$ has N rows with N being the number of singular values of $\mathbf{X}_{M\times T}$, and the columns of whitened matrix $\mathbf{P}_{T\times N}$ are orthogonal with equal variance. Due to whitening, any rotation of $\mathbf{P}_{T\times N}$ will preserve the property that its column vectors are uncorrelated. The algorithm then tries to find a rotation matrix $\mathbf{V}_{N\times N}$ such that

the column vectors of the rotated $\mathbf{P}_{T\times N}$ are as independent as possible. The maximum independence is achieved when the fourth-order cross-cumulants between column vectors are zero and their auto-cumulants maximal. Once $\mathbf{V}_{N\times N}$ has been identified, the demixing matrix can be computed as

$$\mathbf{W}^{+}_{N\times M} = \mathbf{V}_{N\times N} \times \mathbf{B}_{N\times M}, \tag{6.2}$$

and the source matrix as

$$\mathbf{S}_{N\times T} = \mathbf{W}^{+}_{N\times M} \times \mathbf{X}_{M\times T}, \tag{6.3}$$

.

6.1.7 Fingerprinting with Multiple Level-Crossing Sampling

Once the sentinels obtain the breathing patterns of individual targets, it applies the fingerprinting function, $\phi(\cdot)$, to obtain the patterns' binary representations. To be used by the two sentinels to reaffirm the patient's identity and evolve the shared security key, the binary strings must meet two criteria: (1) they should look sufficiently similar in Hamming space if they represent the breathing process of the same person, and (2) they should preserve the uniqueness of the breathing dynamic that distinguishes among individuals.

To achieve both objectives, $\phi(\cdot)$ breaks down a continuous breathing pattern into series of codewords by comparing sampled values at equally-spaced time instants with two predefined thresholds. Specifically, let q_+ q_- be the thresholds values such that $q_+ > q_-$, we define a quantizer $(\cdot)$:

$$(x) = \begin{cases} 10 & if\ x \geq q_+ \\ 01 & if\ x \leq q_- \\ 00 & if\ q_- < x < q_+ \end{cases} \tag{6.4}$$

Let τ be the time interval between adjacent sampling instants. The binary sequence obtained by $\phi(\cdot)$ is $\mathrm{F} = \phi\left(C(t_{str}, t_{end})\right) = [\,(C(t_{str}))\,,\ (C(t_{str}+\tau))\,,\ \ldots\,,$
$\left(C(t_{str} + \lfloor \frac{t_{end}-t_{str}}{\tau} \rfloor \tau\right)]$.

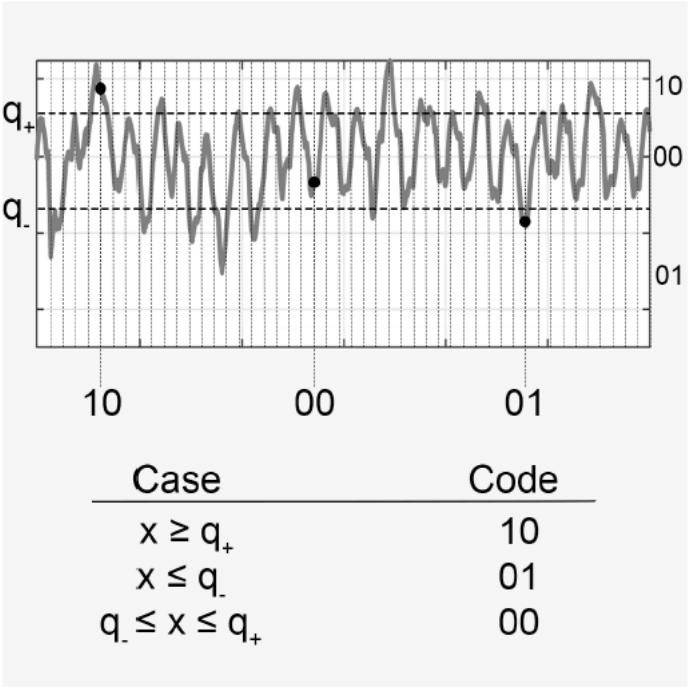

Figure 6.4 Fingerprinting with multiple level crossing sampling

If the binary sequence is longer than the length of the commitment, $\|\lambda\|$, we pad and divide it multiple subsequences, $F = [f_1, f_2, ..., f_n]$ to compute

$$\delta = f_1 \ominus f_2 \ominus ... \ominus f_n \ominus \lambda, \tag{6.5}$$

and

$$\hat{\lambda} = \hat{f}_1 \ominus \hat{f}_2 \ominus ... \ominus \hat{f}_n \ominus \delta, \tag{6.6}$$

The level-crossing quantization described above is an event-based sampling procedure as the crossing events are encoded as changes in the binary patterns. When the signal remains above/below the levels, it produces fixed patterns, which can be exploited to further compress the binary before transmission[2]. However, a single pass of level-crossing binary

[2]Techniques to produce a compressed the binary string that are satisfiable to the two criteria is beyond the scope of this article and will be investigated in the future.

quantization is bound to loss information contained in the original breath pattern, which fails the second objective.

To address this issue, we apply multiple passes of level-crossing binary quatizations, each at a distinct pairs of levels, q_{i+}, q_{i-}, and produce a set of binary sequences $\{F_1, F_2, ...F_n\}$ for the fuzzy commitment. Intuitively, it is equivalent to create a pair-wise linear approximation of the original breathing pattern, with quantization error equals to the level density. Since the human breathing signal is bandlimited, we can eliminate alias in the approximation by setting the sampling frequency to above the Nyquist rate.

6.2 Implementation and Evaluation

We empirically evaluated the performance of MASCOT via our laboratory prototype of the modality-switching compliance tracking system (Fig. 6.5), which consists of one Android-based OSA application, one Bluetooth enabled chestband sensor with one piezo-electric respiration transducer interfacing with an external microcontroller, and one mmWave radar systems implemented with software-defined radios in conjunctions with mmWave radio heads. All experiments with human subjects are approved by the Institutional Review Board (IRB), and we have obtained informed consent from all human subjects.

6.2.1 Implementing MASCOT

Our MASCOT prototype was developed and tested from 2019 to 2020, with two mmWave radars implemented for the preliminary system. One design employs a commercial off-the-shelf 4-channel 24GHz monopulse radar transceiver (K-MC4 from RFbeam Microwave GmbH) interfacing a LabVIEW controlled DAQ through four LNA's (SR560 from Stanford Research System). The 3dB beam aperture is 12° horizontally and 30° vertically. The angle coverage is between +/-15° horizontally. The other design utilizes a mmWave beamforming development kit (BBox one/UD box from TMYTEK) consisting of a 16-channel 24-31GHz phased array antenna, and a frequency Up/Down converter, which

Figure 6.5 Implementation of MASCOT with, an android application, a chest band sensor, and mmWave Radar

interfaces with a LabVIEW controlled USRP (USRP-2974 from NI). The 3dB beam aperture is 13° horizontally and 14° vertically. The angle coverage is +/-45° horizontally and +/-60° vertically.

The skin-contacting compliance tracker is implemented with a piezo-electric respiration transducer (Model 1132 Pneumotrace II from UFI), which interfaces with a LabVIEW controlled DAQ. The Android application communicates via Bluetooth Low Energy (BLE) with the host computers that control the mmWave radar(s) and the respiration transducer to execute the modality-switching and data logging functionality. The implementation leverages the Android BLE APIs to connect to the Generic Attribute Profile (GATT) servers set up by the LabVIEW Bluetooth Toolkit on the host computers.

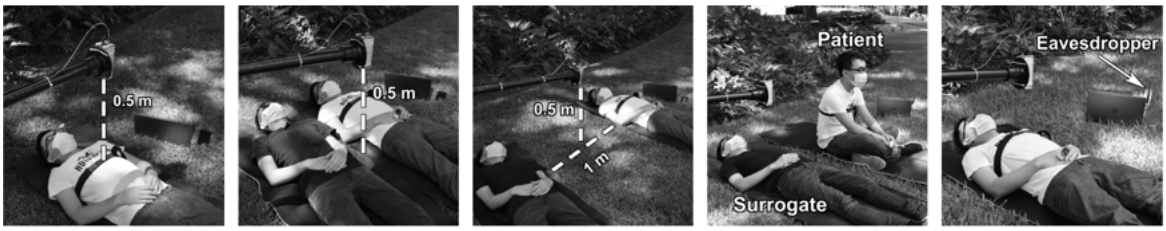

Figure 6.6 Left to right: (a) One person scenario for compliance tracking with patient; (b) Mix-up: patient lies together with non-patient in close distance; (c) Mix-up: patient lies separately with non-patient; (d) Surrogate: radar tracks non-patient; (e) Eavesdropper records signal from radar.

6.2.2 Experiment Set-up

We conducted laboratory and field experiments over a one-month period with the MASCOT prototype and 20 subjects selected through a random sample recruitment process. The subjects are between the ages of 16 and 35, weigh between 42 to 85 kilograms, and have no prior history of heart disease. The subjects are asked to participate in multiple trials of sleep studies under laboratory and everyday settings with environmental and adversarial complications detailed below.

Sleep Environment and Data Collection. We furnished two sleep environments for experimentation. The indoor laboratory environment consists of 2 twin size beds under a quiet and dim ambience. The outdoor field environment consists of two beach mats and umbrellas set up at a local beach park. During each trial, the subjects are attached with chestband sensors and positioned 0.5 meters below the mmWave radar system for data collection. We continuously monitor the respiration of the subjects for 1 hour, during which modality-switches and adversarial activities (if planned) are attempted every 10 minutes. After the experiment, we extract a 60-second data segment around each modality-switch to evaluate MASCOT's performance, with the remaining data to serve as references. Overall, we collected approximately 30,000 breathing cycle samples for each subject.

Mix-Up/Surrogate. We designed the mix-up and surrogate scenarios via a single-blind experiment set-up. For the mix-up scenario, we randomly paired subjects during each

trial. Both subjects were asked to each wear a chestband and lay down under a mmWave radar throughout the experiment, without knowing which subject was the patient. A third-party was assigned to execute the modality switches via the OSA application paired with the patient's chestband and the mmWave radar. For the surrogate scenario, we paired subjects with similar physique during each trial. Both subjects were asked to wear a chestband but lay down under two separate mmWave radars throughout the experiment, without knowing which subject was the patient. A third-party was assigned to execute the modality switches via the OSA application paired with the patient's chestband and the non-patient's mmWave radar.

Eavesdrop/Spoof. We designed the eavesdropping and spoofing attacks against MASCOT via a BLE sniffer and spoofer, implemented via Ubertooth and Kismet []. During each experiment, one subject was asked to wear a chestband and lay down under a mmWave radar. A third-party was assigned to execute the modality switches and operate the computer running the Ubertooth. The packets transmitted by the OSA application, the chestband, and the mmWave radar were identified based on their Bluetooth Device Addresses obtained prior of the experiment. To implement the eavesdropping attack, the host's codes recorded the packets containing compliance tracking data during each modality-switch, which were analyzed offline in attempt to decode the content. To implement the spoofing attacks, a pre-recorded sequence was transmitted at higher power during each modality-switch, in attempt to manipulate the OSA application into accepting fraudulent data, which was verified during offline analysis.

6.2.3 Performance of Breathing Separation

During each experiment, the signal (mixture) captured by the mmWave radar (Fig.6.7 (a)) was filtered in real-time by the ICA-JADE-based breathing separation module implemented through a MATLAB script running within LabVIEW. The script filtered the signal with a digital FIR Low pass filter with cut off frequency of 10 Hz to suppress the high-frequency noise while preserving the physiological-related information. The filtered signal

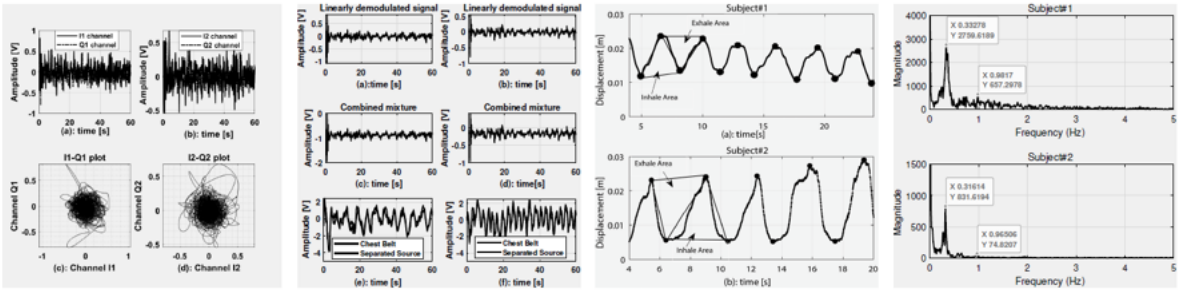

Figure 6.7 Left to right: (a) Raw IQ data received by different RF channels of the the mmWave CW radar; (b) Breathing mixture obtained by (linear) demodulating the raw IQ (top), individual breathing patterns after source separation in comparison with the ones collected by the chestband sensor (bottom); (c,d) time and frequency domain analysis show the inhale and exhale characters are distinct between the two subjects, which allows patient tracking during modality switches.

was linearly demodulated to compute the phase shifts caused by the displacement(s) of the chest(s) surface(s) during breathing (Fig.6.7 (b) top). Specifically, the script calculated the covariance matrices of the I and Q channel signals and applied eigenvalue decomposition to the covariance matrices to extract the maximum chest displacement information. The demodulated signal was separated by the ICA-JADE method to isolate individual respiratory signatures (Fig. 6.7 (b) bottom).

Finally, the script evaluated the performance of ICA-JADE by computing the cross-correlation between the isolated signatures with the ground truth obtained from the respiration transducer. The empirical result shows that the similarity is above 90% when we limit the experiment within 60 seconds. As time increases, the subjects tend to move/turn on the bed, which changes the contribution of their breathing to the signal mixture, e.g., the mixing matrix, and the ICA-JADE result deviates from the truth. Thus, we limited the sensing period of MASCOT during the subsequent experiments to within 60 seconds to achieve a stable source separation.

6.2.4 Performance of Fingerprint Extraction

An individual breathing signature was quantized in parallel by multiple level-crossing LabVIEW VIs to generate the binary fingerprint after the breathing separation. The breathing signature (torso deformation) due to respiratory effort is a complex, three-dimensional pattern, and it varies greatly with subject parameters and activity context. Based on our preliminary data, the thorax motions due to respiration and heartbeat are limited within +/-0.5cm and +/-0.05cm (Fig. 6.8) and the rates of respiration and heartbeat are below 15 and 60 per minute, when the subject is at rest. Therefore, we employed ten level-crossing quantization branches with a quantization step size of 0.05cm at a sample rate of 10 per second, to preserve the fine-grained respiratory motion when extracting the breathing fingerprint.

To be compatible with the key evolution protocol, the quality of the binary fingerprints was evaluated based on the Hamming distances between fingerprints of the same subject observed by different modalities and different subjects observed by different modalities. It has been demonstrated in various works that human subjects can be sufficiently differentiated based on the inhales (local maxima), exhales (local minima), and breathing depth (the area between two consecutive maxima and in between one minima point). The similarities of these features directly translate to the Hamming distances between the quantized fingerprints. Therefore, comparing the Hamming distances is equivalent to constructing an equal-weighted linear classifier for patient identification.

The empirical results (Fig. 6.8 (b)) show that the average Hamming similarity per bit between fingerprints of the same subject observed from different modalities is around 63% when extracted from 6-second breathing signatures (with 2 breathing cycles). The Hamming similarity increases almost logarithmically towards 100% as we extend the duration of the breathing signature to 60 seconds (with 20 breathing cycles). The elevated mean and reduced variance in the Hamming similarity is mostly due to the extended time, which allows repeated measurements of the periodic respiratory effort motion unique to each subject.

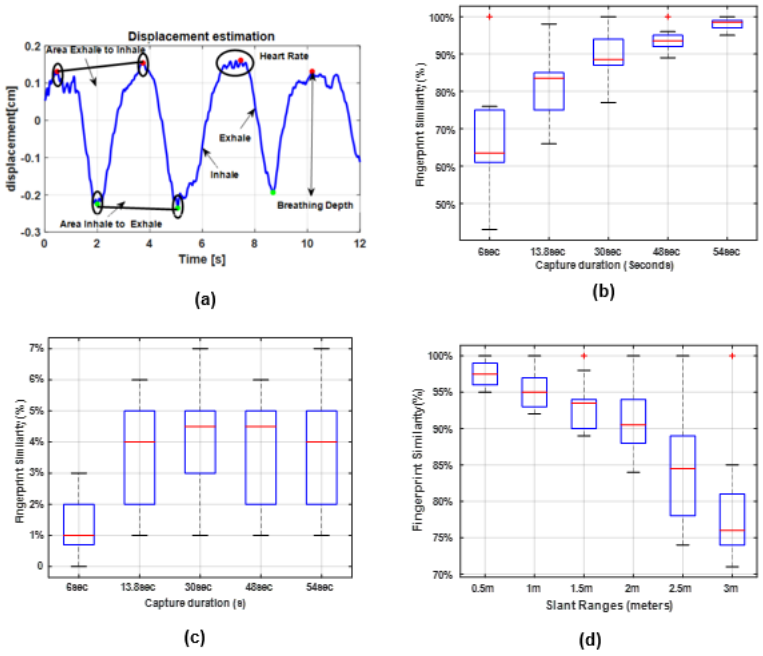

Figure 6.8 (a) Multiple vital related dynamic features, including breathing rate, inhale/exhale area, breathing depth, and heart rate, are preserved after level-crossing quantization; (b) The distributions of fingerprint similarity between chestband-based and mmWave-based modalities, captured from the same subject; (b) The distributions of fingerprint similarity between chestband-based and mmWave-based modalities, captured from different subjects (chestband data from the patient, mmWave radar data from the non-patient); (d) The effect on the fingerprint similarity due to the change of slant range between the mmWave radar and the subject.

On the contrary, the average Hamming similarity per bit between different subjects' fingerprints remains below 5% despite the measurement duration (Fig. 6.8 (c). The position between the mmWave and the subject also poses a significant factor, which attenuates the Hamming similarity. As the subject moves away from the radar's downrange direction, the radar measurements deviate from the ground truth (obtained from the chestband). But their similarity remains sufficiently high compared to the breathing fingerprints between different subjects. Overall, the results show that the Hamming similarity per bit for MASCOT can be set to around 70% to allow accurate patient tracking during modality switches.

6.2.5 Performance of Key Evolution

The binary breathing fingerprints, are chunked into multiple 10-second segments and padded with 0s to meet the codeword length of the $(2^8, 255, n)$ Reed-Solomon codes, e.g., $8 \times 255 = 2040$ bits per padded segment. The particular group of Reed-Solomon codes are chosen to ensure the communicated data are exact multiple of bytes. A key evolution salt of $8 \times n$ bits is randomly selected by the on-duty sentinel and encoded with the $\mathrm{RS}(2^8, 255, n)$ Reed-Solomon encoder to generate the 2040 bits opening value. The opening value and the (multiple) padded fignerprint segments are XORed together to generate the 2040 bits commitment.

We evaluate the security of the fuzzy commitment via a randomness test using the NIST statistical test suite. Based on 10 million randomly generated key evolution salts (with entropy per bit equal to one), we measured the randomness of the opening values and the commitments (Fig. 6.9(a)). The empirical test shows that the entropy per bit drops almost by half when the key salt is converted into a commitment. In other words, the entropy of a 2040-bit commitment is approximately 1000 bits. The primary causes of the reduction are due to the redundancy in the Reed-Solomon codes and the human respiratory motion's cyclic character. Two additional factors that affect the randomness of the commitment are the quantization levels and the number of the XOR operation rounds. When the quantization levels increase, the granularity of the binary sequencing improves, slightly elevating the randomness of the breathing fingerprints, resulting in a higher degree of entropy in the commitments. When the commitment is generated with multiple rounds of XOR operations, the entropy decreases due to the cross-correlation between fingerprint segments[3].

6.2.6 Performance under Adversarial Settings

MASCOT's performance against mix-up and surrogate scenarios is assessed based on the protocol's sensitivity (true positive rate) and specificity (true negative rate) in identifying

[3]In an XOR operation, the higher correlation between the inputs, the less the entropy in the output.

intentional or unintentional identity changes. MASCOT leverages a support vector machine

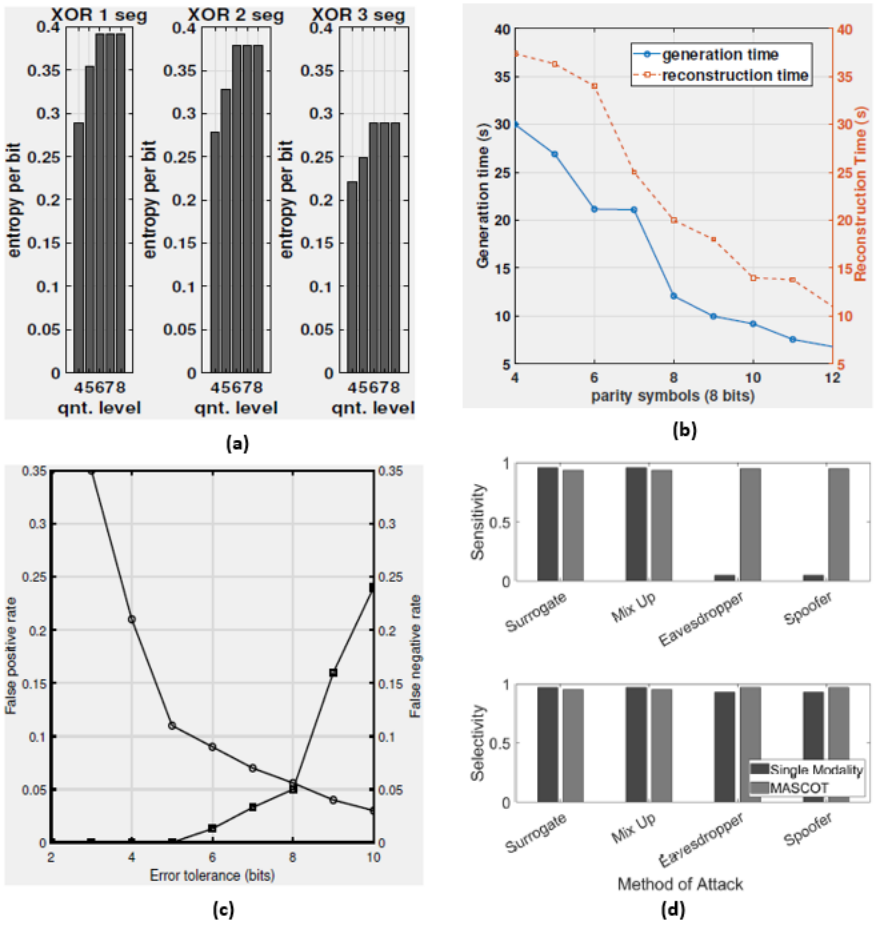

Figure 6.9 Left to right: (a) Average entropy per bit of the fuzzy commitments, e.g., RS encoded key salt XORed with (multiple) fingerprint segments, measured via NIST tests; (b) Commitment time with RS codes of different message lengths; (c)Reconstruction time with RS codes of different message lengths and different bit errors; (d)Overall performance of MASCOT against the four types of adversarial and environmental challenges, in comparison with existing single-modality compliant tracking systems.

(SVM) to detect identity changes (as anomalies in breathing patterns) within a single modality recording and rely on the success/failure of the key evolution to detect identity changes during modality switches. The overall sensitivity and specificity are calculated as the average among single modality and modality switching cases. Our implementation ensures a fair comparison between fuzzy commitment and SVM by using a linear SVM,

whose decision boundary can be interpreted as a weighted Hamming distance between binary breathing fingerprints. The empirical results show that the MASCOT' scores are close to the single modality SVM approach, lower by 1.1% and 1.5% in sensitivity and specificity. The performance of single modality SVM approach is close but not precisely 100%, due to the variance of human respiratory motions. Not that single modality contact-based methods can achieve 100% detection accuracy if more rigid rules, such as prohibiting sensor disconnection, are enforced through the hardware. However, the detrimental effect of contact sensor toward the quality of the OSA screening data renders it inferior to MASCOT, as discussed before.

MASCOT's performance against eavesdropping and spoofing is evaluated by comparing the aggregated bit error rate (BER) at the receiving sentinel versus the aggregated BER at the attacker. Due to the application of fuzzy commitment, the key evolution protocol allows a maximum of 27% BER in the breathing fingerprints (when using $(2^8, 255, 201)$ Reed-Solomon codes) to recover the key salt. Such BER alone prevents any outsider attackers who cannot observe and mimick the patient's breathing fingerprint from stealing the key salt. Our experiments further showed that the jamming signal could suppress the attacker's BER to approximately 50% anywhere within the on-duty sentinel's transmission range, rendering the modality-switching message undecidable, even if an attacker could obtain the patient's breathing fingerprint. Overall, the CDF of the accumulated BERs for any attackers concentrated between 41% to 50%, well beyond the correctable range of the selected Reed-Solomon codes. Thus, the combination of both techniques ensures sufficient and complete protection of the security key during modality-switching against both outsider and insider attacks.

6.2.7 Conclusion

In this chapter, we tested the feasibility of radio-based identity authentication system for in-home sleep apnea screening. An extensive cryptographic analysis has been presented here. Additionally, we developed a cryptographic three-party key evolution protocol for

ensuring the authenticity and integrity of the data. We also analyzed different attack schemes (eavesdropping, spoofing, surrogate and mix-up) to test the resistance capability of our proposed system.

References

[1] F. Lin, C. Song, Y. Zhuang, W. Xu, C. Li, and K. Ren, "Cardiac Scan: A Non-contact and Continuous Heart-based User Authentication System," in *Proceedings of the 23rd Annual International Conference on Mobile Computing and Networking - MobiCom '17*, (Snowbird, Utah, USA), pp. 315–328, ACM Press, 2017.

[2] A. Rahman, V. M. Lubecke, O. Boric-Lubecke, J. H. Prins, and T. Sakamoto, "Doppler Radar Techniques for Accurate Respiration Characterization and Subject Identification," *IEEE Journal on Emerging and Selected Topics in Circuits and Systems*, vol. 8, pp. 350–359, June 2018.

[3] K. Shi, C. Will, R. Weigel, and A. Koelpin, "Contactless person identification using cardiac radar signals," in *2018 IEEE International Instrumentation and Measurement Technology Conference (I2MTC)*, (Houston, TX), pp. 1–6, IEEE, May 2018.

[4] S. M. M. Islam, A. Rahman, N. Prasad, O. Boric-Lubecke, and V. M. Lubecke, "Identity Authentication System using a Support Vector Machine (SVM) on Radar Respiration Measurements," in *2019 93rd ARFTG Microwave Measurement Conference (ARFTG)*, (Boston, MA, USA), pp. 1–5, IEEE, June 2019.

[5] G. Benchetrit, "Breathing pattern in humans: diversity and individuality," *Respiration Physiology*, vol. 122, pp. 123–129, Sept. 2000.

[6] S. M. M. Islam, A. Rahman, E. Yavari, M. Baboli, O. Boric-Lubecke, and V. M. Lubecke, "Identity Authentication of OSA Patients Using Microwave Doppler radar

and Machine Learning Classifiers," in *2020 IEEE Radio and Wireless Symposium (RWS)*, (San Antonio, TX, USA), pp. 251–254, IEEE, Jan. 2020.

[7] M. Baboli, A. Singh, B. Soll, O. Boric-Lubecke, and V. M. Lubecke, "Good Night: Sleep Monitoring Using a Physiological Radar Monitoring System Integrated with a Polysomnography System," *IEEE Microwave Magazine*, vol. 16, pp. 34–41, July 2015.

[8] L. Almazaydeh, "AN INTERACTIVE, REAL-TIME, HIGH PRECISION AND PORTABLE MONITORING SYSTEM OF OBSTRUCTIVE SLEEP APNEA," p. 82.

[9] M. Bruyneel and V. Ninane, "Unattended home-based polysomnography for sleep disordered breathing: Current concepts and perspectives," *Sleep Medicine Reviews*, vol. 18, pp. 341–347, Aug. 2014.

[10] "https://patents.google.com/patent/US8679012B1/en."

[11] S. M. M. Islam, E. Yavari, A. Rahman, V. M. Lubecke, and O. Boric-Lubecke, "Separation of Respiratory Signatures for Multiple Subjects Using Independent Component Analysis with the JADE Algorithm," in *2018 40th Annual International Conference of the IEEE Engineering in Medicine and Biology Society (EMBC)*, (Honolulu, HI), pp. 1234–1237, IEEE, July 2018.

[12] S. M. M. Islam, E. Yavari, A. Rahman, V. M. Lubecke, and O. Boric-Lubecke, "Direction of Arrival Estimation of Physiological Signals of Multiple Subjects Using Phase Comparison Monopulse Radar," in *2018 Asia-Pacific Microwave Conference (APMC)*, (Kyoto), pp. 411–413, IEEE, Nov. 2018.

[13] S. M. M. Islam, E. Yavari, A. Rahman, V. M. Lubecke, and O. Boric-Lubecke, "Multiple Subject Respiratory Pattern Recognition and Estimation of Direction of Arrival using Phase-Comparison Monopulse Radar," in *2019 IEEE Radio and Wireless Symposium (RWS)*, (Orlando, FL, USA), pp. 1–4, IEEE, Jan. 2019.

[14] S. M. M. Islam, O. Boric-Lubecke, and V. M. Lubekce, "Concurrent Respiration Monitoring of Multiple Subjects by Phase-Comparison Monopulse Radar Using Independent Component Analysis (ICA) with JADE Algorithm and Direction of Arrival (DOA)," *IEEE Access*, pp. 1–1, 2020.

[15] "http://www.sleepreviewmag.com/2018/06/tech-fraudulent-sleep-data/."

[16] N. A. Fox, R. Gross, J. F. Cohn, and R. B. Reilly, "Robust Automatic Human Identification Using Face, Mouth, and Acoustic Information," in *Analysis and Modelling of Faces and Gestures* (D. Hutchison, T. Kanade, J. Kittler, J. M. Kleinberg, F. Mattern, J. C. Mitchell, M. Naor, O. Nierstrasz, C. Pandu Rangan, B. Steffen, M. Sudan, D. Terzopoulos, D. Tygar, M. Y. Vardi, G. Weikum, W. Zhao, S. Gong, and X. Tang, eds.), vol. 3723, pp. 264–278, Berlin, Heidelberg: Springer Berlin Heidelberg, 2005.

[17] F. F. Li, "Sound-Based Multimodal Person Identification from Signature and Voice," in *2010 Fifth International Conference on Internet Monitoring and Protection*, (Barcelona, Spain), pp. 84–88, IEEE, 2010.

[18] A. Abushariah, T. Gunawan, J. Chebil, and M. Abushariah, "Voice based automatic person identification system using Vector Quantization," in *2012 International Conference on Computer and Communication Engineering (ICCCE)*, (Kuala Lumpur, Malaysia), pp. 549–554, IEEE, July 2012.

[19] R. Collins, R. Gross, and Jianbo Shi, "Silhouette-based human identification from body shape and gait," in *Proceedings of Fifth IEEE International Conference on Automatic Face Gesture Recognition*, (Washington, DC, USA), pp. 366–371, IEEE, 2002.

[20] P. Connor and A. Ross, "Biometric recognition by gait: A survey of modalities and features," *Computer Vision and Image Understanding*, vol. 167, pp. 1–27, Feb. 2018.

[21] "https://www.nhlbi.nih.gov/health-topics/sleep-deprivation-and-deficiency."

Chapter 7

Non-Contact RF-Based Continuous Identity Authentication Challenges and Future Work

For practical application, the proposed non-contact RF-based continuous identity authentication system requires further improvement. One of the important performance metrics for identity authentication is the authentication time. The critical reviewers also wonder about the processing time of the proposed non-contact authentication system. Another concern is the breathing pattern may change with emotional stress and physical activities. In our proposed system we mostly extracted respiratory features by utilizing our algorithm but recently, using artificial intelligence automatic unique feature extraction is also possible. This chapter presents some insight into the investigation of answering some of these crucial questions.

7.1 Introduction

In this section we will try to illustrate different terms related to performance metric from user's point of view. In general, a practical user authentication system should not only be identifying people accurately and invalid attackers, but also it should be time-efficient technique in processing authentication [1]. We defined the authentication time,T_a in terms

of total time required to recognize people accurately.

$$T_a = T_(cardiac_motion_sensing) + T_(machine_learning_classification) \tag{7.1}$$

where, $T_(cardiac_motion_sensing)$ is the window size of the radar captured respiration pattern need to extract the respiratory features to identify people and $T_processing$ is the time required for classifiers to uniquely identify people, given that the classifier will be trained before integrating with the system. We also performed accuracy analysis for having different window size of the breathing pattern for twenty different participants. Additionally, in our proposed system we extracted respiratory related features using our own algorithm. But with the advancement of AI, automatic unique feature extraction is also possible.Development of future fusion topology also remains our future work to develop. For initial verification of our proposed system, we also performed experiment in controlled environment. But in realistic scenarios, there may have random body movement and other motion artifacts, so we will describe the prior attempt to overcome this challenges. Integration of this techniques with our system also remains our future work to explore.

7.1.1 Accuracy vs Latency for Identification

We also conducted experiment on evaluating the performance of the proposed system in terms of recognizing people accurately with the window size of the radar captured respiration patterns.The result varied participant to participant but it showed a good trend in terms of window size and accuracy. There are some important findings from this investigations. For an example, if the window size is above 20 second, which contains almost four complete

breathing cycle provides an accuracy of almost 100%. But having window size almost 12 second also provides a reasonable accuracy of 97.5%. With the increase in breathing cycle the latency of the system increases considerably.The results are presented in the subsequent tables and figures. Table 7.1 illustrates the accuracy of outperformed classifier SVM for different window sizes for participant-2. Figure 7.1 also illustrates the window size vs

Table 7.1 Accuracy for different window size of for participant-3 with SVM classifier with quadratic function.

Window Size (seconds)	**Accuracy**
60 s	100%
50 s	100%
45 s	100%
40 s	100%
30 s	100%
20 s	100%
15 s	96.5%
10 s	74%
6 s	64%

recognition accuracy for participant-2. We also experimented for other participants. From our investigation we found that with the increase in window size or number of breathing cycles then extraction of unique features become more dominant.

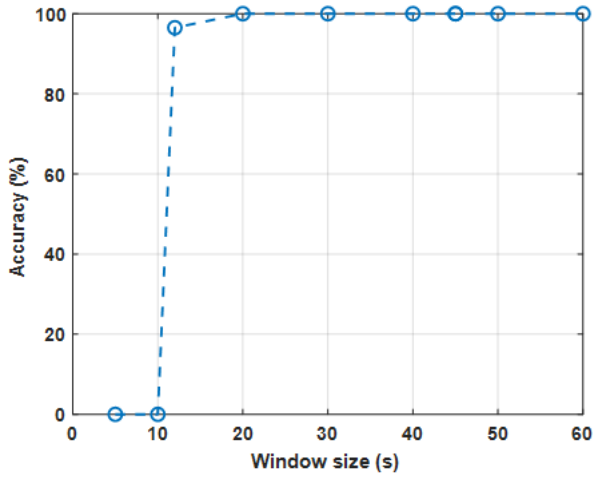

Figure 7.1 Window size vs detection accuracy for participant 2. When window size crosses 12 second the accuracy of the system also increases significantly.If there is multiple breathing cycle then algorithm can extract uniquely identifiable features.

7.1.2 FFT Window size limit

Based on our analysis, we found that, at least without 12-second data set, the algorithm can not extract features reliably. In our feature extraction process, we also extracted breathing rate related information using FFT of the samples [2]. So, minimum window size of the sample required also depends on the FFT resolution limit.

The purpose of windowing your data before processing it with a discrete Fourier transform (DFT or FFT), is to minimize spectral leakage, which happens when you try to Fourier-transform non-cyclical data.Windowing works by forcing your data smoothly to zero at exactly the start and end of the sequence, but not before. Shortening your window destroys information unnecessarily.So window length should match the length of your sample sequences. For instance, with 1024 samples,window length should be 1024 samples to extract the vibrational frequency reliably.

In our experimental setup, DAQ sampling frequency was around 100 Hz. If the FFT window size is 128 then the minimum number of samples required to extract breathing rate related information is 12800 samples.So, when the window size crosses certain threshold limit FFT can extract the breathing rate related information.

7.1.3 Hyper-parameter optimization of Machine Learning Classifiers

After choosing a particular type of machine learning model to train, for example a decision tree or a support vector machine (SVM), we need to tune the model by selecting different advanced options.For example, we can change the maximum number of splits for a decision tree or the box constraint of an SVM. Some of these options are internal parameters of the model, or hyperparameters, that can strongly affect its performance. Instead of manually selecting these options, we also used hyperparamater optimization within the Classification learner app in Matlab for the selection of best hyperparameter value. For instance, for the best hyperparameter selection we repeated the simulation 30 times to find the best hyperparameter value.Figure 7.2 shows the minimum classification error plot with

the number of iterations. Medium KNN classifier with ten neighbor shows the minimum classification error of 0.14 with an accuracy of almost 86%.

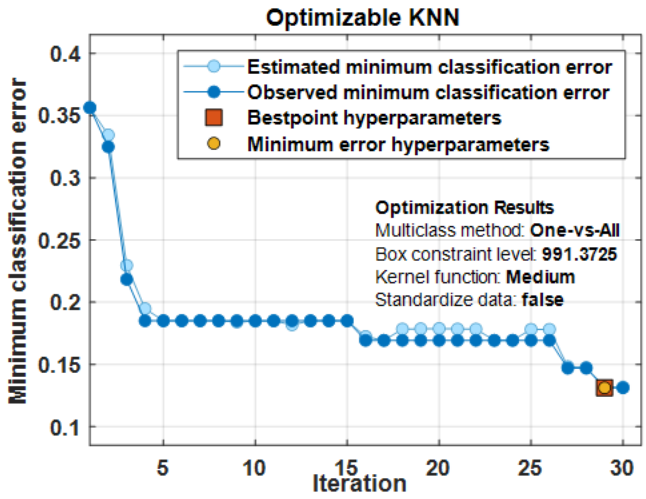

Figure 7.2 Minimum classification error plot for KNN classifier. Medium KNN with neighbor 10 has an accuracy of 86.9%

For the selection of the best hyperparameter, we need to find the best hyperparameter for selecting the highest accuracy. For choosing the best hyperparameter, we need to run the simulation which also increases the processing time. There is always a trade-off between processing time and accuracy. With the sophisticated processing power of the computer, the number of iteration of 30 times can take place within 2-4 seconds.

7.1.4 Future Feature Fusion Topology Development

Additional feature may help to achieve better performance in terms of recognizing people more accurately. One of the challenge of respiratory-based recognition system is variability of breathing dynamics with the change of emotional stress and physiological activities [3].Integrating more cardiopulmonary related dynamic features may help to improve the robustness of the proposed system.Additionally, the advancement of feature engineering also enables us to extract different unique features or pattern to develop multi-modal

recognition system to cooperate with multiple features.So, developing a fusion of feature topology remains our future work to explore.

7.1.5 Challenges in Real-World Settings

Non-contact radar-based continuous authentication systems may ultimately resolve the trade-off between security and utility that plague existing authentication systems, provided that current reliability limitations can be overcome. Current implementations in this category are mostly experimental, with their performance unsatisfactory for practical use. Fundamentally, the difficulty is due to the narrow margin of tolerances toward false/missed detection during system authentication. Unlike other non-critical applications, false/missed detection in authentication could result in irreversible credential revocation and permanent loss of access privilege. This risk is amplified by unpredictable events and noise within a casual sensing environment. For instance, when multiple subjects present close to the sensor, identification might be challenging due to the mixture of signal reflection. Existing studies mostly focus on identification of isolated single subjects without random movement. However, if the system cannot isolate respiratory signatures reliably for multiple subjects, the identity authentication system performance will deteriorate in practice. Furthermore, methods intended to separate subjects [4] may detrimentally discard information that is relied upon for identification. Another potential limitation is that the sample sizes of existing experimental efforts are often limited. Some respiratory or heart-related features need to be validated for a large population to show their uniqueness. So far, results based on small scale studies reported by different researchers appear promising, but further exploration is required. Finally, authentication measurements are subject not only to natural environmental interference, but also to intentional subversion which poses further difficulty.

One of the major challenges in radar-based non-contact continuous identity authentication results from the motion noise produced by random body movement during respiration sensing and by the presence of multiple subjects [4]. While much research

relies on the recognition and exploitation of common opportunities for analyzing time periods of sedentary physiological motion [5][6], successful Doppler radar respiration sensing during random body movement has also been demonstrated in the literature [7] [8]. Prior research has demonstrated the efficacy of a Doppler radar sensor with a camera aided random body movement cancellation technique. In the associated methodology, random body movement can be mitigated by utilizing three different strategies, such as using (1) phase compensation at the Doppler RF front-end (2) phase compensation for baseband complex signals, and (3) cancellation during demodulation techniques [7] [8]. It has also been demonstrated that using multiple transceivers (bio-radar technique), different body movement can be cancelled [8]. Additionally, blind source separation (BSS), or independent component analysis (ICA), has been utilized to extract breathing rate and heart rate with the presence of two subjects [9] and to cancel random body movement. Phased array radar systems with beamforming techniques have also been investigated to isolate the respiratory signature based on estimation of the direction of arrival of the subject [10][11]. In addition to that, frequency modulated continuous wave (FMCW) radar integrated with beam steering technique has been investigated to isolate the respiratory signatures in multiple subject scenarios [12]. In addition, a portable handheld radar-based cardiopulmonary monitoring system has also been investigated, where motion compensation was performed by integrating the EMD technique to reliably extract the respiratory information [13].These proposed solutions have demonstrated the efficacy of radar-based respiration sensing techniques under random body movement or in the presence of multiple subjects. Future non-contact radar authentication research will likely involve the integration of these and other motion-noise suppression techniques to create a robust real-world continuous authentication solution.

7.2 Conclusion

This thesis contributes to the development and feasibility validation of non-contact radar-based identity authentication system in multiple subject scenarios. The feasibility of

this type of identity authentication system was also examined and demonstrated for the application of unobtrusive sleep apnea assessment in home environments. We developed a modality switch tracking protocol to facilitate secure sleep study. We also extracted highly distinguishable breathing related dynamic features from respiratory signatures, including breathing rate/heart rate, inhale/exhale area for identity verification. Moreover, we also performed extensive security analysis, i.e. calculation of the empirical entropy of breathing related hyper-features, and determined that the entropy of hyper-feature sets (approximately 3 bits) is insufficient for secure identity verification. We also combined Fuzzy extractors with linear coding to transform the hyper-feature set into strong biometric keys compatible with machine learning classifiers. This is the first research contribution to achieve secure radio-based multi-subject identity verification for in-home OSA screening, by harnessing the combined power of Doppler radar and Fuzzy key extractors.

For future work, artificial intelligence (AI) or deep learning can be employed to perform analytics, optimization and extract unique features automatically from radar received respiratory pattern. Additionally, automatic feature extraction using AI can reduce the processing time or the latency of the proposed system. One of the potential benefits of this system is that health status monitoring is also possible along with identity authentication. This work mostly concentrate on recognizing people from their sedentary breathing patterns. So, recognizing people for varied breathing pattern remains as future work. We also explored initial feasibility of utilizing ICA-JADE and DOA methods together to isolate respiratory patterns from varied combined breathing patterns [14][15][16][17][18]. Large scale study to prove the efficacy of the system also remains our future work. Development of future feature fusion topology will also make the system more robust and fault tolerant.

References

[1] F. Lin, C. Song, Y. Zhuang, W. Xu, C. Li, and K. Ren, "Cardiac Scan: A Non-contact and Continuous Heart-based User Authentication System," in *Proceedings of the 23rd Annual International Conference on Mobile Computing and Networking*, (Snowbird Utah USA), pp. 315–328, ACM, Oct. 2017.

[2] S. M. M. Islam, A. Rahman, N. Prasad, O. Boric-Lubecke, and V. M. Lubecke, "Identity Authentication System using a Support Vector Machine (SVM) on Radar Respiration Measurements," in *2019 93rd ARFTG Microwave Measurement Conference (ARFTG)*, (Boston, MA, USA), pp. 1–5, IEEE, June 2019.

[3] G. Benchetrit, "Breathing pattern in humans: diversity and individuality," *Respiration Physiology*, vol. 122, pp. 123–129, Sept. 2000.

[4] S. M. M. Islam, O. Boric-Lubecke, and V. M. Lubekce, "Concurrent Respiration Monitoring of Multiple Subjects by Phase-Comparison Monopulse Radar Using Independent Component Analysis (ICA) With JADE Algorithm and Direction of Arrival (DOA)," *IEEE Access*, vol. 8, pp. 73558–73569, 2020.

[5] W. Massagram, V. Lubecke, A. Host-Madsen, and O. Boric-Lubecke, "Assessment of Heart Rate Variability and Respiratory Sinus Arrhythmia via Doppler Radar," *IEEE Transactions on Microwave Theory and Techniques*, vol. 57, pp. 2542–2549, Oct. 2009.

[6] W. Massagram, V. M. Lubecke, and O. Boric-Lubecke, "Feasibility assessment of Doppler radar long-term physiological measurements," in *2011 Annual International*

Conference of the IEEE Engineering in Medicine and Biology Society, (Boston, MA), pp. 1544–1547, IEEE, Aug. 2011.

[7] Changzhi Li and Jenshan Lin, "Random Body Movement Cancellation in Doppler Radar Vital Sign Detection," *IEEE Transactions on Microwave Theory and Techniques*, vol. 56, pp. 3143–3152, Dec. 2008.

[8] C. Gu, G. Wang, Y. Li, T. Inoue, and C. Li, "A Hybrid Radar-Camera Sensing System With Phase Compensation for Random Body Movement Cancellation in Doppler Vital Sign Detection," *IEEE Transactions on Microwave Theory and Techniques*, vol. 61, pp. 4678–4688, Dec. 2013.

[9] S. M. M. Islam, E. Yavari, A. Rahman, V. M. Lubecke, and O. Boric-Lubecke, "Separation of Respiratory Signatures for Multiple Subjects Using Independent Component Analysis with the JADE Algorithm," in *2018 40th Annual International Conference of the IEEE Engineering in Medicine and Biology Society (EMBC)*, (Honolulu, HI), pp. 1234–1237, IEEE, July 2018.

[10] S. M. M. Islam, E. Yavari, A. Rahman, V. M. Lubecke, and O. Boric-Lubecke, "Direction of Arrival Estimation of Physiological Signals of Multiple Subjects Using Phase Comparison Monopulse Radar," in *2018 Asia-Pacific Microwave Conference (APMC)*, (Kyoto), pp. 411–413, IEEE, Nov. 2018.

[11] S. M. M. Islam, E. Yavari, A. Rahman, V. M. Lubecke, and O. Boric-Lubecke, "Multiple Subject Respiratory Pattern Recognition and Estimation of Direction of Arrival using Phase-Comparison Monopulse Radar," in *2019 IEEE Radio and Wireless Symposium (RWS)*, (Orlando, FL, USA), pp. 1–4, IEEE, Jan. 2019.

[12] S. M. M. Islam, N. Motoyama, S. Pacheco, and V. M. Lubecke, "Non-Contact Vital Signs Monitoring for Multiple Subjects Using a Millimeter Wave FMCW Automotive Radar," (Los Angeles, California, USA), p. 4, IEEE International Micorwave Symposium (IMS'20), June 2020.

[13] I. Mostafanezhad, E. Yavari, O. Boric-Lubecke, V. M. Lubecke, and D. P. Mandic, "Cancellation of Unwanted Doppler Radar Sensor Motion Using Empirical Mode Decomposition," *IEEE Sensors Journal*, vol. 13, pp. 1897–1904, May 2013.

[14] S. M. M. Islam, and V. Lubecke, "Extracting Individual Respiratory Signatures from Combined Multi-Subject Mixtures with Varied Breathing Pattern Using Independent Component Analysis with the JADE Algorithm," (Hong Kong), IEEE Asia-Pacific Microwave Conference (APMC'20), Dec. 2020.

[15] S. M. M. Islam, C. Grado, L. Lubecke,and V. Lubecke, "An Adaptive Filter Technique for Platform Motion Compensation in Unmanned Aerial Vehicle Based Remote Life Sensing Radar," (Utrecht, Netherland), European Microwave Week (EuMw'20), Jan. 2021.

[16] S. M. M. Islam, C. Grado, L. Lubecke,and V. Lubecke, "UAV Radar Sensing of Respiratory Variations for COVID-Type Disorders," (Hong Kong), IEEE Asia-Pacific Microwave Conference (APMC'20), Dec. 2020.

[17] F. Snigdha, S. M. M. Islam, V. Lubecke, and O. Boric-Lubecke, "Obstructive Sleep Apnea (OSA) Stage Classification by Effective Radar Cross Section (ERCS) Method Using Microwave Doppler Radar," (Toulouse, France), IEEE MTT-S International Microwave Biomedical Conference (IMBioc'20), Dec. 2020.

[18] S. M. M. Islam, O. Boric-Lubecke,and V. Lubecke, "Comparative Analysis of Phase-Comparison Monopulse and MUSIC Algorithm Methods for Direction of Arrival (DOA) of Multiple-Subject Respiration Measured with Doppler Radar," (Hong Kong), IEEE Asia-Pacific Microwave Conference (APMC'20), Dec. 2020.